

https://dspace.org/

Modelling geological and mineral resources uncertainty in stratabound and stratiform deposits of the Witwatersrand Basin, South Africa

Mashala, Prudence G.

2025

University of the Witwatersrand, Johannesburg

https://hdl.handle.net/10539/50274

Mashala, Prudence G.. (2025). Modelling geological and mineral resources uncertainty in stratabound and stratiform deposits of the Witwatersrand Basin, South Africa [Master's dissertation, University of the Witwatersrand, Johannesburg]. WIReDSpace. https://hdl.handle.net/10539/50274

Downloaded from a DSpace repository. https://dspace.org/

Modelling geological and mineral resources uncertainty in stratabound and stratiform deposits of the Witwatersrand Basin, South Africa



Prudence G. Mashala

(1706065)

A thesis submitted to the Faculty of Science, University of the Witwatersrand, Johannesburg in fulfilment of the requirements for the degree Master of Science

Supervisor: Prof. Glen T. Nwaila

Co-Supervisors: Dr. Steven E. Zhang and Dr. Julie E. Bourdeau

19 October 2025

DECLARATION

This thesis, submitted for the Degree Master of Science at the University of the Witwatersrand, Johannesburg, is my own work. It has not been submitted for any degree or examination at any other institution.



(Signature of candidate)

19th day of October 2025 at Secunda, Mpumalanga

ABSTRACT

Accurate estimation of mineral resources and the quantification of uncertainty associated with kriged estimates are of paramount importance. However, uncertainty in mineral resource estimation is often unquantified and unreported, limiting the ability to make informed decisions. This study aims to integrate statistical and geostatistical methods to characterise mineral resources, quantify their uncertainty, and propose improvements for more reliable estimates. Sampling data from the Middelvlei Reef within the Driefontein area (South Africa) was used as a case study for this research. Resource estimation and uncertainty analysis were conducted using ordinary kriging and confidence intervals methods, with supplementary assessments using kriging validation metrics. The Python programming language within Jupyter Notebook was employed in this study. Key findings highlight that uncertainty analyses, and therefore mineral resource classification, is heavily influenced by variography, model parameters, geological domaining and the choice of the uncertainty quantification method. To improve mineral resource classification and uncertainty assessments, there should be emphasis on the need for infill drilling in high uncertainty and low sample density zones, followed by refinement of variogram parameters post-infill drilling, and a continuous assessment of the relationship between kriged estimates and their confidence intervals. Integrating these approaches will allow mining professionals to develop data-driven resource models, ensuring sustainable and efficient mineral extraction.

DEDICATION

This thesis is dedicated to my parents, who supported the decision to further my studies with no expectations of me fulfilling other roles.

ACKNOWLEDGEMENTS

To the Almighty, Sovereign God who wills and perfects, I am deeply grateful.

I would like to express my sincere gratitude to my supervisor, Prof. G.T. Nwaila, for his invaluable guidance and for sharing his expertise in statistics and mineral resource estimation throughout this research project. I also extend my appreciation to my co-supervisors, Dr J.E. Bourdeau and Dr S.E. Zhang, for their contributions to my knowledge of geostatistics and scientific writing. I would also like to acknowledge Johan van Eeden, the former Chief Geologist at Sibanye Stillwater, for supplying the data that enabled this study.

To my family, I am immensely grateful for the unwavering mental and emotional support I received during my studies. Thank you for providing a shoulder to lean on during challenging times. To my sister, Mrs J.M. Malatji, thank you for being a strong, consistent, and stable anchor. To my friends, Mr M.P. Magagula, Mr S.H. Lifhiga, Ms N.B. Mkasi, and Ms P. Mokadi, thank you for constantly providing much-needed support and sharing encouraging words with me.

TABLE OF CONTENTS

DECLARATION ii
ABSTRACT iii
DEDICATION iv
ACKNOWLEDGEMENTS v
TABLE OF CONTENTS vi
LIST OF FIGURES viii
LIST OF TABLES xvii
LIST OF EQUATIONS xix
1. INTRODUCTION 1
1.1. Aim 5
1.2. Objectives 5
1.3. Scope and Limitation 6
1.4. Thesis Outline 6
2. GEOLOGICAL SETTING 10
2.1. Regional Geology 10
2.2. Geology of the Middelvlei Reef 14
3. GEOSTATISTICAL METHODS OF RESOURCE ESTIMATION 17
3.1. Inverse Distance Weighting 18
3.2. Nearest Neighbour Interpolation 19
3.3. Kriging 21
3.4. Geo-domaining 28
4. MINERAL RESOURCE ESTIMATION AND UNCERTAINTY QUANTIFICATION 31
4.1. Mineral Resource Estimation 31
4.2. Geological and Geostatistical Uncertainty 32
4.3. Geostatistical Uncertainty Quantification 34
4.4. Mineral Resource Classification Using Uncertainty 40
5. STUDY AREA AND METHODOLOGY 44
5.1. Study Area and Dataset 44
5.2. Statistical Analysis 45
5.3. Creating Geo-Domain Boundaries 47
5.4. Variography 47
5.5. Quantitative Kriging Neighbourhood Analysis 49

5.6. Ordinary Kriging 50
5.7. Confidence Intervals 50
6. RESULTS 55
6.1. Exploratory Data Analysis 55
6.2. Domain Boundaries 73
6.3. Variography 82
6.4. Kriging Neighbourhood Analysis 106
6.5. Ordinary Kriging 116
6.6. Confidence Quantification and Mineral Resource Classification 141
7. DISCUSSION 162
7.1. Spatial Variability 162
7.2. Resource Estimation 165
7.3. Confidence Intervals, Uncertainty Analysis, and Uncertainty Classification 170
7.4. Uncertainty Management 173
8. CONCLUSION 176
REFERENCES 178
APPENDIX 189

LIST OF FIGURES

Figure 1.1: A diagram depicting how mineral reserves and resources are classified, considering mining, processing, marketing, legal, environmental, infrastructure, social, and governmental factors as well as increasing levels of geological knowledge and confidence. Adapted from CRIRSCO (2012).

Figure 2.1: A figure showing the geographical and geological setting and location of the Witwatersrand Supergroup and the exposed Archaean rocks in the central Kaapvaal Craton region in Johannesburg, South Africa. The Kaapvaal Craton is outlined in red stippled lines. The red star indicates the location of the study area. Figure modified from Tucker *et al*. (2016).

Figure 2.2: A generalised stratigraphic column of the Witwatersrand Supergroup showing the stratigraphic position of different reefs. The thickness of the stratigraphic sequence is not to scale. Figure adapted from Frimmel (2014).

Figure 2.3: Generalised stratigraphy for Type A (insert A) and Type B (insert B) lithofacies assemblages. Adapted from Krige (1951).

Figure 3.1: A diagram depicting how Thiessen polygons are used to obtain estimates through nearest neighbour interpolation. The black dots represent sampled locations. Insert A shows the area to be estimated; insert B shows how Thiessen polygons are created around sampled locations, and insert C shows the final estimates as a result of partitioning the region of interest.

Figure 3.2: A graph showing terms used in variography: a sill, range, and nugget effect.

Figure 5.1: A map showing spatial locations of gold assay samples and their associated grades, as represented by the colour bar. The black polygon represents the study area. The red and green lines show faults and dykes, respectively.

Figure 5.2: A methodology workflow diagram summarising sequential steps involved in this research.

Figure 6.1: Graphs of z-score values for different variables before and after outlier removal. CMGT z-score, CW z-score and Au z-score represent the gold accumulation (cm.g/t), channel width (cm) and Au (g/t) z-score values, respectively.

Figure 6.2: Boxplots, per variable of interest, of the dataset before and after outlier treatment. CMGT represents the gold accumulation (cm.g/t), CW represents the channel width (cm), and Au represents the Au (g/t).

Figure 6.3: Histogram and boxplot of the entire dataset for gold accumulation (cm.g/t).

Figure 6.4: Histogram and boxplot of the entire dataset for channel width (cm).

Figure 6.5: Histogram and boxplot of the entire dataset for Au (g/t).

Figure 6.6: A correlation matrix heatmap for the entire dataset. The colour gradient represents the correlation relationship, ranging from weak (blue) to strong (red), indicating areas with correlation. X and Y represent the X- and Y-coordinates, CMGT represents the gold accumulation (cm.g/t), CW represents the channel width (cm), and Au represents Au (g/t).

Figure 6.7: Histograms showing the distribution and statistical analysis of data within each variable for domain 8. The red stippled line is a trendline.

Figure 6.8: Histograms showing the distribution and statistical analysis of data within each variable for domain 14. The red stippled line is a trendline.

Figure 6.9: Histograms showing the distribution and statistical analysis of data within each variable for domain 18. The red stippled line is a trendline.

Figure 6.10: Histograms showing the distribution and statistical analysis of data within each variable for domain 19. The red stippled line is a trendline.

Figure 6.11: A map of the study area showing data point locations incorporating geological structures such as faults and dykes. The colour gradient represents the domain into which each sample is categorised.

Figure 6.12: F1 and accuracy scores of various machine learning algorithms and their best models through fivefold cross-validation.

Figure 6.13: Contour plots of the different classifiers and their predicted domain boundaries. The various sample locations are plotted according to their domain classification, and the scale bar represents the different domains into which the samples are classified.

Figure 6.14: Classifier polygons exported as shapefiles. The navy-blue colour shades domain 8, green shades domain 14 and yellow shades both domains 18 and 19.

Figure 6.15: Final domain boundary map from the support vector model. The blue represents the region of interest and its immediate surroundings, and the white lines represent the domain boundaries delineated using the support vector machine model. The domain boundaries extend outside the study area because the maximum and minimum X- and Y-coordinate values in the dataset were used to limit the GridSearchCV process instead of the study area.

Figure 6.16: A map showing the location of sample points and the domains they are classified to fall into, incorporating geological structures and domain boundaries.

Figure 6.17: Scatter-line plot of declustered mean versus cell size for gold accumulation (cm.g/t) in domain 8.

Figure 6.18: Scatter-line plot of declustered mean versus cell size for channel width (cm) in domain 8.

Figure 6.19: Scatter-line plot of declustered mean versus cell size for Au (g/t) in domain 8.

Figure 6.20: Scatter-line plot of declustered mean versus cell size for gold accumulation (cm.g/t) in domain 14.

Figure 6.21: Scatter-line plot of declustered mean versus cell size for channel width (cm) in domain 14.

Figure 6.22: Scatter-line plot of declustered mean versus cell size for Au (g/t) in domain 14.

Figure 6.23: Scatter-line plot of declustered mean versus cell size for gold accumulation (cm.g/t) in domain 18.

Figure 6.24: Scatter-line plot of declustered mean versus cell size for channel width (cm) in domain 18.

Figure 6.25: Scatter-line plot of declustered mean versus cell size for Au (g/t) in domain 18.

Figure 6.26 Scatter-line plot of declustered mean versus cell size for gold accumulation (cm.g/t) in domain 19.

Figure 6.27: Scatter-line plot of declustered mean versus cell size for channel width (cm) in domain 19.

Figure 6.28: Scatter-line plot of declustered mean versus cell size for Au (g/t) in domain 19.

Figure 6.29: Domain 8 variogram maps for different variables. The colour scale represents the semi-variance, with blue indicating low semi-variance and red indicating high semi-variance.

Figure 6.30: Domain 8 fitted semi-variogram models. Each graph represents an experimental semi-variogram (black circles) fitted with a spherical model (magenta curve), with the nugget effect (dotted red line) indicating short-range variability.

Figure 6.31: Domain 14 variogram maps for different variables. The colour scale represents the semi-variance, with blue indicating low semi-variance and red indicating high semi-variance.

Figure 6.32: Domain 14 fitted semi-variogram models. Each graph represents an experimental semi-variogram (black circles) fitted with a spherical model (magenta curve), with the nugget effect (dotted red line) indicating short-range variability.

Figure 6.33: Domain 18 variogram maps for different variables. The colour scale represents the semi-variance, with blue indicating low semi-variance and red indicating high semi-variance.

Figure 6.34: Domain 18 fitted semi-variogram models. Each graph represents an experimental semi-variogram (black circles) fitted with a spherical model (magenta curve), with the nugget effect (dotted red line) indicating short-range variability.

Figure 6.35: Domain 19 variogram maps for different variables. The colour scale represents the semi-variance, with blue indicating low semi-variance and red indicating high semi-variance.

Figure 6.36: Domain 19 fitted semi-variogram models. Each graph represents an experimental semi-variogram (black circles) fitted with a spherical model (magenta curve), with the nugget effect (dotted red line) indicating short-range variability.

Figure 6.37: Graphs showing how discretisation varies with sample in-block variance for different variables of each domain. CMGT represents the gold accumulation (cm.g/t), CW represents the channel width (cm), and Au represents Au (g/t).

Figure 6.38: Graph showing how the slope of regression and kriging efficiency change with increasing number of search data for each variable within each domain. The graphs also indicate the optimal number of samples that should be used for kriging. CMGT represents the gold accumulation (cm.g/t), CW represents the channel width (cm), Au represents Au (g/t), KEFF represents the kriging efficiency, and SLOR represents the slope of regression.

Figure 6.39: Kriged estimates map of the gold accumulation (cm.g/t) incorporating geological structures such as faults and dykes, as well as domain boundaries. The colour gradient represents estimated gold accumulation index values, ranging from low (blue) to high (red), indicating areas with varying levels of gold accumulation.

Figure 6.40: Kriged estimates map of channel width (cm) incorporating geological structures such as faults and dykes, as well as domain boundaries. The colour gradient represents estimated gold accumulation index values, ranging from low (blue) to high (red), indicating areas with varying levels of gold accumulation.

Figure 6.41: Kriged estimates map of Au (g/t) incorporating geological structures such as faults and dykes, as well as domain boundaries. The colour gradient represents estimated gold accumulation index values, ranging from low (blue) to high (red), indicating areas with varying levels of gold accumulation.

Figure 6.42: Kriged variance map of the gold accumulation (cm.g/t) incorporating geological structures such as faults and dykes, as well as domain boundaries. The colour gradient represents kriging variance values, ranging from low (blue) to high (red), indicating areas with varying kriging variance values.

Figure 6.43: Kriged variance map of the channel width (cm) thickness incorporating geological structures such as faults and dykes, as well as domain boundaries. The colour gradient represents kriging variance values, ranging from low (blue) to high (red), indicating areas with varying kriging variance values.

Figure 6.44: Kriged variance map of Au (g/t) incorporating geological structures such as faults and dykes, as well as domain boundaries. The colour gradient represents kriging variance values, ranging from low (blue) to high (red), indicating areas with varying kriging variance values.

Figure 6.45: Kriged efficiency map of the gold accumulation (cm.g/t) incorporating geological structures such as faults and dykes, as well as domain boundaries. The colour gradient represents kriging efficiency values, ranging from low (blue) to high (red), indicating areas with varying kriging efficiency values.

Figure 6.46: Kriged efficiency map of channel width (cm) thickness incorporating geological structures such as faults and dykes, as well as domain boundaries. The colour gradient represents kriging efficiency values, ranging from low (blue) to high (red), indicating areas with varying kriging efficiency values.

Figure 6.47: Kriged efficiency map of Au (g/t) incorporating geological structures such as faults and dykes, as well as domain boundaries. The colour gradient represents kriging

efficiency values, ranging from low (blue) to high (red), indicating areas with varying kriging efficiency values.

Figure 6.48: Slope regression map of the gold accumulation (cm.g/t) incorporating geological structures such as faults and dykes, as well as domain boundaries. The colour gradient represents kriging efficiency values, ranging from low (blue) to high (red), indicating areas with varying slope of regression values.

Figure 6.49: Slope regression map of channel width (cm) thickness incorporating geological structures such as faults and dykes, as well as domain boundaries. The colour gradient represents kriging efficiency values, ranging from low (blue) to high (red), indicating areas with varying slope of regression values.

Figure 6.50: Slope regression map of Au (g/t) incorporating geological structures such as faults and dykes, as well as domain boundaries. The colour gradient represents kriging efficiency values, ranging from low (blue) to high (red), indicating areas with varying slope of regression values.

Figure 6.51: Confidence percentage map of the gold accumulation (cm.g/t) calculated through the normal score transformation method incorporating geological structures such as faults and dykes, as well as domain boundaries. The colour gradient represents the confidence percentage, ranging from low (blue) to high (red), indicating areas with varying certainty.

Figure 6.52: Confidence percentage map of the channel width (cm) thickness calculated through the normal score transformation method incorporating geological structures such as faults and dykes, as well as domain boundaries. The colour gradient represents the confidence percentage, ranging from low (blue) to high (red), indicating areas with varying certainty.

Figure 6.53: Confidence percentage map of Au (g/t) calculated through the normal score transformation method incorporating geological structures such as faults and dykes, as

well as domain boundaries. The colour gradient represents the confidence percentage, ranging from low (blue) to high (red), indicating areas with varying certainty.

Figure 6.54: Uncertainty classification map of the gold accumulation (cm.g/t) calculated through the logarithmic transformation method incorporating geological structures such as faults and dykes, as well as domain boundaries. The colour gradient represents the level of uncertainty, ranging from low (blue) to high (red), indicating areas with varying uncertainty.

Figure 6.55: Uncertainty classification map of channel width (cm) thickness calculated through the logarithmic transformation method incorporating geological structures such as faults and dykes, as well as domain boundaries. The colour gradient represents the level of uncertainty, ranging from low (blue) to high (red), indicating areas with varying uncertainty.

Figure 6.56: Uncertainty classification map Au (g/t) calculated through the logarithmic transformation method incorporating geological structures such as faults and dykes, as well as domain boundaries. The colour gradient represents the level of uncertainty, ranging from low (blue) to high (red), indicating areas with varying uncertainty.

Figure 6.57: Swath plots for the gold accumulation (cm.g/t) along the X- and Y-directions. The plot compares the kriged model estimates with the sample values. Sample counts are represented by grey bars, while the pink and green lines indicate sample and model gold accumulation (cm.g/t) values, respectively.

Figure 6.58: Swath plots for channel width (cm) thickness along the X- and Y-directions. The plot compares the kriged model estimates with the sample values. Sample counts are represented by grey bars, while the pink and green lines indicate sample and model gold accumulation index values, respectively.

Figure 6.59: Swath plots for Au (g/t) along the X- and Y-directions. The plot compares the kriged model estimates with the sample values. Sample counts are represented by grey

bars, while the pink and green lines indicate sample and model gold accumulation index values, respectively.

Figure A1: Pairwise plots showing the relationships between different variables within each domain.

Figure A2: Pearson's correlation heatmaps for the different domains.

Figure A3: Scatter plots and histograms showing histograms and scatter plots for each variable-domain's combination for the declustered estimation data.

Figure A4: Experimental semi-variograms created for the variable-domain combinations at 15◦ intervals.

Figure A5: Histograms of each domain-variable combination's raw data, normal score transformed data and back-transformed data distribution.

LIST OF TABLES

Table 4.1: Potential error levels at the 90% confidence level for mineral resource or reserve classification as suggested by Dominy et al. (2002).

Table 4.2: Mineral resource classification criteria at the 90% confidence level as proposed by Yamamoto (1999).

Table 6.1: A selection of data points from the raw datasheet showing different sample properties. XPT, YPT and ZPT represent the X-, Y- and Z- coordinates, respectively.

Table 6.2: A selection of data points after QA/QC.

Table 6.3: Table presenting descriptive statistics for spatial coordinates, domain classifications, and three key variables of the dataset after QA/QC was applied.

Table 6.4: Table showing summary statistics of the dataset following outlier treatment.

Table 6.5: Summary statistics of the different variables per domain.

Table 6.6: Table showing hyperparameters used in domain boundary classification.

Table 6.7: Table showing test score summary (accuracy and F1 score) for each classifier.

Table 6.8: Table showing selected weights and normal score values obtained for each variable-domain combination.

Table 6.9: Variogram summary parameters for different variables within the domains. X and Y represent the X- and Y-coordinates, CMGT is the gold accumulation index, CW is the channel width, and Au represents the gold concentration.

Table 6.10: Table showing a selection of the first ten rows of results from the quantitative kriging neighbourhood analysis post-validation results. CMGT represents the gold accumulation index.

Table 6.11: Table summarising minimum and maximum samples required for optimal estimation of reserves.

Table 6.12: Table summarising the parameters used for kriging as determined from variography and quantitative kriging neighbourhood analysis.

Table 6.13: Summary statistics of results obtained through ordinary kriging, including values that are NaN.

Table 6.14: Summary statistics of results obtained through ordinary kriging, excluding blocks that were not estimated due to insufficient sample numbers.

Table 6.15: Table showing selected results from the logarithmic transformation of the estimation dataset in preparation for confidence interval calculation.

Table 6.16: Summary table of the gold accumulation (cm.g/t) confidence interval results and their associated logarithmic transformed values.

Table 6.17: Summary table of the channel width (cm) confidence interval results and their associated logarithmic transformed values.

Table 6.18: Summary table of the Au (g/t) confidence interval results and their associated logarithmic transformed values.

Table 6.19: Table summarising the uncertainty classification used in this study.

Table A1: Within-block variance for various discretisation block and discretisation number combinations for each variable.

Table A2: Table showing results from quantitative neighbourhood analysis post-validation.

LIST OF EQUATIONS

Equation 3.1: Inverse distance weighting

Equation 3.2: Inverse distance weighting estimates

Equation 3.3: Nearest neighbour interpolation

Equation 3.4: Basic equation for kriging

Equation 3.5: Simple kriging

Equation 3.6: Ordinary kriging

Equation 3.7: Search neighbourhood

Equation 3.8: Root mean-square error

Equation 4.1: Simple kriging variance

Equation 4.2: Ordinary kriging variance

Equation 4.4: Kriging efficiency

Equation 45: Kriging slope of regression

Equation 5.1: Formula for calculating z-score values.

Equation 5.2: Logarithmic transformation of data

Equation 5.3: Logarithmic variance computation

Equation 5.4: Dispersion variance calculation

Equation 5.5: Scaling the logarithmic variance

Equation 5.6: Kriging standard deviation in logarithmic space

Equation 5.7: Conversion of kriging estimates to logarithmic space

Equation 5.8: Lower-bound logarithmic confidence interval calculation

Equation 5.9: Upper-bound logarithmic confidence interval calculation

Equation 5.10: Lower-bound logarithmic confidence interval conversion to raw space

Equation 5.12: Logarithmic variance computation

Equation 5.13: Scaling the log kriging variance.

Equation 5.14: Kriging standard deviation in normal space

Equation 5.15: Conversion of kriging estimates to log space.

Equation 5.16: Lower-bound log confidence interval calculation

Equation 5.17: Upper-bound log confidence interval calculation

Equation 5.18: Lower-bound log confidence interval conversion to raw space

1. INTRODUCTION

Resource estimation is crucial for the success of any mining project and cannot be performed without sampling and geoscientific information. Resource estimation is the outcome of a procedure that begins with gathering data, proceeds to geological interpretation, and may be concluded when the deposit's geology is interpreted, which may involve geological and geostatistical models as well as the reporting and reconciliation of mineral resource estimates (McManus *et al.,* 2021). Resource estimation includes the analysis of numerical and geological data to provide estimated tonnages and grades to guide ore extraction (Coombes, 2008). Globally, the Committee for Mineral Reserves International Reporting Standards (CRIRSCO) and its members generally categorise mineral resources into three main groups: (1) inferred, (2) indicated, and (3) measured mineral resources, considering the degree of geoscientific knowledge and confidence in techno-economic factors (Dominy *et al.*, 2002) (Fig. 1.1). Mineral resources are converted into mineral reserves (i.e., probable and proved mineral reserves) based on techno-economic viability regarding mining, processing, marketing, legal, environmental, infrastructural, social, and governmental factors (CRIRSCO, 2012) (Fig. 1.1).

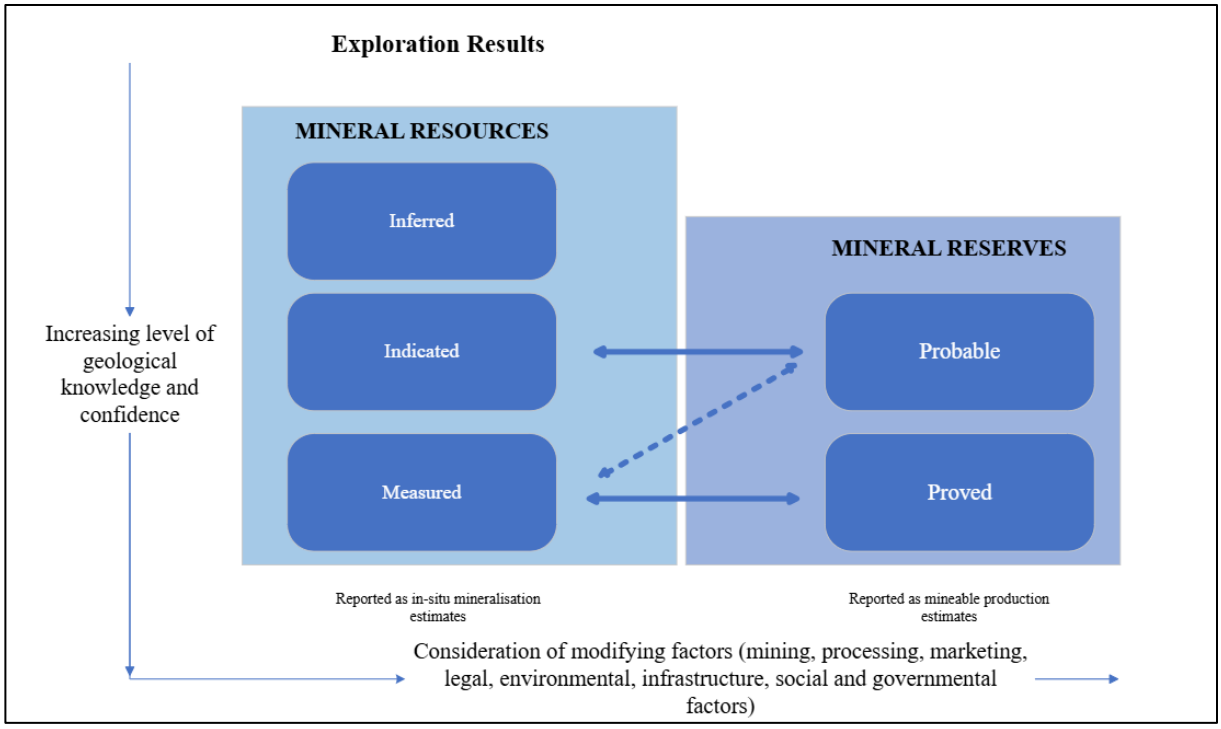


Figure 1.1: A diagram depicting how mineral reserves and resources are classified, considering mining, processing, marketing, legal, environmental, infrastructure, social, and governmental factors, as well as increasing levels of geological knowledge and confidence. Adapted from CRIRSCO (2012).

Several challenges may be encountered when estimating resources: (1) inaccuracy in geoscientific information and interpretations; (2) grade variability, which is a function of continuity and distribution; (3) technological and external factors; and (4) the experience and assumptions applied by the competent person (Ortiz, 2006; Owusu and Dagdelen, 2024). Typically, orebodies are known to be anisotropic, *i.e.*, they are discontinuous and have varying thicknesses and orientations. The geology and the sample size in an area may be similar, but variation between samples a small distance apart (termed the nugget effect) can vary with sample orientation; in turn, changing the values of distribution (Camana and Deutsch, 2019). Grade variability and the nugget effect are affected by errors in measurements and differences

in sampling and drilling orientation. Since measurement errors affect the grade variability and nugget effect, simple interpolation methods are not ideal for estimating thin, tabular, anisotropic mineral resources (Abzalov and Humphreys, 2002). Enhancement in the accuracy of a mineral resource's grade and tonnage estimation could therefore better guide mine planning, decision-making procedures, and assist in the effective extraction of mineral resources.

Geological considerations such as mineral and grade continuity and geological structures are used to determine block model estimates (Deustch *et al*., 2014). When most conditionally biased resource estimation techniques became insufficient for estimating mineral resource grades and an improvement in mine valuation methods became necessary, kriging, a geostatistical estimation method, was applied to the South African ore as a mineral resource estimation method (Krige, 1951). Geostatistical methods were introduced because they can recognise and model anisotropy, decluster data, and create unbiased estimates (Amwaama, 2018). Geostatistical estimation techniques are widely used in the South African gold mining industry to assess mineral resources and reserves and to assist with daily mine valuation and mine planning (Mpanza, 2015; Bargawa and Tobing, 2020). Specifically, most of the gold mined in South Africa is extracted from the Witwatersrand Basin and is hosted within conglomerates, with gold assay data and channel thickness measurements used to estimate the gold grade (Muntean *et al*., 2005). Gold assay data and channel width measurements are supplemented with qualitative geological information such as particle size, packing density, and weight percentage of minerals such as pyrite, uraninite, quartz, and carbon, providing additional insights into geological domains for subsequent resource estimation (Letanta, 2020).

Geostatistical methods for estimating reserves are advantageous because they provide a measure of accuracy for all their estimates (Mpanza, 2015). Kriging is used as a primary resource estimation technique over other linear estimation methods because it provides more

precise estimates and it minimises the estimation variance while accounting for variability within the study area, thereby providing a measure of uncertainty of the estimates (Daya and Bejari, 2015). Although kriging is the primary technique for mineral reserve estimation, most studies that have applied and investigated this technique demonstrated kriging's limitations in independently quantifying uncertainty (*e.g.*, Emery et al., (2006); Delbari *et al*., (2009); and Mpanza, (2015)).

A common issue encountered in the mining industry is that the level of uncertainty related to estimating mineral resources is often left unreported and unquantified (McManus *et al*., 2021). The lack of transparency can significantly impact mining decisions by introducing concerns related to the difference between predicted and extracted grades and reducing the accuracy of uncertainty assessments, in turn affecting the decision-making process and the business's profitability (Delbari *et al*., 2009). There is also a scarcity of studies that address the effect of leaving uncertainties unreported on decision-making, and it has been argued by McManus *et al*. (2021) that the inclusion of uncertainty helps inform investment decisions and provide appropriate mineral resources and reserves. Reporting a resource and reserve estimate in compliance with one of the reporting codes (*e.g*., South African Mineral Reporting Code, Joint Ore Reserves Committee, and National Instrument 41-100) does not necessarily mean that it is a quality estimate; it simply means that the process is clear, transparent, and that the figures were reported in a prescribed manner. Actual confidence levels can be determined through geostatistical applications (Dominy *et al*., 2002). This research endeavour will employ linear geostatistical techniques to quantify uncertainty in mineral resource estimation.

1.1. Aim

The study aims to utilise statistical techniques and ordinary kriging to quantify and effectively manage uncertainties associated with mineral resource estimation of stratabound and stratiform deposits. By employing linear geostatistical approaches, an insight into the spatial distribution and variability of mineral resources within the deposit will be achieved, ultimately enhancing decision-making processes such as resource assessment and extraction. The Middelvlei Reef, within the Driefontein area (South Africa), will serve as the subject of this study.

1.2. Objectives

To fulfil the above aim, the following was carried out:

i. Characterisation of the spatial variability and distribution of mineral resources within the Middelvlei Reef of the Witwatersrand Basin. Spatial variability assessment will focus on analysing and understanding the geological and geostatistical characteristics of the deposit, including the variations in grade, thickness, continuity, and other relevant parameters.

ii. Mineral resource estimation using ordinary kriging. Estimating the mineral resource entailed employing ordinary kriging, a geostatistical method, to calculate the mineral resources in the Middelvlei Reef. The aim was to establish precise and dependable estimates of mineral grades and volumes by integrating information from surrounding samples while considering the spatial dependence and variability evident in the deposit.

iii. Confidence interval calculation for uncertainty analysis. The analysis of uncertainty involved calculating kriging validation metrics and confidence intervals to assess and quantify uncertainty associated with mineral resource estimation. The goal was to capture and provide insights into the level of uncertainty in the estimates by determining

the extent to which estimates may deviate from actual sample values. Results from confidence interval analysis will aid in decision-making during mineral resource extraction planning.

iv. Propose strategies that can be used for uncertainty management and resource optimisation. The findings from the above objectives were used to provide suggestions to effectively manage uncertainty and provide a guide to decision-makers in terms of mine design and extraction planning.

1.3. Scope and Limitation

To accurately estimate mineral resources, historical data from the Middelvlei Reef in the Witwatersrand Basin, gathered over 30 years through exploration, underground sampling, drillhole sampling, and statistical inference, was utilised. The data was sourced from Sibanye Stillwater and was collected through different methods by individuals with varying expertise and goals. This introduces potential uncertainties related to data collection practices, focal areas in drill core logging and sampling, and inconsistencies in assay methods over time. Therefore, Quality Assurance and Quality Control (QA/QC) of the database is essential before its use in the study.

1.4. Thesis Outline

This section outlines the layout of the thesis. The report is made up of a total of eight chapters with supplementary material added at the end of the report as appendices.

Chapter 1 is the Introduction. The chapter provides essential context for the research. The introduction begins with a detailed background on the study, highlighting its significance within the broader context of mineral resource estimation and uncertainty analysis. The introduction

chapter clearly defines the aim and outlines specific objectives designed to achieve the aim. The scope and limitations of this study are presented, ensuring clarity on what the study seeks to accomplish and the boundaries within which it operates. The introduction also explores the rationale behind conducting such studies, emphasising their advantages in improving resource estimation accuracy and decision-making processes.

Chapter 2 is the Geological Setting. The chapter provides an in-depth examination of the geological context and theoretical foundations of this study. The literature review begins with a detailed overview of the regional geology, including the subdivision of geological units, the depositional environment, and key structural features within the study area. The focus then shifts to the Middelvlei Reef, emphasising its sedimentary characteristics, including its formation, thickness variations, and mineral assemblages.

Chapter 3 is Geostatistical Methods of Resource Estimation. The chapter provides a theoretical background of the geostatistical methodologies employed in this study, offering insights into the geostatistical techniques, estimation processes, and uncertainty analysis approaches utilised to achieve the study's objectives. The chapter also highlights the advantages and disadvantages of the methods employed in this study.

Chapter 4 focuses on Mineral Resource Estimation and Uncertainty Quantification. The chapter presents the South African standards applied in mineral resource estimation and the need for quantification of resources and their estimates. Following the necessary background on mineral resource estimation, the chapter presents an overview of sources of uncertainty in mineral resource estimation and classification methods that are used to quantify uncertainty, and the advantages and disadvantages of using each classification method.

Chapter 5 provides an overview of the study area and details the methodologies employed in this research. The chapter begins by outlining the type of data that was received and used in this study. The chapter gives a step-by-step account of the processes followed in analysing the dataset, highlighting the considerations and assumptions applied throughout the analysis. Documenting the methodology in a structured manner, the chapter establishes a clear foundation for understanding and verifying the research findings, thereby ensuring transparency and reproducibility.

Chapter 6 consolidates the findings from the methodologies used in this research. The chapter begins with the results of the statistical analysis applied to the dataset and is followed by the delineation of geological domains within the study region. The chapter then presents the results of variography, outlines the step-by-step process of determining parameters for ordinary kriging through quantitative kriging neighbourhood analysis, and further presents the results of ordinary kriging. Finally, the chapter details the uncertainty associated with kriged estimates. By integrating all aspects of the research analysis, the results chapter provides a holistic view of outcomes from the workflow.

Chapter 7 is dedicated to discussing the results. The chapter provides an interrogation of the results obtained throughout the research and evaluates their alignment with the study's aims and objectives. The discussion chapter begins by analysing key findings, focusing on the spatial variability, resource estimation, and uncertainty quantification achieved through the methodologies employed. The effectiveness of the geostatistical techniques used in resource estimation, strategies for uncertainty management, and uncertainty analysis are also examined in the results chapter.

The final chapter reflects on the implications of this study's findings. Chapter 8 is dedicated to the conclusion. The chapter provides a concise summary of the study, highlighting how the objectives were achieved and the significance of findings in advancing mineral resource estimation and classification analysis, particularly for stratiform deposits. The conclusion chapter also identifies limitations encountered during the study and suggests areas for future research.

2. GEOLOGICAL SETTING

This chapter presents relevant geological background information on the Witwatersrand Supergroup and the Middelvlei Reef, which is the subject of the study. The chapter begins by outlining the broader regional geology in South Africa and that of the Witwatersrand Supergroup, and finally ties them to the geology of the Middelvlei Reef.

2.1. Regional Geology

The southern African Kaapvaal Craton, which is surrounded by the Kalahari and Zimbabwe cratons, contains some of the world's oldest Archaean rocks (Tucker *et al*., 2016). The Kaapvaal Craton is approximately 585,000 kilometres in area, with most of the Craton located in South Africa (Mpanza, 2015) (Fig. 2.1). This craton hosts granitoids, gneisses, and greenstone belt Archaean basement rocks, which are overlain by metamorphosed volcanic and clastic sedimentary rocks of the ±2700 Ma Dominion Group (Tucker *et al*., 2016). The Witwatersrand Basin, within the centre of the Kaapvaal Craton, is one of the largest sedimentological hosts of gold and uranium ores (Frimmel, 2019a; Muntean *et al.,* 2005). The Mesoarchean-aged Witwatersrand Basin developed in a compressive foreland setting, possibly related to the Limpopo Orogeny (located further north). The basin is composed of Witwatersrand Supergroup rocks and is located South of Johannesburg (McCarthy, 1994).

Overlying the siliciclastic and volcanic Dominion Group or the Archaean granite-greenstone basement in some places (Fig. 2.1), the Witwatersrand Basin was formed through a series of crustal plate movements (Tucker *et al*., 2016; Nwaila *et al*., 2021). The 2900 Ma Witwatersrand Supergroup is divided into the Central and the West Rand groups, which are separated by an unconformity (Frimmel, 2014). The groups are further subdivided into Subgroups and Formations (e.g., Fig. 2.2). Numerous geological structures exist within the basin: compressional faults, extensive faults, and igneous intrusions. Three primary

deformation events are related to the formation of the Witwatersrand Basin: (1) early syn-depositional deformation, (2) late syn-depositional deformation, and (3) post-Transvaal age deformation (Myers *et al.,* 1990).

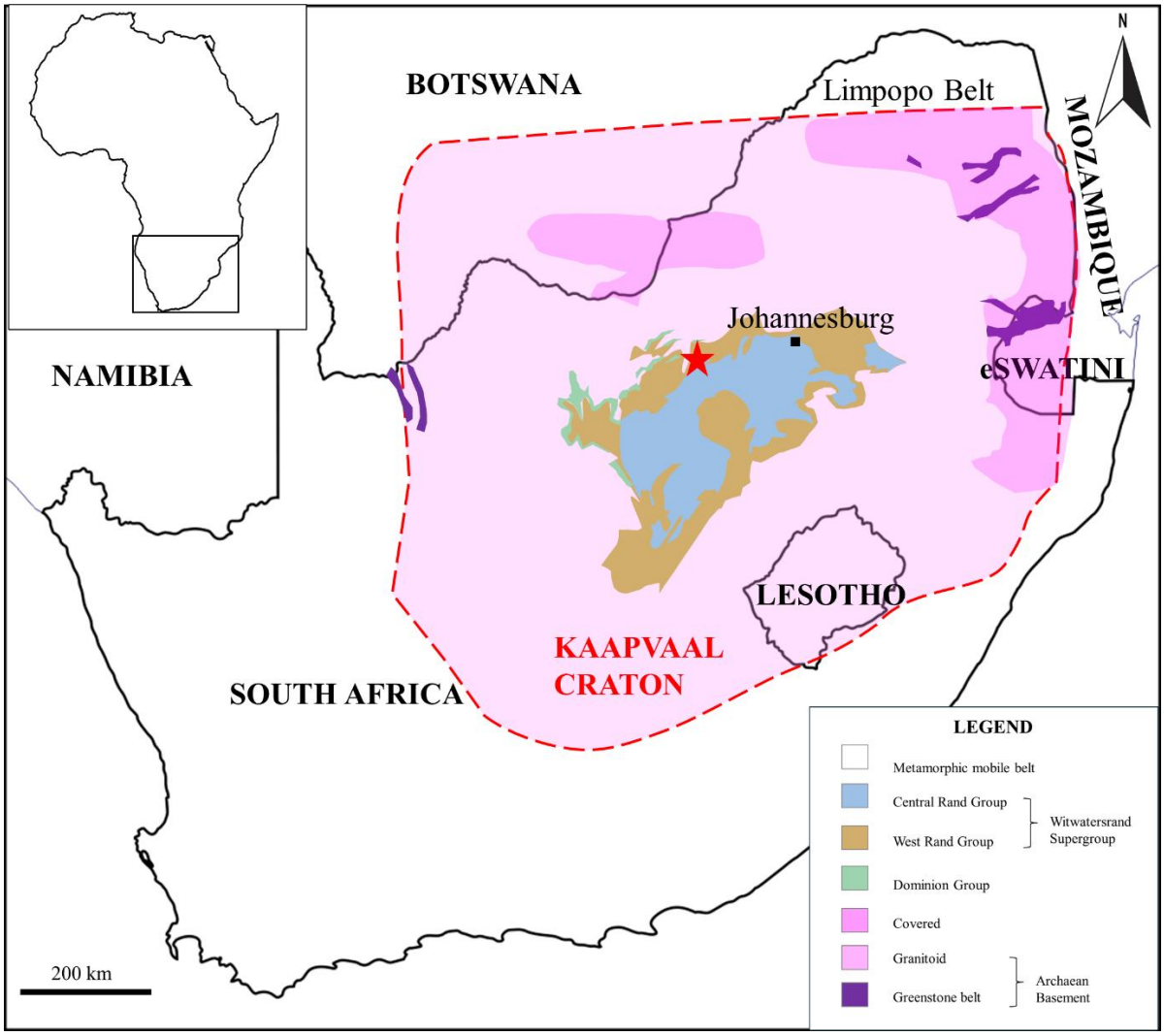


Figure 2.1: A figure showing the geographical and geological setting and location of the Witwatersrand Supergroup and the exposed Archaean rocks in the central Kaapvaal Craton region in Johannesburg, South Africa. The Kaapvaal Craton is outlined in red stippled lines. The red star indicates the location of the study area. Figure modified from Tucker *et al*. (2016).

The 2895 to 2914 Ma West Rand Group is divided from the bottom upwards into the Hospital Hill, Government, and Jeppestown Subgroups (Frimmel, 2019b) (Fig. 2.2). The West Rand Group is dominantly characterised by alternating cycles of pyrite-rich sandstone and magnetitic shales, thin conglomerate beds, mudstones, glaciogenic diamictites, and a single volcanic unit (Frimmel, 2014; Letanta, 2020; Nwaila *et al*., 2021). Tensional rifting of the Dominion Group in a shallow marine to fluvial-deltaic environment resulted in the formation of the West Rand Group (McCarthy, 1994; Gibson *et al*., 2000; Frimmel, 2014). The rifting made way for the deposition of the Central Rand Group in a tectonically stable environment (Tucker *et al*., 2016).

The West Rand Group is overlain by the 2790 ± 8 Ma Central Rand Group, which is divided into the Johannesburg and Turffontein Subgroups from the bottom upwards (Frimmel, 2019a) (Fig. 2.2). The Central Rand Group is characterised by fluvial to fluvial-deltaic sandstones and conglomerates, with minor debris flow diamictites (Tucker *et al*., 2016; Frimmel, 2019b). The Central Rand Group contains most of the gold mineralisation within the Witwatersrand Supergroup, typically hosted within commonly lens- or sheet-like conglomerate bed units (Frimmel, 2014, 2019a; Muntean *et al*., 2005; Nwaila *et al*., 2021). Sedimentological deposition of the Central Rand Group took place at the same time as folding, faulting, and uplift of the margins of the Witwatersrand Basin, resulting in multiple unconformities (Frimmel, 2014). Tensional rifting during the late deposition of the West Rand Group led to the formation of a foreland basin into which the Central Rand Group was deposited, with the Rand Anticline and Bank Thrust controlling the deposition of the Central Rand Group (Gibson et al., 2000; Tucker *et al*., 2016).

The formation, origin, and precipitation of the gold within the Witwatersrand Supergroup sediments is a widely debated topic. Notably, different models have been proposed to explain

the origin of gold: (1) the placer model, which states that gold was introduced to the basin as clastic particles (Phillips and Law, 2000; Frimmel, 2019b); (2) the hydrothermal model, which states that gold was introduced through structurally channelled hydrothermal aqueous solutions (Muntean *et al*., 2005; Frimmel, 2019b); and (3) the modified placer/precipitation model, which states that gold was introduced as a detrital clastic material mobilised from the Archaean granite-greenstone terrane after burial (Muntean *et al*., 2005; Tucker et al., 2016; Nwaila *et al*., 2021). The nature, texture, mineralogical zoning, host rock composition, gold grain shape, and distribution of gold throughout the basin are used as evidence to suggest the origin and concentration of gold by Phillips and Law (2000), Muntean *et al*. (2005), Tucker *et al*. (2016), Nwaila *et al*. (2021), and references therein. Although the formation of gold is a fascinating subject, it lies beyond the scope of this study. This study focuses on adapting and applying a geostatistical method to quantify uncertainty in mineral resource estimation.

Most of the Witwatersrand gold is confined to fluvial conglomerates, pebble arenites, and quartz arenites with minor amounts hosted in carbon-rich kerogen seams (Frimmel, 2019). The gold within the Witwatersrand Basin occurs in different textures such as: (1) minute inclusions in porous, laminated euhedral pyrite; (2) associated with bitumen and chlorite; (3) within carbon-rich kerogen seams; and as (4) discrete toroidal to spheroid-shaped micro-nuggets (Frimmel, 2014; de Costa *et al*., 2020).

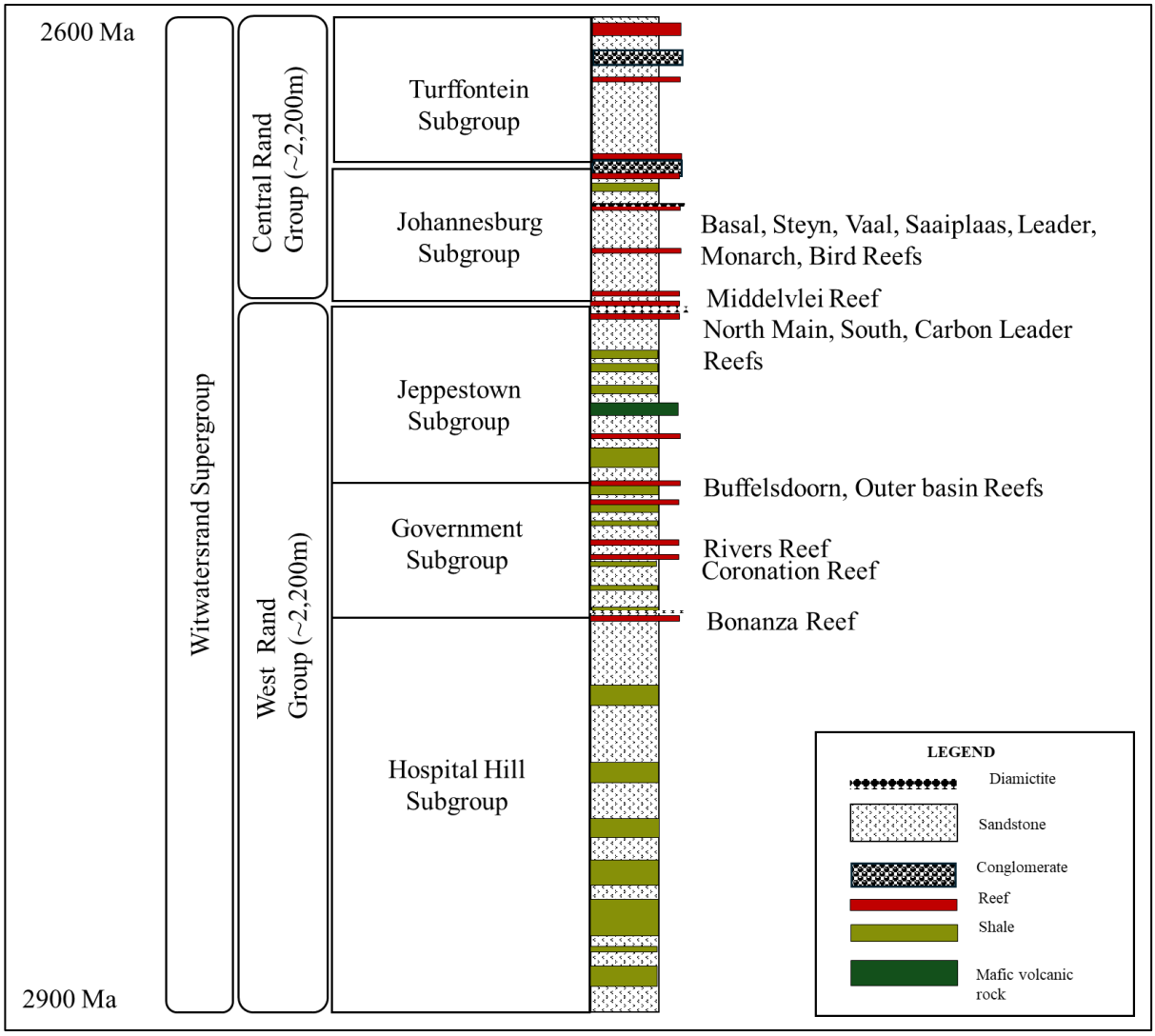


Figure 2.2: A generalised stratigraphic column of the Witwatersrand Supergroup showing the stratigraphic position of different reefs. The thickness of the stratigraphic sequence is not to scale. Figure adapted from Frimmel (2014).

2.2. Geology of the Middelvlei Reef

The Witwatersrand Basin hosts nine major goldfields distributed along the edge of the basin (Tucker *et al.,* 2016; Letaba, 2020). The Middlevlei Reef, located in the Carletonville Goldfield, stratigraphically within the Main Conglomerate Formation of the Johannesburg Subgroup (Fig. 2.2), will be the focus of this study.

The approximately 7 m thick Middelvlei Reef, consisting of massive conglomerate beds, is a gold palaeoplacer deposit which is found near the base of the Central Rand Group (Els, 1988, 1993). The Middelvlei Reef contains quartz- and pyrite-rich matrix, which hosts interbedded sandstones and oligomictic, auriferous conglomerates (Letanta, 2020). Three depositional systems are used to characterise the Middelvlei Reef: (1) the Footwall Sequence, composed predominantly of trough-bedded sandstones, lag conglomerates, and thin siltstone beds and laminae; (2) the Middelvlei Sequence, which contains interbedded quartz-pebble conglomerates, quartz wackes and thin siltstone; and (3) the Hanging Wall Sequence, composed of trough cross-bedded quartz wackes which typically rest upon conglomerates (Jolly, 1984). The sedimentological characterisation of the Middelvlei Reef by Els and Beukes (1987) led to the conclusion that it is fluvial in origin and was deposited in a braided stream environment. The Middelvlei Reef is affected by two sets of normal faulting and intrusive dykes that follow the strike of the faults (Jolly, 1984; Els, 1987).

Areas of high gold concentration within Middelvlei Reef at the Driefontein Mine were investigated by Jolly (1984). To locate these areas, Jolly (1984) built depositional models using sedimentological and stratigraphical descriptions. From the study, Jolly (1984) recognised nine lithofacies: six major (*viz.,* clast-supported conglomerate, matrix-supported conglomerate, thin single pebble beds, mixed massive sandstone, flat-bedded sandstone, and planar cross-stratified sandstones) and three minor lithofacies (*viz.,* ripple cross-laminated sandstone, scour fill sandstone, and siltstone lamina) based on composition and sedimentological structures. An assessment of the grain size, composition, conglomerate thickness, and proportion in the reef resulted in further categorisation into two lithofacies assemblages (Fig. 2.3):

- Type A lithofacies assemblage: dominated by conglomerates and clast- or matrix-supported basal units, thicknesses greater than 32cm. The type A lithofacies consists of thin lag pebble beds overlain by clast-supported conglomerates.
- Type B lithofacies assemblage consists of thin pebble matrix- or clast-supported conglomerates overlying scour-and-fill sandstone. The basal reef is less than 32 cm thick.

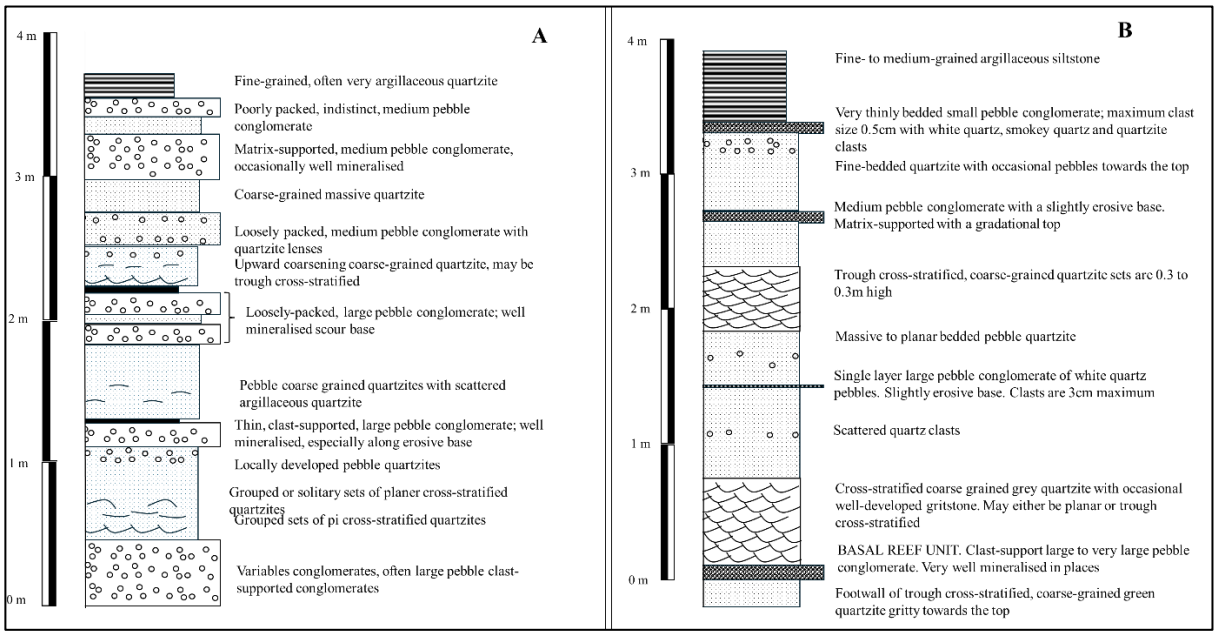


Figure 2.3: Generalised stratigraphy for Type A (insert A) and Type B (insert B) lithofacies assemblages. Adapted from Krige (1951).

3. GEOSTATISTICAL METHODS OF RESOURCE ESTIMATION

This chapter presents the theoretical background on the various geostatistical methods relevant to this study, their applications, and the advantages and disadvantages of their use. Geostatistics is a spatial interpolation method used extensively in resource and reserve estimation to describe the relationship between sampled and unsampled locations within a region (Daya and Bejari, 2014; Oliver and Webster, 2015). Geostatistics is also used to determine the spatial variation of a variable in space through kriging methods (Delbari *et al*., 2009). The use of geostatistics in resource estimation is advantageous as it provides a measure of accuracy of its estimates and can be used to determine the optimal sampling pattern (Mpanza, 2015). Geostatistics aims to incorporate spatial correlation between variables, as described by the semi-variogram, into an estimation process.

Estimation methods can be broadly categorised into two types: linear and non-linear methods. The key characteristic of linear methods, such as Ordinary Kriging, Simple Kriging, and Inverse Distance Weighting, is that the estimated value is a linear combination of known values determined by assigning weights to surrounding sampled data points (Choudhury, 2015). These weights are usually based on the spatial configuration and distance between the sampled and unsampled locations (Coombes, 2008).

Non-linear estimation methods such as Artificial Neural Networks, Random Forests, and Support Vector Machine are typically data-driven and are used when the relationship between variables is complex, not adequately captured by linear models and do not rely directly on spatial location in a linear fashion (Choudhury, 2015). Instead, they compute the relationship between a set of independent variables and the dependent variable through non-linear models (Glacken and Snowden, 2001).

The following subsections outline common linear estimation methods applied to Witwatersrand gold and similar deposits. Inverse distance weighting and nearest neighbour interpolation methods are benchmarks, as ordinary kriging is the preferred method for estimation.

3.1. Inverse Distance Weighting

Inverse distance weighting is a linear interpolation method that aims to determine the value of a variable at an unsampled location by evaluating the relationship between sampled and unsampled locations (Li and Heap, 2014). The inverse distance weighting method assumes that the sampled location's influence on an unsampled location's estimate diminishes as the distance between these samples increases (Coombes, 2008). Accordingly, samples closer to the sampled location are given greater weight compared to samples that are further from the sampled location (Coombes, 2008; Letanta, 2020). When the power of the inverse distance weighting is increased, the closer sample receives more emphasis, resulting in a detailed contour. The common formula used to determine inverse distance weighting is:

$$\lambda_i = \frac{d_{ij}^{-P}}{\sum_{i=1}^{n} d_{ij}^{-P}},$$

Equation 3.1: Inverse distance weighting

where P is the weighted power, d_{ij} is the distance between the grid node, i, and the neighbouring points, j, and λ_i is the weight of the observation points. Once the relative influence of each sample point around the unsampled location has been determined, the estimated value at the unsampled location is computed using the equation:

$$Z(X_0) = \sum_{i=1}^{n} \lambda_i Z(X_i)$$

Equation 3.2: Inverse distance weighting estimates

where X_0 is the estimated value at the unsampled location and $Z(x_i)$ is the true value at the sampled location.

The value of the weighted power can be chosen based on the variogram, where a low nugget effect indicates good reproducibility and a high nugget effect suggests poor reproducibility; hence, the use of a low power for inverse distance weighting (Coombes, 2008). Unlike kriging, inverse distance weighting does not minimise the estimation variance and is not subject to conditions such as providing the best estimate possible by a linear combination of the available weighted data and minimising the error variance of the estimate (Mpanza, 2015). However, the weighted power is an arbitrary value chosen at the discretion of the competent person, where a lower power results in smoother estimates (Glacken and Snowden, 2001).

Inverse distance weighting is an exact interpolator, meaning the estimated values at sampled points are equal to the true values, ensuring consistency with the underlying data (Liu *et al*., 2021). The disadvantages of inverse distance weighting are that it is dependent on the choice of the inverse power, where the quality of interpolation decreases if the sample distribution is uneven, and maximum and minimum interpolation values can only occur at sample data points (O'Donohue, 2023). Inverse distance weighting assumes that the variables being estimated are uniformly distributed and tends to perform poorly in areas with clustered or unevenly distributed data (Liu *et al*., 2021; Ohlert *et al*., 2023). Inverse distance does not provide an assessment of the error from an estimate, making it unsuitable for this study (Li and Heap, 2014).

3.2. Nearest Neighbour Interpolation

Nearest neighbour interpolation is a linear spatial estimation technique that assigns the value of an unsampled location to that of its nearest sampled point (Coombes, 2008). The

method is parameter-free, computationally efficient, and easy to implement, making it suitable for spatial datasets with irregular sampling distributions (Etherington, 2020; Holbert, 2023). A key advantage is that it preserves the original sampled values without introducing smoothing or modification, but a disadvantage is that it produces blocky and discontinuous surfaces that may misrepresent natural spatial variability (Burrough and McDonnell, 1998; Li and Heap, 2014). Mathematically, the estimated value of a variable at an unsampled location x_0 can be expressed as:

$$Z(X_0) = Z(X_i),$$

Equation 3.3: Nearest neighbour interpolation

where $Z(X_0)$ is the estimated value of the variable at x_0 and $Z(X_i)$ is the observed value at the nearest sampled location.

The most common application of nearest neighbour interpolation is through the use of Thiessen polygons, also known as Voronoi diagrams. The polygons allow us to estimate an unsampled location by constructing polygons around the region of interest such that each polygon contains one sample point and then assigning the value of the sampled point closest to the polygon to the unsampled location as an estimate (Fig. 3.1) (Brus *et al*., 1996; Hartkamp *et al.,* 1999).

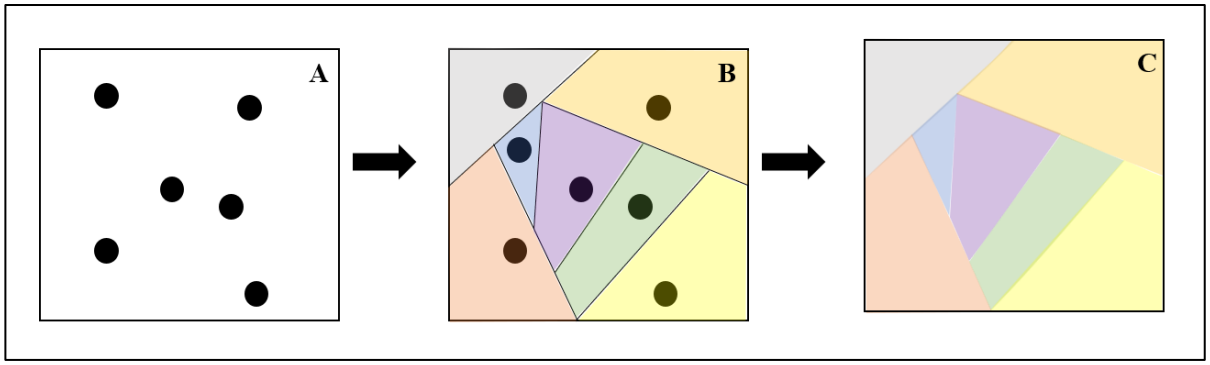


Figure 3.1: A diagram depicting how Thiessen polygons are used to obtain estimates through nearest neighbour interpolation. The black dots represent sampled locations. Insert A shows the area to be estimated; insert B shows how Thiessen polygons are created around sampled locations, and insert C shows the final estimates as a result of partitioning the region of interest.

3.3. Kriging

Kriging is a term used to describe a spatial interpolation method that is employed to obtain the best, minimum variance estimates at a location using the least-squares regression method (Mpanza, 2015). Kriging uses the spatial correlation between data, through the variogram function, to assume the relationship between sampled and unsampled locations (Daya and Bejari, 2015; Ibrahim and Nasser, 2017; Letanta, 2020). The basic equation for kriging is:

$$Z(X_0) = \sum_{i=1}^{n} \lambda_i \cdot Z(X_i),$$

Equation 3.4: Basic equation for kriging

where $Z(X_0)$ is the variable being estimated, n is the number of observation points in an area, $Z(X_i)$ are values of scattered observation points around the variable being estimated, and λ_i are the weights based on the variogram model.

There are two common kriging techniques whose results are influenced by the spatial distribution of the variable being estimated: simple and ordinary kriging (Mpanza, 2015). The

simple kriging estimation method aims to minimise variance between sampled and unsampled locations by using the average value of the variable being estimated to produce a smooth result (Daya and Bejari, 2015; Bai and Tahmasebi, 2022). Simple kriging assumes that there is variation in the variable being estimated and that the data has a constant average throughout the region of interest (Mpanza, 2015; de Smith *et al.,* 2021). The following equation is used to estimate unknown points using simple kriging:

$$Z(X_0) = m(1 - \sum_{i=1}^{N} \lambda_i) + \sum_{i=1}^{N} \lambda_i \cdot Z(X_i),$$

Equation 3.5: Simple kriging

where m is the weight of the regional mean.

Ordinary kriging estimates the local constant mean at an unsampled location by using the local search window's mean (Daya and Bejari, 2015). Ordinary kriging assumes that the regionalised variables are stationary, the average value of the variable being estimated is unknown, and that the weights of values sum up to one. Since there is a constraint that the sum of weights must be one, there is a need to ensure the optimisation of weights by using the Lagrange multiplier as a factor to balance the weights such that they are one (Mpanza, 2015). To avoid bias in ordinary kriged estimates, a high data density is required. Estimation of variables through ordinary kriging is achieved through the following equation:

$$Z(X_0) = \sum_{i=1}^{N} \lambda_i \cdot Z(X_i)$$

Equation 3.6: Ordinary kriging

The effectiveness of the kriging system in producing reliable weights in kriging depends on: (1) the kriging type, (2) the quantity of samples at each location; (3) spatial location of the samples within a deposit; (4) distance between samples and the point or block being estimated;

and (5) spatial continuity of the variable considered (Deustch *et al*., 2014; Mpanza, 2015). The use of kriging in mineral resource estimation may result in conditional bias. To address the conditional bias that results from ordinary kriging, increased block sizes can be employed in simple kriging. However, increasing block sizes may lead to an overly smoothed representation of the variable being estimated (Nwaila *et al*., 2021)

3.3.1. Variography

Variography is the analysis of grade continuity by comparing samples according to the distance and orientation between them (*e.g*., Fig. 3.2) (Coombes, 2008). A variogram is a graph that describes the distance and orientation at which samples correlate to one another (Mpanza, 2015). According to Emery *et al.* (2006) and Coombes (2008), variogram analysis assumes that samples are representative of the dataset; hence, (1) data integrity, (2) geological context and domains, as well as (3) statistical analysis, should be considered. This is because (1) incorrect application of data will affect the nugget effect (Fig. 3.2) (which is the difference between samples adjacent to each other) and the perceived grade continuity; (2) understanding the geological context, including structural elements or various phases of mineralisation provides an assessment of grade continuity; and (3) understanding the variability within and between domains helps govern expectations of the dataset when comparing samples.

The nature and distribution of the mineral deposits determine which variogram type will be used to characterise spatial continuity (Mpanza, 2015). For accurate characterisation of the spatial structure, it is necessary to perform individual analysis in multiple azimuth directions to identify and manage anisotropy in the data (Daya and Bejari, 2014). The process of variogram construction begins by calculating the semi-variance values for increasing lag distances between sample pairs, which are then plotted on experimental semi-variograms (Mpanza,

2015). Once the experimental variograms are established, theoretical models are used to capture the underlying structure and parameters such as the nugget, sill, and range, as guided by spatial continuity (Kim and Deutsch, 2022). The azimuth directions with a long range are considered major directions of continuity and will be used in the estimation model (Goovaerts, 1997).

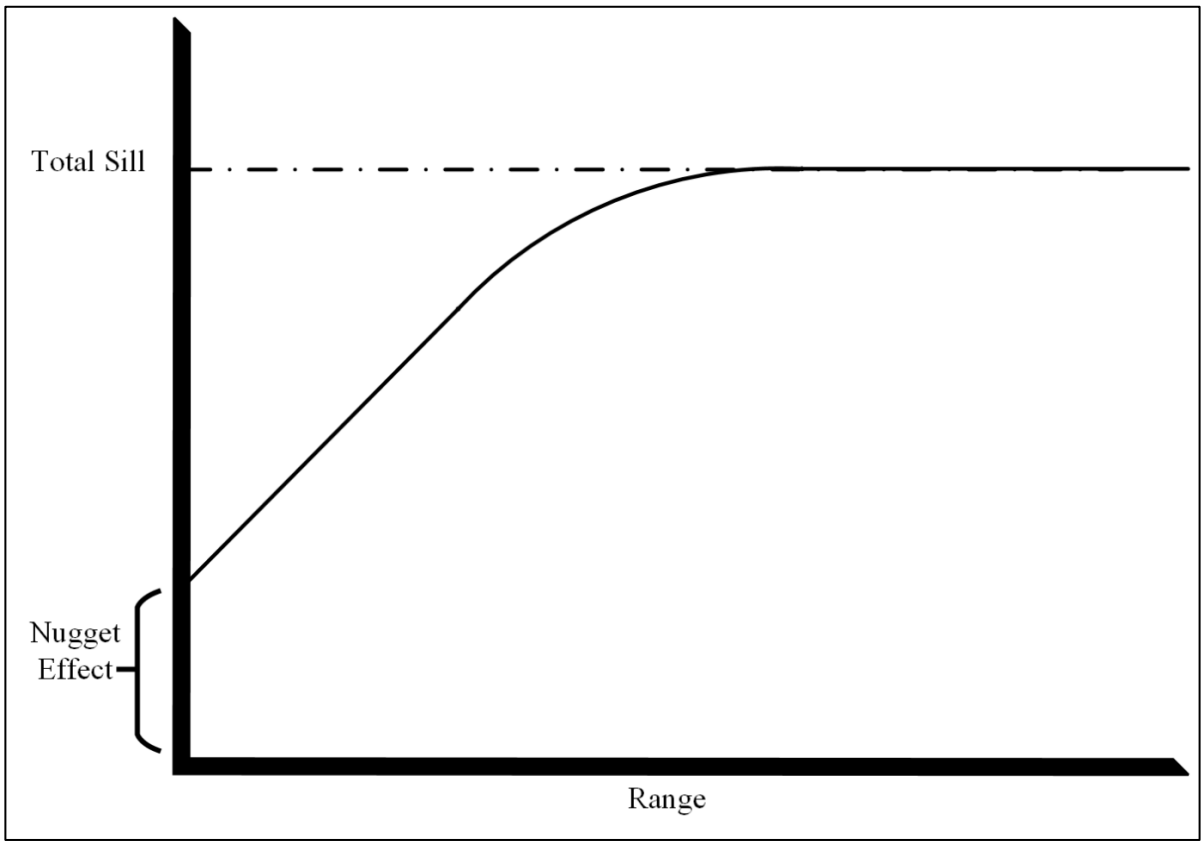


Figure 3.2: A graph showing terms used in variography: a sill, range, and nugget effect.

3.3.2. Search parameters

To accelerate the estimation process, a maximum limit on the number of samples required for ore grade estimation at any point is calculated (Coombes, 2008). The limit on the number of samples is known as the search neighbourhood. The search neighbourhood is

defined by a search radius, *R*, and the number of drill holes, n_{dh}, (Silva and Boisvert, 2014), and it is calculated through the equation:

$$Search\ Neighbourhood: R(2/n_{dh})^{\frac{1}{2}}$$

Equation 3.7: Search neighbourhood

The decision on search parameters is dependent on results from variography and includes a maximum range around the location being estimated, the number of samples to be used, and the maximum number of samples that can be used in estimation (Deustch *et al.,* 2014). Ideal search parameters decrease the mean root square error, increase the kriging efficiency and slope of regression, and decrease the conditional bias (Coombes, 2008). The following should be considered when selecting estimation parameters: geological domains, block sizes, discretisation, search ellipsoids, minimum and maximum number of samples, and samples per drillhole (Coombes, 2008).

3.3.3. Smallest mining unit criteria

The smallest mining unit refers to the minimum support upon which decisions on mining equipment size, mining method, direction of mining and the depositional environment, amongst other factors, can be made (Leuangthong *et al*., 2004). The smallest mining unit is usually smaller than the sampling grid dimensions (Choudhury, 2015). The choice of the smallest mining unit affects the variability observed within the estimates (Dominy *et al.*, 2002). An estimation block size, which is different from the smallest mining unit, is a grid support that minimises estimation variance and the spatial correlation structure (Leuangthong *et al*., 2004). The smallest mining unit thus reflects operational constraints while the estimation block size addresses statistical precision (Jara *et al*., 2006).

Direct estimation at the smallest mining unit scale often produces unstable or biased results when drillhole spacing is greater than the smallest mining unit, since sparse sampling cannot capture local grade variability (Fonseca *et al*., 2021). The bias may be a result of the low variability in sample grades and sparsely spaced data (Mudau, 2014). The use of small estimation blocks is generally suitable for global resource models, as small block size models are intended to guide mine planning since large block models are not useful for extraction-level planning (Hundelshaussen *et al.,* 2018). Consequently, the block sizes must be adjusted during mineral resource estimation such that they reflect the smallest mining unit (Emery *et al*., 2006). Practitioners therefore reconcile the discrepancy by estimating on larger, statistically robust estimation blocks and then deriving the smallest mining unit-scale information via change-of-support techniques, conditional simulation, proportion or indicator methods, or by staged grade-control sampling, prior to production (Hekmat *et al*., 2011).

3.3.4. Kriging neighbourhood analysis

The optimisation of key features such as (1) block size, (2) minimum and maximum sample numbers, (3) search range, and (4) discretion points to minimise conditional bias and over-smoothing is known as kriging neighbourhood analysis (Mandava *et al*., 2016; Amwaama, 2018; Letanta, 2020). Kriging neighbourhood analysis seeks to optimise the search neighbourhood by minimising errors between true and estimated values through a quantitative analysis of kriging efficiency or slope of regression while accounting for support-volume considerations (Hundelshaussen *et al*., 2018; Sunday and Deutsch, 2020).

Kriging neighbourhood analysis can be conducted on a single (global) or customised (local) neighbourhood, but recent studies have shown that the local neighbourhood approach produces better outcomes as compared to the global neighbourhood approach (Fonseca *et al.*, 2021). To determine search neighbourhoods, the following are considered: (1) weight of

the mean for kriging and slope of regression; (2) number of samples required for estimation and their usability; and (3) the distribution of kriging weights and kriging variance (Amwaama, 2018). The definition of the search neighbourhood can have a significant impact on the outcome of the kriging estimate (Khakestar *et al.,* 2013). The best estimation parameters are achieved by selecting the block sizes that maximise kriging efficiency and slope of regression through kriging neighbourhood analysis (Coombes, 2008).

3.3.5. Kriging cross-validation

Validation of mineral resource estimates is an essential step to ensure that geostatistical models are reliable. The comparison between kriged values and true values to evaluate prediction accuracy is known as cross-validation (Bardossy, 2017). Cross-validation allows for a comparison of estimated and true values using information available in the dataset, giving users the ability to examine and reformulate models to better utilise the data (Ortiz, 2006). Cross-validation can be used to detect outliers of the measurement value and to find the most suitable model, but it does not provide a definitive measure of the goodness of an estimation method (Camana and Deutsch, 2019). In typical practice, the root mean-square error, which is used to measure the difference between the actual values and those predicted by the model, is used to measure the difference between estimated and true values through the equation:

$$RMSE = \sqrt{1/n \sum_{i=1}^{n} (z^*(x_i) - Z(x_i)^2)}$$

Equation 3.8: Root mean-square error

Diagnostic measures such as mean error, mean squared error, and slope of regression are assessed to evaluate the adequacy of variogram models and kriging parameters (Boyle,

2010; Deustch *et al*., 2014). Local validation techniques, such as swath or trend plots, evaluate spatial alignment between samples and estimates along key directions, highlighting local bias or smoothing effect (Vann *et al*., 2003). While effective for assessing internal model consistency, cross-validation does not directly evaluate broader spatial patterns or the overall representativeness of estimates (Dominy *et al*., 2002).

3.4. Geo-domaining

In resource estimation, a domain is a spatial volume where the geology is consistent, contains a single grade population and has a single orientation (Coombes, 2008). To ensure that models are accurate and useful for extraction guidance, the populations of interest are determined by considering the limits of each mineralisation population and understanding and defining domains before creating envelopes of the population (Coombes, 2008). This is because ore bodies are often complex, with variations in lithology, grade distribution, and structural features that necessitate the creation of distinct domains to reflect these heterogeneities (Gilday and Emsley, 2017). For this reason, the regional (genesis, lithology, domain, structural controls, weathering, mineralogy) and local (geological structures, weathering, relevant features) controls in the geology are considered when delineating geological boundaries (Zhang *et al.,* 2023). The purpose of building a domain is to restrict the use of sample data during estimation to ensure that only data relevant to the body is being estimated. Probabilistic definition of domains includes two main steps: (1) indicator probability maps for the probability of each block exceeding the chosen threshold value; and (2) grouping of blocks according to how their probability to exceed the threshold using a model that will fill the gaps between blocks (Emery *et al.*, 2006).

Domain boundaries are typically classified into hard, soft, and transitional types, each representing a unique approach to boundary definition and data integration (Zhang *et al.,* 2023). Hard domain boundaries are the most rigid and are typically defined by geological boundaries, such as lithological contacts, fault zones, and metallurgical test work (Gilday and Emsley, 2017). Soft domain boundaries are less rigid, often used where boundaries are yet to be confirmed, and can use data from adjacent domains to influence estimates (Zhang *et al.,* 2023). Soft domains are useful in situations where data density is insufficient to clearly define hard boundaries, as they allow for more robust interpolation in uncertain zones (Lindi *et al*., 2024). Transitional, or overlapping, domain boundaries are the most difficult to determine, exist along gradational contacts, and are common in deposits with complex ore systems or in the presence of faults and structural controls that cause a gradual change in grade of ore types (Atalay, 2025).

Abzalov and Humphreys (2002) investigated the effect of domaining on mineral resource estimates by using non-linear geostatistics on the structurally complex and discontinuous mesothermal gold deposit of the Tiriganiaq lode-gold deposit. The indicator probability model was used to subdivide gold lodes of the Tiriganiaq lode-gold deposit into geostatistically defined domains. This study's findings demonstrate that when domaining has not been applied to a deposit, ordinary kriged estimates will result in significant errors, which may result in grade smoothing, and that uniform conditioning allows for estimation of local resources at various smallest mining units that can be lower than the drilling density without bias or excessive smoothing of local values. This is because the structural complexity of the mineralised zones, together with the highly irregular distribution of the gold-bearing minerals, prevents unambiguous delineation of the mineralised domains by conventional deterministic contouring methodologies.

The literature on geostatistical resource estimation highlights the close integration between geological interpretation and statistical modelling. A consistent theme is the importance of creating estimation domains that respect geological boundaries, since failure to do so can introduce artificial continuity and bias into the estimates. Experimental variograms are constructed to capture spatial dependence, with attention given to the choice of directions and the identification of anisotropy, both of which strongly influence the fitted models. However, studies also emphasise the need to consider the limitations of kriging, particularly its reliance on the variogram model and sensitivity to data configuration. The chapter demonstrates that effective geostatistical estimation requires both geological insight and rigorous statistical modelling, with domains, variograms, and kriging forming the core methodological pillars.

4. MINERAL RESOURCE ESTIMATION AND UNCERTAINTY QUANTIFICATION

Mining is a primary source of raw materials and an integral part of South Africa's economy, as it substantially contributes to the sustainability and growth of the country's economy (Emery *et al*., 2006). Mineral resources and their subsequent conversion to mineral reserves are of key importance to mining companies within South Africa (Bosman, 2013), meaning the accuracy of resource estimation is important as investment and operational decisions must be made on relevant and reliable information. Consequently, mineral resource classification standards were designed to define rules for public disclosure of mineral projects following a series of technical studies on a deposit: scoping, pre-feasibility, and feasibility studies (Dominy *et al*., 2002). Reliable mineral resource estimates are essential for the day-to-day operation of a mine.

4.1. Mineral Resource Estimation

South Africa follows mineral resource estimation and reporting standards set out in the South African Code for Reporting of Mineral Resources and Mineral Reserves, commonly known as the SAMREC Code (2016). The code, which draws from the CRIRSCO-style reporting standard, sets out minimum standards, recommendations, and guidelines for public reporting of exploration results and mineral resource and reserve estimation (SAMREC, 2016). The SAMREC Code (2016) states that the estimation of mineral resources and reserves must be carried out by a competent person who possesses sufficient knowledge in the mineral resource being estimated. However, several factors, such as model selection and uncertainty quantification, are left to the discretion of the competent person (McManus *et al.,* 2021). This liberty to choose which method to use in resource estimation and uncertainty calculation usually results in variations between reports, and may imply that the information that the competent person did not consider relevant will not be disclosed (Owusu and Dagdelen, 2024).

The South African gold mining sector commonly employs geostatistical approaches to estimate gold reserves and resources and to aid in daily mine evaluation and planning (Mpanza, 2015; Letanta, 2020). Geostatistical methods are used to produce the best linear unbiased estimates of metal accumulation by incorporating geological interpretations and applying restrictions to mineralisation (Rezaee and Asghari, 2012). The confidence of grade estimates and mineralisation continuity in each model block size is dependent on (1) exploration drilling records, (2) survey accuracy, (3) sample density, (4) mineral assays, (5) underground observations, (6) geological continuity, and (7) grade continuity characteristics (Mandaav *et al*., 2016).

4.2. Geological and Geostatistical Uncertainty

There are two types of uncertainty in mineral resource estimation: geological and geostatistical uncertainty. Geological uncertainty arises from incomplete knowledge of the geometry, boundaries, lithological and structural continuity, and the distribution of mineralisation controls (Journel and Huijbregts, 1978; Sinclair and Blackwell, 2002; Shishvan and Benndorf, 2016). Geological uncertainty is strongly influenced by sampling density, drill-hole orientation, geological interpretation, depositional boundaries, sample selection, sample preparation and assaying, geological modelling error, and database construction errors, meaning it reflects conceptual and structural ambiguity (Dominy *et al*., 2002; Phoona *et al*., 2022). Geostatistical uncertainty is a result of the spatial variability of grade values within defined geological domains, selection and application of estimation methods, planned extraction methods, and the limitations of interpolation or simulation methods to capture variability (Goovaerts, 1997; Dominy *et al*., 2002). Geological and geostatistical uncertainty are interrelated because a misinterpretation of grades or geological domains directly propagates into geostatistical uncertainty, which may result in increased conditional bias or smoothing (Phoona *et al*., 2022).

A key assumption of both geological and geostatistical uncertainty is that the geological model and sample data are representative of the deposit (Randle *et al.,* 2019). Geological models incorporate geological, structural, and depositional knowledge but are interpretive, subjective, and non-unique as multiple geological models can explain the same dataset, making geological uncertainties difficult to quantify (Dominy *et al*., 2002; Rezaee and Asghari, 2012). Geostatistical uncertainty, however, is quantifiable, reproducible, and based on formal statistical theory, enabling the calculation of estimation errors (Goovaerts, 1997). However, geostatistical uncertainty is sensitive to variogram modelling, sampling configuration, and parameter selection and does not capture uncertainty in geological interpretation or model misspecification (Dominy *et al*., 2002; Randle *et al*., 2019).

A range of methods can be used to quantify uncertainty. Geological uncertainty can be quantified using stochastic geological modelling, multiple-point geostatistics, and boundary simulation to capture the variability of alternative interpretations (Phoona *et al*., 2022). Geostatistical uncertainty can be quantified using kriging variance, conditional simulation, cross-validation statistics, and confidence intervals derived from estimation distributions (Emery *et al*., 2006; McManus *et al.,* 2021). However, this study will focus on geostatistical uncertainty quantified using kriging variance and confidence intervals.

Kriging variance was adopted because it directly reflects sample configuration and spatial continuity as defined by the variogram, while confidence intervals complement kriging variance by introducing a probabilistic perspective on estimate reliability, highlighting zones of high and low confidence (Shishvan and Benndorf, 2016; Frost, 2020). Confidence intervals mitigate some of the weaknesses of relying solely on kriging variance by providing a distributional range of estimates (Emery *et al*., 2006; Lindi *et al.*, 2024). The absence of

stochastic simulations or geological model alternatives means that structural uncertainty is not explicitly assessed (Emery *et al*., 2006). Omitting alternative approaches such as multiple realisation simulations or explicit geological uncertainty quantification narrows the scope of the uncertainty analysis (Delbari *et al*., 2009). However, this limitation is mitigated by adopting a conservative interpretation of uncertainty outputs, using uncertainty maps to flag zones requiring additional sampling, and situating classification outcomes within the broader context of data quality and geological knowledge.

4.3. Geostatistical Uncertainty Quantification

Kriged estimates at each location have an estimation error, which should be quantified and accounted for in decision-making. According to Coombes (2008), the uncertainty associated with kriging is related to sample configuration and computational efficiency. Mineral resource classification is a key step in mineral resource estimation, as capital investment decisions are influenced by the confidence level displayed in the mineral resources and reserves (Bosman, 2013). There are various methods applied to quantify uncertainty, some more preferred than others. The methods are categorised into geometric and geostatistical methods, where geometric methods consider the quantity, proximity, and location of data available for block estimation, while geostatistical methods quantify uncertainty on a given production period (Owusu and Dagdelen, 2019). Although there are no standard procedures for categorising mineral resource estimates, geostatistical methods have been preferred over the years because they consider the spatial continuity of the data in characterising uncertainty (Dohm, 2005).

Confidence in mineral resource and reserve estimation is affected by (1) the reliability of the geological model, (2) spatial continuity and variability of the deposit, (3) quality and configuration of the sample data, and (4) the evaluation of the method's reliability (Dominy *et al*., 2002; Dohm, 2005). Although quantitative methods of expressing uncertainty are uncommon, there are ways that uncertainty can be further interpreted to provide a realistic measure of project viability (McManus *et al*., 2021). The following paragraphs outline the methods that can be used to quantify and account for the uncertainty of kriged estimates and measure the goodness of fit to evaluate the appropriateness of the parameters used for estimation (Coombes, 2008).

4.3.1. Kriging variance

Kriging variance is the minimised mean square error (Deustch *et al*., 2014). Kriging variance accounts for the uncertainty associated with the neighbouring data and for the spatial variability described by the variogram and the sampling grid configuration of the block being estimated (Coombes, 2000; Dohm, 2005; Emery *et al.,* 2006; Letanta, 2020). Kriging variance is dependent on variogram parameters but independent of true values, making it a useful tool for mineral resource classification (Emery *et al*., 2006; Silva and Boisvert, 2014). The kriging variance is calculated independently of the actual estimates as the difference between the weighted sum of the true grades and the estimation block (Dohm, 2005). The following formulas can be used to determine the kriging variances using the two common kriging methods:

$$\sigma_{SK}^2 = C\ (V,V) - \sum \lambda_i' \cdot C \cdot (\ x_i, V)$$

Equation 4.1: Simple kriging variance

for simple kriging estimates, while the kriging variance for the ordinary kriging estimates is:

$$\sigma_{OK}^2 = \sum \lambda_i \cdot \gamma(x_i, V) - \gamma\,(V, V) + \mu,$$

Equation 4.2: Ordinary kriging variance

where λ_i are the weights based on the variogram, $\gamma(X_i, V)$ is the average variance between the point x_i and the volume V, $C\,(V, V)$ is the variance of the block V, $\gamma\,(V, V)$ is the average variogram between two points x and x' within the volume V and μ is the Lagrange multiplier.

The key advantage of using kriging variance as a classification criterion is its ability to account for the spatial structure of the feature and the redundancy between samples (Owusu and Dagdelen, 2019). However, kriging variance often results in classification with undesirable artifacts, particularly near sample locations, where patches of measured blocks may appear within indicated zones (Silva & Bossert, 2014). Since kriging variance remains unchanged regardless of data values, it does not account for the proportional effect; a significant limitation when dealing with the highly skewed distributions typical in the mining industry (Phoona et al., 2002; Lindi *et al*., 2024).

The kriging variance approach for mineral resource classification incorporates geostatistical parameters that integrate both geometric and geological inputs to characterise the uncertainty associated with estimation parameters (Owusu and Dagdelen, 2019). Measured mineral resources are associated with lower kriging variance values, indicating higher confidence, whereas indicated resources have higher kriging variance and reduced confidence (Emery *et al.,* 2006). Blocks extrapolated beyond the variogram's range of influence are classified as inferred resources (Dohm, 2005).

4.3.2. Kriging efficiency

Kriging efficiency, a scaled estimate that does not exceed one, is a measure of the relationship between kriged estimates and true values (Amwaama, 2018; Letanta, 2020). A negative kriging efficiency value indicates a weak relationship between kriged estimates and true block values, while high kriging efficiency values indicate that the variance between kriged estimates and true block values is almost equal (Coombes, 2008; Amwaama, 2018). The equation used to calculate the kriging efficiency is:

$$Kriging\ efficiency = \frac{\sigma_B^2 - \sigma_K^2}{\sigma_B^2},$$

Equation 4.3: Kriging efficiency

where σ_B^2 is the block variance, and σ_K^2 is the kriging variance.

An evaluation of a model's kriging efficiency provides an indication of the degree of accuracy in the estimate (Coombes, 2008). Kriging efficiency can be used to assess the conditional bias, goodness of fit, and departure from theoretical optimality of estimates (Deustch *et al.,* 2014). If the kriged variance is greater than the true block variance, the kriging efficiency will be negative (Barboza and Deutsch, 2024). A high kriging efficiency means that the kriging variance is low and the variance of the block estimates is approximately equal to the variance of the true block estimates (Deustch *et al*., 2014).

4.3.3. Kriging slope of regression

The slope of regression is a measure of the degree of conditional bias on estimates, and it depends on the Lagrange multiplier, block variance, and kriging variance (Letanta, 2020; Fonseca *et al*., 2021). The slope of regression value is used as a diagnostic for conditional bias against the true sample grades (Deustch *et al*., 2014). The slope of regression can only

be between zero and one, where values further from one indicate conditional bias (Nwaila *et al*., 2021). The slope of regression for simple kriging estimates is exactly one, and ordinary kriged estimates are conditionally biased unless the slope of regression is equal to one (Deustch *et al*., 2014). The slope of regression values are calculated using the equation:

$$Slope\ of\ regression = \frac{\sigma_B^2 - \sigma_K^2 + \mu}{\sigma_B^2 - \sigma_K^2 + 2\mu}$$

Equation 4.4: Kriging slope of regression

4.3.4. Conditional simulation

Conditional simulation is a non-linear statistical method used to classify mineral resources based on local uncertainty, confidence levels, and confidence associated with production volumes (Emery *et al.,* 2006; Dominy *et al.,* 2002). Conditional simulation models are often employed as a complementary approach to ordinary kriging and are widely used to evaluate the risk associated with mining decisions (Nwaila *et al.,* 2021). Conditional simulation allows for the testing of different realisations of the same model while measuring the range of impact of grade variability (Glacken and Snowden, 2001; Coombes, 2008). In addition to overcoming the smoothing effect that results from kriging approaches, conditional simulation models create a more accurate representation of variability as described by the variogram, thereby increasing confidence in the kriging estimates and improving grade distribution across a variety of cut-off grades (Delbari *et al.,* 2009; Nwaila *et al*., 2021; Bai and Tahmasebi, 2022).

The range of grade and tonnage outcomes derived from conditional simulation can be used to quantify and report the risk in resource estimates for different cut-off grades, block sizes, or mine layouts across various mining periods (Dominy *et al.*, 2002). The variation among realisations from conditional simulation provides a quantitative measure of spatial

uncertainty in estimates (Delbari *et al.*, 2009). Compared to kriging variance and other validation techniques, conditional simulation is considered a more effective approach for assessing uncertainty (Dominy *et al*., 2002; Delbari *et al*., 2009; Silva and Boisvert, 2014). However, a key limitation of using conditional simulation to assess uncertainty is that classification results are highly sensitive to the chosen estimation parameters, potentially reducing transparency in resource disclosure for investors (Silva and Boisvert, 2014). Conditional simulation is an alternative to generating some measure of grade variability on a local scale and can be used to evaluate the risk associated with variability in estimated grades and to quantify risk classification (Coombes, 2008).

4.3.5. Confidence intervals

A confidence interval is a range of values, calculated from sample data, that is expected to contain the true population parameter a specified proportion of the time if the sampling process were repeated many times (Holbert, 2023b). For example, a 95% confidence interval for a grade mean represents the probability that if sampling were to be undertaken in the same conditions, 95% of the constructed intervals would contain the true mean (Davies and Crombie, 2009). Confidence intervals quantify the level of uncertainty within a deposit, serve as a statistical measure of the reliability of estimated values, and are essential for the classification of mineral resources (Owusu and Dagdelen, 2019). The calculation of confidence intervals requires consideration of key factors such as the quantity and spatial configuration of neighbourhood data as well as the spatial continuity of estimated grades, typically measured using the variogram (Rezaee and Asghari, 2012).

Associated with a confidence interval is a confidence level. A confidence level is the probability that a series of confidence intervals will contain the true value of the population

parameter, where a wide confidence interval implies a larger margin of error, and therefore, an imprecise estimate that results from an extensive range (Frost, 2020). According to Hespanol *et al*. (2019) and Frost (2020), confidence intervals depend on sample size, sample variability, and confidence level (a methodology independent of sample characteristics), where larger sample sizes result in a narrower confidence interval and high sample variability increases the confidence interval.

Understanding confidence intervals is critical as they define a range within which the true value of a variable is likely to lie, thereby reflecting the uncertainty in sample estimates (Davies and Crombie, 2009). A widely accepted industry practice for mineral resource classification based on confidence intervals is ensuring that the estimated metal content falls within ±15% relative precision at a 90% confidence level (Owusu and Dagdelen, 2019; Rezaee and Asghari, 2012). Different studies apply varying confidence levels to categorise mineral resource estimates as inferred, indicated, or measured, reflecting the level of certainty in the estimation process.

4.4. Mineral Resource Classification Using Uncertainty

Mineral resources are classified based on increasing geological knowledge and certainty (e.g., Fig. 1.1). The classification of mineral resources is dependent on the search neighbourhood, kriging variance, and conditional variance (Emery *et al.,* 2006; Lindi *et al*., 2024). Coombes (2008) used the following descriptions to differentiate between measured, indicated, and inferred mineral resources:

- Measured mineral resources are the highest confidence category and describe the portion of the resource that is exhaustively drilled, has a high quality in sample collection, assaying, logging, and surveying, with sufficient evidence to support both interpreted controls and spatial estimates of mineralisation.

- Indicated mineral resource typically refers to the portion of the resource model that lacks data, information, and/or quality for a few criteria
- Inferred mineral resources refers to the portion of a resource model that falls short of being classified as an indicated mineral resource

McManus *et al.* (2021) conducted an empirical study of 142 Australian Securities Exchange reports submitted to the Joint Ore Reserves Committee (JORC) 2012 in the year 2020. The aim was to assess how many of these reports contained uncertainty assessments and, in cases where it was measured, assess how it was reported. A review of these reports indicates that the basis of mineral resource classification for each mineral resource was variable and dependent on several factors such as mineralisation style, methodology used in mineral resource and reserve estimation, and the experience of the competent person. Not all the reports contained uncertainty measurements, and this led to the use of vague words such as “well documented and understood”, “acceptable”, “satisfactory”, and “adequate” used to communicate the quality, and therefore uncertainty, of these assessments.

Although kriging variance does not measure the error between true values and kriged estimates but rather reflects the geometry of sample distribution and the spatial continuity defined by the variogram model, kriging variance’s computational efficiency and direct link to kriging parameters make it a widely adopted tool in resource classification schemes, such as distinguishing measured, indicated, and inferred resources (Emery *et al*., 2006; Silva and Boisvert, 2014). To address kriging variance limitations, confidence intervals were calculated as an additional measure of uncertainty. Unlike kriging variance, confidence intervals are sensitive to both spatial continuity and the underlying grade distribution, making them a more representative measure of uncertainty in resource estimates (Holbert, 2023b). Confidence

intervals strengthen the uncertainty analysis by explicitly quantifying grade variability and producing ranges that are directly interpretable in the context of resource confidence and mine planning (Frost, 2020). The integration of both approaches ensures that uncertainty is not underestimated and supports more reliable, risk-informed decision-making in mineral resource evaluation.

Dominy *et al*. (2002) conducted a study on potential sources of error that may occur during mineral resource estimation, with emphasis on the quality of data and continuous management improvement. Dominy *et al*. (2002) suggested potential precision levels for mineral resources and reserves at a 90% confidence level that may be used for mineral resource classification (Table 4.1). However, a widely used mineral resource classification criterion based on confidence intervals is from Yamamoto (1999), as outlined in Table 4.2.

Table 4.1: Potential error levels at the 90% confidence level for mineral resource or reserve classification as suggested by Dominy *et al*. (2002).

Mineral Resources	Error
Measured	±10-15%
Indicated	±25-35%
Inferred	±35-100%

Table 4.2: Mineral resource classification criteria at 90% confidence level as proposed by Yamamoto (1999).

Mineral Resources	Error
Measured	0-20%
Indicated	20-50%
Inferred	>50%

This chapter underscores the importance of geological interpretation and geostatistical modelling in producing reliable resource models. A key theme across studies is that estimation should be conducted within geologically meaningful domains. Geostatistical uncertainty reflects the variability in grade estimates arising from data density, spatial continuity, and estimation parameters. Although the classification of mineral resources is dependent on geological interpretation and grade continuity, sound quality data is important in ensuring that non-flawed data is used in mineral resource classification.

5. STUDY AREA AND METHODOLOGY

This chapter summarises relevant information on the study area, the dataset, and the methodology used to obtain results.

5.1. Study Area and Dataset

This study was conducted using a legacy dataset that was collected between 1982 and 2017 by multi-generation mine geologists, within the Carletonville Goldfield's Driefontein Mining Complex. The geologists were associated with various gold mining companies, including, but not limited to, Goldfields, Sibanye Gold, and Sibanye Stillwater. The 19,531 data points were collected from underground mining stopes and raise line stratigraphic chip samples. It is assumed that QA/QC was carried out based on methods available at the time of analysis and that Au assay detection limits were greater than 0.1 g/t.

The data used in this study was received as comma delimited (.csv) files containing (1) the study area polygon; (2) structure polygons, which are a combination of dykes and faults; (3) contours; (4) lithofacies; and (5) Au (g/t) assays (Fig. 5.1). The following is assumed about the data: (1) data values are precise; (2) data values are accurate; (3) data values are random and independent; (4) samples are a small proportion of the population; and (5) all samples were collected from the same elevation. The study area has been subdivided into four geological domains at the discretion of the mine geologists at the time.

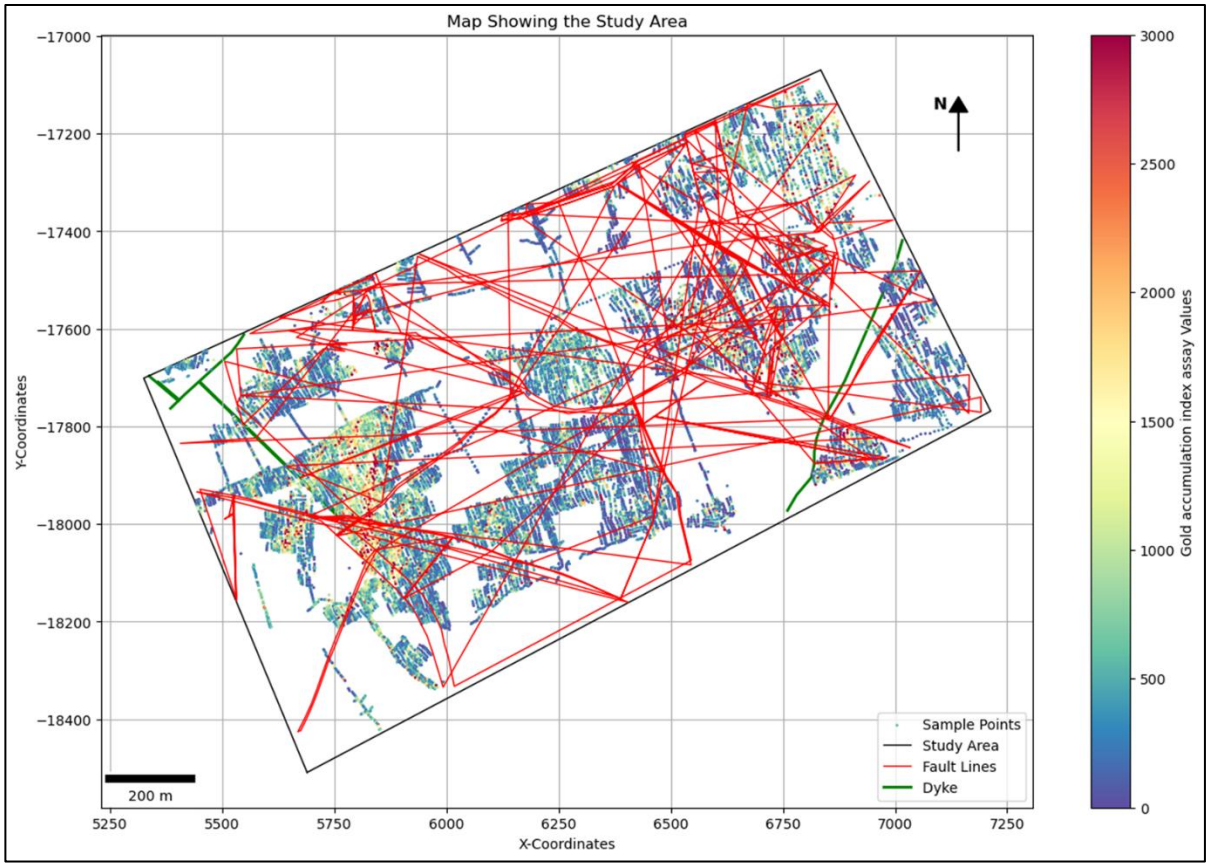


Figure 5.1: A map showing spatial locations of gold assay samples and their associated grades, as represented by the colour bar. The black polygon represents the study area. The red and green lines show faults and dykes, respectively.

5.2. Statistical Analysis

Statistical analysis was performed using data analysis and statistical libraries in Python. Statistical analysis begins with QA/QC of the data and is followed by exploratory data analysis. QA/QC and exploratory data analysis ensure that decisions on project value and progression are sound and that poor-quality data is not publicised (Coombes, 2008). QA/QC was achieved by assessing patterns and setting control limits through good statistical practice standards to ensure the use of non-erroneous data.

The following QA/QC steps were followed:

- Importing necessary Python and geostatistical libraries such as Matplotlib, NumPy and Seaborn
- Importing the dataset file that contains information on stratigraphic chip samples
- Deleting empty rows and columns
- Deleting points outside the study area
- Deleting rows that will not be required (e.g., sample name, sample type, date, z-value)

Following the above QA/QC steps, outliers were treated using z-score intervals, and the data was visualised using boxplots and histograms. Outliers were treated by removing values that are outside the 98% confidence interval (i.e., z-score values outside 2.58) through the formula:

$$z = \frac{(x - \mu)}{\sigma}$$

Equation 5.1: Formula for calculating z-score values

Z-scores assume that the data follows a bell-shaped distribution, and the cut-off would be misleading if the data is skewed, heavy-tailed or multi-modal in distribution (Montgomery and Runger, 2014). The treatment of outliers using a z-score of 2.58 is justified by the fact that mining data that may appear to be an outlier could represent true high-grade mineralisation rather than noise, and to ensure that the data is preserved to the fullest extent. The data was described using statistical properties such as central tendencies, skewness, and kurtosis to recognise distributions and spatial variability within the dataset. These statistical properties are detailed in section 6.1 of the results section. To visualise the distribution of the data before and after outlier treatment, understand the relationship between variables, and analyse patterns in

the dataset, results from exploratory data analysis were visualised using histograms, boxplots, pairwise plots, and heatmap plots.

5.3. Creating Geo-Domain Boundaries

To ensure that an acceptable resource estimation model is created, populations of interest that should be estimated are determined by considering the limits of each mineralisation population and understanding and defining domain populations before creating envelopes of the population (Coombes, 2008). The envelopes ensure that one population does not influence estimates of the adjacent population and vice versa. The study area has already been subdivided into populations considering the regional (e.g., genesis, lithology, domain, structural controls, weathering, mineralogy) and local (e.g., geological structures, weathering, relevant variables) geological controls. In this study, geo-domain boundaries were created around populations to control the influence of samples from one population on the adjacent population through machine learning algorithms. A more detailed account of the methodology used to create domain boundaries is presented in the results section.

5.4. Variography

Geostatistical analysis for kriging was performed using Geostatistical Libraries such as SciPy, GeostatsPy, and GeoPandas. First, the filtered estimation dataset was declustered and transformed into normal space to minimise bias caused by preferential sampling. From there, variogram maps were created to assess each variable’s general trend of continuity within each domain. For a clearer picture of mineralisation continuity, experimental semi-variogram graphs were modelled at 15° intervals, standardised to a distribution of 1. Experimental semi-variogram modelling was achieved through four critical steps: (1) preparation, (2) calculation, (3) modelling, and (4) interpretation.

The preparation stage involved cell declustering and normal score transformation of the estimation dataset to counteract dense and preferential sampling. The calculation step involved creating variogram maps to assess the mineral grade continuity and cyclicity within the study area. The modelling step involved creating experimental semi-variograms along a range of directions to assess the extent of sample influence. The final, and most important step is interpretation, where the experimental semi-variograms along the identified major and minor directions are automatically fitted with consideration of the range, nugget effect and sill contribution values. The following sub-sections detail the steps involved in variography.

5.4.1. Cell declustering

Cell declustering was applied to the variables of interest to overcome the bias caused by random sampling. A total of 500 cells were interpolated from 1m to 1000m, and 25 random cell offsets were used to decluster the dataset. The declustered weights were added to the dataset to yield more representative statistics compared to using naïve data. Summary statistics and minimised cell sizes of the declustered data were calculated for each variable-domain combination. The data from cell declustering was then used to plot scatter line plots to show the typical relationship between increasing cell sizes and the average declustered mean per block.

5.4.2. Variogram modelling

Variogram maps were created to give a general overview of the major directions of grade continuity, assess the degree of anisotropy, and identify directions of cyclicity for each variable-domain combination. The maps were created using normal score transformation values obtained during the cell declustering stage. From there, experimental semi-variograms were

created for each variable-domain combination at 15° intervals. Major and minor directions of continuity were identified for each variable-domain combination and subsequently modelled such that the nugget effect, sill, and range were fitted onto an exponential graph. The parameters used for variography and cell declustering are similar.

5.5. Quantitative Kriging Neighbourhood Analysis

Quantitative kriging neighbourhood analysis is a process employed to optimise resource estimation by determining parameter values that should be used to estimate resources to avoid over-smoothing and bias (Mandava *et al*., 2016). The purpose of quantitative neighbourhood analysis is to determine estimation parameters that will improve mineral resource estimation accuracy, handle non-stationarity, and better apply the variogram model to estimate values within smaller sub-blocks while accounting for support-volume considerations (Sunday and Deutsch, 2020). The process of quantitative kriging neighbourhood analysis involves block discretisation and the calculation of kriging validation matrices using variogram parameters.

Block discretisation was used to determine the number of partitions that minimises error and provide the most unbiased estimation as outlined by Coombes (2008). Block discretisation was achieved by dividing estimation blocks into smaller sub-blocks and calculating the variance within sub-blocks at different discretisation levels for each variable-domain combination. The within-block variance values at different discretisation levels were then plotted against each other and the optimal discretisation level was identified using the KneeLocator. If the KneeLocator function does not find an inflection point on the in-block versus discretisation, the fallback is a random choice number between four and seven. From there, kriging validation metrics and performance scores were calculated across a range of sample sizes with interval values between 5 and 35, resulting in a gridded dataframe for each

variable-domain combination, thereby providing a continuous representation of the performance matrices over various sample sizes.

5.6. Ordinary Kriging

A Python-based workflow adopted from Pyrcz (2023) was used for ordinary kriging through parallel processing of spatial data variables within each domain. To accurately model spatial relationships, variogram parameters such as the nugget effect, sill, range, and major and minor directions of continuity were extracted from the dataset. Interpolation was applied using the ordinary kriging method to calculate kriged estimates, kriged estimate variance, kriged estimate efficiency and slope of regression on a 20 × 20 m grid cell size, which is the cell size that maximises kriging efficiency and slope of regression. The discretisation size and constraints on the minimum and maximum number of samples were defined before kriging to ensure sound spatial estimation. Kriging was then performed for each variable-domain combination with spatial coordinates adjusted to cell centres and domains for accuracy. Finally, the kriging results were validated by analysing metrics such as kriging variance and kriging efficiency and visualised as spatial plots, enabling detailed and further analysis of the results.

5.7. Confidence Intervals

Confidence intervals were calculated using both the raw data and the kriged estimates. The methodology was adopted from Holbert (2023b). Confidence interval calculation is a structured process that involves (1) the transformation of raw data, (2) the computation variances for the transformed raw data, (3) scaling of the kriging variance, (4) conversion of kriged estimates into normal or logarithmic space, (5) calculation of the 90% confidence intervals and finally, (6) the back-transformation of the confidence intervals to raw space for data validation. Confidence intervals can be calculated using the normal score or the

logarithmic transformation method. However, this study will follow the logarithmic transformation method. The step-by-step methodology employed in confidence interval calculation is detailed below.

The raw data is transformed into normal space through the equation:

$$Z = \ln(A + \beta),$$

Equation 5.2: Logarithmic transformation of data

where A is the variable being transformed and β is a positive constant added to minimise the skewness of the data to create a standardised Gaussian moment transformation. Logarithmic transformation of the data ensures that the data follows a standard normal distribution, with a mean of 0 and a variance of 1. The positive constant β was determined and calculated through geostatistical code in Jupyter Notebook and was established to have different values for the variables being estimated. These values are shown in Table 6.15.

The variance of the above transformed data is computed using the equation:

$$LogVar = VAR(Z),$$

Equation 5.3: Logarithmic variance computation

where $LogVar$ is the log variance of the raw data.

The selection of block sizes introduces variability (Dominy *et al*., 2002). To account for the variability introduced by the selection of block sizes in kriging estimates, the dispersion variance, also referred to as the sample variance, is calculated using the equation:

$$D^2(V, K) = D^2(v, K) - D^2(v, V)$$

Equation 5.4: Dispersion variance calculation

where $D^2(V,K)$ is the dispersion variance of the larger unit, V, (*e.g.*, domain) within the entire deposit K, $D^2(v,K)$ is the dispersion variance of a small unit (*e.g.*, model block) within the entire deposit, and $D^2(v,V)$ is the dispersion variance of the small unit within the larger unit.

The dispersion variance quantifies the variability introduced by the block size, accounts for the spatial averaging effect because of the block size, and ensures that the kriging variance is scaled accordingly (Haslwanter, 2022). The dispersion variance value is then used to scale the logarithmic kriging variance, thereby quantifying the variability introduced by the block size and accounting for the spatial averaging effect that results from block size selection, through equation 5.5:

$$LogKVar = \sigma_K^2 \cdot D^2(V,K)$$

Equation 5.5: Scaling the logarithmic kriging variance

where σ_K^2 is the normalised kriging variance from the variogram model. The kriging log-transformed standard deviation is calculated using the equation:

$$LogKSD = \sqrt{LogKVar}$$

Equation 5.6: Kriging standard deviation in logarithmic space

where and $LogKSD$ is the kriging standard deviation in the log space.

To ensure that the same units of measure are used, kriging estimates are then transformed to logarithmic space through the equation:

$$KrigingEstimate_{log} = \ln\left(Estimate_{raw} + \beta\right)$$

Equation 5.7: Conversion of kriging estimates to logarithmic space

where $KrigingEstimate_{log}$ is the logarithmic value of the kriged estimate, $Estimateraw$ is the kriged estimate value.

The logarithmic transformation values of kriged estimates, the z-score value associated with the 90% confidence level, and the logarithmic standard deviation value of a block size were used to calculate the 90% confidence interval, such that:

$$CI_{lower,log} = \left(KrigingEstimate_{log}\right) - Z_x \cdot LogKSD$$

Equation 5.8: Lower-bound logarithmic confidence interval calculation

for the lower-bound confidence interval and equation 5.9 is used for the upper-bound confidence interval.

$$CI_{upper,log} = \left(KrigingEstimate_{log}\right) + Z_x \cdot LogKSD$$

Equation 5.9: Upper-bound logarithmic confidence interval calculation

where CI is the confidence and Z_x is the z-score corresponding to a one-tailed confidence interval.

The lower- and upper-bound confidence interval values must be constrained within the kriged estimate values such that the upper-bound confidence interval values do not exceed the maximum kriged estimate value for a variable. The confidence interval results are back transformed into raw space using the equation:

$$CI_{lower,raw} = \exp\left(CI_{lower,log} + (LogVar/2)\right) - \beta$$

Equation 5.10: Lower-bound log confidence interval conversion to raw space

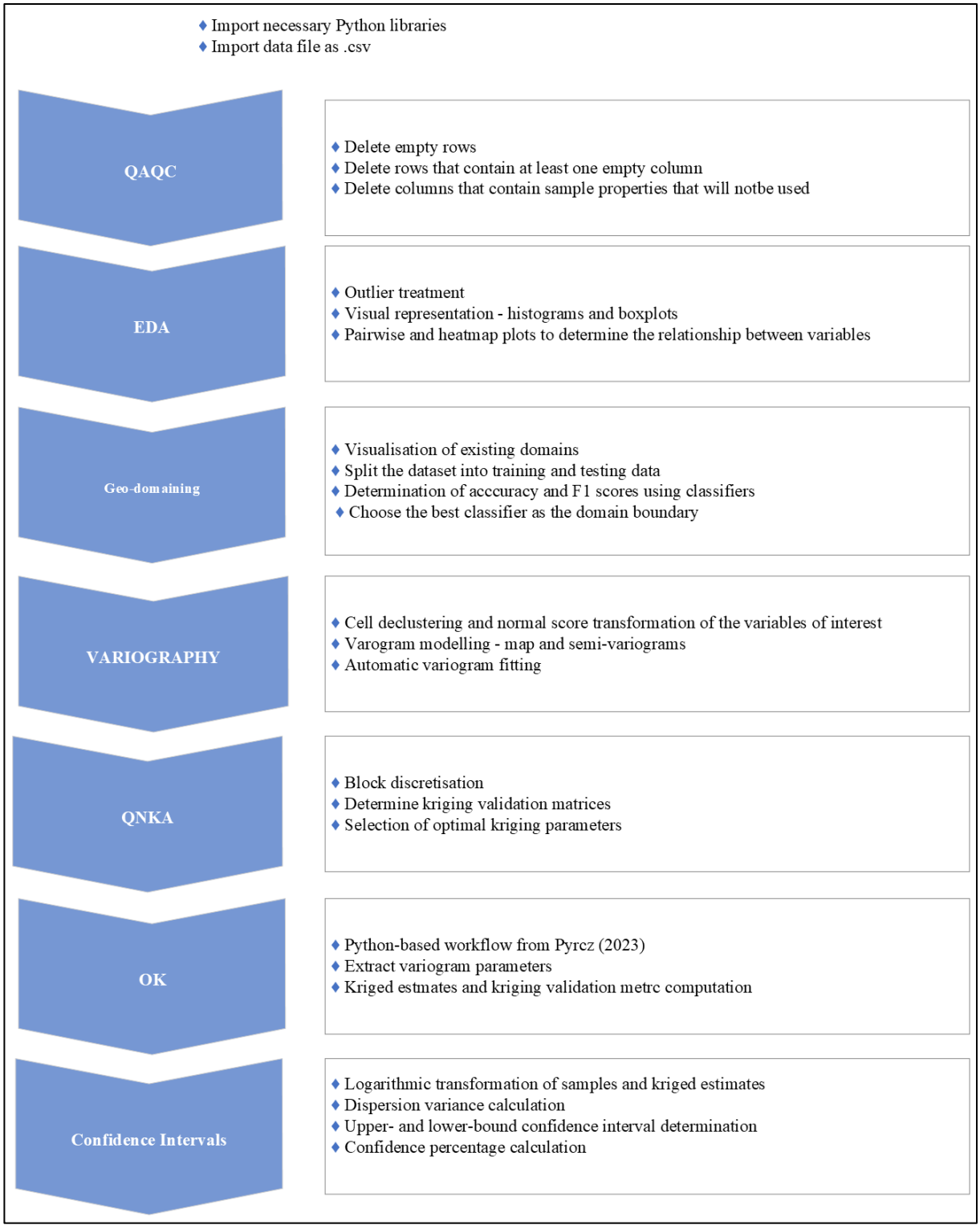


Figure 5.2: A methodology workflow diagram summarising sequential steps involved in this research.

6. RESULTS

This chapter presents results derived from the methodologies detailed in Chapter 5. The chapter begins with an exploratory data analysis, focusing on statistical analysis and an assessment of the relationships that exist between the different variables. The next section outlines how the study area's various domains were delineated into polygons. The third section summarises the results from variography, emphasising findings from cell declustering and experimental variogram modelling. Variography results are followed by the results from quantitative kriging neighbourhood analysis, ensuring that parameters that will produce unbiased estimates are selected for ordinary kriging analysis. Quantitative kriging neighbourhood analysis is then applied to the subsequent sections, where results from ordinary kriging are presented alongside kriging validation matrices. The final section of the results chapter details the confidence percentages associated with kriging estimates, determined through two different methodologies, and validates confidence percentages using correlation analysis and swath plots.

6.1. Exploratory Data Analysis

The section details the results obtained through QA/QC and exploratory data analysis. QA/QC is a data pre-processing step that ensures the use of non-erroneous data and ensures that results obtained from estimation are a good representation of the sample data. From the assay data sheet obtained, the variables of interest are the gold accumulation (cm.g/t), channel width (cm), and Au (g/t). For graphical representation, the variables of interest will be referred to as CMGT, CW, and Au, representing the gold accumulation index (cm.g/t), channel width (cm), and Au (g/t), respectively.

6.1.1. Sample dataset

The raw data comprises 19,532 data points and 11 sample properties (Table 6.1). Each sample is associated with X-, Y- and Z-coordinates and is classified to belong to a ZONE (later referred to as a domain). Gold accumulation index (cm.g/t), channel width (cm), Au (g/t), stoping width (cm), vertical length (cm), sample type, and the date (DATE) that the sample was collected are also described in the raw assay data file. The coordinates are shown in the Gauss conform coordinate system and represent longitudes and latitudes, respectively. Sample properties that were not of interest (e.g., ZPT, SMPTYPE, and DATE) and rows that contained at least one empty column were removed from the dataset. The dataset was then left with a total of 19,504 points (Table 6.2), on which outlier treatment was performed. Summary statistics of the data after QA/QC are shown in Table 6.3.

Table 6.1: A selection of data points from the raw datasheet showing different sample properties. XPT, YPT and ZPT represent the X-, Y- and Z- coordinates, respectively.

XPT	YPT	ZPT	ZONE	CMGT	CW	SW	VL	SMPTYPE	DATE
5365.4	-17708.5	0	18	603.2	90	0	0	2	20120822
5368.2	-17708.8	0	18	547.2	70	0	0	2	20120822
5370.7	-17708.2	0	18	158	73	0	0	2	20120822
5373.1	-17707.1	0	18	405.2	53	0	0	2	20120822
5373.2	-17682.6	0	18	249.34	124	0	0	2	20121126
5374.5	-17684.9	0	18	315.84	91	0	0	2	20121126
5375.6	-17706.4	0	18	332	20	0	0	2	20120822
5376	-17687.2	0	18	444.56	65	0	0	2	20121126
5377.2	-17681.4	0	18	1017.38	144	0	0	2	20121212
5377.3	-17689.6	0	18	331.61	25	0	0	2	20121126

Table 6.2: A selection of data points after QA/QC.

X	Y	Domain	CMGT	CW	Au
5365.40	-17708.50	18	603.20	90.00	6.70
5368.20	-17708.80	18	547.20	70.00	7.82
5370.70	-17708.20	18	158.00	73.00	2.16
5373.10	-17707.10	18	405.20	53.00	7.65
5373.20	-17682.60	18	249.34	124.00	2.01
5374.50	-17684.90	18	315.84	91.00	3.47
5375.60	-17706.40	18	332.00	20.00	16.60
5376.00	-17687.20	18	444.56	65.00	6.84
5377.20	-17681.40	18	1017.38	144.00	7.07
5377.30	-17689.60	18	331.61	25.00	13.26
5377.90	-17705.20	18	892.80	12.00	74.40

Table 6.3: Table presenting descriptive statistics for spatial coordinates, domain classifications, and three key variables of the dataset after QA/QC was applied.

	X	Y	Domain	CMGT	CW	Au
Count	19504	19504	19504	19504.00	19504.00	19504.00
Mean	6241.033	-17758.2	11.27	643.03	47.39	23.70
Standard deviation	434.48	262.69	4.51	899.11	43.15	39.62
Minimum	5365.4	-18421.3	8	0.00	3.00	0.00
25th percentile	5861.1	-17690.5	8	161.12	13.00	4.44
Median	622.35	-17778.2	8	383.00	30.00	11.82
75th percentile	6610.7	-17582.9	18	791.00	70.00	27.00
Maximum	7165.93	-17103.8	19	27086.76	328.00	1062.06

6.1.2. Outlier treatment

Outliers were treated using equation 5.1. Values that are beyond the z-score of 2.58 were considered outliers. Following outlier treatment, a total of 18,676 points remained. The datapoints will be used for resource estimation, and their summary statistics are shown in Table 6.4 below.

Table 6.4: Table showing summary statistics of the dataset following outlier treatment.

	X	Y	Domain	CMGT	CW	Au
Count	18676	18676	18676	18676	18676	18676
Mean	6233.56	-17760.3	11.356	658.28	47.79	24.20
Standard deviation	435.90	263.9149	4.55	807.51	43.19	36.30
Minimum	5365.4	-18421.3	8	9.6	4.00	0.24
25th percentile	5854.18	-17962.9	8	185.51	13	5.14
Median	6212.7	-17782.7	8	406	30	12.51
75th percentile	6606.83	-17586.8	18	814.39	71	27.87
Maximum	7165.93	-17103.8	19	11541.08	328	454.79

The effect of outlier treatment was assessed by visualising the distribution of the dataset before and after outlier removal. The z-score distribution histogram of the dataset before outlier treatment shows that the data is negatively (left) skewed; that is, the mean is less than the median (Fig. 6.1). Channel width (cm) does not display a symmetrical bell shape as compared to the gold accumulation index (cm.g/t) and Au (g/t). The non-normal distribution exhibited by channel width (cm) may be caused by subpopulations that exist within the channel width.

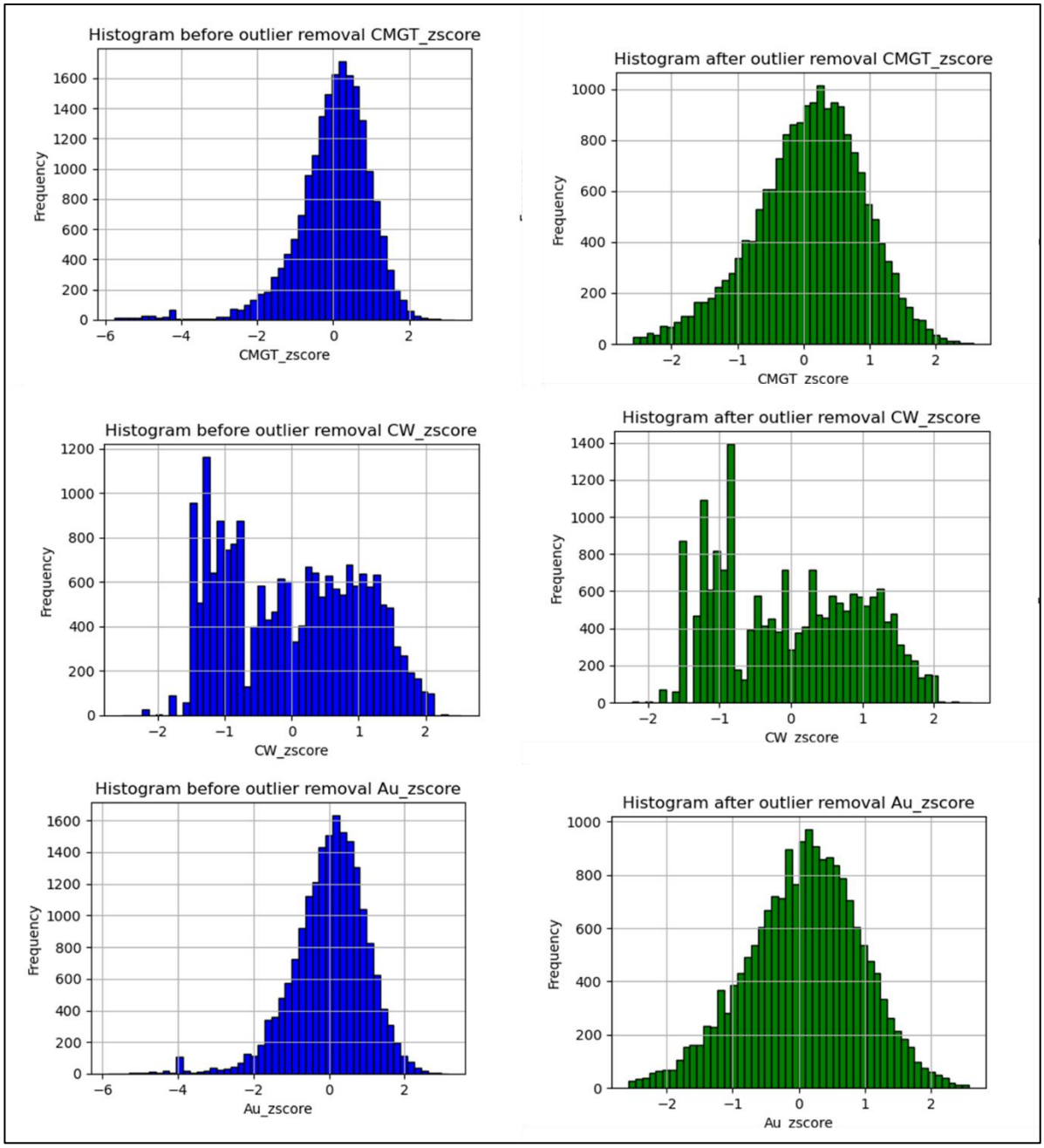


Figure 6.1: Graphs of z-score values for different variables before and after outlier removal. CMGT z-score, CW z-score and Au z-score represent the gold accumulation (cm.g/t), channel width (cm) and Au (g/t) z-score values, respectively.

The following boxplots (Fig. 6.2) serve as a visual representation of the effects of outlier treatment. Detailed observation of the dataset indicates that there is a change in the distribution

and count of the data points within every variable. However, there is a minimal difference in the summary statistics of the channel width (cm). Although outliers were treated, the boxplots show that outliers still exist according to the interquartile range. This is because high z-score values were used to treat outliers in order to preserve the dataset and ensure that it remains representative.

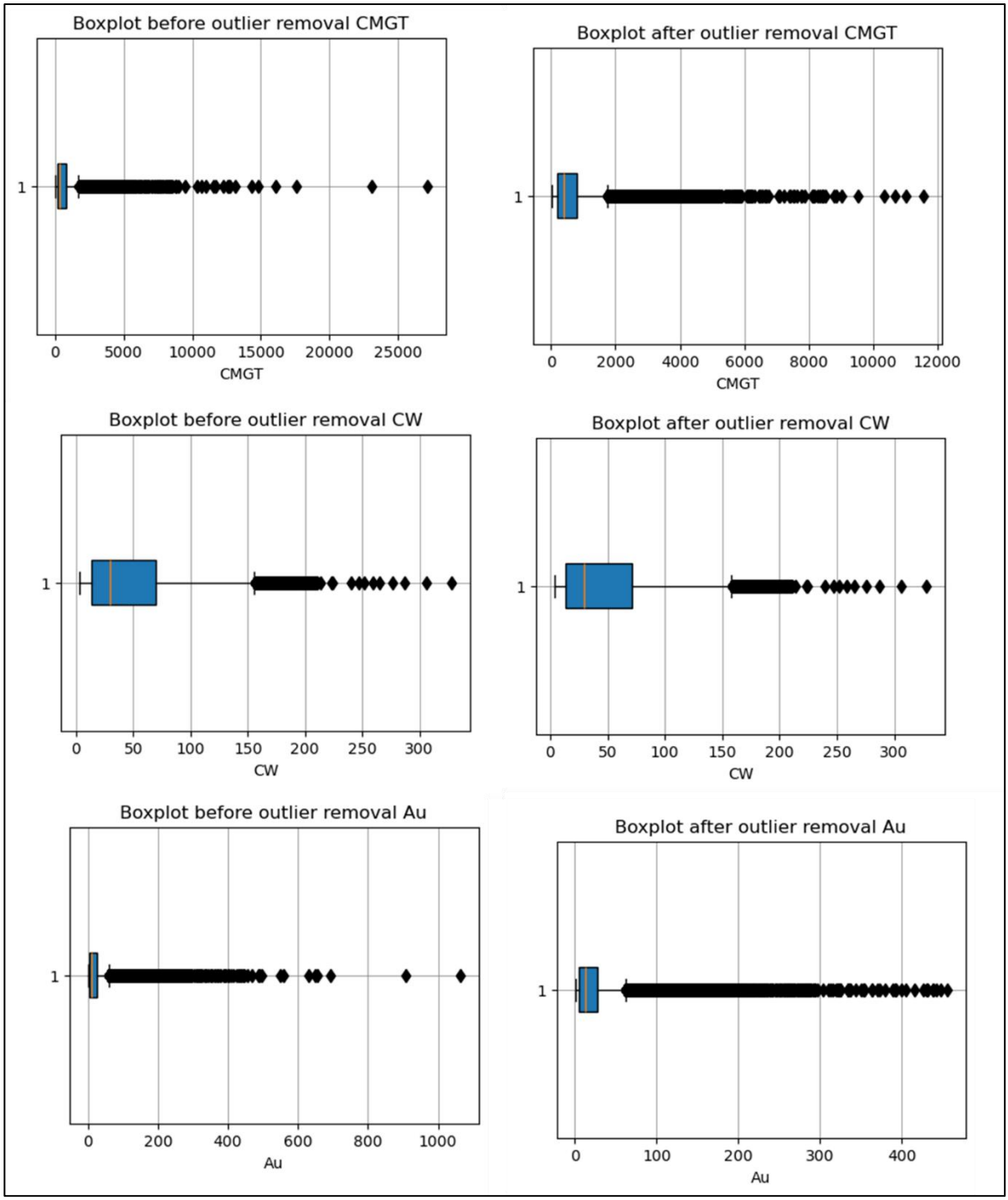


Figure 6.2: Boxplots, per variable of interest, of the dataset before and after outlier treatment. CMGT, CW and Au represent the gold accumulation (cm.g/t), channel width (cm) and Au (g/t).

6.1.3. Variable analysis

The variable analysis subsection examines the statistical properties and spatial distribution of the gold accumulation (cm.g/t), channel width (cm), and Au (g/t) within the dataset. Statistical analysis includes descriptive statistics, distribution patterns, and spatial variability assessments, and aims to provide insights into the nature and behaviour of the variables under investigation. Table 6.4 summarises the descriptive statistics of the different variables within the study area.

6.1.3.1. Gold accumulation (cm.g/t)

The gold accumulation (cm.g/t) is a continuous quantitative variable, ranging from a minimum of 9.6 cm.g/t to a maximum of 11,541.08 cm.g/t. Statistical analysis reveals a mean value of 658.28 cm.g/t with a standard deviation of 807.51 cm.g/t, indicating variability in the dataset. The box-and-whisker plot and histogram illustrate a right-skewed distribution, suggesting the presence of high-value samples (Fig. 6.3). Both the boxplot and histogram confirm that most data points are concentrated below 1000 cm.g/t, highlighting the dominance of lower gold accumulation (cm.g/t) values across the dataset.

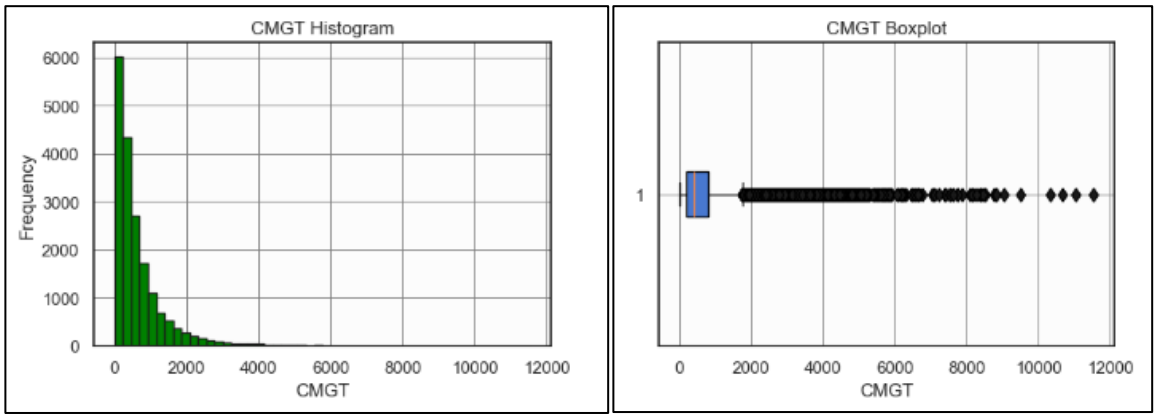


Figure 6.3: Histogram and boxplot of the entire dataset for gold accumulation (cm.g/t).

6.1.3.2. Channel width (cm)

Channel width (cm) is a continuous quantitative variable, ranging from a minimum of 4 cm to a maximum of 328 cm. Statistical analysis reveals a mean value of 47.79 cm with a standard deviation of 43.19 cm, indicating variability in the dataset. The box-and-whisker plot and histogram illustrate a right-skewed distribution, suggesting the presence of high-value samples (Fig. 6.4). Both the boxplot and histogram confirm that most data points are concentrated below 100 cm, highlighting the dominance of lower channel width (cm) values across the dataset.

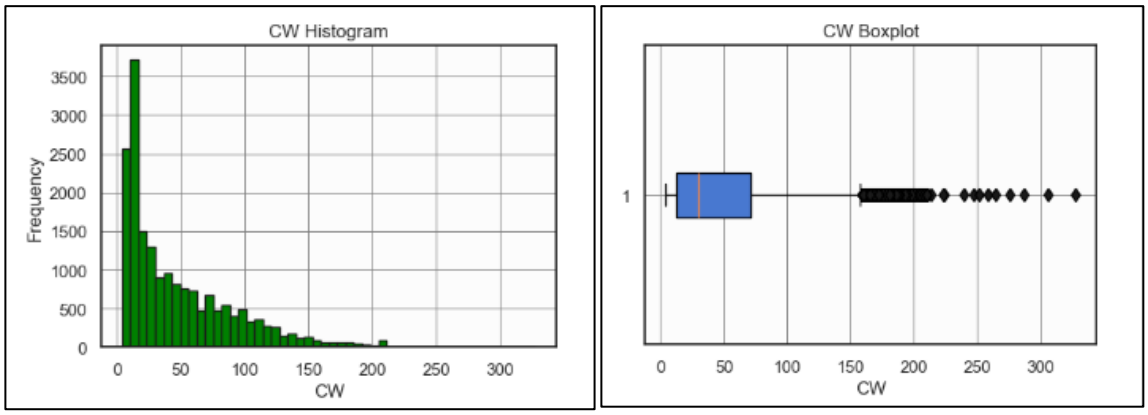


Figure 6.4: Histogram and boxplot of the entire dataset for channel width (cm).

6.1.3.3. Au (g/t)

Au (g/t) is a continuous quantitative variable, ranging from a minimum of 0.2g/t to a maximum of 454.79 g/t cm. Statistical analysis reveals a mean value of 24.20 g/t with a standard deviation of 36.30 g/t cm, indicating variability in the dataset. The box-and-whisker plot and histogram illustrate a right-skewed distribution, suggesting the presence of high-value samples (Fig. 6.5). Both the boxplot and histogram confirm that most data points are concentrated below 50 g/t, highlighting the dominance of lower accumulation values across the dataset.

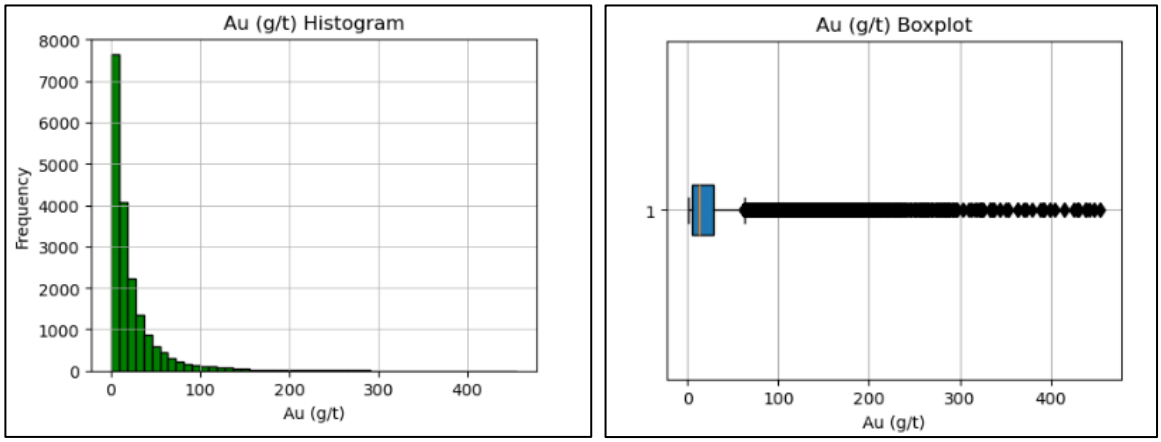


Figure 6.5: Histogram and boxplot of the entire dataset for Au (g/t).

6.1.4. Data relationships – correlation heatmaps

The correlation heatmap provides a visual representation of relationships between variables, offering insights into potential dependencies. The Pearson correlation matrix was used to quantify the relationships between variables. The results indicate the following: (1) a strong positive correlation exists between the gold accumulation (cm.g/t) and Au (g/t); (2) a weaker positive correlation is observed between channel width (cm) and the gold accumulation (cm.g/t); (3) channel width (cm) shows a weak correlation with both the gold accumulation (cm.g/t) and Au (g/t); (4) a slight positive correlation is identified between channel width (cm) and Y-coordinates (Fig. 6.6). Pairwise and correlation heatmap plots of variables, per variable, are shown by figures A1 and A2 in the appendix, respectively.

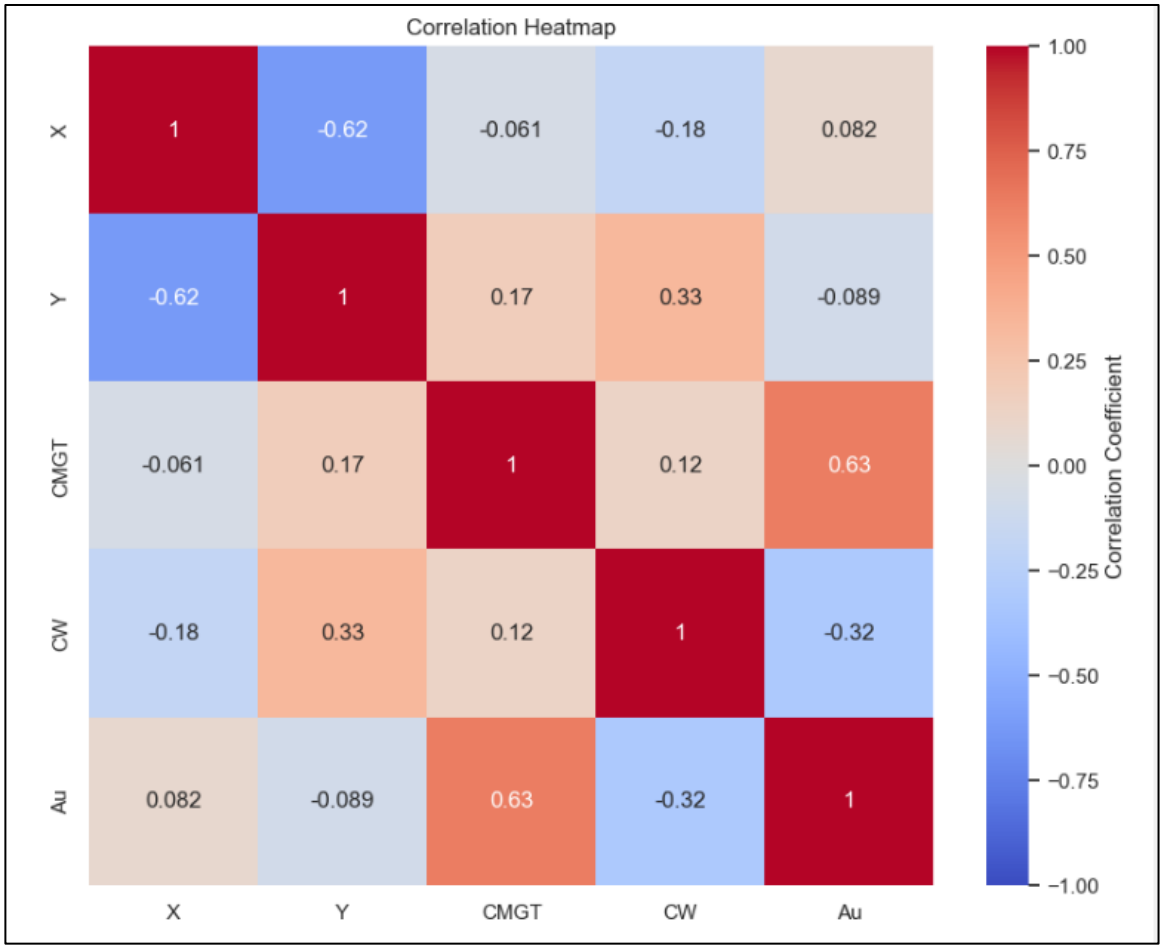


Figure 6.6: A correlation matrix heatmap for the entire dataset. The colour gradient represents the correlation relationship, ranging from weak (blue) to strong (red), indicating areas with correlation. X and Y represent the X- and Y-coordinates, CMGT represents the gold accumulation (cm.g/t), CW represents the channel width (cm), and Au represents the Au (g/t).

6.1.5. Statistical analyses

Statistical analysis of the validated and filtered Middelvlei Reef data, including sample statistics, was carried out. Table 6.5 below details the summary statistics for the different variables within each domain. Basic statistical properties of each domain are described in terms of central tendency, standard deviation, variance, coefficient of variation, skewness, and

kurtosis. The sub-section presents detailed statistical analysis for each variable presented per domain.

Table 6.5: Statistics of the different variables per domain.

Domain	Variable	Count	Mean	Standard deviation	Minimum	25th percentile	Median	75th percentile	Maximum	Variance	Skewness	Kurtosis
8	Gold accumulation (cm.g/t)	11777	584.30	781.57	9.60	154.24	339.57	698.38	11029.35	610801.14	4.16	27.67
	Channel width (cm)		42.43	41.22	4.00	12.00	25.00	61.00	328.00	1699.35	1.69	3.07
	Au (g/t)		25.87	40.14	0.24	4.51	12.06	29.92	447.40	1611.29	4.01	23.02
14	Gold accumulation (cm.g/t)	1979	748.75	894.75	10.00	224.00	495.00	906.00	11541.08	800179.12	3.86	26.36
	Channel width (cm)		96.10	48.15	6.00	62.00	95.00	129.00	210.00	2317.23	0.15	-0.55
	Au (g/t)		10.64	17.85	0.25	2.71	5.24	10.94	260.74	318.33	4.49	44.63
18	Gold accumulation (cm.g/t)	3327	811.30	822.01	11.70	265.94	583.44	1053.97	7760.02	67598.29	2.71	11.36
	Channel width (cm)		42.07	34.17	6.00	14.00	30.00	59.00	210.00	1166.96	1.22	1.00
	Au (g/t)		25.30	29.63	0.33	10.22	16.99	29.88	454.79	877.88	5.27	46.70
19	Gold accumulation (cm.g/t)	1593	773.30	782.00	13.40	285.63	539.04	966.72	6762.41	611135.71	2.73	10.72
	Channel width (cm)		39.36	27.11	8.00	17.00	33.00	53.00	159.00	734.48	1.09	0.72
	Au (g/t)		26.44	32.46	0.39	8.98	16.02	31.02	392.63	1052.90	4.02	24.73

6.1.5.1. Domain 8

Gold accumulation (cm.g/t)

Domain 8 consists of 11,777 samples, exhibiting a right-skewed distribution with a mean gold accumulation of 584.30 cm.g/t and a median of 339.57 cm.g/t. The standard deviation is 781.54 cm.g/t while the coefficient of variation is 133.76%, both indicating variability and high relative dispersion. The distribution is highly skewed at 4.16, with a leptokurtic kurtosis (27.67). The gold accumulation spans a wide range from 9.6 cm.g/t to 11,029.35 cm.g/t, reflecting significant gold accumulation (cm.g/t) variability within the domain.

Channel Width (cm)

Domain 8 consists of 11,777 samples, exhibiting a right-skewed distribution with a mean channel width of 42.43 cm and a median of 25 cm. The standard deviation is 41.22 cm, while the coefficient of variation is 97.16%, both indicating variability and high relative dispersion. The distribution is highly skewed at 1.69, with a leptokurtic kurtosis (3.07). The channel width within domain 8 spans a wide range from 4 cm to 328 cm, reflecting significant channel width (cm) thicknesses within the domain.

Au (g/t)

Domain 8 has a total of 11,777 samples, exhibiting a right-skewed distribution with a mean concentration of 25.87 g/t and a median of 12.06 g/t. The standard deviation is 40.14 g/t while the coefficient of variation is 155.18%, both indicating variability and high relative dispersion. The distribution is highly skewed at 5.49, with a leptokurtic kurtosis (44.63). The Au concentration within domain 8 spans a wide range from 0.24 g/t to 447.4 g/t.

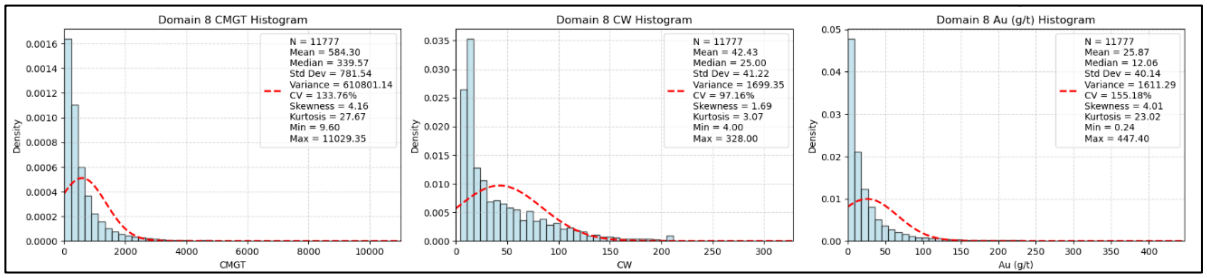


Figure 6.7: Histograms showing the distribution and statistical analysis of data within each variable for domain 8. The red stippled line is a trendline.

6.1.5.2. Domain 14

Gold accumulation (cm.g/t)

Domain 14 has a total of 1,979 samples, exhibiting a right-skewed distribution with a gold accumulation of 748.75 cm.g/t and a median of 495 cm.g/t. The standard deviation is 894.53 cm.g/t while the coefficient of variation is 119.47%, both indicating variability and high relative dispersion. The distribution is highly skewed at 5.49, with a leptokurtic kurtosis (26.36). The gold accumulation (cm.g/t) within domain 14 spans a wide range from 10 cm.g/t to 11,541.08 cm.g/t.

Channel width (cm)

Domain 14 has a total of 1,979 samples, exhibiting a normal distribution with a mean channel width of 96.1 cm and a median of 95 cm. The standard deviation is 48.14 cm while the coefficient of variation is 50.09%, indicating moderate variability and relative dispersion. The distribution has a low skewness at 0.15, with a mesokurtic kurtosis (-0.55). The channel width (cm.g/t) within domain 14 spans a wide range from 6 cm to 210 cm.

Au (g/t)

Domain 14 has a total of 1,979 samples, exhibiting a right-skewed distribution with a mean of 10.64 g/t and a median of 5.24 g/t. The standard deviation is 17.84 g/t while the coefficient of variation is 167.84%, indicating variability and high relative dispersion. The distribution is highly skewed at 5.49, with a leptokurtic kurtosis (44.63). The Au (g/t) concentration within domain 14 has a wide range from 0.25 g/t to 260.74 g/t.

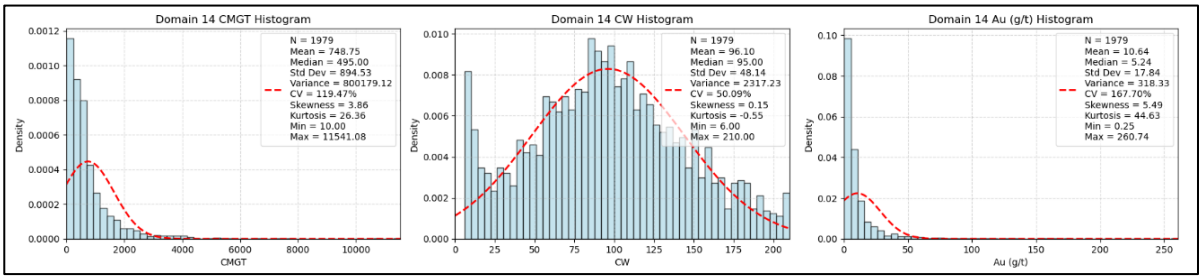


Figure 6.8: Histograms showing the distribution and statistical analysis of data within each variable for domain 14. The red stippled line is a trendline.

6.1.5.3. Domain 18

Gold accumulation (cm.g/t)

Domain 18 has a total of 3,327 samples, exhibiting a right-skewed distribution with a mean of 811.30 cm.g/t and a median of 583.44 cm.g/t. The standard deviation is 821.89 cm.g/t while the coefficient of variation is 101.31%, indicating variability and high relative dispersion. The distribution is highly skewed at 2.71, with a leptokurtic kurtosis (11.36). The gold accumulation concentration within domain 18 has a wide range from 11.70 cm.g/t to 7,760 cm.g/t.

Channel width (cm)

Domain 18 has a total of 3,327 samples, exhibiting a normal distribution with a mean of 42.07 cm and a median of 30 cm. The standard deviation is 34.16 cm while the coefficient of variation is 81.2%, indicating variability and moderate relative dispersion. The distribution is highly skewed at 10.22 with a platykurtic kurtosis. The channel width (cm) within domain 18 has a wide range from 6 cm to 210 cm.

Au (g/t)

Domain 18 has a total of 3,327 samples, exhibiting a right-skewed distribution with a mean of 25.3 g/t and a median of 16.99 g/t. The standard deviation is 29.63 g/t while the coefficient of variation is 117.13%, indicating variability and high relative dispersion. The distribution is highly skewed at 5.27, with a leptokurtic kurtosis (46.7). The gold accumulation concentration range within domain 18 is wide, from 0.33 g/t to 454.79 g/t.

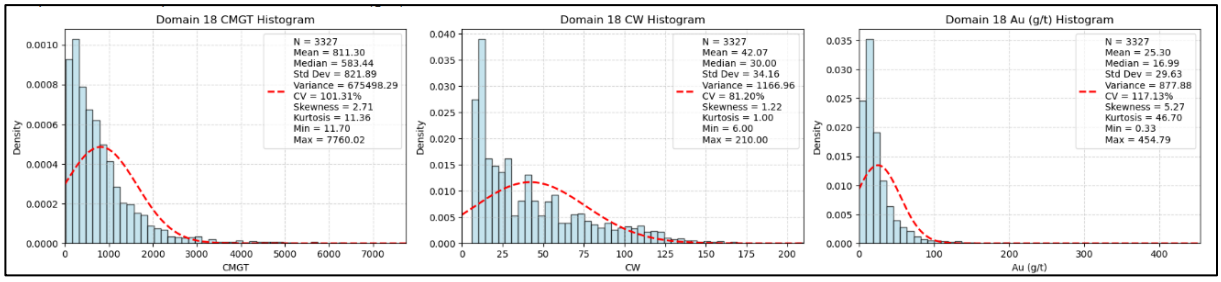


Figure 6.9: Histograms showing the distribution and statistical analysis of data within each variable for domain 18. The red stippled line is a trendline.

6.1.5.4. Domain 19

Gold accumulation (cm.g/t)

Domain 19 has a total of 1,593 samples, exhibiting a right-skewed distribution with a mean of 773.3 cm.g/t and a median of 539.04 cm.g/t. The standard deviation is 781.75 cm.g/t while the coefficient of variation is 101.09%, indicating variability and high relative dispersion. The distribution is highly skewed at 2.73, with a leptokurtic kurtosis (10.73). The gold accumulation range within domain 19 is wide, ranging from 13.40 cm.g/t to 6,762.41 cm.g/t.

Channel width (cm)

Domain 19 has a total of 1,593 samples, exhibiting a normal distribution with a mean of 39.37 cm and a median of 33 cm. The standard deviation is 27.1 cm while the coefficient of variation is 68.86%, indicating variability and relative dispersion. The distribution is highly skewed at 1.09 with a platykurtic kurtosis (0.72). The channel widths within domain 19 is wide, ranging between 8 cm to 159 cm.

Au (g/t)

Domain 19 has a total of 1,593 samples, exhibiting a right-skewed distribution with a mean of 26.44 g/t and a median of 16.02 g/t. The standard deviation is 32.45 g/t while the coefficient of variation is 122.71%, indicating variability and high relative dispersion. The distribution is highly skewed at 4.02 with a leptokurtic kurtosis (24.73). The Au (g/t) concentration within domain 19 is wide, from 0.39 g/t to 392.63 g/t.

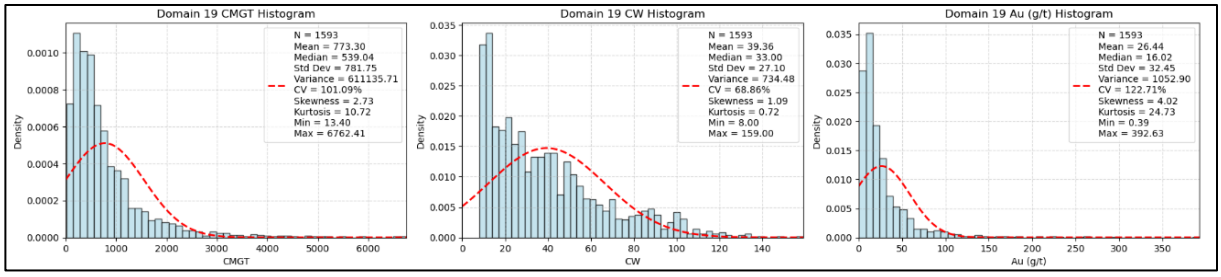


Figure 6.10: Histograms showing the distribution and statistical analysis of data within each variable for domain 19. The red stippled line is a trendline.

6.2. Domain Boundaries

To ensure that the influence of mineral grade continuity between adjacent domains is minimised, domain boundaries were defined to constrain mineral resource estimates within each domain, as recommended by Ortiz and Emery (2006). Hard domain boundaries were created for the geological domains within the study areas. The delineation of domains using hard boundaries was achieved with machine-learning algorithms using Scikit Learn libraries. The aim was to ensure that variable values and properties from across the boundaries are disregarded when estimating the variables within a given domain, to minimise the spatial influence of one domain on the other.

First, the different domains that exist within the study area were visualised using a scatter plot (Fig. 6.11). From there, the dataset was split into 80% training and 20% testing data. The training dataset was used to fit classifiers, while the testing data served to validate the models' performance. Classifiers such as k-Nearest Neighbours (kNN), Support Vector Machines (SVM), Random Forest (RF), Gradient Boosting (GB), Multi-Layer Perceptron (MLP), and AdaBoost were applied to the data to predict domain boundaries (Emery *et al.*, 2006; Gilday and Emsley, 2017; Kundu, 2022; Zhang *et al.,* 2023). The hyperparameters used to predict the best domain boundary model through different machine learning algorithms are summarised

in Table 6.6. The accuracy and F1 scores from classifiers were compared to each other to predict the best-performing model.

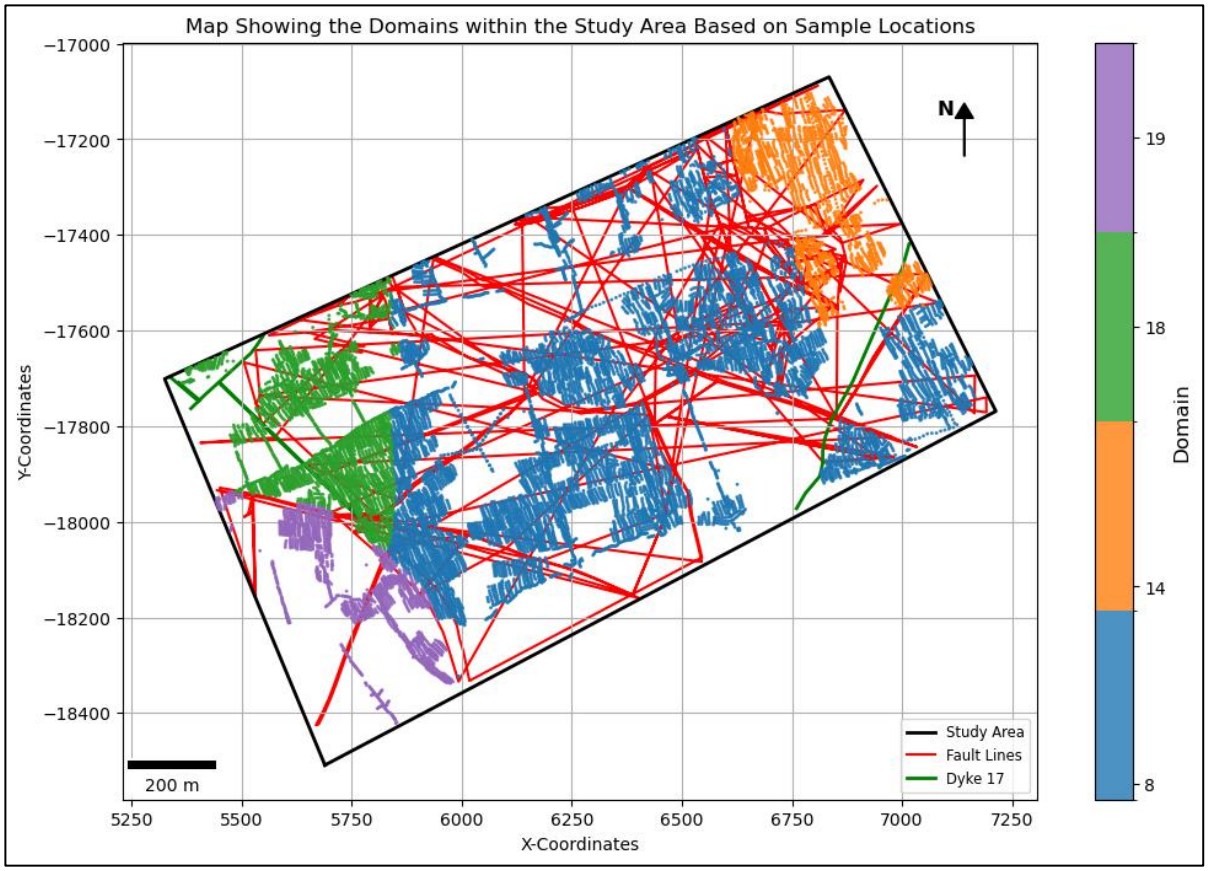


Figure 6.11: A map of the study area showing data point locations incorporating geological structures such as faults and dykes. The colour gradient represents the domain into which each sample is categorised.

Table 6.6: Table showing hyperparameters used in domain boundary classification.

Classifier	Hyperparameter	Assigned Values
k-Nearest Neighbours (kNN)	neighbours	2, 4, 6, 8, 10, 20
	weights	uniform, distance
	algorithm	Auto, ball tree, k-dimensional tree, brute
Support Vector Machine (SVM)	kernel	Linear, polynomial, radial basis, sigmoid
	C	0.1, 1, 10, 100, 500
	gamma	[scale, auto, 0.001, 0.01, 0.1, 1]
Random Forest (RF)	estimators	[100, 200, 500]
	criterion	[gini, entropy]
	Maximum features	[auto, sqrt, log2]
	Maximum depth	[None, 5, 10, 15]
Gradient Boosting (GB)	Number of estimators	[100, 200, 500]
	Learning rate	[0.01, 0.1, 0.2]
	Maximum depth	[3, 5, 8]
	subsample	[0.7, 0.9, 1.0]
Multi-Layer Perceptron (MLP)	Hidden layer sizes	[(50,), (100,), (50, 50), (100, 50)]
	activation	Tangent, rectified linear unit
	solver	Stochastic gradient descent, adaptive moment estimation
	alpha	[0.0001, 0.001, 0.01]
	Learning rate	[constant, adaptive]
AdaBoost (AB)	Number of estimators	[50, 100, 200, 500]
	Learning rate	[0.01, 0.1, 1.0]
	algorithm	Discrete, real

The optimal parameters for each classifier were determined using the GridSearchCV process, which performs an exhaustive search over specified parameter values. The GridSearchCV process was combined with cross-validation to ensure that the models were not overfit. For each model, the cross-validation results were analysed to compute evaluation matrices such as accuracy and F1 score (a metric that measures a model's performance by combining precision and recall into a single value, with higher values indicating better quality classifiers) (Kundu, 2022). The accuracy and F1 scores were averaged over multiple runs to assess the reliability and validity of the models, and results are tabulated in Table 6.7 and graphically represented in Figure 6.12.

Table 6.7: Table showing the classification test score summary (accuracy and F1 score) for each classifier.

Method	Accuracy	F1
k-Nearest Neighbours	0.996471	0.996469
Support Vector Machines	0.994512	0.994513
Random Forest	0.995883	0.995882
Gradient Boosting	0.995559	0.995557
Multi-Layer Patching	0.992338	0.992338
AdaBoost	0.960826	0.959478

After training the dataset, the decision boundaries between domains were identified based on changes in the predicted labels, representing the spatial extent of each domain as defined by the classifiers. Contour plots were generated to visualise the decision boundaries, overlain by scatter plots of the original data points (Fig. 6.12) to visually validate that the classifier-derived boundaries aligned with the actual domain data.

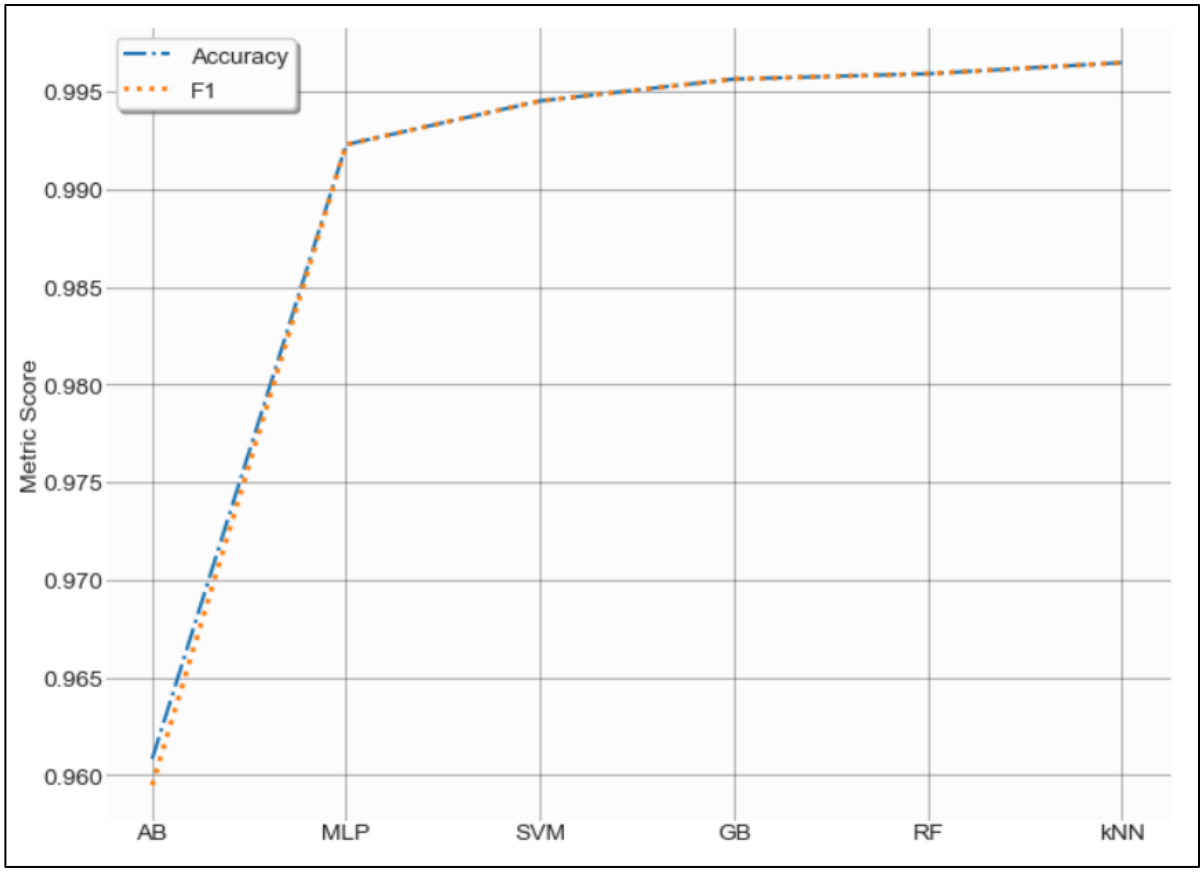


Figure 6.12: F1 and accuracy scores of various machine learning algorithms and their best models through fivefold cross-validation.

After training the dataset, the decision boundaries between domains were identified based on changes in the predicted labels, representing the spatial extent of each domain as defined by the classifiers. Contour plots were generated to visualise the decision boundaries, overlain by scatter plots of the original data points (Fig. 6.13) to visually validate that the classifier-derived boundaries aligned with the actual domain data.

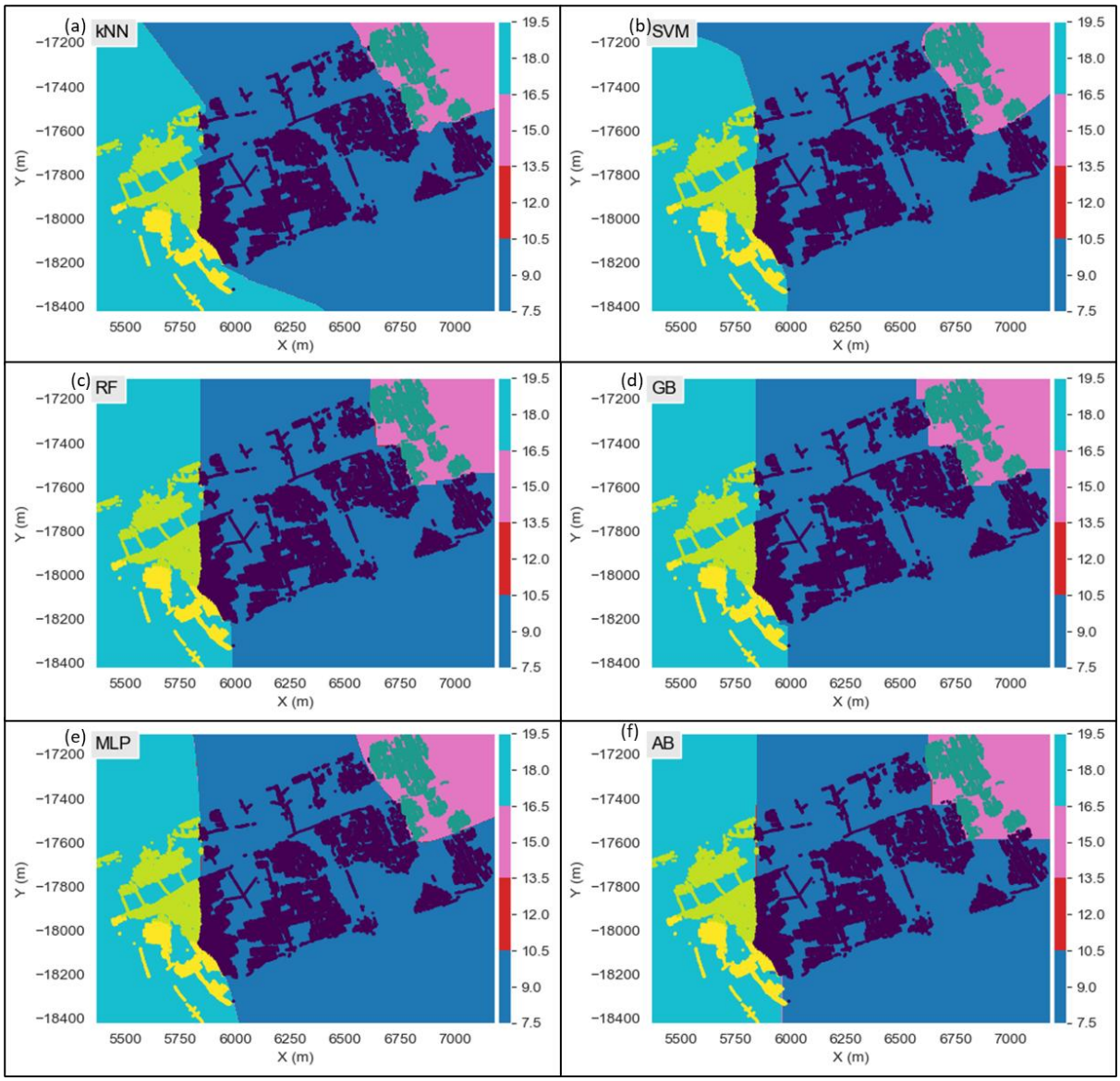


Figure 6.13: Contour plots of the different classifiers and their predicted domain boundaries. The various sample locations are plotted according to their domain classification, and the scale bar represents the different domains into which the samples are classified.

The decision boundaries derived from the classifiers were then converted into polygon geometries for practical use in geospatial analysis. The polygons were exported as shapefiles and plotted on maps enhanced with variables such as colour schemes, grid lines, and labelled regions to improve interpretability (Fig. 6.14). Enhancements ensured that the maps clearly

depicted the distinct regions segmented by each classifier, providing a good visual representation of the domain boundaries.

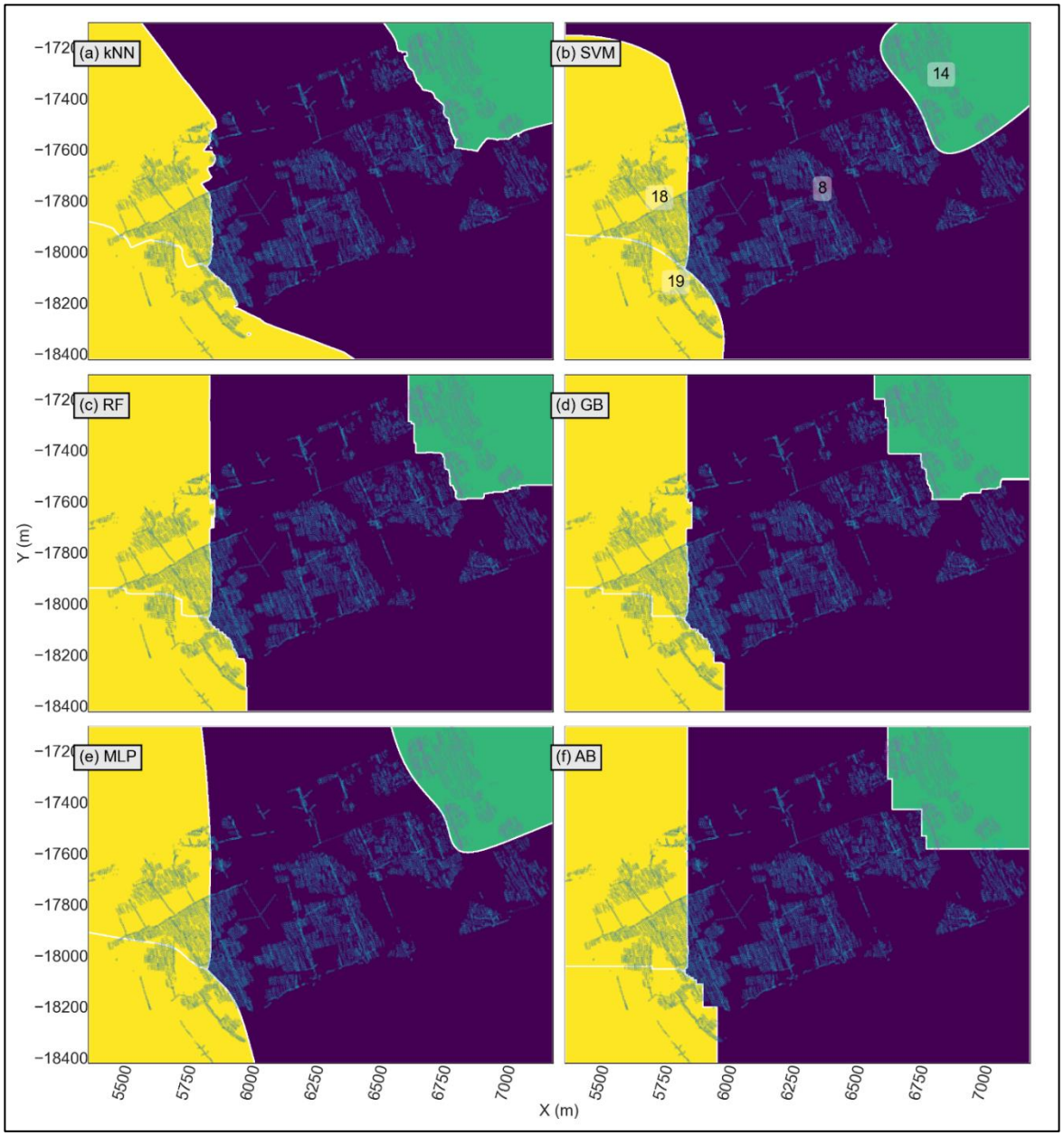


Figure 6.14: Classifier polygons exported as shapefiles. The navy-blue colour shades domain 8, green shades domain 14 and yellow shades both domains 18 and 19.

From the classification results, the support vector machine classifier is used as the best geo-domain boundary shapefile (Fig. 6.15). The support vector machine classifier achieved an accuracy of 0.994512 and an F1 score of 0.994513, placing it as one of the top-performing classifiers. While k-Nearest Neighbours, Random Forest and Gradient Boosting slightly outperformed the support vector machine, the differences in matrices are minimal and likely within the margin of error for many datasets (Kundu, 2022). Support vector machine's F1 score matches its accuracy, demonstrating reliability across different aspects.

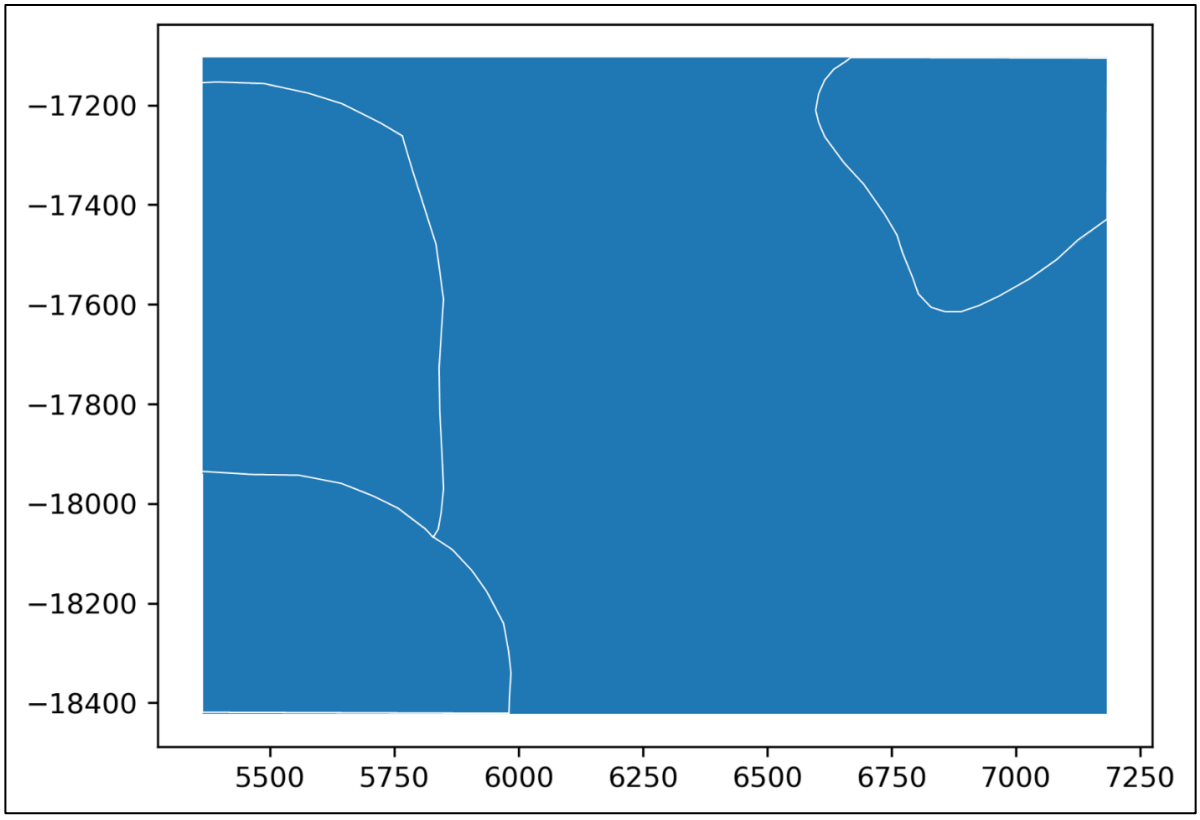


Figure 6.15: Final domain boundary map from the support vector machines model. The blue represents the region of interest and its immediate surroundings, and the white lines represent the domain boundaries delineated using the support vector machine model. The domain boundaries extend outside the study area because the maximum and minimum X- and Y-coordinate values in the dataset were used to limit the GridSearchCV process instead of the study area.

Finally, the support vector machine model is overlain on Figure 6.11 to assess the reliability and effectiveness of delineating domains (Fig. 6.16).

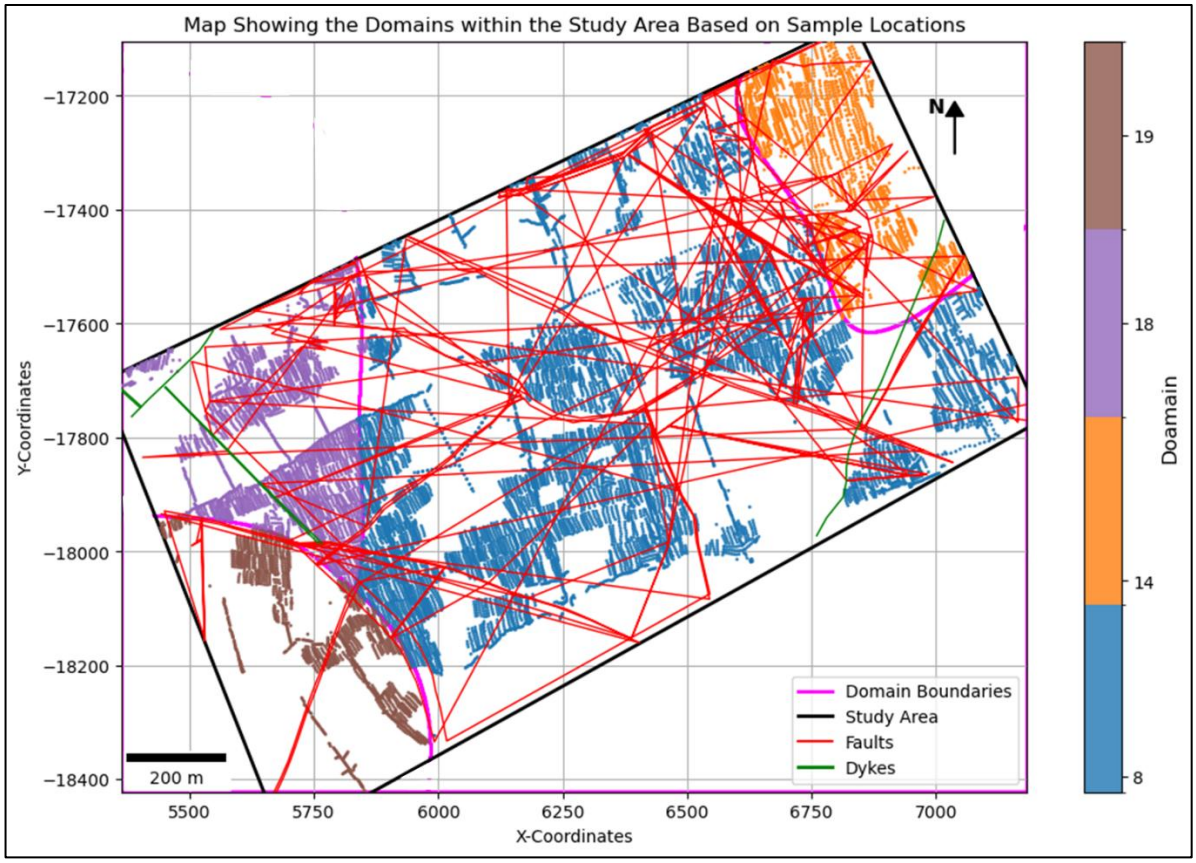


Figure 6.16: A map showing the location of sample points and the domains they are classified to fall into, incorporating geological structures and domain boundaries.

6.3. Variography

Variography assesses the spatial continuity, cyclicity, and the degree of anisotropy in an area. The variography subsection details results obtained from variography. First, results from cell declustering and normal score transformation are shared, followed by variogram maps and experimental variograms.

6.3.1. Cell declustering and normal score transformation

The results obtained from cell declustering are presented below. The naïve mean represents the raw data without declustering, whereas the declustered mean accounts for the declustering

weights assigned to each sample. Table 6.8 shows a selection of results obtained from cell declustering and normal score transformation.

6.3.1.1. Domain 8

Gold accumulation (cm.g/t)

The graph below illustrates the relationship between the declustered mean gold accumulation (cm.g/t) and cell size for domain 8, comparing the declustered mean against the naïve mean and the declustered mean at the smallest (minimised) cell size (Fig. 6.17). The declustered mean at very small cell sizes is high, at approximately 580 cm.g/t, but drops to below 500 cm.g/t from a cell size of approximately 80. The declustered mean fluctuates between cell sizes of 100 and 800, showing an increasing trend. Beyond 800 meters, the values stabilise at approximately 550 cm.g/t.

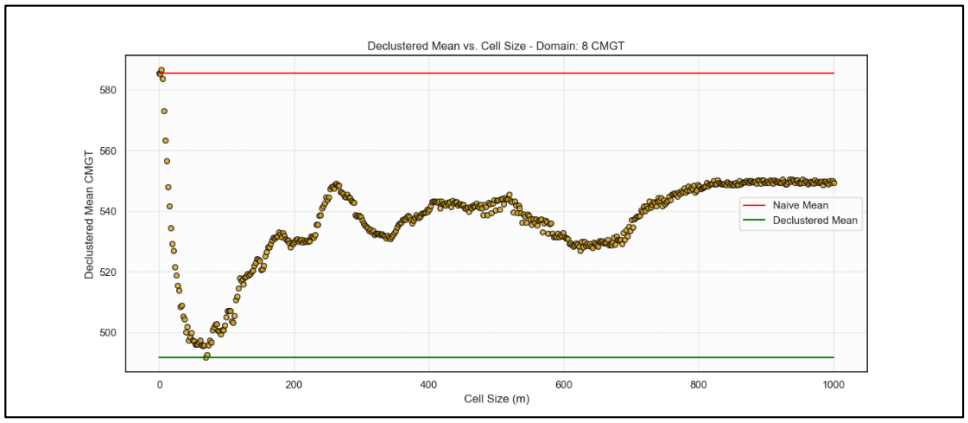


Figure 6.17: Scatter-line plot of declustered mean versus cell size for the gold accumulation (cm.g/t) in domain 8.

Table 6.8: Table showing selected weights and normal score values obtained for each variable-domain combination. X and Y represent the X- and Y-coordinates, respectively.

X	Y	Domain	Gold accumulation (cm.g/t)	Channel width (cm)	Au (g/t)	Gold accumulation (cm.g/t) declustering weights	Channel width (cm) declustering normal score	Channel width (cm) declustering weights	Channel width (cm) normal score	Au (g/t) declustering weights	Au (g/t) normal score weights
5365.4	-17708.5	18	603.2	90	6.7	7.18	0.16	1	1.21	9.89	-0.89
5368.2	-17708.8	18	547.2	70	7.82	7.18	0.06	1	0.84	9.91	-0.72
5370.7	-17708.2	18	158	73	2.16	7.18	-1.03	1	0.9	6.89	-1.82
5373.1	-17701.1	18	405.2	53	7.65	7.18	-0.23	1	0.54	6.89	-0.76
5373.2	-17682.6	18	249.34	124	2.01	7.26	-0.66	1	1.99	6.99	-1.87
5374.5	-17684.9	18	315.84	91	3.47	5.05	-0.46	1	1.22	5.76	-1.53
5375.6	-17706.4	18	332	20	16.6	4.96	-0.4	1	-0.34	5.7	0.13
5376	-17687.2	18	444.56	65	6.84	5.05	-0.15	1	0.75	5.76	-0.87
5377.2	-17681.4	18	1017.38	144	7.07	5.05	0.71	1	2.41	5.8	-0.83
5377.3	-17689.6	18	331.61	25	13.26	5.02	-0.4	1	-0.16	5.73	-0.14

Channel width (cm)

The graph below illustrates the relationship between the declustered mean channel width (cm) and cell size for domain 8, comparing the declustered mean against the naïve mean and the declustered mean at the smallest (minimised) cell size (Fig. 6.18). The declustered mean at very small cell sizes is approximately 42 cm, but drops to below 41 cm from a cell size of approximately 420. The declustered mean fluctuates between cell sizes of 0 and 800. Beyond 800 m, the values stabilise at approximately 42 cm.

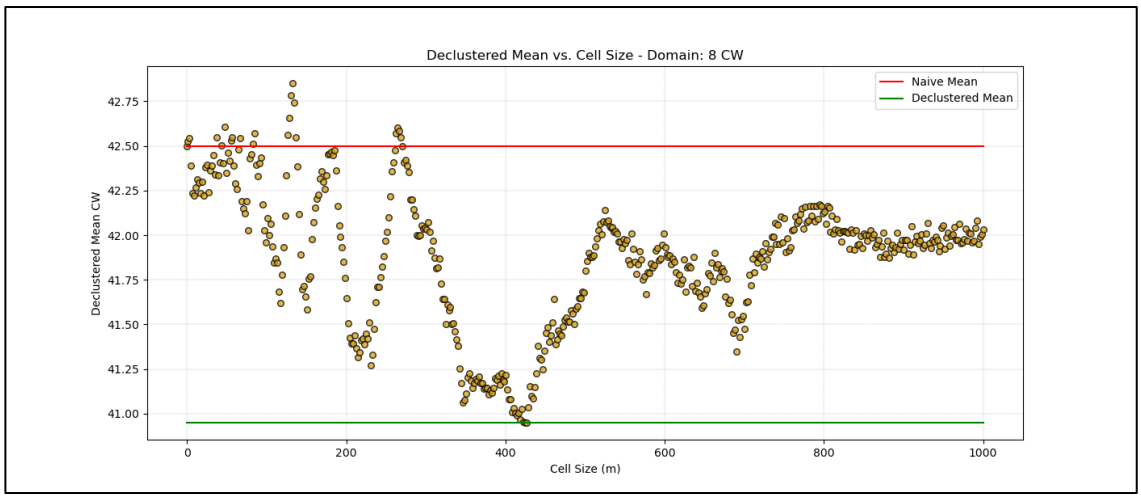


Figure 6.18: Scatter-line plot of declustered mean versus cell size for the channel width (cm) in domain 8.

Au (g/t)

The graph below illustrates the relationship between the declustered mean Au (g/t) and cell size for domain 8, comparing the declustered mean against the naïve mean and the declustered mean at the smallest (minimised) cell size (Fig. 6.19). The declustered mean at very small cell sizes is high, at approximately 26 g/t, but drops to below 22 g/t from a cell size

of approximately 80. The declustered mean fluctuates between cell sizes of 100 and 800, showing an increasing trend. Beyond 800 m, the values stabilise at approximately 23 cm.

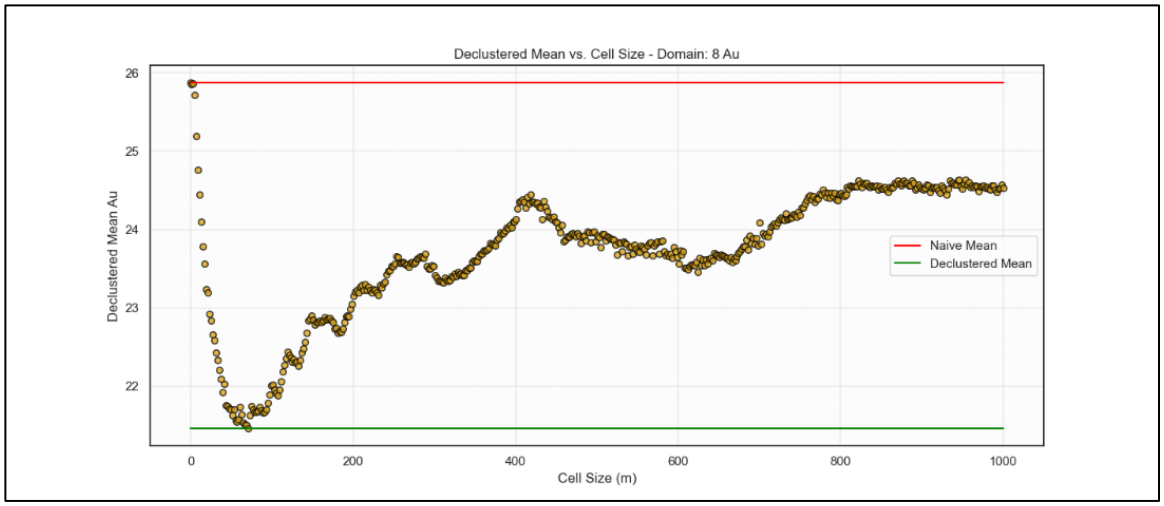


Figure 6.19: Scatter-line plot of declustered mean versus cell size for Au (g/t) in domain 8.

6.3.1.2. Domain 14

Gold accumulation (cm.g/t)

The graph below illustrates the relationship between the declustered mean gold accumulation (cm.g/t) and cell size for domain 14, comparing the declustered mean against the naïve mean and the declustered mean at the smallest minimised cell size (Fig. 6.20). The declustered mean at very small cell sizes is high, at approximately 780 cm.g/t but drops to below 670 cm.g/t from a cell size of approximately 220. The declustered mean fluctuates between cell sizes of 200, showing an increasing trend. The declustered mean value does not reach a cell size where it stabilises.

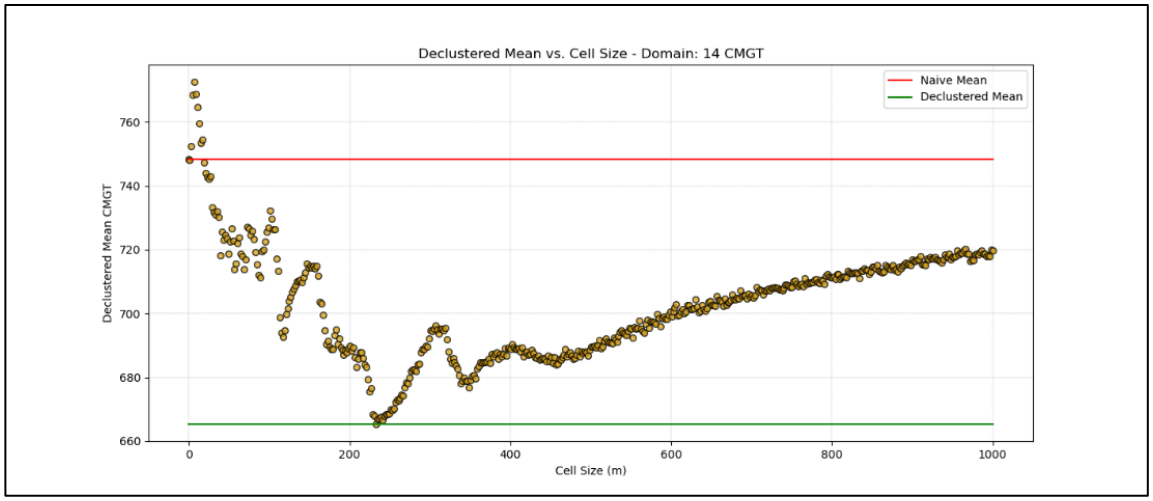


Figure 6.20: Scatter-line plot of declustered mean versus cell size for the gold accumulation (cm.g/t) in domain 14.

Channel width (cm)

The graph below illustrates the relationship between the declustered mean channel width (cm) and cell size for domain 14, comparing the declustered mean against the naïve mean and the declustered mean at the smallest (minimised) cell size. (Fig. 6.21) The declustered mean at very small cell sizes is high, at approximately 96 cm, but drops to below 93 cm from a cell size of approximately 300. The declustered mean fluctuates between cell sizes of 0 and 1000, showing an increasing trend from a cell size of 300. The declustered mean value does not reach a cell size where it stabilises.

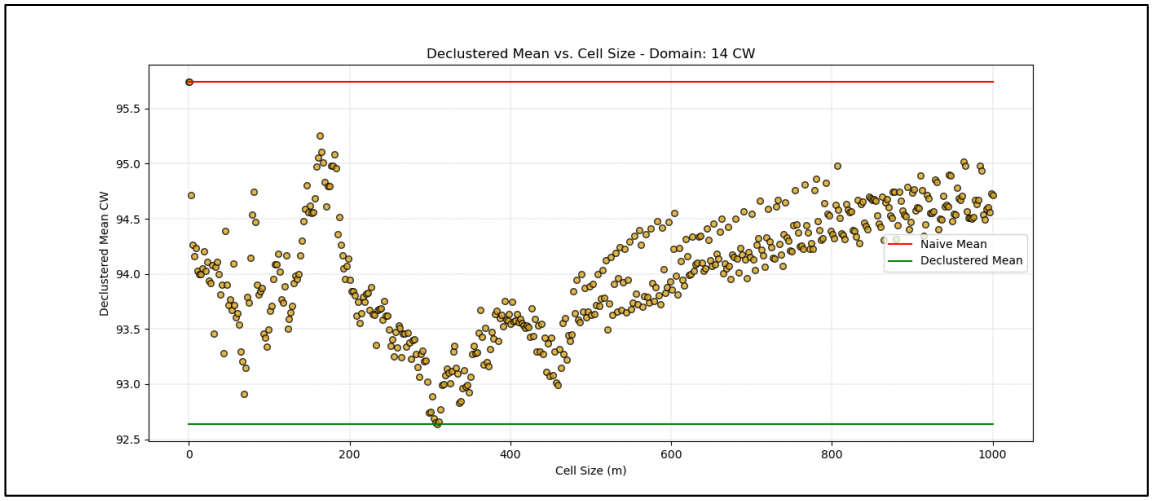


Figure 6.21: Scatter-line plot of declustered mean versus cell size for the channel width (cm) in domain 14.

Au (g/t)

The graph below illustrates the relationship between the declustered mean Au (g/t) and cell size for domain 14, comparing the declustered mean against the naïve mean and the declustered mean at the smallest (minimised) cell size (Fig. 6.22). The declustered mean at very small cell sizes is high, at approximately 11.20 g/t, but drops to below 10 g/t from a cell size of approximately 180. The declustered mean fluctuates between cell sizes of 0 and 400, showing an increasing trend. Beyond 450 m, the values stabilise at approximately 10.50 g/t.

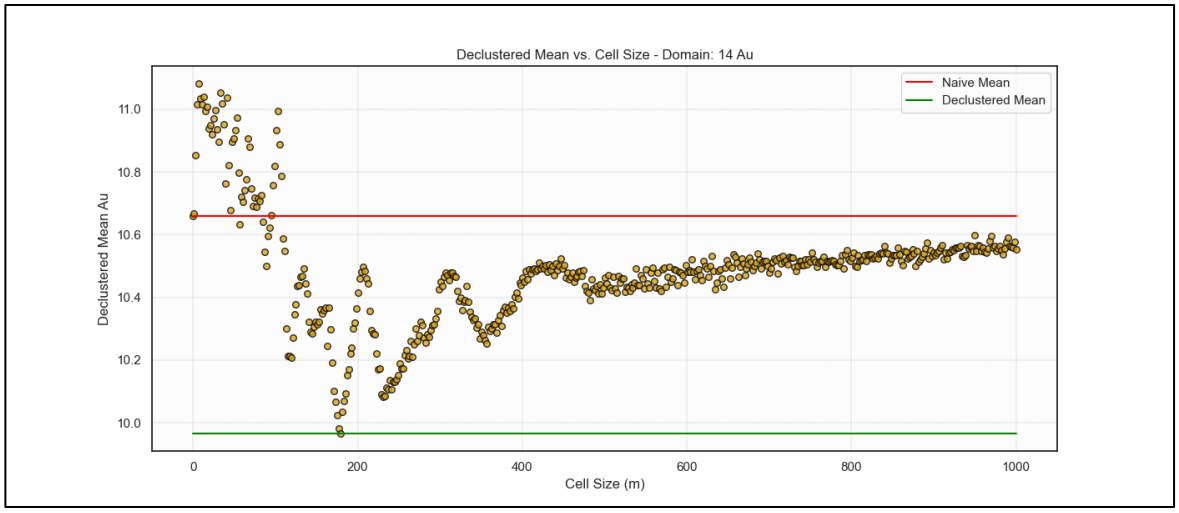


Figure 6.22: Scatter-line plot of declustered mean versus cell size for Au (g/t) in domain 14.

6.3.1.3. Domain 18

Gold accumulation (cm.g/t)

The graph below illustrates the relationship between the declustered mean gold accumulation (cm.g/t) and cell size for domain 18, comparing the declustered mean against the naïve mean and the declustered mean at the smallest (minimised) cell size (Fig. 6.21). The declustered mean at very small cell sizes is high, at approximately 825 cm.g/t, but drops to below 770 cm.g/t from a cell size of approximately 350. The declustered mean fluctuates between cell sizes of 0 and 500. Beyond 500 m, the declustered mean values steadily increase.

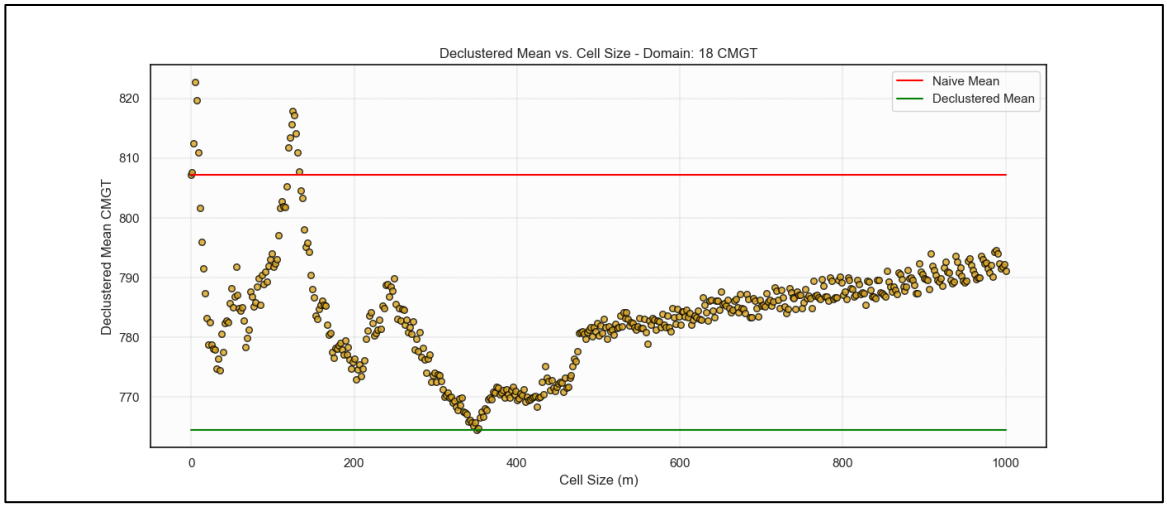


Figure 6.23: Scatter-line plot of declustered mean versus cell size for the gold accumulation (cm.g/t) in domain 18.

Channel width (cm)

The graph below illustrates the relationship between the declustered mean channel width (cm) and cell size for domain 14, comparing the declustered mean against the naïve mean and the declustered mean at the smallest (minimised) cell size (Fig. 6.24). The declustered mean at very small cell sizes is low, at approximately 42 cm, but increases to above 45 cm from a cell size of approximately 150. The declustered mean fluctuates between cell sizes of 0 and 400, showing an increasing trend until a cell size of 220. Beyond 220 m, the declustered mean values decrease.

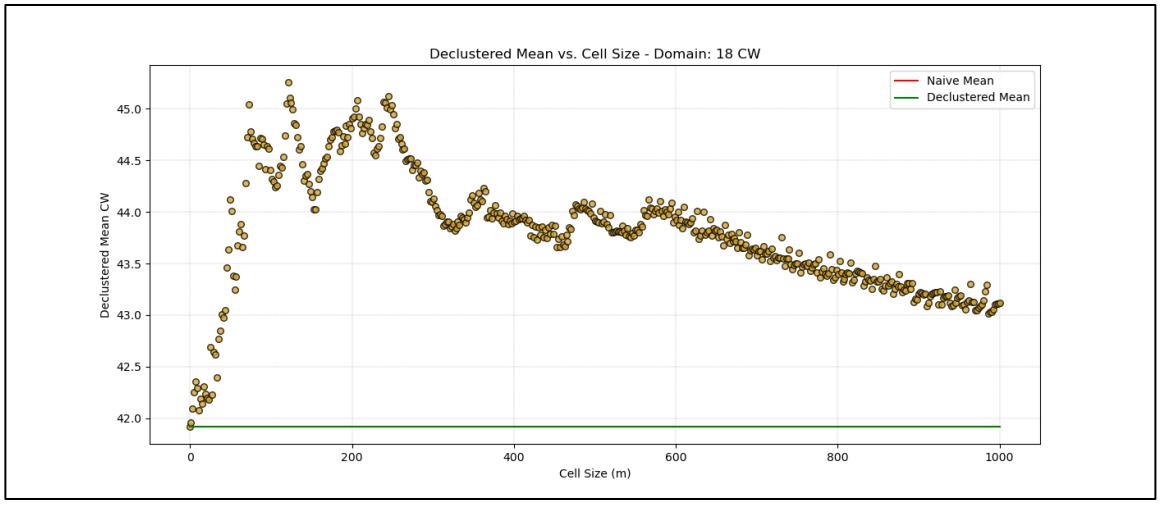


Figure 6.24: Scatter-line plot of declustered mean versus cell size for the channel width (cm) in domain 18.

Au (g/t)

The graph below illustrates the relationship between the declustered mean Au (g/t) and cell size for domain 18, comparing the declustered mean against the naïve mean and the declustered mean at the smallest (minimised) cell size (Fig. 6.25). The declustered mean at very small cell sizes is high, at approximately 25.40 g/t, but drops to below 22.5 g/t from a cell size of approximately 200. The declustered mean fluctuates between cell sizes of 200 and 1000, showing an increasing trend. The declustering cell sizes do not reach a point of stability.

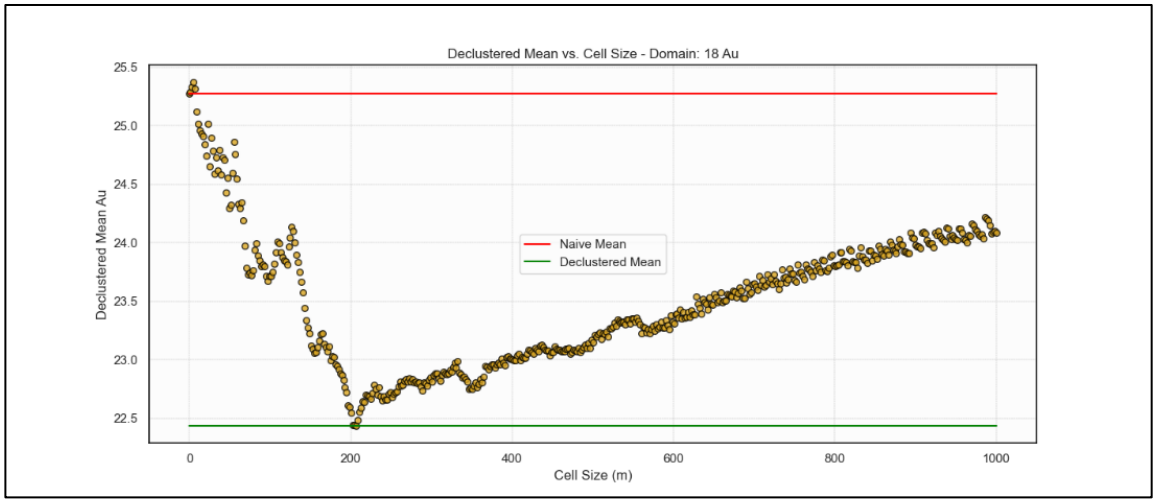


Figure 6.25: Scatter-line plot of declustered mean versus cell size for Au (g/t) in domain 18.

6.3.1.4. Domain 19

Gold accumulation (cm.g/t)

The graph below illustrates the relationship between the declustered mean gold accumulation (cm.g/t) and cell size for domain 19, comparing the declustered mean against the naïve mean and the declustered mean at the smallest (minimised) cell size (Fig. 6.26). The declustered mean at very small cell sizes is high, at approximately 780 cm.g/t, but drops to below 680 cm.g/t from a cell size of approximately 80. The declustered mean fluctuates between cell sizes of 100 and 700, showing an increasing trend. Beyond 700 m, the declustered cell size values stabilise at approximately 750 cm.g/t.

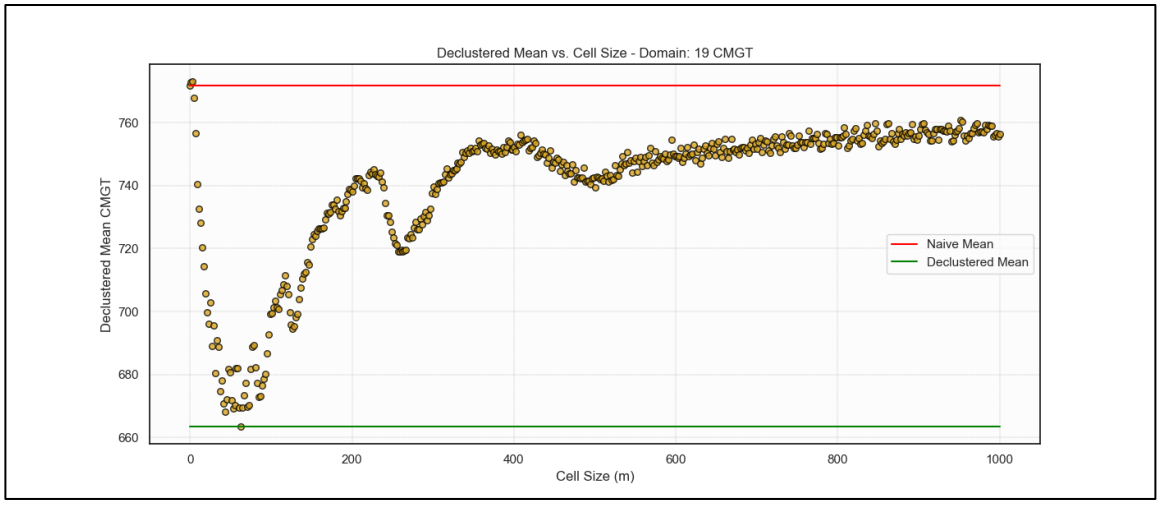


Figure 6.26: Scatter-line plot of declustered mean versus cell size for the gold accumulation (cm.g/t) in domain 19.

Channel width (cm)

The graph below illustrates the relationship between the declustered mean channel width (cm) and cell size for domain 19, comparing the declustered mean against the naïve mean and the declustered mean at the smallest (minimised) cell size (Fig. 6.27). The declustered mean at very small cell sizes is high, at approximately 40 g/t, but drops to below 35.50 g/t from a cell size of approximately 180. The declustered mean fluctuates between cell sizes of 0 and 700. Beyond 700 m, the declustered cell size values steadily increase.

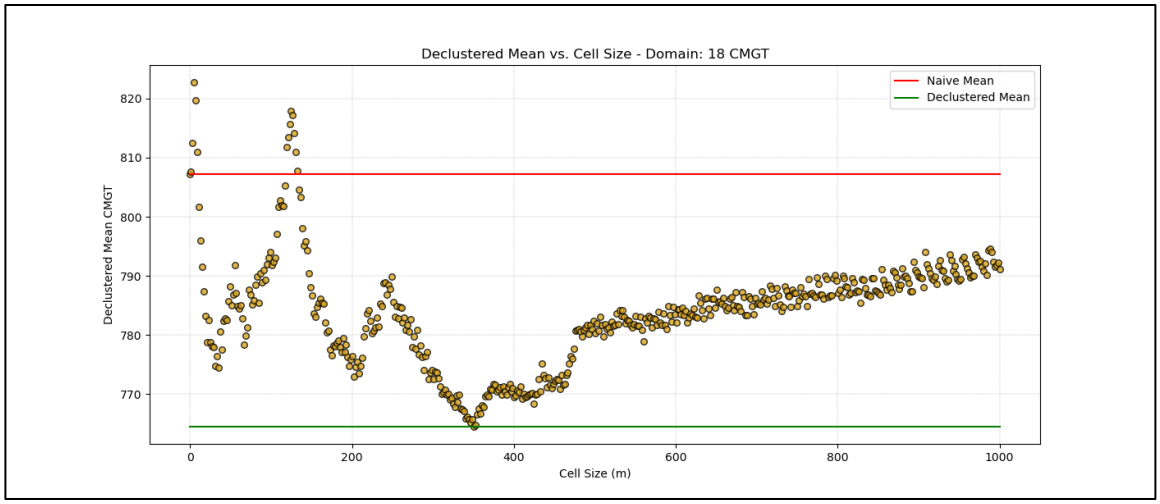


Figure 6.27: Scatter-line plot of declustered mean versus cell size for the channel widths in domain 19.

Au (g/t)

The graph below illustrates the relationship between the declustered mean Au (g/t) and cell size for domain 19, comparing the declustered mean against the naïve mean and the declustered mean at the smallest (minimised) cell size (Fig. 6.28). The declustered mean at very small cell sizes is high, at approximately 26.50 g/t but drops to below 23.5 g/t from a cell size of approximately 100. The declustered mean fluctuates between cell sizes of 100 and 550, showing an increasing trend.

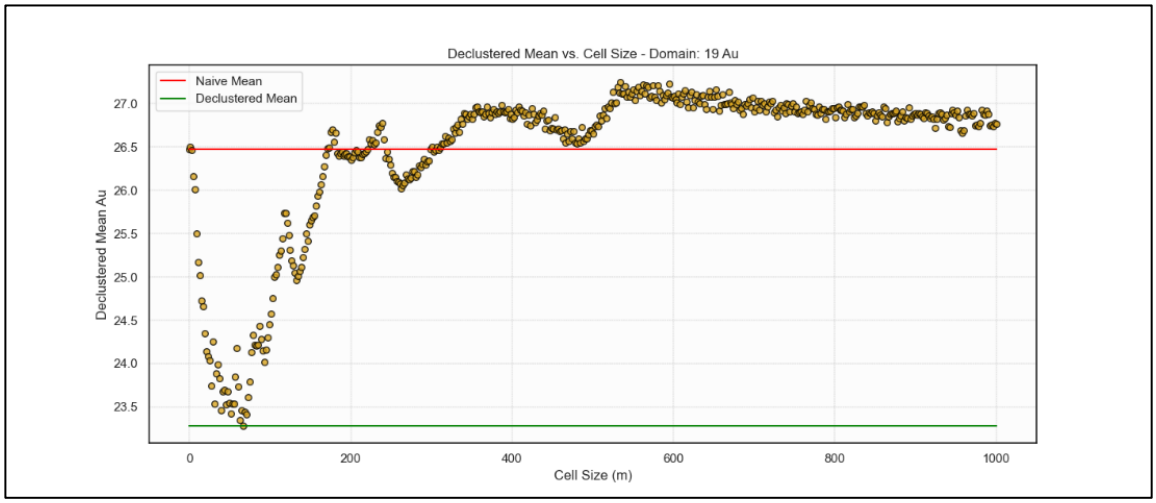


Figure 6.28: Scatter-line plot of declustered mean versus cell size for Au (g/t) in domain 19.

6.3.2. Variogram maps and experimental semi-variograms

Variogram maps and experimental semi-variograms were modelled to analyse the anisotropy, cyclicity, and continuity of the variables of interest using normal score-transformed values to provide insights into directional dependencies and structural variations within the dataset. The results from the variogram modelling are presented below, focusing on the directions of major continuity, while semi-variograms for all azimuths are included in the appendix for reference.

6.3.2.1. Domain 8

The variogram maps presented in the figure illustrate the directional continuity of different variables within domain 8 (Fig. 6.29). The results indicate that the strongest spatial continuity is observed along the north-south direction for all variables, suggesting that the underlying geological structure or mineralisation follows the same trend. There are noticeable patterns of high and low variance along the northeast-southwest directions, indicating cyclic

variations in spatial continuity. Localised high-variance zones are indicated by the red patches scattered across the maps, suggesting the presence of geological structures. Experimental semi-variogram models at 15° intervals were used to quantify the exact orientation and range of anisotropy, and major directions of continuity are modelled and fitted as shown in Figure 6.30.

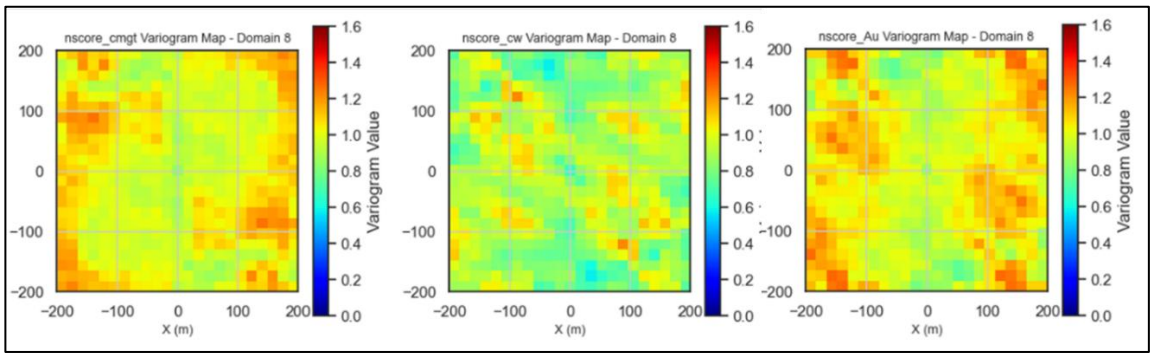


Figure 6.29: Domain 8 variogram maps for different variables. The colour scale represents the semi-variance, with blue indicating low semi-variance and red indicating high semi-variance.

Gold accumulation (cm.g/t)

The gold accumulation (cm.g/t) in domain 8 has a major direction of continuity of 165° with an orthogonal minor direction of 75°. The structure contributes 0.32 to the semi-variance and reaches a range of 148.55 m, beyond which spatial correlation diminishes. The nugget effect of 0.68 suggests moderate short-scale variability. The relatively long range indicates that gold accumulation (cm.g/t) remains spatially correlated over larger distances.

Channel width (cm)

The channel width (cm) in domain 8 has a major direction of continuity of 150° with an orthogonal minor direction of 60°. The structure contributes 0.65 to the semi-variance and

reaches a range of 134.92 m, beyond which spatial correlation diminishes. The nugget effect of 0.35 suggests less short-scale variability. The channel width (cm) measurements exhibit more spatial consistency, following a more continuous spatial pattern.

Au (g/t)

The Au (g/t) in domain 8 has a major direction of continuity of 165° with an orthogonal minor direction of 75°. The structure contributes 0.42 to the semi-variance and reaches a range of 111.57 m, beyond which spatial correlation diminishes. The nugget effect of 0.58 suggests moderate short-scale variability. The relatively shorter range indicates that the spatial correlation diminishes more quickly compared to the gold accumulation (cm.g/t) and channel width (cm).

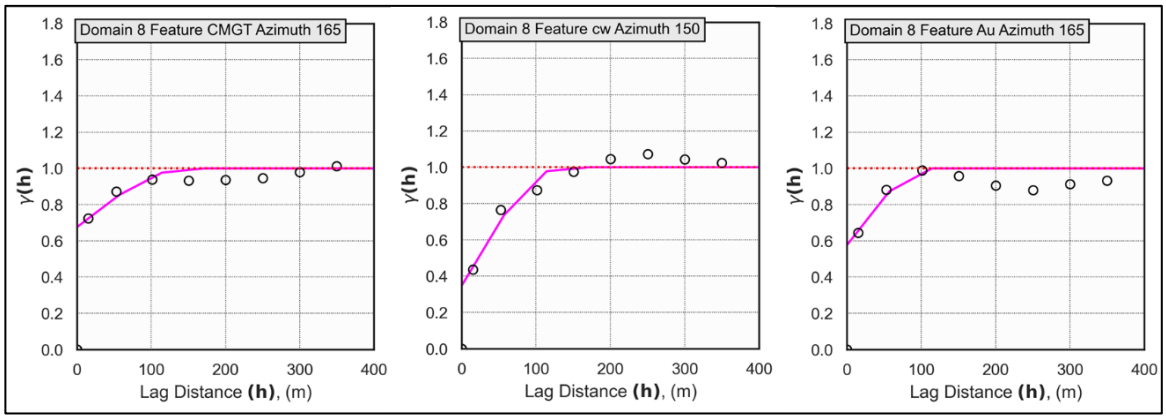


Figure 6.30: Domain 8 fitted semi-variogram models. Each graph represents an experimental semi-variogram (black circles) fitted with a spherical model (magenta curve), with the nugget effect (dotted red line) indicating short-range variability.

6.3.2.2. Domain 14

The variogram maps presented in the figure illustrate the directional continuity of different variables within domain 14 (Fig. 6.31). The results indicate that the strongest spatial continuity is observed along the northeast-southwest direction for all variables, suggesting that the underlying geological structure or mineralisation follows the same trend. There are noticeable patterns of high and low variance along the northwest-southeast directions, indicating cyclic variations in spatial continuity. Localised high-variance zones are indicated by the red patches scattered across the maps, suggesting the presence of geological structures. Experimental semi-variogram models at 15° intervals were used to quantify the exact orientation and range of anisotropy, and major directions of continuity are modelled and fitted as shown in Figure 6.32.

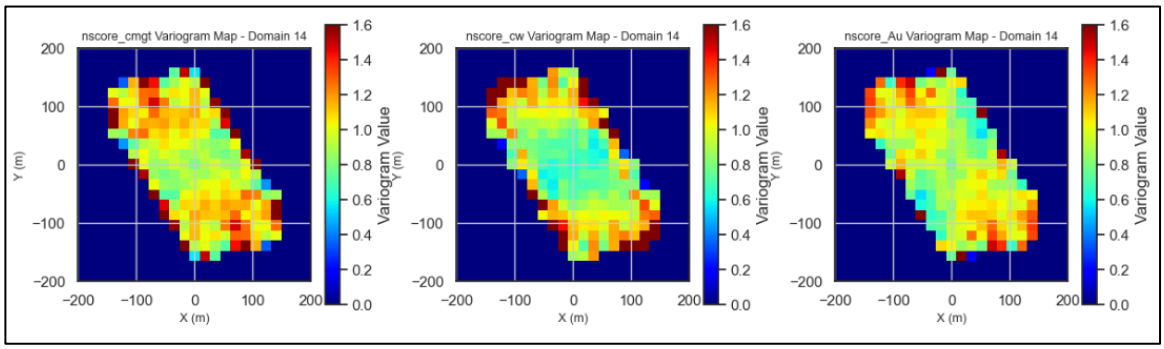


Figure 6.31: Domain 14 variogram maps for different variables. The colour scale represents the semi-variance, with blue indicating low semi-variance and red indicating high semi-variance.

Gold accumulation (cm.g/t)

The gold accumulation (cm.g/t) in domain 14 has a major direction of continuity of 150° with an orthogonal minor direction of 60°. The structure contributes 0.44 to the semi-variance

and reaches a range of 168.74 m, beyond which spatial correlation diminishes. The nugget effect of 0.56 suggests moderate short-scale variability. The long range indicates that gold accumulation (cm.g/t) remains spatially correlated over larger distances.

Channel width (cm)

The channel width (cm) in domain 14 has a major direction of continuity of 120° with an orthogonal minor direction of 30°. The structure contributes 0.43 to the semi-variance and reaches a range of 166.61 m, beyond which spatial correlation diminishes. The nugget effect of 0.57 suggests moderate short-scale variability. The long range indicates that channel width (cm) remains spatially correlated over larger distances.

Au (g/t)

The Au (g/t) in domain 14 has a major direction of continuity of 150° with an orthogonal minor direction of 60°. The structure contributes 0.45 to the semi-variance and reaches a range of 165.68 m, beyond which spatial correlation diminishes. The nugget effect of 0.55 suggests moderate short-scale variability. The long range indicates that Au (g/t) remains spatially correlated over larger distances.

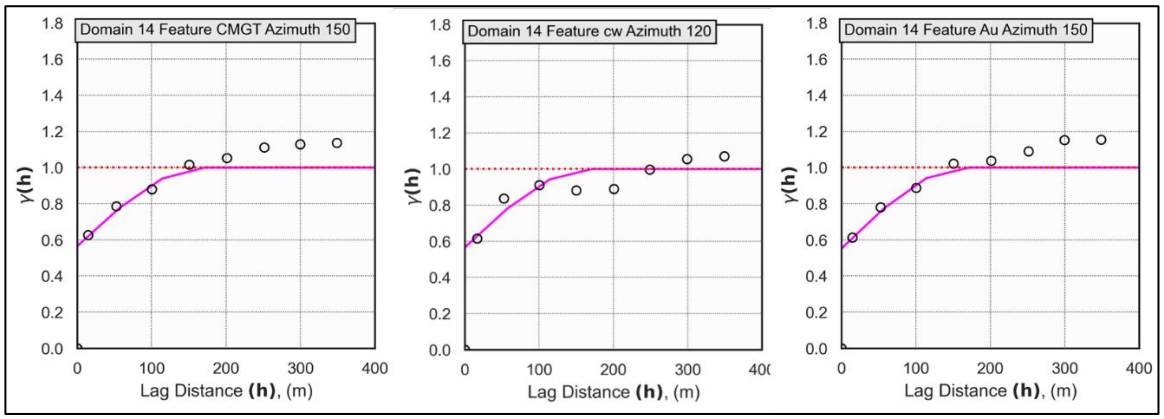


Figure 6.32: Domain 14 fitted semi-variogram models. Each graph represents an experimental semi-variogram (black circles) fitted with a spherical model (magenta curve), with the nugget effect (dotted red line) indicating short-range variability.

6.3.2.3. Domain 18

The variogram maps presented in the figure illustrate the directional continuity of different variables within domain 18 (Fig. 6.33). The results indicate that the strongest spatial continuity is observed along the northeast-southwest direction for the gold accumulation (cm.g/t) and channel width, and the northwest-southeast direction for Au, suggesting that the underlying geological structure or mineralisation follows the same trend. There are noticeable patterns of high and low variance along the northwest-southeast directions for gold accumulation and channel width and in the northeast-southwest direction for Au, indicating cyclic variations in spatial continuity. Localised high-variance zones are also indicated by the red patches scattered across the maps, suggesting the presence of geological structures. Experimental semi-variogram models at 15° intervals were used to quantify the exact orientation and range of anisotropy, and major directions of continuity are modelled and fitted as shown in Figure 6.34.

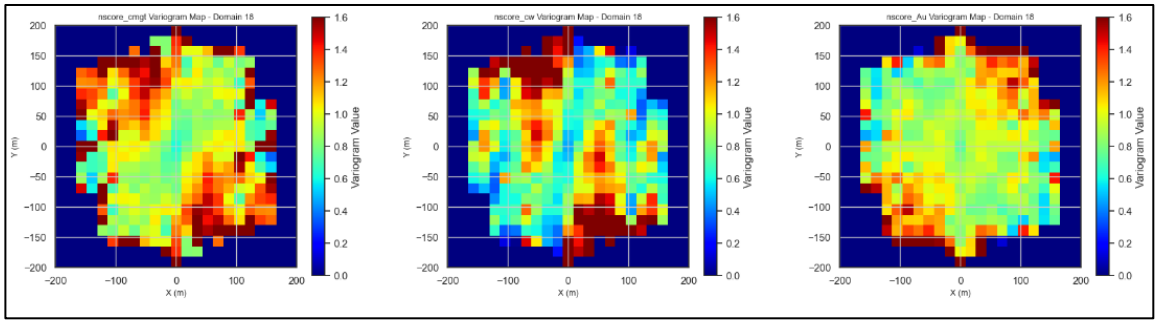


Figure 6.33: Domain 18 variogram maps for different variables. The colour scale represents the semi-variance, with blue indicating low semi-variance and red indicating high semi-variance.

Gold accumulation (cm.g/t)

The gold accumulation (cm.g/t) in domain 18 has a major direction of continuity of 30° with an orthogonal minor direction of 120°. The structure contributes 0.55 to the semi-variance and reaches a range of 225.09 m, beyond which spatial correlation diminishes. The nugget effect of 0.45 suggests moderate short-scale variability. The long range indicates that gold accumulation (cm.g/t) remains spatially correlated over larger distances.

Channel width (cm)

The channel width (cm) in domain 18 has a major direction of continuity of 0° with an orthogonal minor direction of 90°. The structure contributes 0.77 to the semi-variance and reaches a range of 318.94 m, beyond which spatial correlation diminishes. The nugget effect of 0.23 suggests high short-scale variability. The long range indicates that channel width (cm) remains spatially correlated over larger distances.

Au (g/t)

The Au (g/t) in domain 18 has a major direction of continuity of 165° with an orthogonal minor direction of 75°. The structure contributes 0.37 to the semi-variance and reaches a range of 147.85 m, beyond which spatial correlation diminishes. The nugget effect of 0.63 suggests moderate short-scale variability. The relatively short range indicates that Au (g/t) spatially correlations diminish over larger distances.

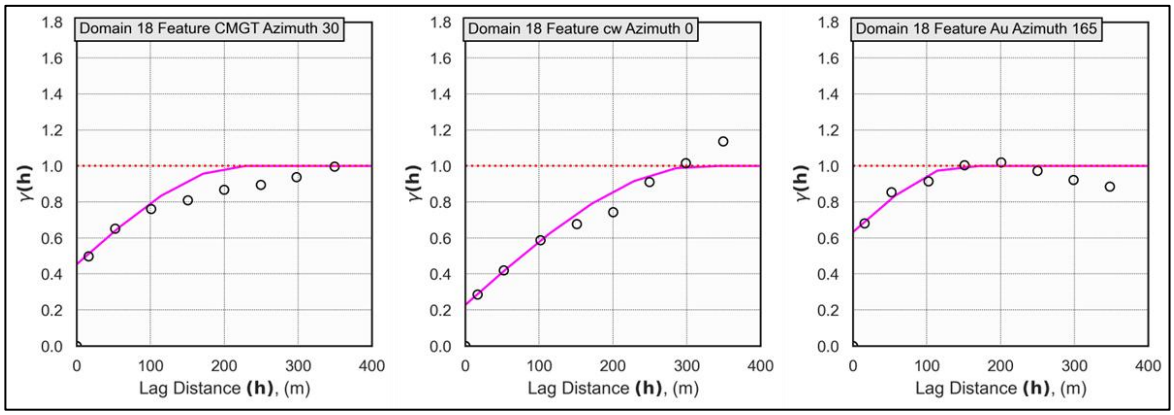


Figure 6.34: Domain 18 fitted semi-variogram models. Each graph represents an experimental semi-variogram (black circles) fitted with a spherical model (magenta curve), with the nugget effect (dotted red line) indicating short-range variability.

6.3.2.4. Domain 19

The variogram maps presented in the figure illustrate the directional continuity of different variables within domain 19 (Fig. 6.35). The results indicate that the strongest spatial continuity is observed along both the northwest-southeast and northeast and southwest directions for all variables, suggesting that the underlying geological structure or mineralisation follows the same trend. There are noticeable patterns of high and low variance along the northeast-southwest directions, indicating cyclic variations in spatial continuity. Localised high-variance zones are also indicated by the red patches scattered across the maps, suggesting

the presence of geological structures. Experimental semi-variogram models at 15◦ intervals were used to quantify the exact orientation and range of anisotropy, and major directions of continuity are modelled and fitted as shown in Figure 6.36.

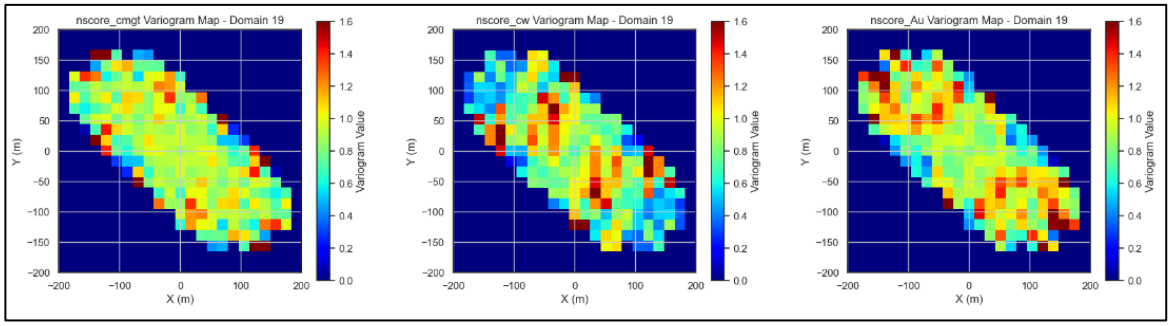


Figure 6.35: Domain 19 variogram maps for different variables. The colour scale represents the semi-variance, with blue indicating low semi-variance and red indicating high semi-variance.

Gold accumulation (cm.g/t)

The gold accumulation (cm.g/t) in domain 19 has a major direction of continuity of 0° with an orthogonal minor direction of 90°. The structure contributes 0.41 to the semi-variance and reaches a range of 99.55 m, beyond which spatial correlation diminishes. The nugget effect of 0.59 suggests moderate short-scale variability. The short range indicates that gold accumulation (cm.g/t)'s correlation diminishes over shorter distances.

Channel width (cm)

The channel width (cm) in domain 19 has a major direction of continuity of 165° with an orthogonal minor direction of 75°. The structure contributes 0.7 to the semi-variance and reaches a range of 134.92 m, beyond which spatial correlation diminishes. The nugget effect

of 0.30 suggests low short-scale variability. The relatively long range indicates that channel width (cm) remains spatially correlated over larger distances.

Au (g/t)

The Au (g/t) in domain 19 has a major direction of continuity of 60° with an orthogonal minor direction of 150°. The structure contributes 0.29 to the semi-variance and reaches a range of 111.57 m, beyond which spatial correlation diminishes. The nugget effect of 0.71 suggests high short-scale variability. The relatively long range indicates that Au (g/t) remains spatially correlated over larger distances.

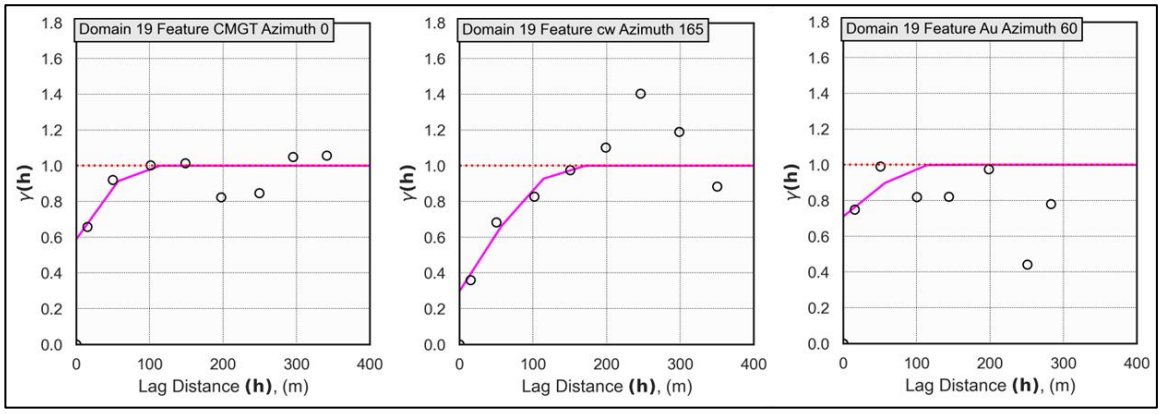


Figure 6.36: Domain 19 fitted semi-variogram models. Each graph represents an experimental semi-variogram (black circles) fitted with a spherical model (magenta curve), with the nugget effect (dotted red line) indicating short-range variability.

Results from variogram modelling are summarised in Table 6.9.

Table 6.9: Variogram summary parameters for different variables within the domains. X and Y represent the X- and Y-coordinates.

Domain	Variable	Major Azimuth	Major Range	Major Nugget	Major Contribution to sill	Major sill	Minor Azimuth	Minor Range	Minor Nugget	Minor Contribution to sill	Minor sill
8	Gold accumulation (cm.g/t)	165	148.55	0.68	0.32	1	75	122.48	0.72	0.28	1
	Channel width (cm)	150	134.92	0.35	0.65	1	60	87.39	0.42	0.58	1
	Au (g/t)	165	111.56	0.58	0.42	1	75	101.41	0.68	0.32	1
14	Gold accumulation (cm.g/t)	150	168.74	0.56	0.44	1	60	125.44	0.72	0.28	1
	Channel width (cm)	120	166.61	0.57	0.43	1	30	155.02	0.66	0.34	1
	Au (g/t)	150	165.68	0.55	0.45	1	60	0	0.76	0.24	1
18	Gold accumulation (cm.g/t)	30	225.09	0.45	0.55	1	120	139.41	0.49	0.51	1
	Channel width (cm)	0	318.94	0.23	0.77	1	90	104.33	0.3	0.7	1
	Au (g/t)	165	147.86	0.63	0.37	1	75	91.1	0.69	0.31	1
19	Gold accumulation (cm.g/t)	0	95.55	0.59	0.41	1	90	50.55	0.66	0.34	1
	Channel width (cm)	165	157.81	0.3	0.7	1	75	55.41	0.15	0.84	1
	Au (g/t)	60	122.2	0.71	0.23	1	150	63.03	0.57	0.43	1

6.4. Kriging Neighbourhood Analysis

Kriging metrics such as block size, optimal number of samples, search range and discretisation numbers required for ordinary kriging were determined through quantitative kriging neighbourhood analysis. Quantitative kriging neighbourhood analysis is a process that involves determining the discretisation size, block size, search radius and the number of samples required to accurately estimate mineral resources to avoid bias and over-smoothing. The following are results obtained from the methodology outlined in Chapter 5.

6.4.1. Discretisation

Discretisation is the process of subdividing estimation blocks into smaller sub-blocks, and the discretisation value is the number of subdivisions per block (Amwaama, 2018). In this study, the KneeLocator was unsuccessful in detecting the inflection point. Consequently, random values were selected as possible discretisation values. However, five was chosen as the discretisation number for all variable-domain combinations. A discretisation value of five is acceptable as the discretisation versus variance curves begin to flatten and the sample variance is relatively low (Fig. 6.37). Discretisation values were used to optimise kriging parameters across different sample numbers and evaluate the quality of kriging estimates for various variable-domain combinations. Variogram parameters and discretisation values were extracted to determine the search neighbourhood size for kriging. If the minimum required sample count was met, kriging was executed to generate estimation matrices.

A range of quantitative kriging neighbourhood analysis metric values, including kriging efficiency, slope of regression, and the mean kriging-derived estimate, were obtained from the quantitative kriging neighbourhood analysis (e.g., Table 6.10). Finally, the kriged estimates computed are validated by calculating absolute error (*i.e.*, the absolute difference between the

mean of the observed sampled data values and the kriging-estimated mean). Graphs of kriging variance against discretisation values are created to visualise how the change in kriging variance within the estimation blocks at different discretisation levels (Fig. 6.37).

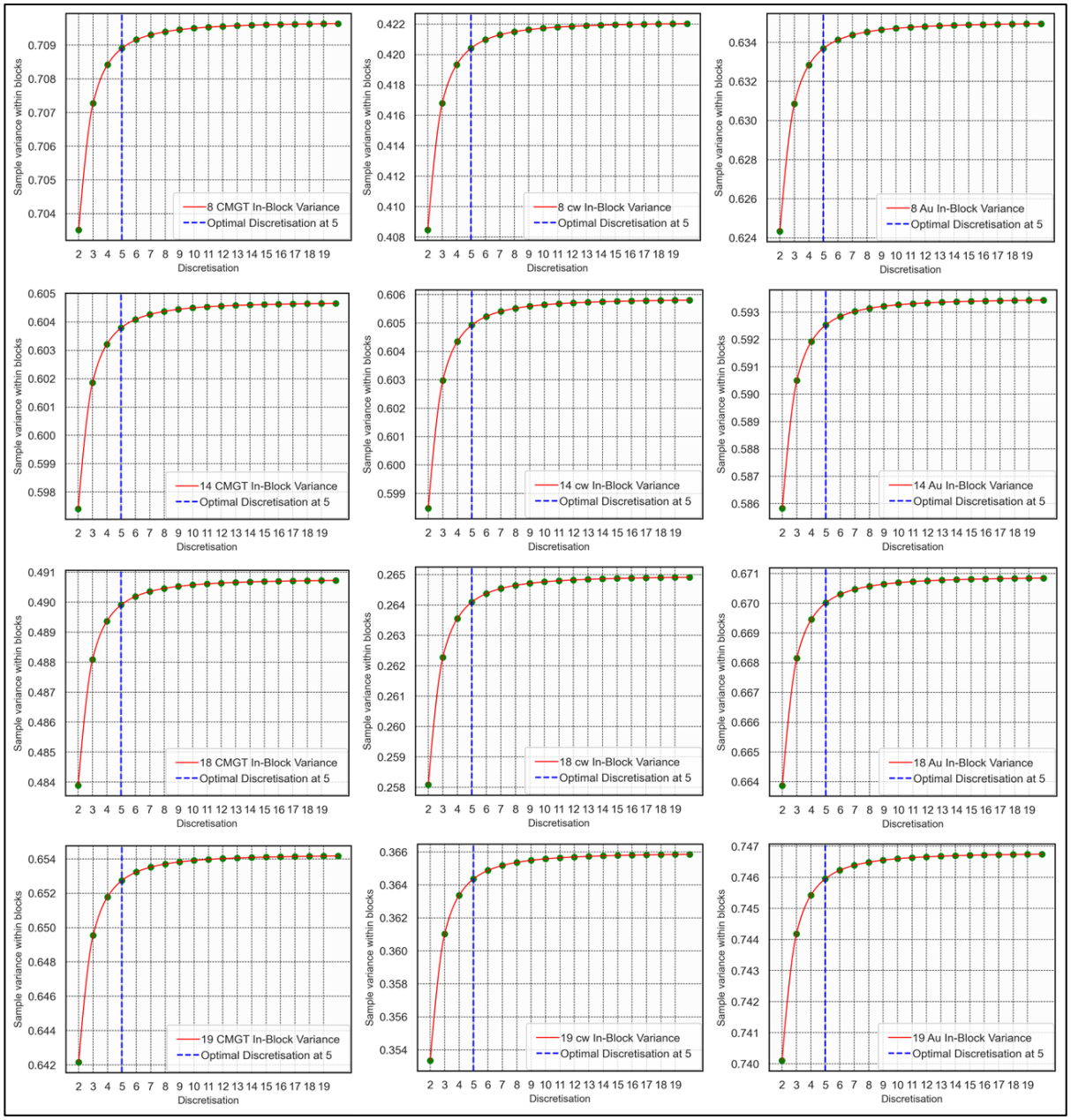


Figure 6.37: Graphs showing how discretisation varies with sample in-block variance for different variables of each domain. CMGT represents the gold accumulation (cm.g/t), CW represents the channel width (cm), and Au represents Au (g/t).

6.4.2. Optimal sample numbers

A range of values for the declustered mean, kriged mean, estimated value of kriging, kriging efficiency, kriging slope of regression, and absolute error were obtained for the different sample numbers used in the estimation of each variable for each domain (Table 6.10). Kriging efficiency and slope of regression point scores were plotted against the number of samples for each variable-domain combination to determine the optimal sample size required for estimation using the KneeLocator method (Fig. 6.38).

Table 6.10: Table showing a selection of the first ten rows of results from the QKNA post-validation results.

Domain	Variable	Declustered mean	Kriging mean	Kriged estimate	Kriging efficiency	Slope of regression	Number of samples	Absolute Error
8	Gold accumulation (cm.g/t)	585.50	494.95	494.95	0.94	0.91	5.00	90.54
8	Gold accumulation (cm.g/t)	585.50	497.24	497.24	0.95	0.92	7.00	88.25
8	Gold accumulation (cm.g/t)	585.50	498.99	498.99	0.96	0.93	9.00	86.51
8	Gold accumulation (cm.g/t)	585.50	501.72	501.72	0.96	0.94	11.00	83.78
8	Gold accumulation (cm.g/t)	585.50	500.24	500.24	0.97	0.95	13.00	85.26
8	Gold accumulation (cm.g/t)	585.50	499.86	499.86	0.97	0.95	15.00	85.63
8	Gold accumulation (cm.g/t)	585.50	499.66	499.66	0.97	0.95	17.00	85.84
8	Gold accumulation (cm.g/t)	585.50	501.33	501.33	0.97	0.96	19.00	84.16
8	Gold accumulation (cm.g/t)	585.50	501.74	501.74	0.98	0.96	21.00	83.76
8	Gold accumulation (cm.g/t)	585.50	504.20	504.20	0.98	0.96	23.00	81.30

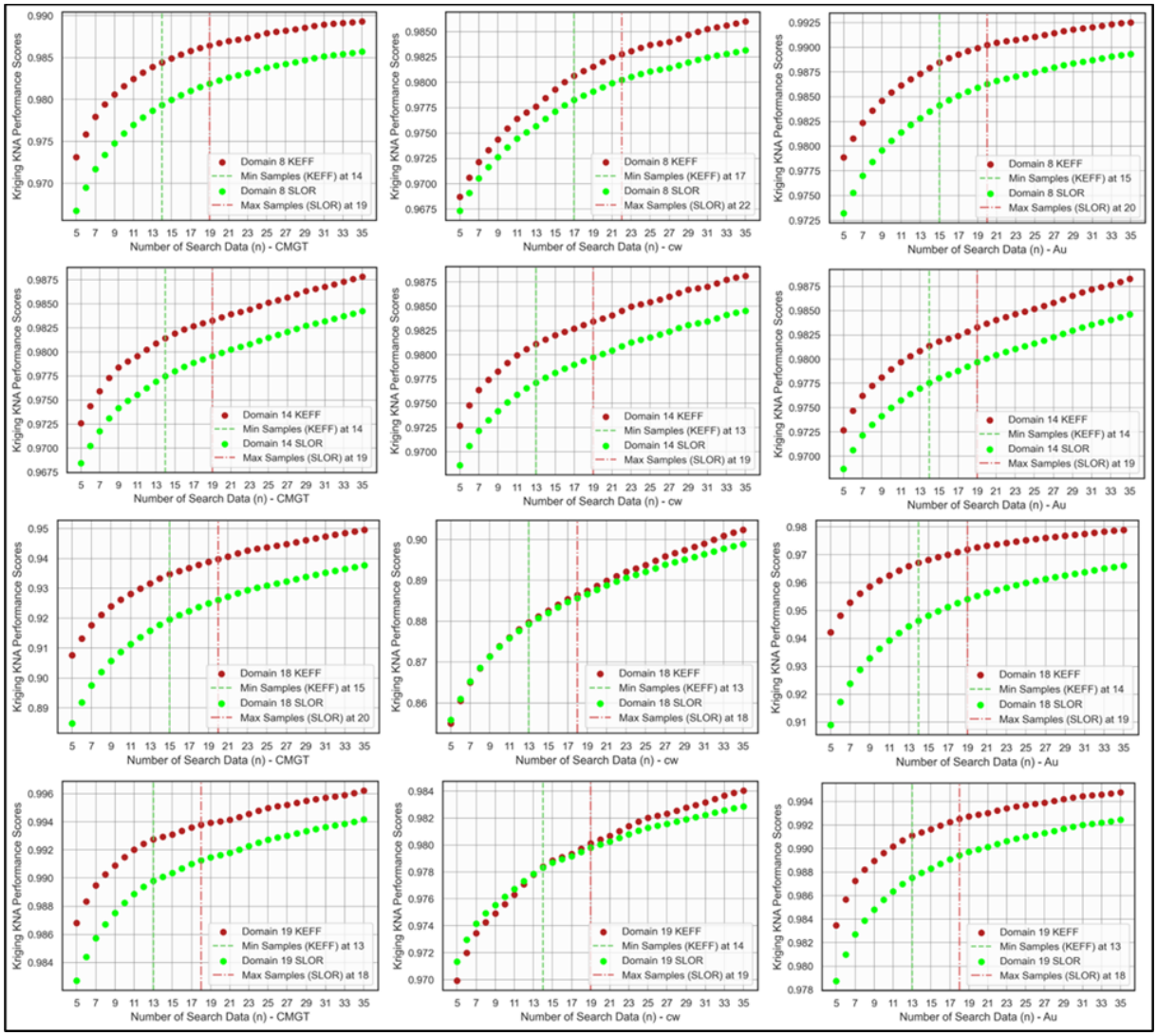


Figure 6.38: Graph showing how the slope of regression and kriging efficiency change with increasing number of search data for each variable within each domain. The graphs also indicate the optimal number of samples that should be used for kriging. CMGT represents the gold accumulation (cm.g/t), CW represents the channel width (cm), Au represents Au (g/t), KEFF represents the kriging efficiency, and SLOR represents the slope of regression.

Table A1 shows the results from quantitative neighbourhood analysis. A discretisation value of five in a 20 × 20 m estimation block, with sample numbers ranging between five and thirty-five, yields varying kriging efficiency and slope of regression values for the different variable-domain combinations. The minimum kriging efficiency and slope of regression values are 0.896 and 0.908, respectively, while the maximum values are 0.996 and 0.992, respectively (Fig. 6.39). The highest values correspond to domain 19's the gold accumulation values at a sample number of thirty-five, whereas the lowest values are associated with domain 18's channel width (cm) values at a sample number of five.

All kriging efficiency and slope of regression values are positive and close to one, indicating that the block variance is approximately equal to the true block variance and that the kriged estimates exhibit a low degree of conditional bias when using variogram parameters. Slope of regression values closer to one are linked to a higher number of samples, which is generally desirable; however, an excessive number of samples can lead to over-smoothing of estimates.

Table 6.11: Table summarising minimum and maximum samples required for optimal estimation of reserves.

Domain	Variable	Minimum Samples	Maximum Samples
8	Gold accumulation (cm.g/t)	13	19
	Channel width (cm)	15	20
	Au (g/t)	13	19
14	Gold accumulation (cm.g/t)	11	17
	Channel width (cm)	11	17
	Au (g/t)	14	19
18	Gold accumulation (cm.g/t)	16	19
	Channel width (cm)	18	21
	Au (g/t)	16	21
19	Gold accumulation (cm.g/t)	17	21
	Channel width (cm)	15	20
	Au (g/t)	13	19

Kriging efficiency and slope of regression values were used to determine the optimal number of samples for estimation by plotting kriging efficiency against the number of samples and applying the Knee Locator method to identify the point where the curves begin to flatten.

A close assessment of results from Tables 6.10, 6.11, and A2 aided in the choice of estimation parameters. The following was observed: kriging efficiency and slope of regression increase with an increase in the number of samples used in estimation and a decrease in the absolute error; the kriged estimate and kriged mean values are equal, as expected; the

declustered mean never equals the kriged mean for each sample size; it is always larger between sample sizes of 5 to 35.

The 20 x 20 m block size was selected based on quantitative kriging neighbourhood results, ensuring a balance between estimation accuracy, data support, and kriging efficiency. A minimal difference between the absolute error of a 19 x 19 m and a 21 x 21 m block size was observed compared to other block sizes. The two block sizes under consideration exhibited a high kriging efficiency and a slope of regression close to one, indicating a strong correlation between true and estimated values. Additionally, the 20 x 20 m block size minimised kriging variance and reduced estimation uncertainty while maintaining spatial resolution. The selection also considered adequate data support, ensuring each block contained sufficient sample data without over-smoothing. The table below (Table 6.11) summarises different kriging parameters used in determining the kriging parameters that will be used.

Table 6.12: Table summarising the parameters used for kriging as determined from variography and quantitative kriging neighbourhood analysis.

Parameter	Description	Value (if assigned)
xmin	Minimum X-coordinate of the grid.	Calculated from domain_poly_points.X.min()
xmax	Maximum X-coordinate of the grid.	Calculated from domain_poly_points.X.max()
ymin	Minimum Y-coordinate of the grid.	Calculated from domain_poly_points.Y.min()
ymax	Maximum Y-coordinate of the grid.	Calculated from domain_poly_points.Y.max()
xsiz	Grid cell size in the X-direction.	20
ysiz	Grid cell size in the Y-direction.	20
tmin	Minimum threshold for the target variable.	-99999
tmax	Maximum threshold for the target variable.	99999
nst	Number of nested structures in the variogram.	2
it1	Type of variogram for the first nested structure.	1 (spherical)
it2	Type of variogram for the second nested structure.	1 (spherical)
it3	Type of variogram for the third nested structure.	1
min_samples	Minimum number of samples required for kriging.	5
ktype	Type of kriging to be performed (1: Ordinary Kriging).	Ordinary kriging
xmn	X-coordinate of the grid origin (center of the first cell).	xmin + xsiz / 2
ymn	Y-coordinate of the grid origin (center of the first cell).	ymin + ysiz / 2
nx	Number of grid cells in the X-direction.	Calculated as (xmax - xmin) / xsiz
ny	Number of grid cells in the Y-direction.	Calculated as (ymax - ymin) / ysiz
nxdis, nydis	Discretisation values in X and Y directions for blocks.	Derived from optimal_discretisations, clipped to 3–8
ndmin	Minimum number of samples required for kriging per block.	From min_max_samples_dict (default: 10)
ndmax	Maximum number of samples allowed for kriging per block.	From min_max_samples_dict (default: 25)
search_radius	Radius for sample search during kriging.	Equal to hmaj1 (major range of variogram)
keff	Kriging efficiency calculated for each block.	Derived from kriging variance.
slor	Slope of regression for kriging estimates.	Derived from kriging variance and weights.

6.5. Ordinary Kriging

Kriging analysis was conducted for each variable across multiple geological domains. Ordinary kriging results include spatial estimates, kriging variance, kriging efficiency, and slope of regression values, providing insights into the spatial continuity and reliability of predictions. The estimation parameters were based on the spatial distribution of samples and variography. The search radius was set to the major range of the variogram, while the 20 x 20 parent blocks use a discretisation of five with a minimum sample number of five to better represent block volumes based on parameters defined in the quantitative kriging neighbourhood analysis.

The ordinary kriging section will discuss results obtained from kriging, with focus on the variable-domain combination results. A summary of results from the ordinary kriging estimation is tabulated in Table 6.13. Some blocks do not contain kriged estimates due to an insufficient number of samples. The blocks that do not contain kriged estimate values were removed from the kriged estimate results, and their summary statistics were calculated (Table 6.14). Tables 6.13 and 6.14 indicate that from the 72,072 blocks created within the study area, only a total of 13,066 blocks contained enough samples to estimate variables. Some of the blocks that were removed are in areas that were not sampled due to geological structures (*e.g.*, Fig. 5.1). Apart from kriging variance, there is minimal difference between summary statistics in Table 6.13 and Table 6.14. The results summarised in Table 6.14 are used for further analysis of kriging results.

Table 6.13: Summary statistics of results obtained through ordinary kriging, including values that are NaN.

	Variable	Count	Mean	Standard deviation	Minimum	25th percentile	Median	75th percentile	Maximum
Kriged estimates	Gold accumulation (cm.g/t)	6306	625.25	454.96	51.79	309.85	476.37	810.24	3104.34
	Channel width (cm)	6971	51.76	33.27	7.91	26.52	41.11	71.54	206.08
	Au (g/t)	5611	19.57	14.79	1.15	9.52	15.63	25.16	147.68
Kriging variance	Gold accumulation (cm.g/t)	24024	736.83	439.46	0.00	0.47	999.00	999.00	999.00
	Channel width (cm)	24024	709.23	453.22	0.00	0.57	999.00	999.00	999.00
	Au (g/t)	24024	765.72	422.59	0.00	999.00	999.00	999.00	999.00
Kriging efficiency	Gold accumulation (cm.g/t)	24024	0.21	0.35	0.00	0.00	0.00	0.53	1.00
	Channel width (cm)	24024	0.18	0.30	0.00	0.00	0.00	0.43	1.00
	Au (g/t)	24024	0.18	0.34	0.00	0.00	0.00	0.00	1.00
Slope of regression	Gold accumulation (cm.g/t)	24024	0.97	0.06	0.69	1.00	1.00	1.00	1.00
	Channel width (cm)	24024	0.97	0.07	0.65	0.96	1.00	1.00	1.00
	Au (g/t)	24024	0.95	0.10	0.57	0.97	1.00	1.00	1.00

Table 6.14: Summary statistics of results obtained through ordinary kriging, excluding blocks that were not estimated due to insufficient sample numbers.

	Variable	Count	Mean	Standard deviation	Minimum	25th percentile	Median	75th percentile	Maximum
Kriged estimates	Gold accumulation (cm.g/t)	4405	545.94	360.283	51.7903	294.429	453.549	682.591	3104.34
	Channel width (cm)	4512	47.3467	33.9848	7.90734	22.8982	36.0752	62.2985	206.076
	Au (g/t)	4149	20.2382	15.4734	1.15468	9.2078	16.1662	26.5347	147.675
Kriging variance	Gold accumulation (cm.g/t)	4405	0.21196	0.11392	6.4E-05	0.13263	0.2207	0.25477	0.53517
	Channel width (cm)	4512	0.39203	0.17829	0.00011	0.2654	0.42398	0.53025	0.74802
	Au (g/t)	4149	0.21616	0.10203	1.4E-05	0.13593	0.2419	0.30664	0.41727
Kriging efficiency	Gold accumulation (cm.g/t)	4405	0.78804	0.11392	0.46483	0.74524	0.77931	0.86737	0.99994
	Channel width (cm)	4512	0.60797	0.17829	0.25198	0.46975	0.57602	0.7346	0.99989
	Au (g/t)	4149	0.78384	0.10203	0.58273	0.69336	0.7581	0.86407	0.99999
Slope of regression	Gold accumulation (cm.g/t)	4405	0.91189	0.06319	0.65522	0.88578	0.9399	0.95789	1
	Channel width (cm)	4512	0.89128	0.09536	0.57439	0.84067	0.92621	0.96597	1
	Au (g/t)	4149	0.91495	0.06104	0.7092	0.88565	0.9408	0.96065	0.9894

6.5.1. Kriged estimates

Spatial estimates represent the predicted values of the variable throughout the study area. For each variable-domain combination, the kriging estimates were computed on a 20 × 20 m block model size. The kriged estimates highlight regions of high and low concentration, aligning with observed data trends. High variability in the kriged estimates is noted throughout the study area for each variable of interest. The following paragraphs detail results from ordinary kriging.

6.5.1.1. Gold accumulation (cm.g/t)

The gold accumulation (cm.g/t) kriging estimates reveal distinct spatial patterns across the domains, as illustrated in Figure 6.39. The statistical analysis of the gold accumulation (cm.g/t) indicates a minimum value of 51.79 cm.g/t and a maximum of 3,103.34 cm.g/t, with a mean of 545.94 cm.g/t and a standard deviation of 360.28. The statistics highlight the variability in gold accumulation (cm.g/t) across the study area. The distribution of gold accumulation (cm.g/t) values suggests that most estimates are concentrated below 1000 cm.g/t, indicating that high-grade zones are limited to specific areas.

The spatial distribution of gold accumulation (cm.g/t) values reveals that the highest gold accumulation zones are concentrated in the central and southern regions of the study area. Lower gold accumulation (cm.g/t) values dominate the edges of the study area. Analysis of the gold accumulation (cm.g/t) values per domain indicates that there is variability in spatial distribution. Domain 19 contains the highest average gold accumulation (cm.g/t) estimates. Higher estimated values are concentrated along the border between domains 8 and 18, along the eastern portion of domain 8, and along the western portion of domain 14.

Regions with high gold accumulation (cm.g/t) concentrations are affected by faulting (Fig. 6.39). The presence of faults in high gold accumulation (cm.g/t) areas, such as the central region of the study area, implies that these geological structures may have acted as pathways for mineralising fluids or as zones of structural weakness, leading to gold concentration. Similarly, dykes traverse areas of moderate to high gold accumulation (cm.g/t), potentially acting as either barriers or conduits for mineralisation. Preferential sampling is observed within the areas of higher gold accumulation (cm.g/t) estimated values, indicating localised enrichment and sampling bias.

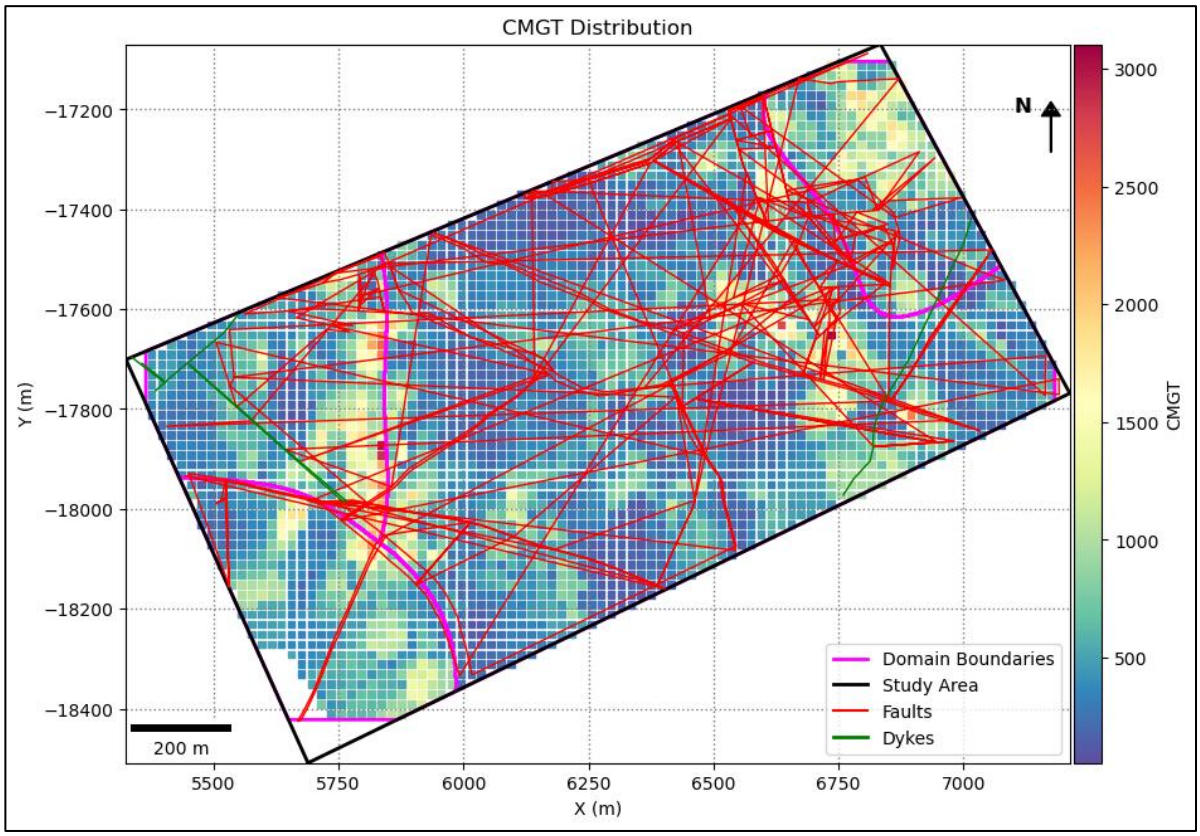


Figure 6.39: Kriged estimate map of the gold accumulation (cm.g/t) incorporating geological structures such as faults and dykes, as well as domain boundaries. The colour gradient represents estimated gold accumulation (cm.g/t) values, ranging from low (blue) to high (red), indicating areas with varying levels of gold accumulation.

6.5.1.2. Channel width (cm)

The channel width (cm) kriging estimates reveal notable spatial patterns across the study area, as illustrated in Figure 6.40. Statistical analysis of the channel width (cm) indicates a minimum value of 7.91 cm and a maximum of 206.08 cm, with a mean of 47.35 cm and a standard deviation of 33.99. The statistics highlight the variability in channel width (cm) across the study area. The distribution of channel width (cm) suggests that most estimates are concentrated within the moderate range, often below 75 cm.

The spatial distribution of channel width (cm) reveals that the thickest channel width (cm) areas are concentrated in the central and north-eastern regions of the study area. Thinner channel width (cm) estimates dominate the edges of the study area, mainly toward the north and west. Analysis of the channel width (cm) thickness per domain indicates that there is variability in spatial distribution. Domain 14 contains the highest average channel width (cm) thickness estimate. Higher channel width (cm) estimated values are concentrated along the border between domains 8 and 18, and in patches throughout domain 8. Thick channel width (cm) areas are generally associated with high gold accumulation (cm.g/t) values.

Generally, areas with thick channel widths (cm) are affected by faulting and dykes, especially in the central and eastern regions of the study area. The presence of faults and dykes in thick channel width (cm) regions suggests a potential influence of geological structures on channel formation, with faulting possibly creating wider channel widths (cm). Apart from domain 14, no preferential sampling is observed within thicker channel width (cm) regions.

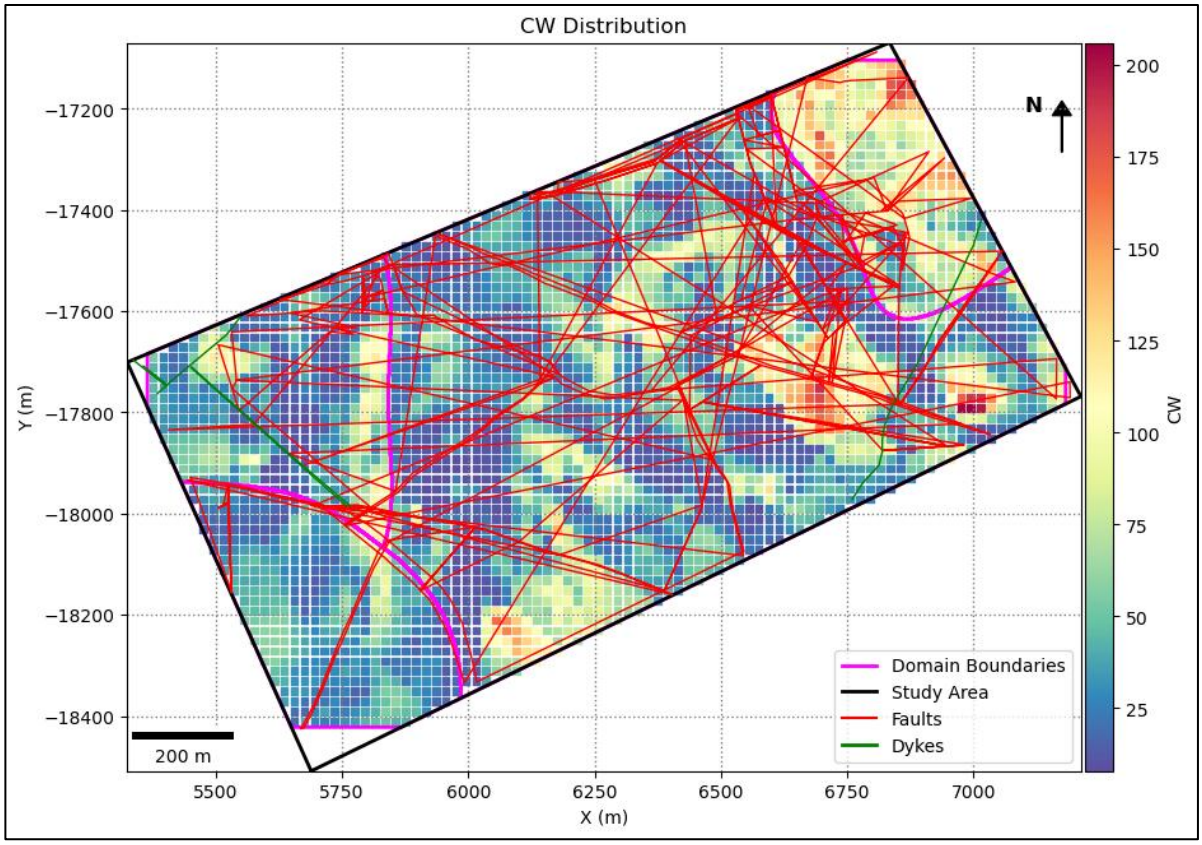


Figure 6.40: Kriged estimate map of the channel widths (cm) incorporating geological structures such as faults and dykes, as well as domain boundaries. The colour gradient represents estimated channel width (cm) values, ranging from low (blue) to high (red), indicating areas with varying channel width thicknesses.

6.5.1.3. Au (g/t)

The Au (g/t) kriging estimates reveal distinct spatial patterns across the domains, as illustrated in Figure 6.41. The statistical analysis of Au (g/t) indicates a minimum value of 1.16 g/t and a maximum of 147.67 g/t, with a mean of 20.24 g/t and a standard deviation of 15.47. The statistics highlight the variability in Au (g/t) across the study area. The distribution of Au (g/t) suggests that most estimates are concentrated below 20 g/t, indicating that high-grade zones are limited to specific areas.

The spatial distribution of Au (g/t) reveals that the highest Au (g/t) estimates are concentrated within pockets in the eastern, western and southern regions of the study area. Lower Au (g/t) values dominate the edges of the study area. Analysis of estimated Au (g/t) values per domain indicates that there is variability in spatial distribution. Domain 18 contains the highest average Au (g/t) estimates, with higher estimated values concentrated along the edges of domain 8 and the eastern regions of domain 18.

Areas with high Au (g/t) estimates are affected by faulting. Regions with high gold accumulation (cm.g/t) values and thick channel widths have lower Au (g/t) estimated values. An example of regions with lower Au (g/t) estimated values is domain 14 and the eastern region of domain 18. However, regions with higher gold accumulation (cm.g/t) estimates and thinner channel width (cm) have higher Au (g/t) estimate values. For example, the northern region of domain 18.

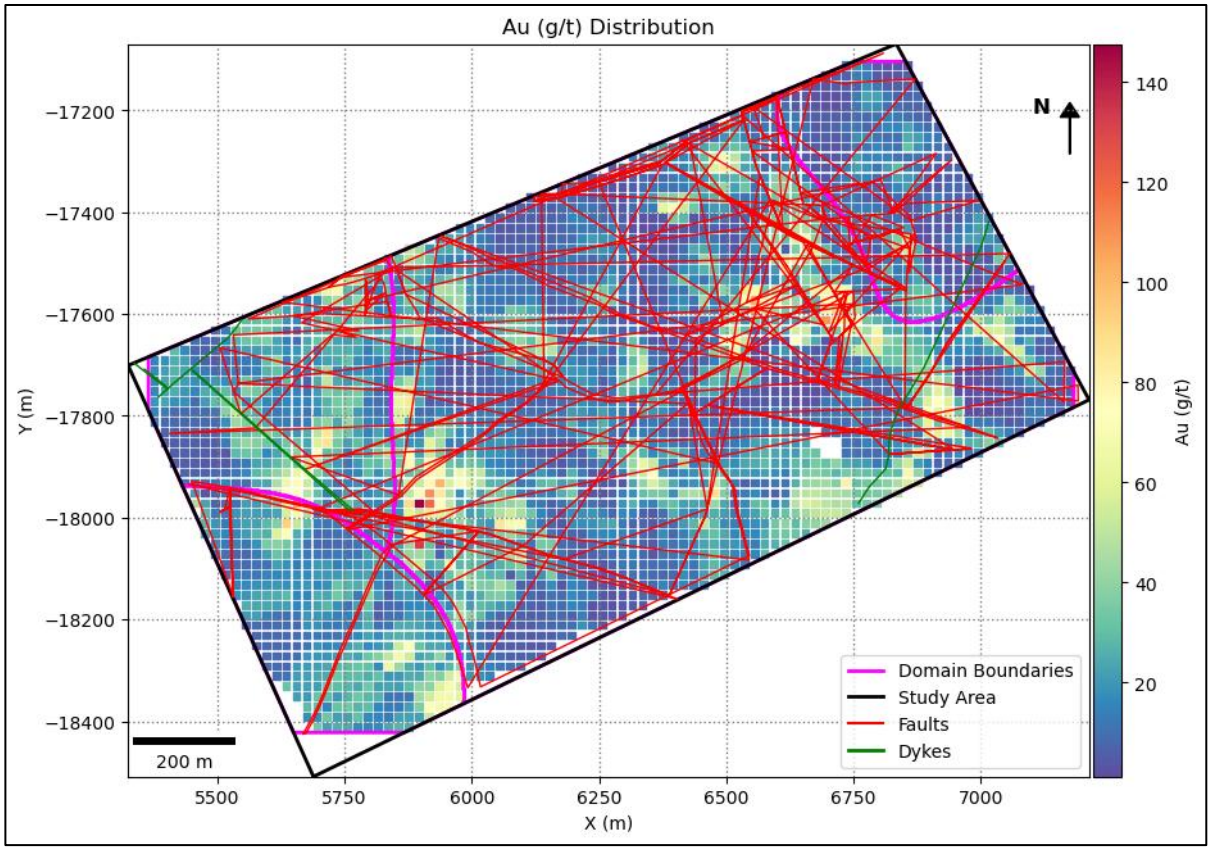


Figure 6.41: Kriged estimate map of Au (g/t) incorporating geological structures such as faults and dykes, as well as domain boundaries. The colour gradient represents estimated Au (g/t) values, ranging from low (blue) to high (red), indicating areas with varying Au (g/t) concentrations.

6.5.2. Kriging variance

Kriging variance maps quantify the uncertainty associated with kriged estimates. Higher kriging variance regions typically coincide with areas of dense sampling. Variability in the kriging variance is observed throughout the study area for each variable of interest. The lowest kriging variance is noted in the gold accumulation (cm.g/t) estimates. The following subsections detail kriging variance results.

6.5.2.1. Gold accumulation (cm.g/t)

The gold accumulation (cm.g/t) kriging estimate's variance reveals distinct spatial patterns across the domains, as illustrated in Figure 6.42. The statistical analysis of the gold accumulation (cm.g/t) indicates a minimum value of 0 and a maximum of 0.54, with a mean of 0.39 and a standard deviation of 0.18. The statistics highlight the variability in variance across the study area.

The gold accumulation (cm.g/t) kriging variance map reveals that the highest kriging variance areas are located in the north western and north-eastern regions of the study area. Lower kriging variance areas are generally concentrated around the peripheral regions of the study area. Analysis of the kriging variance within each domain indicates that the highest average kriging variance is within domain 18, and the lowest kriging variance is within both domains 8 and 19.

There does not appear to be a relationship between geological structures and gold accumulation (cm.g/t) kriging variance. However, higher kriging variance areas are associated with densely sampled areas. Consequently, lower kriging variance regions are associated with unsampled or sparsely sampled areas.

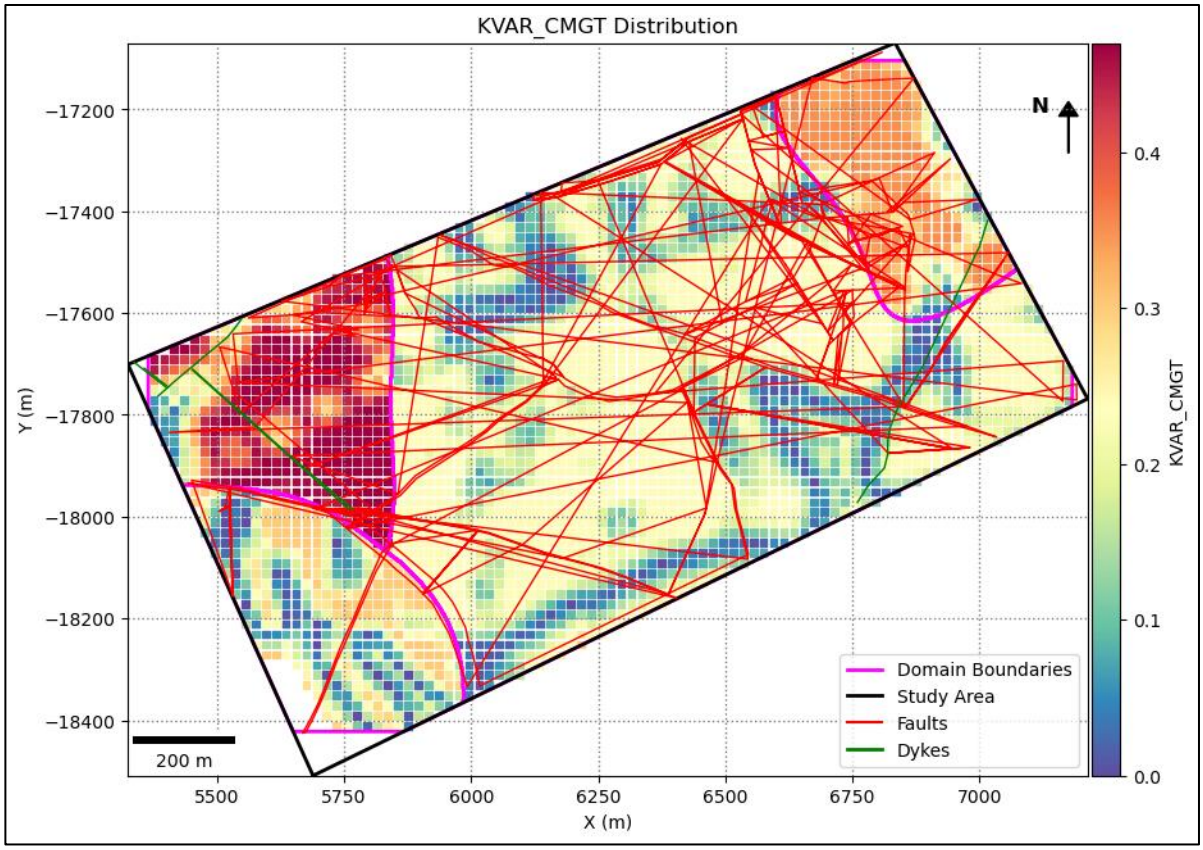


Figure 6.42: Kriging variance map of the gold accumulation (cm.g/t) incorporating geological structures such as faults and dykes, as well as domain boundaries. The colour gradient represents kriging variance values, ranging from low (blue) to high (red), indicating areas with varying kriging variance values.

6.5.2.2. Channel width (cm)

The channel width (cm) kriging estimate's variance reveals distinct spatial patterns across the domains, as illustrated in Figure 6.43. The statistical analysis of the channel width (cm) indicates a minimum value of 0 and a maximum of 0.72, with a mean of 0.39 and a standard deviation of 0.18. The statistics highlight the variability in variance across the study area.

The channel width (cm) kriging variance map reveals that the highest kriging variance areas are located in the north-western region of the study area. Lower kriging variance areas are concentrated in the north-eastern region of the study area and along the periphery of the study area. Analysis of the kriging variance within each domain indicates that the highest average kriging variance is within domain 18 and the lowest kriging variance within domain 14. Domains 8 and 19 contain similar kriging variance values.

There does not appear to be a relationship between geological structures and channel width (cm) kriging variance. However, higher kriging variance areas are associated with densely sampled areas. Consequently, lower kriging variance regions are associated with areas unsampled or sparsely sampled.

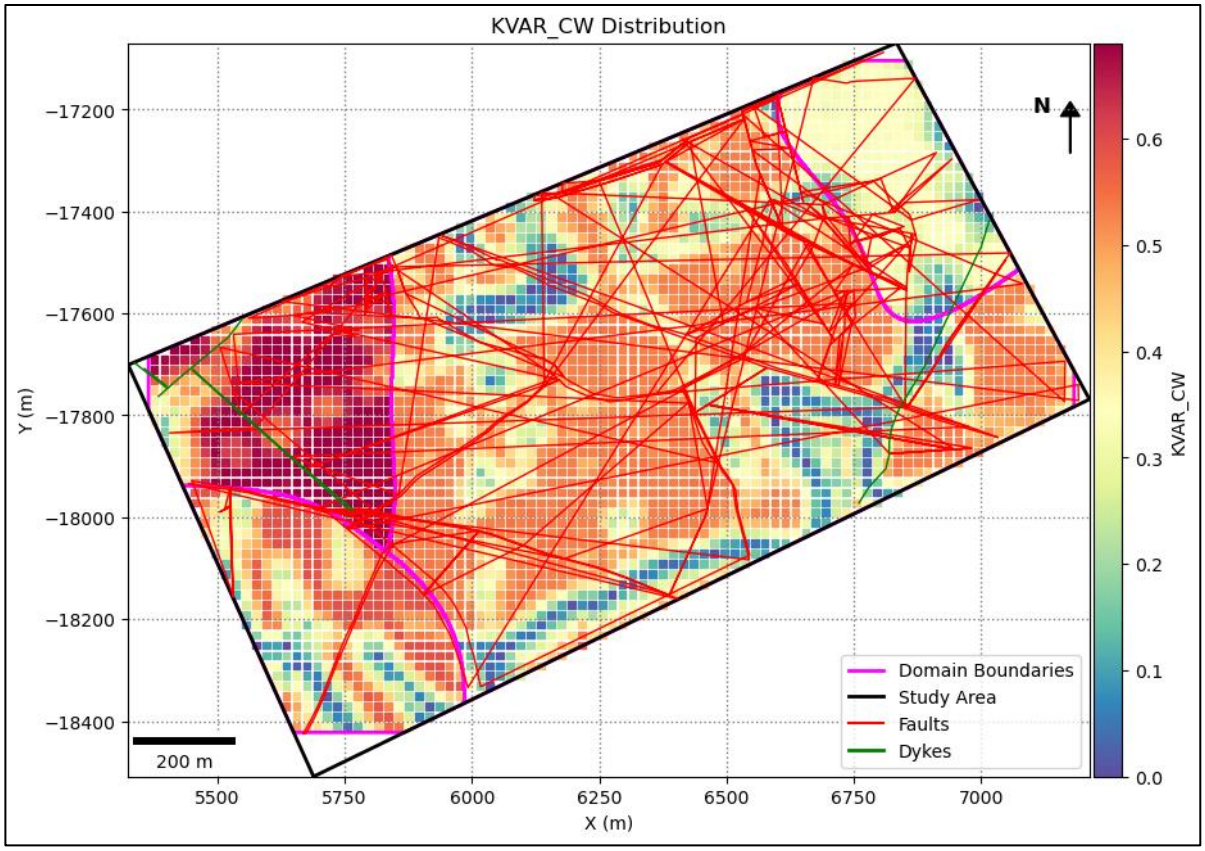


Figure 6.43: Kriging variance map of the channel width (cm) thickness incorporating geological structures such as faults and dykes, as well as domain boundaries. The colour gradient represents kriging variance values, ranging from low (blue) to high (red), indicating areas with varying kriging variance values.

6.5.2.3. Au (g/t)

The Au (g/t) kriging estimate's variance reveals distinct spatial patterns across the domains, as illustrated in Figure 6.44. The statistical analysis of Au (g/t) kriging variance indicates a minimum value of 0 and a maximum of 0.42, with a mean of 0.22 and a standard deviation of 0.10. The statistics highlight the variability in variance across the study area.

The Au (g/t) kriging variance map reveals that Au (g/t) contains the lowest kriging variance values, with the highest kriging variance areas concentrated in the northwestern and northeastern regions of the study area. Lower kriging variance areas are concentrated along the periphery of the study area. Analysis of the kriging variance within each domain indicates that the highest average kriging variance is within domain 18 and the lowest kriging variance is within domains 8 and 19.

There does not appear to be a relationship between geological structures and Au (g/t) kriging variance values. However, higher kriging variance areas are associated with densely sampled areas. Consequently, lower kriging variance regions are associated with areas that are unsampled or sparsely sampled.

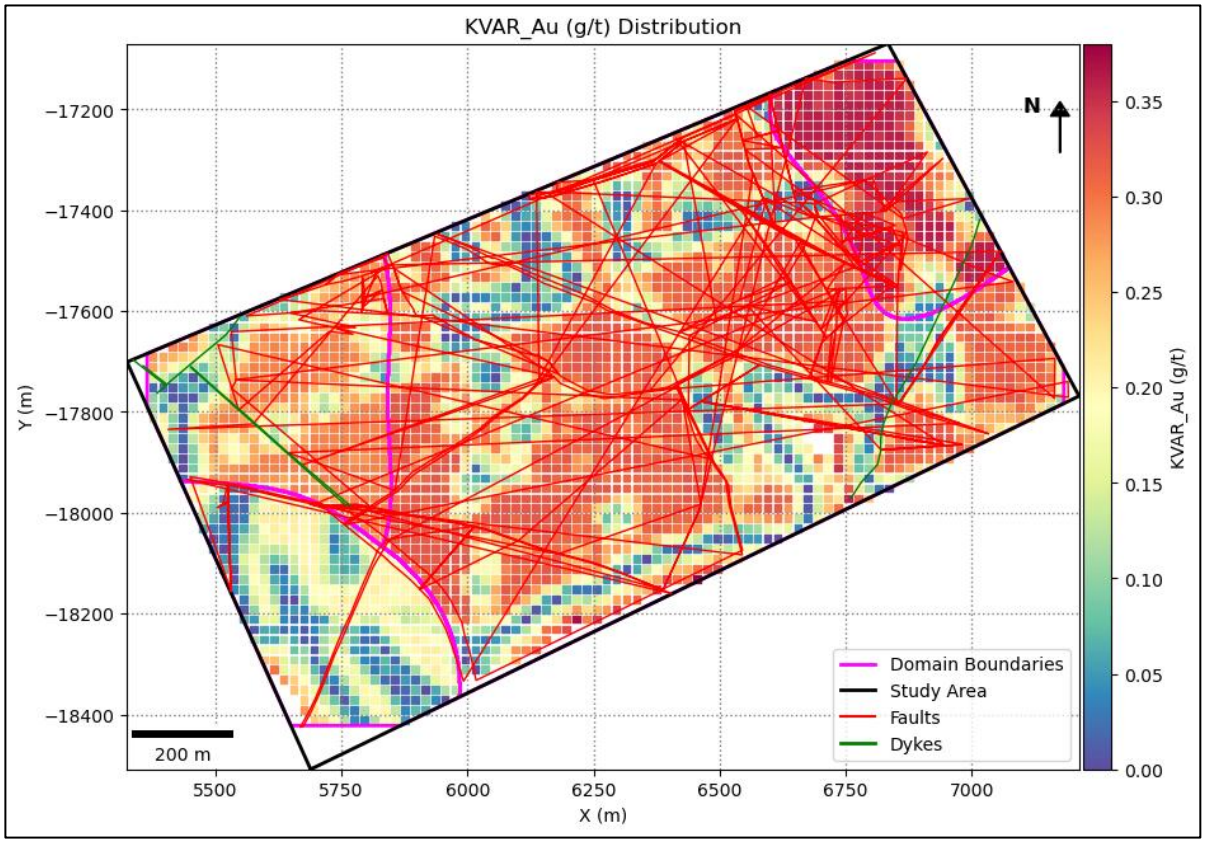


Figure 6.44: Kriging variance map of Au (g/t) incorporating geological structures such as faults and dykes, as well as domain boundaries. The colour gradient represents kriging variance values, ranging from low (blue) to high (red), indicating areas with varying kriging variance values.

6.5.3. Kriging efficiency

Kriging efficiency values, calculated as 1 − kriging variance, indicate the reliability of the kriging estimates. Kriging efficiency values closer to 1 suggest high confidence in predictions, whereas values closer to 0 highlight areas where kriging is less effective. The following subsections detail results obtained from kriging efficiency calculations.

6.5.3.1. Gold accumulation (cm.g/t)

The gold accumulation (cm.g/t) kriging efficiency reveals distinct spatial patterns across the domains, as illustrated in Figure 6.45. The statistical analysis of the gold accumulation (cm.g/t) kriging efficiency indicates a minimum value of 0.76 and a maximum of 0.99, with a mean of 0.79 and a standard deviation of 0.11. The statistics highlight the variability in gold accumulation's kriging efficiency across the study area.

The spatial distribution of the gold accumulation (cm.g/t) kriging efficiency reveals that the highest kriging efficiency regions are concentrated in the central and southwestern regions of the study area. Analysis of the gold accumulation (cm.g/t) values per domain indicates that there is variability in spatial distribution. Domains 8 and 19 contain the highest average gold accumulation (cm.g/t) kriging efficiency. Higher kriging efficiency values are concentrated within domain 14, while domain 18 contains the lowest kriging efficiency values.

Regions of relatively moderate kriging efficiency are truncated by faults and dykes. Higher kriging efficiency areas are associated with sparsely sampled areas. Consequently, lower kriging efficiency regions are associated with areas that are densely sampled.

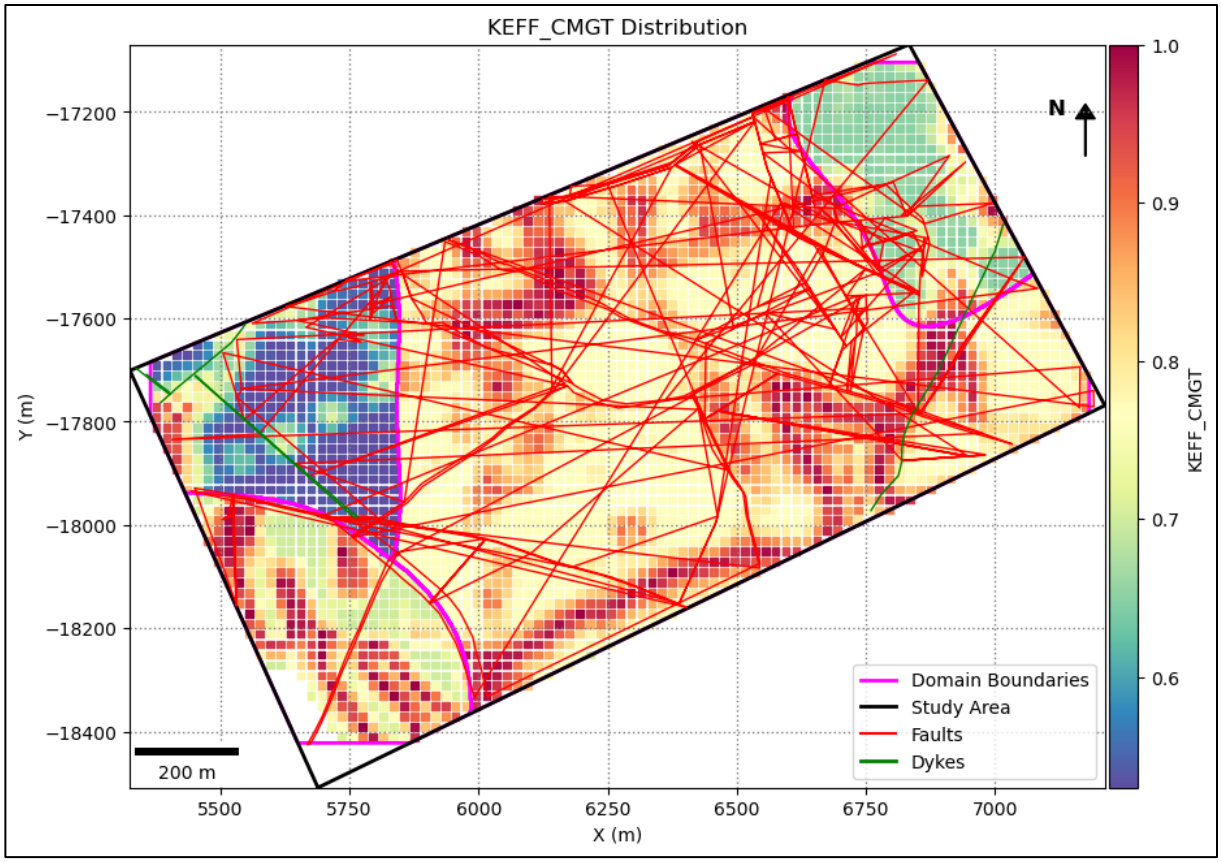


Figure 6.45: Kriging efficiency map of the gold accumulation (cm.g/t) incorporating geological structures such as faults and dykes, as well as domain boundaries. The colour gradient represents kriging efficiency values, ranging from low (blue) to high (red), indicating areas with varying kriging variance values.

6.5.3.2. Channel width (cm)

The channel width (cm) kriging efficiency reveals distinct spatial patterns across the domains, as illustrated in Figure 6.46. The statistical analysis of the channel width (cm) kriging efficiency indicates a minimum value of 0.25 and a maximum of 0.99, with a mean of 0.61 and a standard deviation of 0.17. The statistics highlight the variability in the channel width (cm) kriging efficiency across the study area.

The spatial distribution of the channel width (cm) kriging efficiency reveals that the highest kriging efficiency regions are concentrated in the northeastern region of the study area. Analysis of the channel width (cm) kriging efficiency per domain indicates that there is relatively low variability in spatial distribution. Domain 14 contains the highest average channel width (cm) kriging efficiency. Higher kriging efficiency values are concentrated within both domains 8 and 19, while domain 18 contains the lowest kriging efficiency values.

Regions of relatively moderate kriging efficiency are truncated by faults and dykes. Higher kriging efficiency areas are associated with sparsely sampled areas. Consequently, lower kriging efficiency regions are associated with areas that are densely sampled.

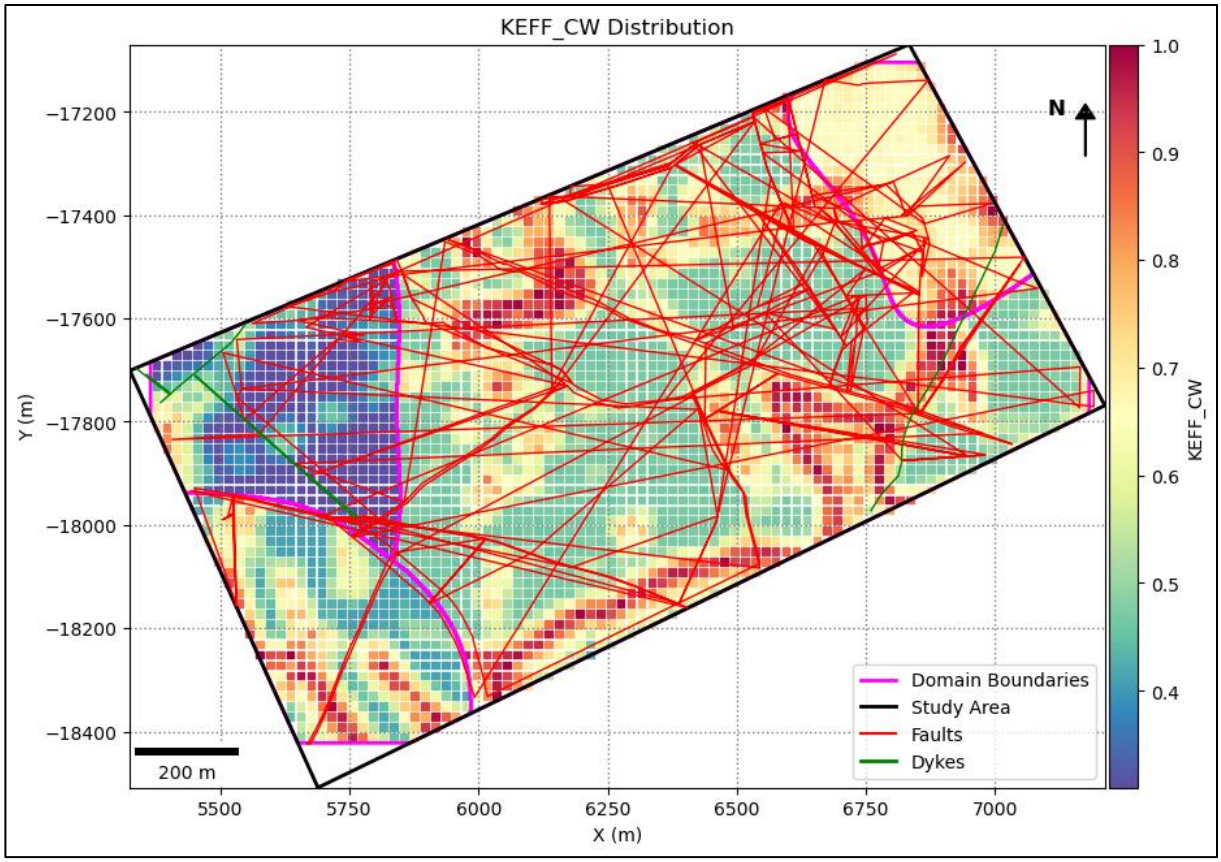


Figure 6.46: Kriging efficiency map of the channel width (cm) thickness incorporating geological structures such as faults and dykes, as well as domain boundaries. The colour gradient represents kriging efficiency values, ranging from low (blue) to high (red), indicating areas with varying kriging variance values.

6.5.3.3. Au (g/t)

The Au (g/t) kriging efficiency reveals distinct spatial patterns across the domains, as illustrated in Figure 6.47. The statistical analysis of Au (g/t) kriging efficiency indicates a minimum value of 0.58 and a maximum of 0.99, with a mean of 0.78 and a standard deviation of 0.10. The statistics highlight the variability in Au (g/t) kriging efficiency across the study area.

The spatial distribution of Au (g/t) kriging efficiency reveals that the highest kriging efficiency regions are concentrated in the central and southwestern regions of the study area. Analysis of the Au (g/t) kriging efficiency per domain indicates that there is variability in spatial distribution. Domain 19 contains the highest average Au (g/t) kriging efficiency. Higher estimated values are concentrated within domains 8 and 18, while domain 14 contains the lowest kriging efficiency values.

Regions of relatively moderate kriging efficiency are truncated by faults and dykes. Higher kriging efficiency areas are associated with sparsely sampled areas. Consequently, lower kriging efficiency regions are associated with areas that are densely sampled.

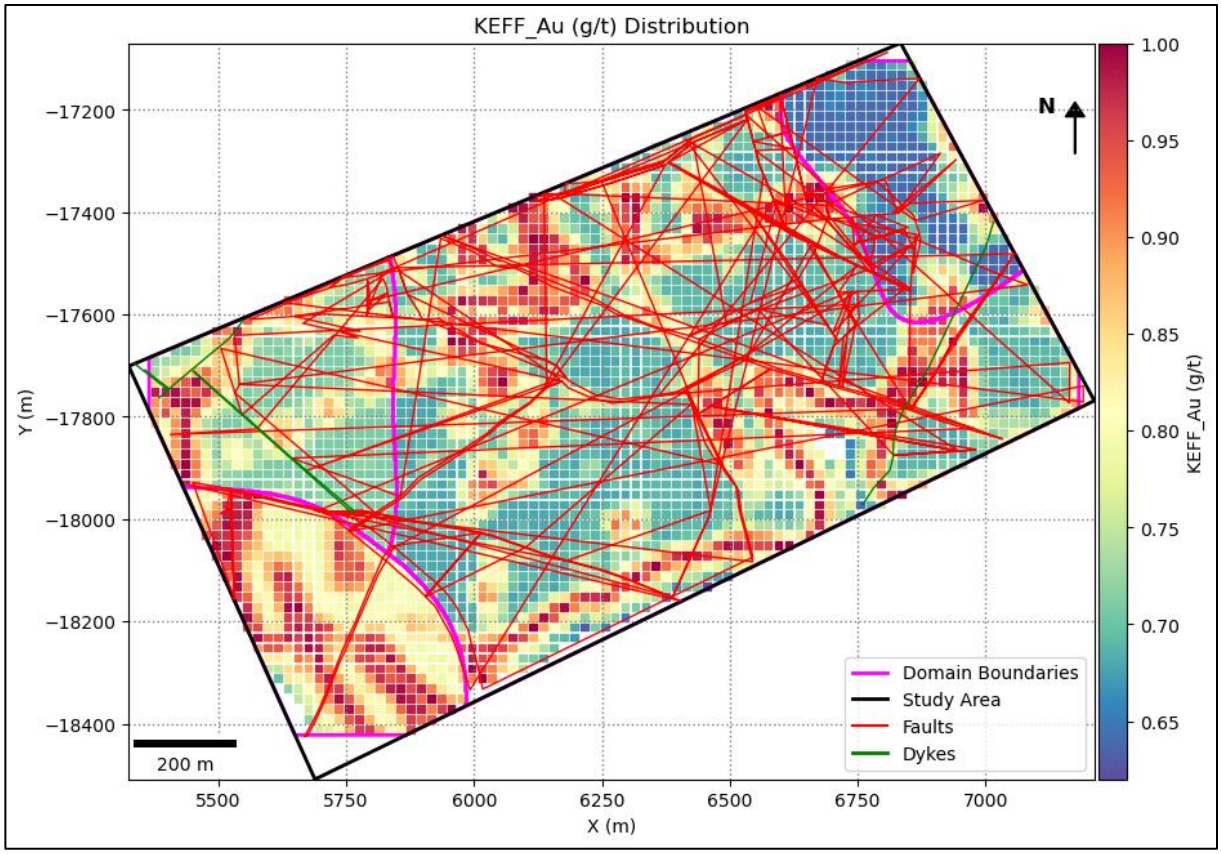


Figure 6.47: Kriging efficiency map of Au (g/t) incorporating geological structures such as faults and dykes, as well as domain boundaries. The colour gradient represents kriging efficiency values, ranging from low (blue) to high (red), indicating areas with varying kriging variance values.

6.5.4. Slope of regression

The slope of regression provides a measure of prediction bias. Values closer to 1 indicate unbiased predictions, whereas values further from 1 suggest potential overestimation or underestimation of variables. Results from the slope of regression analysis indicate that the study area has high slope of regression values across all variables and domains. Relatively lower slope of regression values were calculated along the peripheral regions of the study area.

The following paragraphs detail the slope of regression results per variable of interest within the study area.

6.5.4.1. Gold accumulation (cm.g/t)

The gold accumulation (cm.g/t) slope of regression reveals distinct spatial patterns across the domains, as illustrated in Figure 6.48. The statistical analysis of the gold accumulation (cm.g/t) slope of regression indicates a minimum value of 0.66 and a maximum of 1, with a mean of 0.91 and a standard deviation of 0.06. The statistics highlight low variability in gold accumulation's slope of regression across the study area.

The spatial distribution of the gold accumulation (cm.g/t) slope of regression reveals that most of the study area has a high slope of regression, above 0.95. Regions with a lower slope of regression are concentrated along the peripheral regions of the study area. Analysis of the gold accumulation (cm.g/t) slope of regression values per domain indicates that there is low variability in spatial distribution. Domains 18 and 19 contain the lowest average gold accumulation (cm.g/t) slope of regression. There is no observed relationship between the slope of regression, geological structures, and preferential sampling.

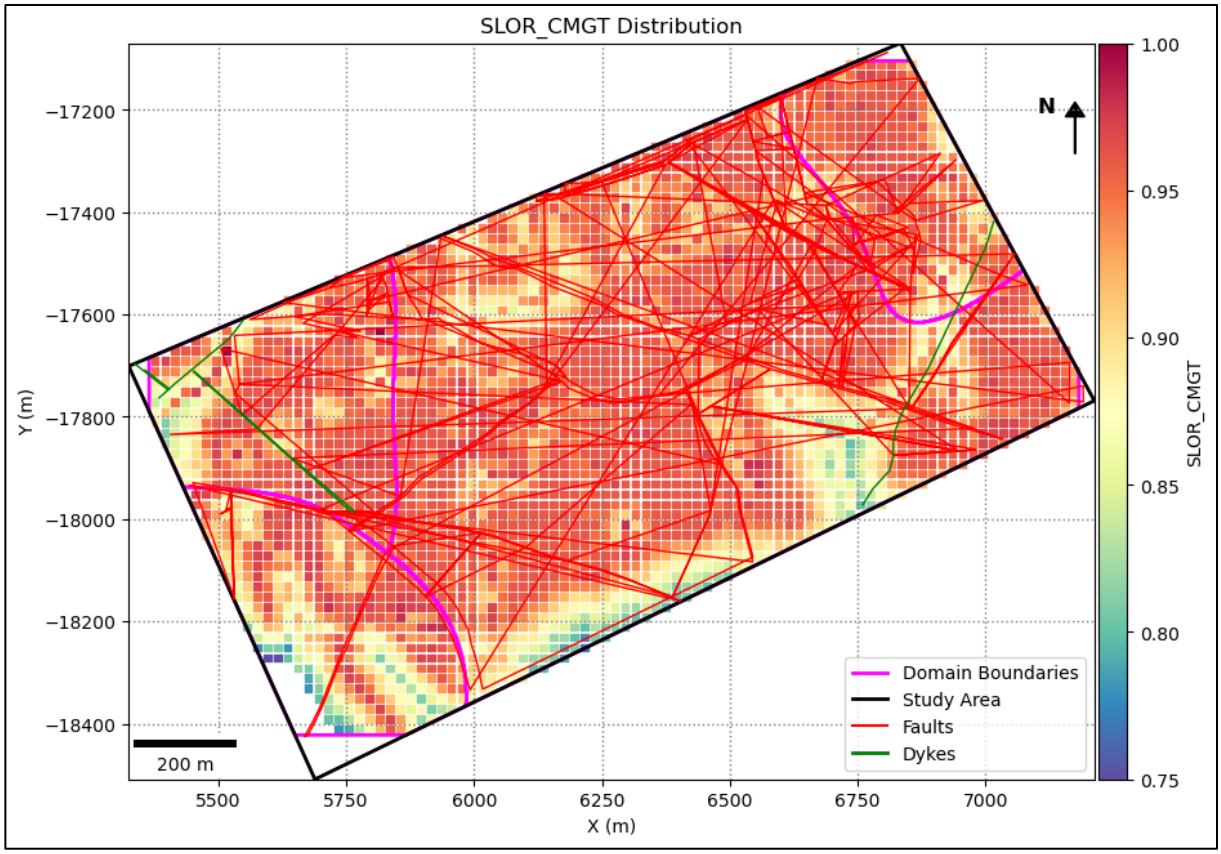


Figure 6.48: Slope of regression map of the gold accumulation (cm.g/t) incorporating geological structures such as faults and dykes, as well as domain boundaries. The colour gradient represents the slope of regression values, ranging from low (blue) to high (red), indicating areas with varying slope of regression values.

6.5.4.2. Channel width (cm)

The channel width (cm) slope of regression reveals distinct spatial patterns across the domains, as illustrated in Figure 6.49. The statistical analysis of channel width (cm) slope of regression indicates a minimum value of 0.57 and a maximum of 1, with a mean of 0.89 and a standard deviation of 0.10. The statistics highlight low variability in the channel width (cm) slope of regression across the study area.

The spatial distribution of the channel width (cm) slope of regression reveals that a majority of the study area has a high slope of regression, above 0.90. Regions with a lower slope of regression are concentrated along the peripheral regions of the study area. Analysis of the channel width (cm) slope of regression values per domain indicates that there is low variability in spatial distribution. There is no observed relationship between the slope of regression, geological structures, and preferential sampling.

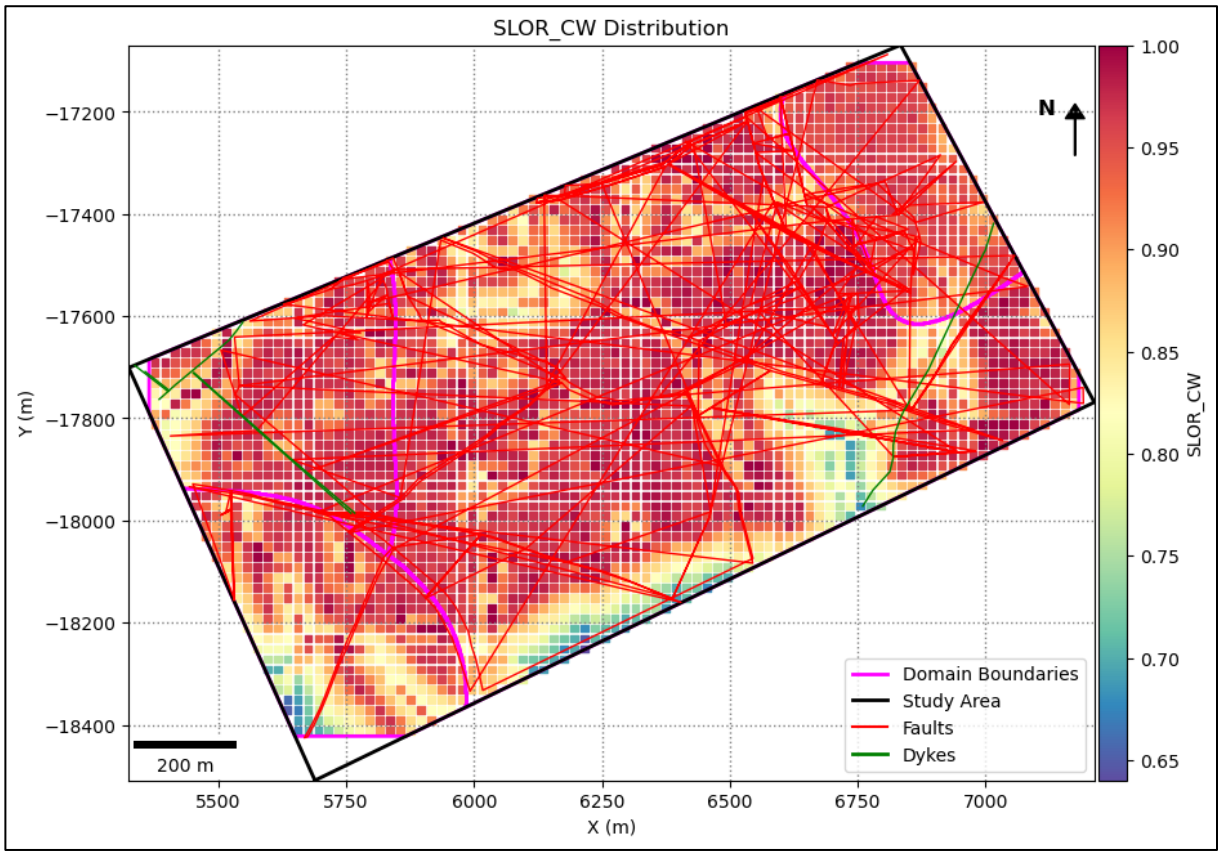


Figure 6.49: Slope regression map of channel width (cm) thickness incorporating geological structures such as faults and dykes, as well as domain boundaries. The colour gradient represents kriging efficiency values, ranging from low (blue) to high (red), indicating areas with varying kriging variance values.

6.5.4.3. Au (g/t)

The Au (g/t) slope of regression reveals distinct spatial patterns across the domains, as illustrated in Figure 6.50. The statistical analysis of the Au (g/t) slope of regression indicates a minimum value of 0.71 and a maximum of 0.99, with a mean of 0.91 and a standard deviation of 0.06. The statistics highlight low variability in the Au (g/t) slope of regression across the study area.

The spatial distribution of the Au (g/t) slope of regression reveals that a majority of the study area has a high slope of regression, above 0.90. Regions with a lower slope of regression are concentrated along the peripheral regions of the study area. Analysis of the Au (g/t) slope of regression values per domain indicates that there is low variability in spatial distribution. There is no observed relationship between the slope of regression, geological structures, and preferential sampling.

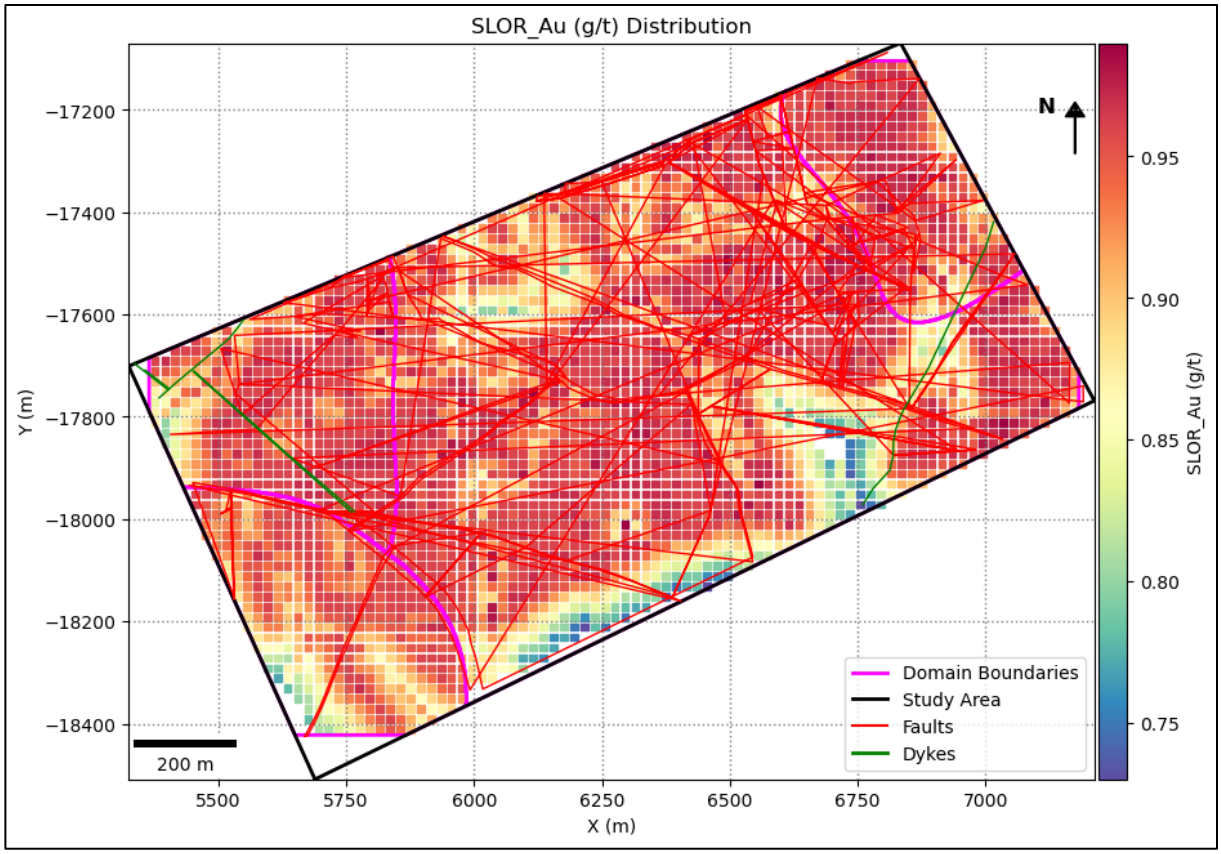


Figure 6.50: Slope of regression map of Au (g/t) incorporating geological structures such as faults and dykes, as well as domain boundaries. The colour gradient represents kriging efficiency values, ranging from low (blue) to high (red), indicating areas with varying kriging variance values.

6.6. Confidence Quantification and Mineral Resource Classification

This section presents the results obtained from confidence interval analysis using the methodologies described in Chapter 5.7, highlighting the uncertainty associated with the mineral resource estimates. Confidence intervals provide a quantitative measure of the reliability of the estimates, offering insights into the precision and range of possible outcomes. Confidence interval analysis serves as a foundation for understanding the spatial distribution of reliability in the estimates.

The method used to determine optimal discretisation was modified such that it includes the calculation of the dispersion variance associated with each sample using variogram parameters on a 20 × 20 m model block size. Confidence intervals were calculated separately for each variable-domain combination and the results combined for assessment and visualisation. The raw data was transformed into the logarithmic space using Equation 5.2 to ensure that it follows a normalised standard distribution. Table 6.15 shows some results from the logarithmic transformation

Table 6.15: Table showing selected results from the logarithmic transformation of the estimation dataset in preparation for confidence interval calculation.

X	Y	Domain	Gold accumulation (cm.g/t)	Channel width (cm)	Au (g/t)	Log transformed gold accumulation (cm.g/t)	Gold accumulation (cm.g/t) optimal beta	Gold accumulation (cm.g/t) log variance	Log transformed channel width (cm)	Channel width (cm) optimal beta	Channel width (cm) log variance	Log transformed Au (g/t)	Au (g/t) optimal beta	Au (g/t) log variance
5365.4	-17709	18	603.20	90.00	6.70	6.42	9.99	1.16	4.50	0.10	0.84	1.97	0.46	1.37
5368.2	-17709	18	547.20	70.00	7.82	6.32	9.99	1.16	4.25	0.10	0.84	2.11	0.46	1.37
5370.7	-17708	18	158.00	73.00	2.16	5.12	9.99	1.16	4.29	0.10	0.84	0.96	0.46	1.37
5373.1	-17707	18	405.20	53.00	7.65	6.03	9.99	1.16	3.97	0.10	0.84	2.09	0.46	1.37
5373.2	-17683	18	249.34	124.00	2.01	5.56	9.99	1.16	4.82	0.10	0.84	0.90	0.46	1.37
6625.8	-17922	8	246.00	30.00	8.20	5.55	9.99	1.16	3.40	0.10	0.84	2.16	0.46	1.37
6655.0	-17330	14	219.00	59.00	3.71	5.43	9.99	1.16	4.08	0.10	0.84	1.43	0.46	1.37
6665.4	-17710	8	72.30	52.07	1.39	4.41	9.99	1.16	3.95	0.10	0.84	0.61	0.46	1.37
6957.0	-17430	14	60.00	6.00	10.00	4.25	9.99	1.16	1.81	0.10	0.84	2.35	0.46	1.37

6.6.1. Confidence intervals

6.6.1.1. Gold accumulation (cm.g/t)

Gold accumulation (cm.g/t) confidence intervals were calculated for the entire dataset and visualised to highlight differences between the domains. The results include the 90% lower-bound kriged estimate values from confidence intervals and the confidence percentage for each block model (e.g., Fig. 6.51). The statistical analysis of the confidence percentages of the gold accumulation (cm.g/t) confidence intervals indicate a minimum confidence percentage of 50.85% and a maximum of 100%, with a mean of 72.19% and a standard deviation of 9.28% (Table 6.16).

Visualisation of confidence percentages reveals variation throughout the study area (Fig. 6.51). The highest gold accumulation (cm.g/t) confidence percentages are concentrated in the southwestern and central regions of the study area. Lower gold accumulation (cm.g/t) percentages are concentrated in the north-eastern and north-western regions of the study area. Analysis of the confidence percentages per domain indicates variability in the confidence associated with kriging estimates, where domains 8 and 19 have the highest confidence percentages for kriged estimates, while domains 18 and 14 show lower confidence percentages.

Regions with the highest gold accumulation (cm.g/t) confidence percentage, especially within domain 18, are affected by faulting. Regions with lower confidence percentages are seldom intersected by faults or dykes. The lower-bound 90% confidence percentage kriged estimates follow similar trends to those exhibited by the gold accumulation (cm.g/t) kriging estimates.

Table 6.16: Summary table of the gold accumulation (cm.g/t) confidence interval results and their associated logarithmic transformed values.

	Count	Mean	Standard deviation	Minimum	25th percentile	Median	75th percentile	Maximum
X	4102	6274.31	484.08	5375.40	5875.40	6275.40	6675.40	7175.40
Y	4102	-17720.30	302.09	-18411.30	-17951.30	-17711.30	-17491.30	-17111.30
Domain	4102	11.37	4.55	8.00	8.00	8.00	18.00	19.00
Gold accumulation (cm.g/t)	4102	547.07	365.61	51.79	293.96	448.72	685.84	3104.34
Gold accumulation (cm.g/t) kriged variance	4102	0.21	0.11	0.00	0.13	0.22	0.24	0.47
Gold accumulation (cm.g/t) slope of regression	4102	0.92	0.05	0.71	0.90	0.94	0.96	1.00
Gold accumulation (cm.g/t) log kriged variance	4102	0.07	0.06	0.00	0.04	0.06	0.08	0.23
Gold accumulation (cm.g/t) log standard deviation	4102	0.25	0.10	0.00	0.19	0.25	0.28	0.48
Log gold accumulation (cm.g/t) kriged estimates	4102	6.10	0.60	4.11	5.69	6.09	6.50	8.01
Lower 90% gold accumulation (cm.g/t) log confidence interval	4102	5.78	0.58	3.87	5.38	5.76	6.17	7.68
Upper 90% gold accumulation (cm.g/t) log confidence interval	4102	6.43	0.64	4.34	5.98	6.41	6.86	8.51
Lower 90% gold accumulation (cm.g/t) kriged estimate	4102	387.42	247.24	38.67	214.69	318.16	488.16	2228.07
Upper 90% gold accumulation (cm.g/t) kriged estimates	4102	784.84	581.76	68.44	394.44	618.31	994.97	5546.00
Gold accumulation (cm.g/t) 90% confidence percentage	4102	72.19	9.28	50.85	68.84	71.51	77.11	100.00

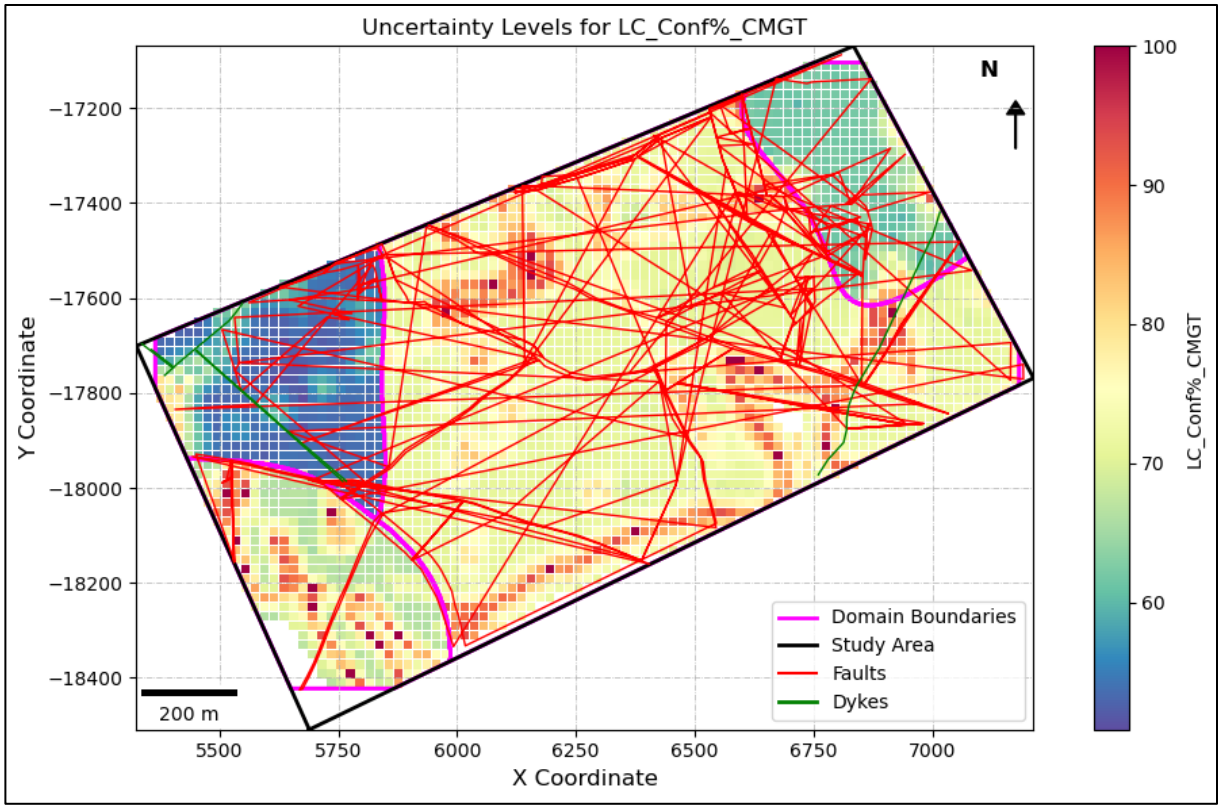


Figure 6.51: Confidence percentage map of the gold accumulation (cm.g/t) calculated through the logarithmic transformation method incorporating geological structures such as faults and dykes, as well as domain boundaries. The colour gradient represents the confidence percentage, ranging from low (blue) to high (red), indicating areas with varying certainty.

6.6.1.2. Channel width (cm)

The channel width (cm) confidence intervals were calculated for the entire dataset and visualised to highlight differences between the domains. The results include the 90% lower bound of the kriged estimate values from confidence intervals and the confidence percentage for each block model. The statistical analysis of the confidence percentages of the channel width (cm) confidence intervals indicates a minimum confidence percentage of 34.43% and a maximum of 100%, with a mean of 55.88% and a standard deviation of 12.03% (Table 6.17).

Visualisation of confidence percentages reveals variation throughout the study area (Fig. 6.52). The highest channel width (cm) confidence percentages are concentrated in the northeastern regions of the study area. Lower channel width confidence percentages are concentrated in the northwestern region of the study area. Both domains 8 and 14 have similar confidence percentage values. Analysis of the confidence percentages per domain indicates variability in the confidence associated with kriging estimates, where domain 14 has the highest confidence percentages for kriged estimates, while domain 18 exhibits lower confidence percentages.

Regions with the moderate channel width (cm) confidence percentages, especially within domain 8, are affected by faulting. Regions with lower confidence percentages are seldom intersected by faults or dykes. The lower-bound 90% confidence percentage kriged estimates follow similar trends to those exhibited by the gold accumulation (cm.g/t) kriging estimates.

Table 6.17: Summary table of channel width confidence intervals results and their associated logarithmic transformed values.

	Count	Mean	Standard deviation	Minimum	25th percentile	Median	75th percentile	Maximum
X	4102	6274.31	484.08	5375.40	5875.40	6275.40	6675.40	7175.40
Y	4102	-17720.30	302.09	-18411.30	-17951.30	-17711.30	-17491.30	-17111.30
Domain	4102	11.37	4.55	8.00	8.00	8.00	18.00	19.00
Channel width (cm)	4102	48.48	34.81	7.91	22.59	37.27	65.40	206.08
Channel width (cm) Kriged variance	4102	0.39	0.18	0.00	0.26	0.42	0.53	0.69
Channel width (cm)Slope of regression	4102	0.91	0.07	0.67	0.87	0.94	0.97	1.00
Channel width (cm) log kriged variance	4102	0.21	0.12	0.00	0.11	0.23	0.28	0.45
Channel width (cm) log standard deviation	4102	0.44	0.14	0.00	0.33	0.48	0.53	0.67
Log channel width (cm) kriged estimates	4102	3.58	0.68	2.11	3.07	3.55	4.09	5.26
Lower 90% channel width (cm) log confidence interval	4102	3.02	0.76	1.39	2.46	2.99	3.53	5.02
Upper 90% channel width (cm) log confidence interval	4102	4.14	0.65	2.61	3.65	4.11	4.66	5.84
Lower 90% channel width (cm) kriged estimate	4102	28.36	23.79	3.38	11.78	20.56	36.50	149.74
Upper 90% channel width (cm) kriged estimates	4102	85.17	57.79	12.14	40.84	66.87	116.06	387.71
Channel width (cm) 90% confidence percentage	4102	55.88	12.03	34.43	47.81	51.82	64.82	100.00

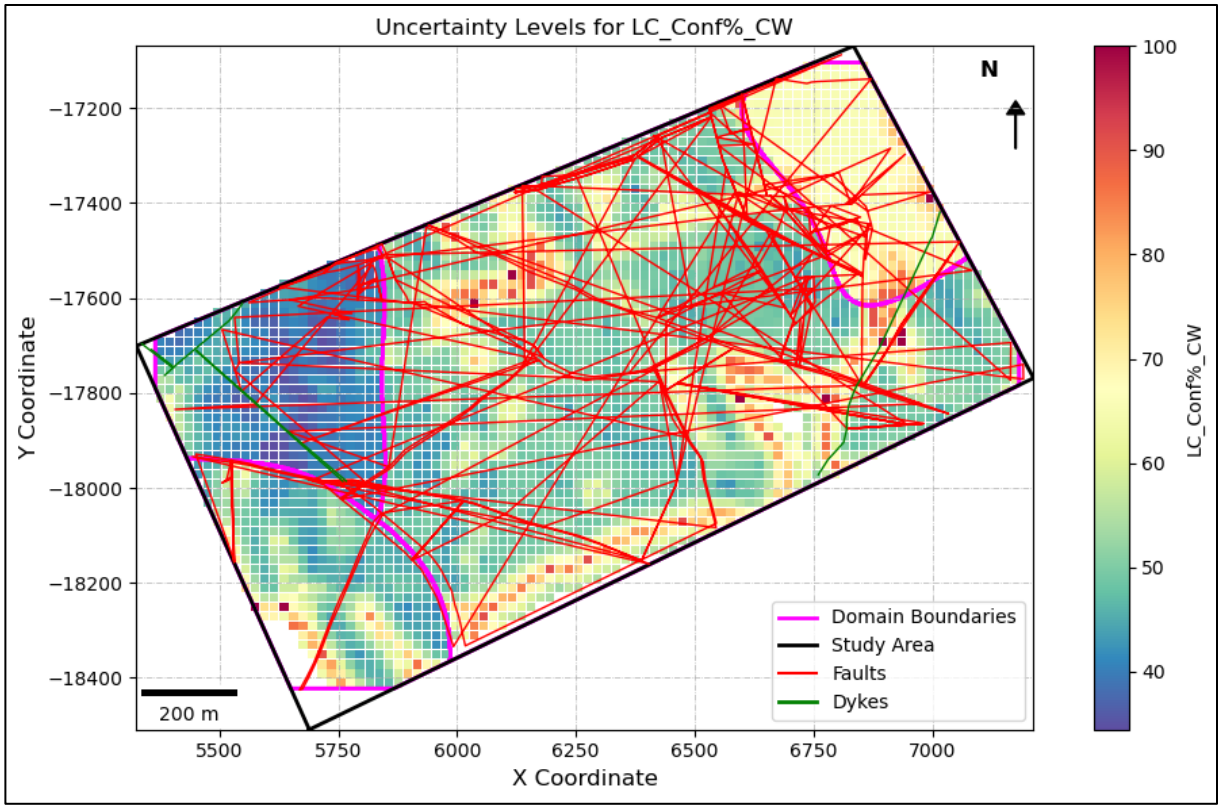


Figure 6.52: Confidence percentage map of channel width (cm) calculated through the logarithmic transformation method incorporating geological structures such as faults and dykes, as well as domain boundaries. The colour gradient represents the confidence percentage, ranging from low (blue) to high (red), indicating areas with varying certainty.

6.6.1.3. Au (g/t)

The Au (g/t) confidence intervals were calculated for the entire dataset and visualised to highlight differences between the domains. The results include the 90% lower bound of the kriged estimate values from confidence intervals and the confidence percentage for each block model. The statistical analysis of the confidence percentages of Au (g/t) confidence intervals indicates a minimum confidence percentage of 55.80% and a maximum of 100%, with a mean of 70.88% and a standard deviation of 8.64% (Table 6.18).

Visualisation of the confidence percentages reveals high variation throughout the study area (Fig. 6.53). The highest Au (g/t) confidence percentages are concentrated in the southwestern region of the study area. Lower Au (g/t) confidence percentages are concentrated in the northeastern region of the study area. Analysis of confidence percentages per domain indicates variability in the confidence associated with kriging estimates, where domain 14 exhibits the lowest confidence percentages for kriged estimates, while domain 19 exhibits lower confidence percentages.

Regions with the low to moderate Au (g/t) confidence percentages, especially within domain 8, are affected by faulting. Regions with the highest confidence percentages are seldom intersected by faults or dykes. The lower-bound 90% confidence percentage kriged estimates follow similar trends to those exhibited by the gold accumulation (cm.g/t) kriging estimates.

Table 6.18: Summary table of Au (g/t) confidence interval results and their associated logarithmic transformed values.

	Count	Mean	Standard deviation	Minimum	25th percentile	Median	75th percentile	Maximum
X	4102	6274.31	484.08	5375.40	5875.40	6275.40	6675.40	7175.40
Y	4102	-17720.30	302.09	-18411.30	-17951.30	-17711.30	-17491.30	-17111.30
Domain	4102	11.37	4.55	8.00	8.00	8.00	18.00	19.00
Au (g/t)	4102	20.24	15.52	1.15	9.21	16.13	26.50	147.68
Au (g/t) kriged variance	4102	0.22	0.10	0.00	0.14	0.24	0.31	0.42
Au (g/t) Slope of regression	4102	0.92	0.06	0.71	0.89	0.94	0.96	0.99
Au (g/t) log kriged variance	4102	0.08	0.04	0.00	0.04	0.08	0.12	0.16
Au (g/t) log standard deviation	4102	0.26	0.09	0.00	0.21	0.29	0.34	0.40
Log Au (g/t) kriged estimates	4102	2.73	0.73	0.34	2.22	2.76	3.25	4.94
Lower 90% Au (g/t) log confidence interval	4102	2.39	0.74	-0.06	1.89	2.41	2.93	4.49
Upper 90% Au (g/t) log confidence interval	4102	3.07	0.74	0.64	2.55	3.09	3.59	5.38
Lower 90% Au (g/t) kriged etsimate	4102	14.36	10.97	0.68	6.54	11.26	19.06	94.51
Upper 90% Au (g/t) kriged estimates	4102	28.84	22.88	1.62	12.87	22.54	37.30	230.66
Au (g/t) 90% confidence percentage	4102	70.88	8.64	55.80	64.07	68.21	75.94	100.00

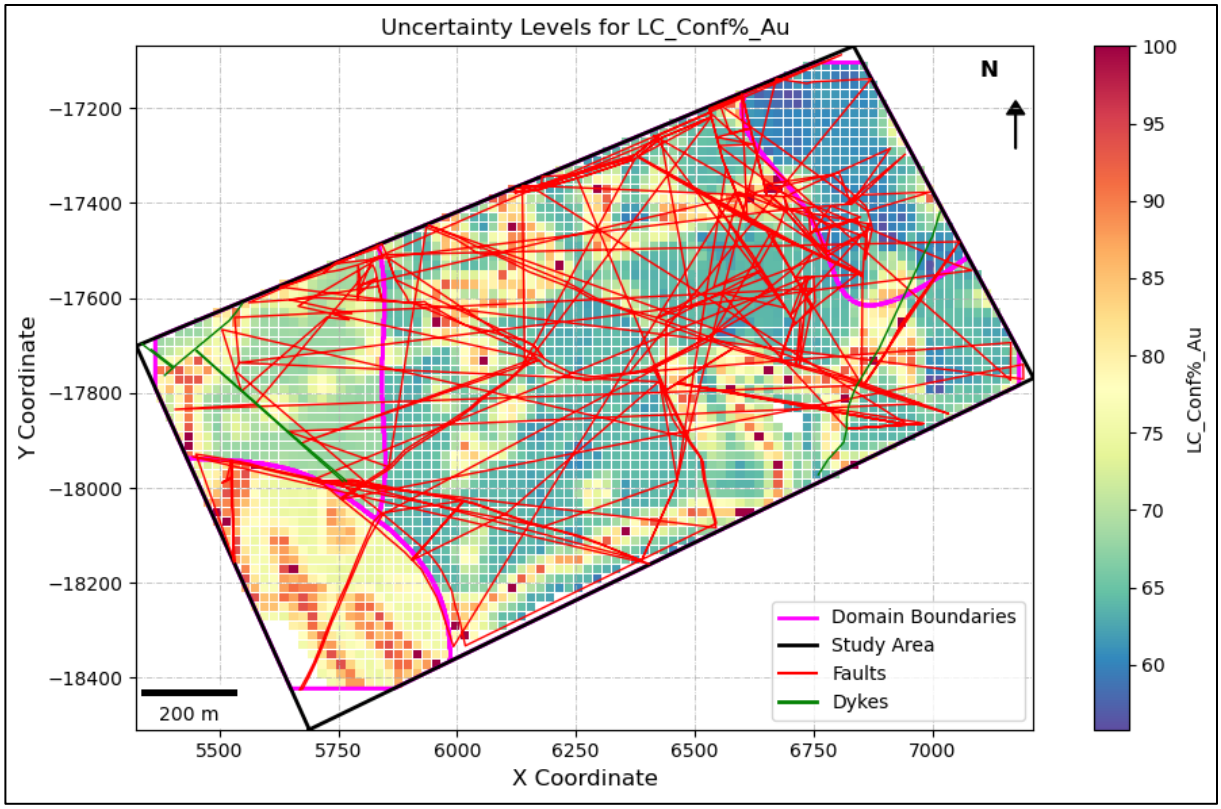


Figure 6.53: Confidence percentage map of Au (g/t) calculated through the logarithmic transformation method incorporating geological structures such as faults and dykes, as well as domain boundaries. The colour gradient represents the confidence percentage, ranging from low (blue) to high (red), indicating areas with varying certainty.

6.6.2. Certainty classification

To help visually categorise and assess the reliability of resource estimates, certainty plots were created from the confidence percentages determined above, following the intervals summarised in Tables 6.16, 6.17 and 6.18. Certainty classification plots were developed to evaluate the reliability of resource estimates by categorising the study area into zones of varying uncertainty levels. The thresholds reflect the relative precision of the estimates, where blocks with a higher confidence interval are classified as having a lower uncertainty and are therefore more reliable.

Table 6.19: Table summarising the uncertainty classification used in this study

Low uncertainty	Medium uncertainty	High uncertainty	Very high uncertainty
>90%	70-90%	50-70%	0-50%

6.6.1.4. Gold accumulation (cm.g/t)

The spatial distribution of the uncertainty in the gold accumulation (cm.g/t) kriged estimates suggests that most areas exhibit medium to high uncertainty (Fig. 6.54). The highest uncertainty regions are concentrated in the north-eastern and western regions of the study area, while lower uncertainty regions occur as scattered patches in the central region.

An analysis of the gold accumulation (cm.g/t) kriged estimate uncertainty per domain indicates moderate to high variability within and between the domains. Domains 14 and 18 exhibit the highest uncertainty levels, while domain 8 exhibits lower uncertainty. Medium and high uncertainty areas are intersected by faults, suggesting that geological structures play a role in the classification of estimates. Preferential sampling played a role in the observed uncertainty patterns, where low-uncertainty areas are typically unsampled or sparsely sampled, whereas medium and high uncertainty regions correspond to areas with denser sampling.

The gold accumulation (cm.g/t) uncertainty classification was compared with the kriging validation maps from the ordinary kriging estimation process to assess the relationship between uncertainty and the kriging validation metrics. Low kriging variance areas are classified as exhibiting low to medium uncertainty, while high kriging variance areas are generally classified as high uncertainty. Conversely, low kriging efficiency areas are classified as high uncertainty, while high kriging efficiency areas are classified as medium to high uncertainty. Since the slope of regression is nearly uniform across the study area, no

comparison was made between the uncertainty classification and the predicted slope of regression values.

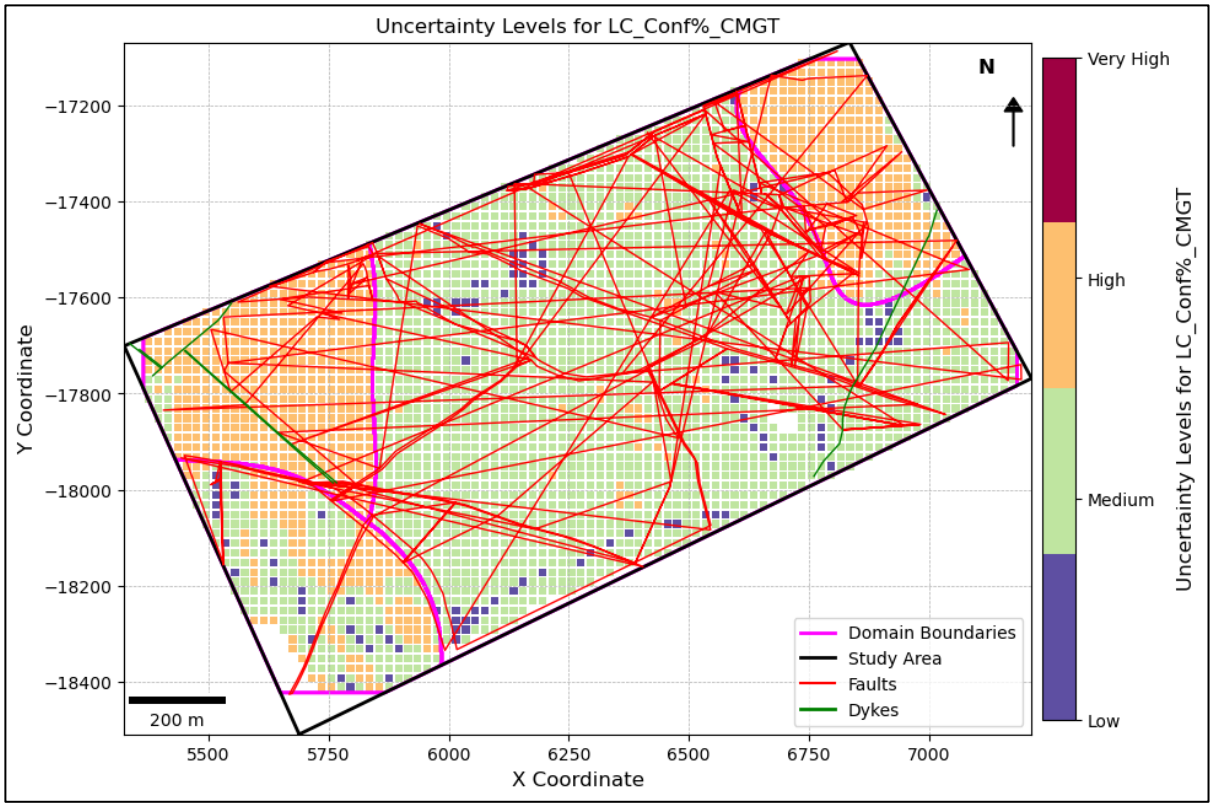


Figure 6.54: Uncertainty classification map of the gold accumulation (cm.g/t) calculated through the logarithmic transformation method incorporating geological structures such as faults and dykes, as well as domain boundaries. The colour gradient represents the level of uncertainty, ranging from low (blue) to high (red), indicating areas with varying uncertainty.

6.6.1.5. Channel width (cm)

The spatial distribution of the uncertainty in the channel width (cm) kriged estimates suggests that most areas exhibit high to very high uncertainty (Fig. 6.55). The highest uncertainty regions are concentrated in the eastern and central regions of the study area, while lower uncertainty regions are concentrated in the north-eastern region.

An analysis of the channel width (cm) kriged estimate uncertainty per domain indicates moderate to high variability within and between the domains. Domain 18 exhibits the highest uncertainty levels, while domain 14 exhibits lower uncertainty. High and very high uncertainty areas are intersected by faults, suggesting that geological structures play a role in the classification of estimates. Preferential sampling played a role in the observed uncertainty patterns, where very high uncertainty areas are typically sampled, while medium and high uncertainty regions are either unsampled or sparsely sampled.

The channel width (cm) uncertainty classification was compared with the kriging validation maps from the ordinary kriging estimation process to assess the relationship between uncertainty and the kriging validation metrics. Low kriging variance areas are classified as exhibiting medium uncertainty, while high kriging variance areas are generally classified as very high uncertainty. Conversely, low kriging efficiency areas are classified as very high uncertainty, while high kriging efficiency areas are classified as medium uncertainty. Since the slope of regression is nearly uniform across the study area, no comparison was made between the uncertainty classification and the predicted slope of regression values.

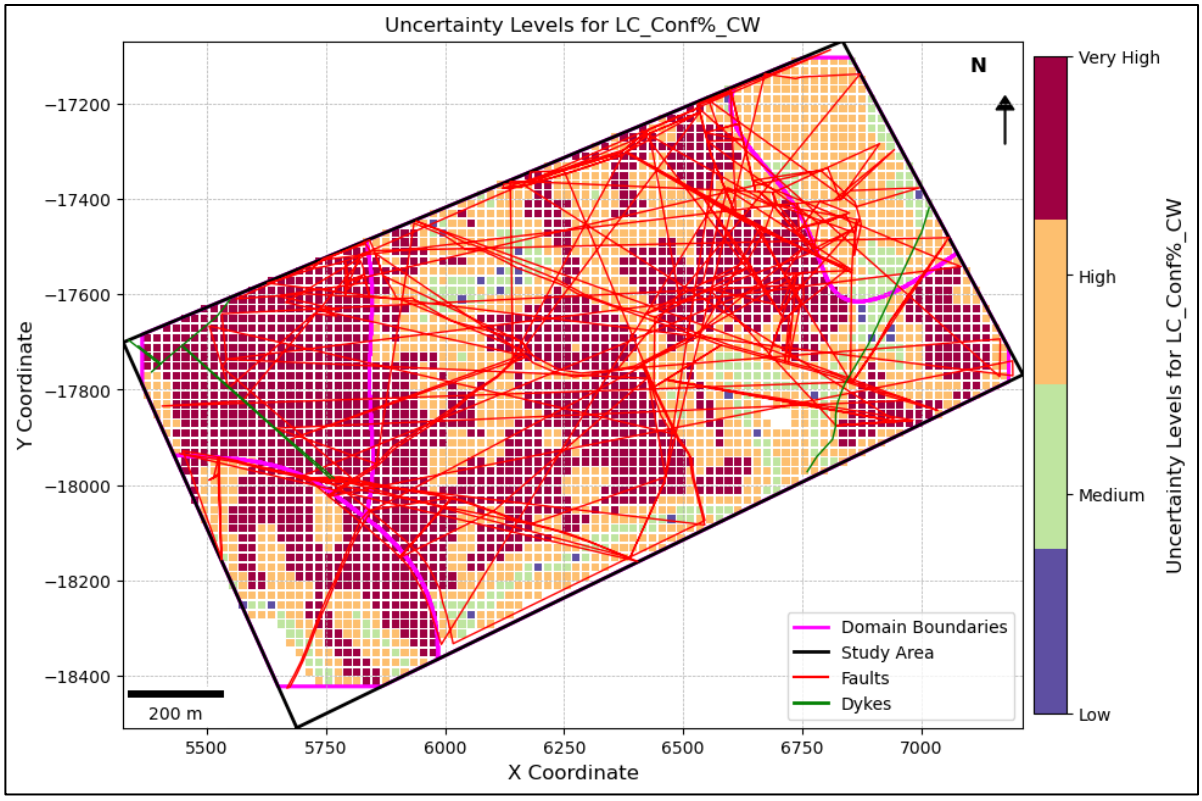


Figure 6.55: Uncertainty classification map of the channel width (cm) calculated through the logarithmic transformation method incorporating geological structures such as faults and dykes, as well as domain boundaries. The colour gradient represents the level of uncertainty, ranging from low (blue) to high (red), indicating areas with varying uncertainty.

6.6.1.6. Au (g/t)

The spatial distribution of the uncertainty in Au (g/t) kriged estimates suggests that most areas exhibit medium to high uncertainty (Fig. 6.56). The highest uncertainty regions are concentrated in the northeastern regions of the study area, while the lower uncertainty regions are concentrated in the southwestern region.

An analysis of the Au (g/t) kriged estimate uncertainty per domain indicates moderate to high variability within and between the domains. Domain 14 exhibits the highest uncertainty

levels, while domain 19 exhibits the lowest uncertainty. Medium uncertainty areas are intersected by faults, suggesting that geological structures play a role in the classification of estimates. Preferential sampling played a role in the observed uncertainty patterns, where high uncertainty areas are typically densely sampled, whereas medium and low uncertainty regions are less densely sampled.

The Au (g/t) uncertainty classification was compared with the kriging validation maps from the ordinary kriging estimation process to assess the relationship between uncertainty and the kriging validation matrices. Low kriging variance areas are classified as exhibiting medium uncertainty, while high kriging variance areas are generally classified as very high uncertainty. Conversely, low kriging efficiency areas are classified as high uncertainty, while high kriging efficiency areas are classified as medium uncertainty. Since the slope of regression is nearly uniform across the study area, no comparison was made between the uncertainty classification and the predicted slope of regression values.

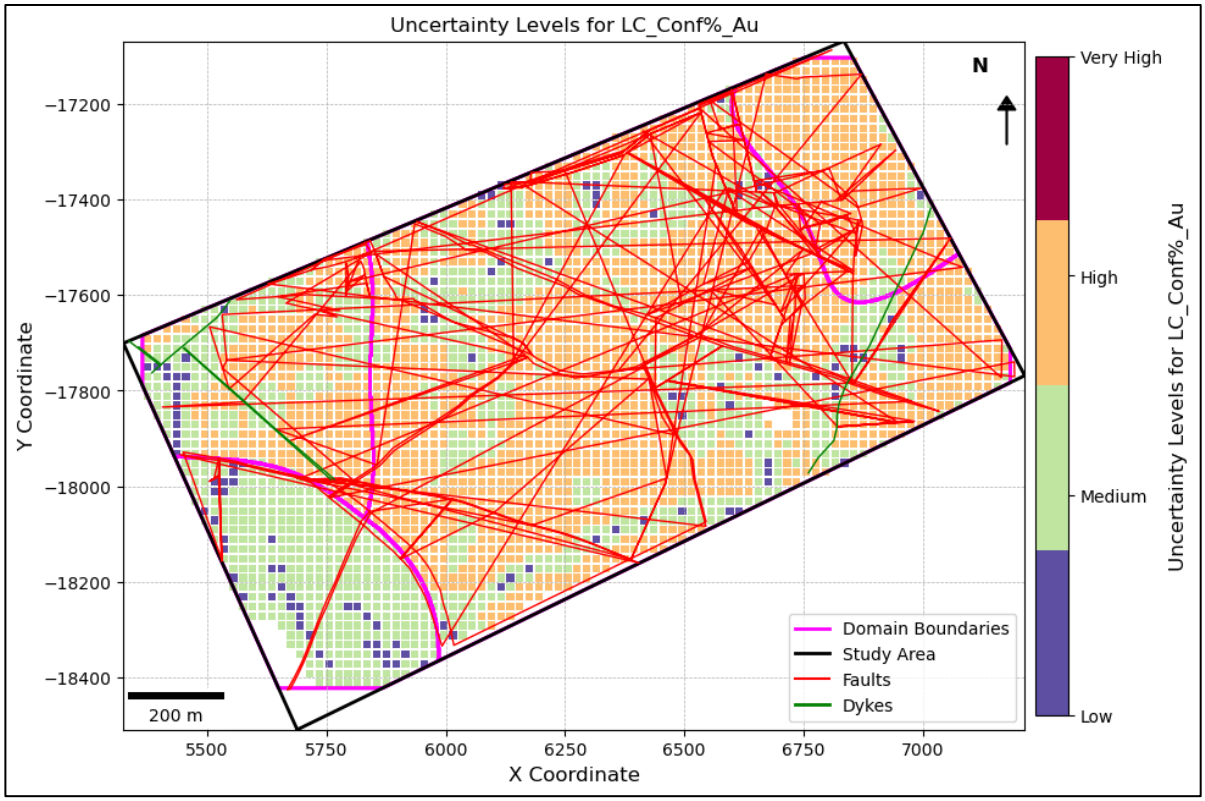


Figure 6.56: Uncertainty classification map of Au (g/t) calculated through the logarithmic transformation method incorporating geological structures such as faults and dykes, as well as domain boundaries. The colour gradient represents the level of uncertainty, ranging from low (blue) to high (red), indicating areas with varying uncertainty.

6.6.3. Swath plots

6.6.3.1. Gold accumulation (cm.g/t)

The gold accumulation (cm.g/t) swath plots along the X and Y-directions show consistent trends between the kriged estimates and sample grades (Fig. 6.57). The kriged estimates of the gold accumulation (cm.g/t) are consistently lower than the sample values and follow a similar trend as the one exhibited by sample numbers, indicating an underestimation of estimated values compared to actual sample values. In the X-direction, the average sample and model gold accumulation (cm.g/t) values follow the same trend as sample counts. A similar

trend is observed in the Y-direction, except along the edges of the study area, where the average sample numbers significantly decrease.

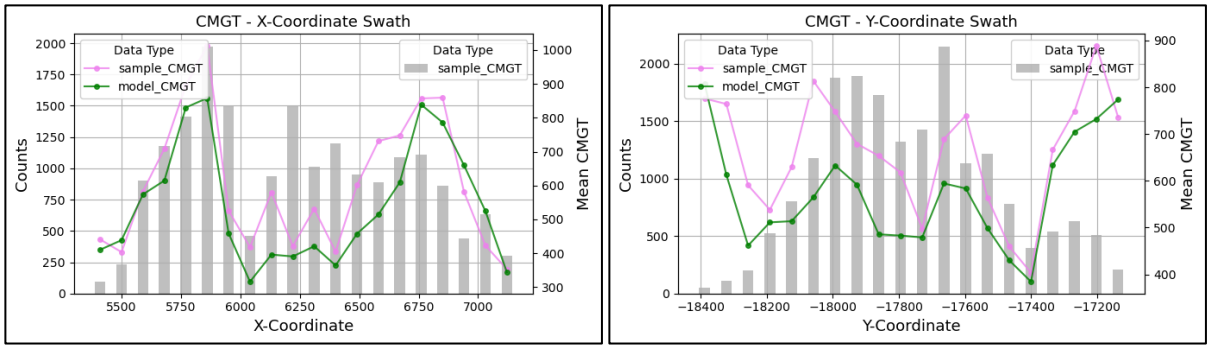


Figure 6.57: Swath plots for the gold accumulation (cm.g/t) along the X- and Y-directions. The plot compares the kriged model estimates with the sample values. Sample counts are represented by grey bars, while the pink and green lines indicate sample and model gold accumulation (cm.g/t) values, respectively.

6.6.3.2. Channel width (cm)

The channel width (cm) swath plots along the X and Y-directions show consistent trends between the model and samples (Fig. 6.58). The model line plots fluctuate between above and below the sample line values. The fluctuation is an indication of underestimation and overestimation of some values within the study area. The sample and model values do not follow the trend exhibited by sample counts; high sample count values are not necessarily associated with high average sample and model values.

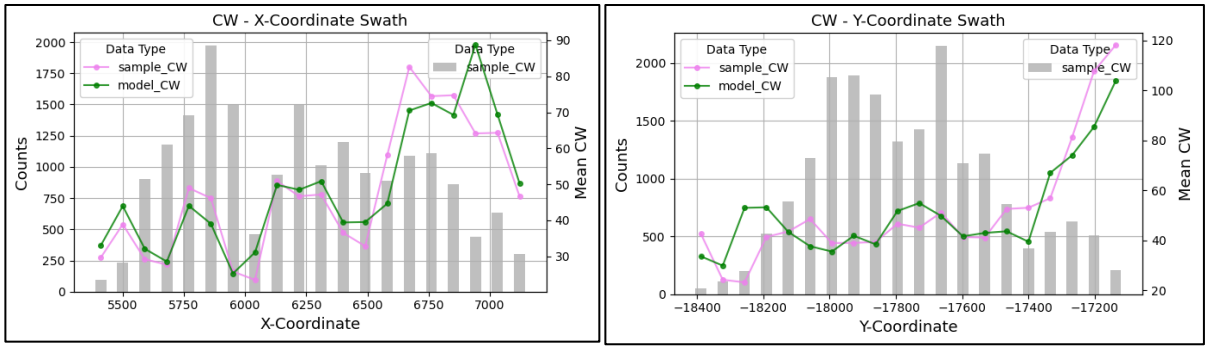


Figure 6.58: Swath plots for channel width (cm) along the X- and Y-directions. The plot compares the kriged model estimates with the sample values. Sample counts are represented by grey bars, while the pink and green lines indicate sample and model channel width (cm) values, respectively.

6.6.3.3. Au (g/t)

The Au (g/t) swath plots along the X and Y-directions show consistent trends between the model and samples (Fig. 6.59). The model estimates are below the sample values, indicating an underestimation of model values compared to the sample values. Average sample and model Au (g/t) do not truly follow the same trend as sample counts in the Y-direction, deviations are noted.

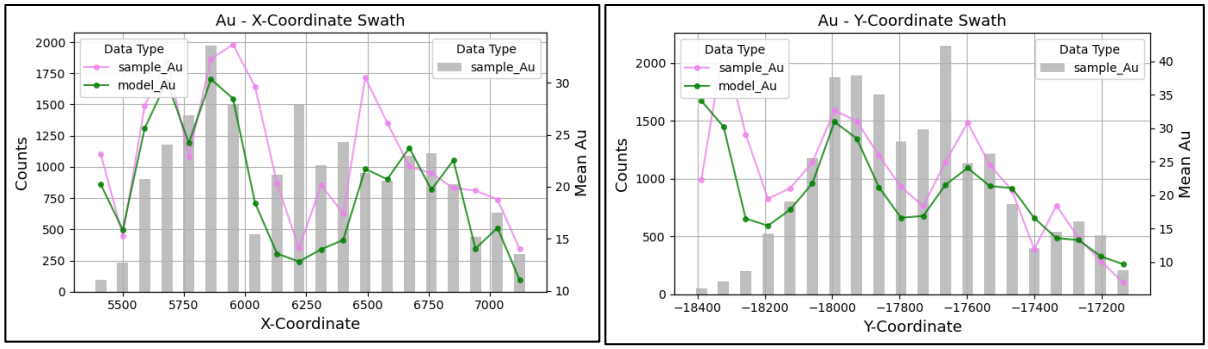


Figure 6.59: Swath plots for Au index along the X- and Y-directions. The plot compares the kriged model estimates with the sample values. Sample counts are represented by grey bars, while the pink and green lines indicate sample and model Au (g/t) values, respectively.

7. DISCUSSION

The discussion chapter interprets the results obtained in this study by addressing the objectives outlined in Chapter 1 and exploring key questions related to these goals. The chapter is divided into four sections, each corresponding to a specific objective detailed in Chapter 1. The first section examines the spatial variability of variables within the study area, as indicated by statistical analysis, variography, and kriged estimate maps. The second section evaluates the results of ordinary kriging, focusing on the differences between true values and estimates and assessing the reliability of kriged estimates. The third section analyses the certainty and confidence of kriging estimates. Finally, the fourth section explores methods for assessing the uncertainty associated with kriging estimates.

7.1. Spatial Variability

The characterisation of spatial variability and mineral distribution is critical in resource estimation as it directly influences the accuracy of reserve quantification and the quality of estimates. Understanding spatial variability patterns allows for improved grade continuity and high-grade concentration predictions. Exploratory data analysis, variography, and kriged estimate maps revealed significant spatial variability within the study area, with each domain exhibiting its own variability trends.

Exploratory data analysis provides insights into spatial trends within the dataset through assessing trends exhibited by the mean, variance, skewness, and kurtosis. Outlier treatment as part of QA/QC preserved a large portion of the dataset, ensuring that the statistics remain relevant and that the estimation dataset is a true representation of the sample population. The z-score histograms, data distribution histograms, and boxplots of the data before outlier

treatment were assessed. The z-score histograms, distribution histograms, and boxplots reveal that the original dataset contained a high concentration of low variable values, which resulted in an asymmetrical distribution of the dataset as seen in Fig. 6.1. Summary statistics of the dataset before outlier treatment indicates large variability due to (1) standard deviation values that are higher than the mean, (2) mean values that are higher than the median, and (3) maximum values that are significantly higher than the 75th percentile for all variables.

The dataset distribution before and after outlier treatment reveals similar trends to the distribution observed before outlier treatment. The z-score distribution histogram after outlier treatment exhibits trends that suggest normal distribution. However, the dataset following outlier treatment is also positively skewed, as evidenced by median values that are lower than the mean. The skewness of the dataset is also observed through maximum values that are significantly higher than the 75th percentile for all variables.

Outlier treatment assisted in stabilising the dataset by reducing the influence of extreme values while maintaining the overall distribution trends. More than 95% of the original data was retained in the dataset after outlier treatment. Outlier treatment improves the reliability of subsequent geostatistical modelling, particularly for variography and kriging. The frequency of extremely high values decreased substantially following outlier treatment, resulting in a more stable dataset. However, the dataset used for estimation contains extreme values that may be considered as outliers, as revealed by the coefficient of variation values of up to 135%. The estimation dataset was not further treated for outlier analysis, as further outlier treatment would lead to less data being available for use in the estimation process.

Spatial variability within the study area is also evidenced by the fluctuations observed on the cell sizes versus declustered means (Fig. 6.17 to Fig. 6.26). Variogram maps for

different variable-domain combinations reveal a preferred spatial continuity in the north-south direction and cyclicity along the northwest-southeast direction. Experimental semi-variograms further confirm that each variable has a distinct major direction of continuity and range of influence. The highest range of influence is observed in domain 18 for the gold accumulation (cm.g/t) and channel width (cm), while domain 14 exhibits the highest range for Au (g/t). The variations in range and nugget effects between each domain-feature variable highlight the spatial variability within the study area, indicating the presence of zonal anisotropy within and between domains.

Statistics from the kriged estimate results indicate spatial variability throughout all variables. The gold accumulation (cm.g/t) shows the highest variability as reflected by its high standard deviation values, a wide range, and significantly higher maximum values relative to the 75th percentile. Following the gold accumulation (cm.g/t), the channel width (cm) exhibits the second highest variability, while Au (g/t) displays the least variation. Spatial location and krige estimate maps confirm that the preferred continuity and cyclicity align with the directions identified in variography. The biased distribution of samples further justified the need for declustering and normal score transformation in variogram modelling.

The influence of geological structures, such as faults and dykes, on spatial variability is assessed across the study area for various variables. Previous analyses have established that major directions of spatial continuity are associated with regions of high variable values. Notably, high gold accumulation (cm.g/t) and channel width (cm) values align with preferred directions of continuity. However, high-value regions are visibly truncated by faults and dykes, indicating that geological structures disrupt continuity, thereby suggesting that faults and dykes may have influenced gold accumulation (cm.g/t) by acting as geological boundaries or remobilisation conduits, leading to localised variations in spatial distribution. The presence of

geological structures likely contributes to anisotropy, affecting both the reliability of kriging estimates and the interpretation of spatial trends.

7.2. Resource Estimation

Kriging results provide a spatially continuous representation of grade distribution across the study area, reflecting the underlying geological controls and the sampling framework. Overall, the kriged block estimates preserve the global mean grades of the input data, consistent with the unbiased nature of the kriging estimator. As expected, the variance of kriged estimates is lower than that of the raw samples, indicating a smoothing effect, particularly evident in areas with sparse drilling.

Ordinary kriging estimates reveal key patterns in the spatial distribution of variables across the study area. High-value estimates were identified in regions with high actual sample values and dense sampling. Areas with no samples have very low kriged estimated values. However, some unsampled areas contain moderate to high estimated values due to extrapolation (*e.g.*, the north-eastern portion of domain 14). The extrapolation is a result of ordinary kriging's inherent nature to balance local trends while maintaining unbiasedness. Kriging results highlight the differences in spatial predictability among the variables, which are then considered when interpreting estimation reliability.

Sample statistics were derived directly from the raw assay or grade data and represent the observed distribution at the sampling support, while kriged estimate statistics were derived from block or grid estimates generated through kriging, incorporate both data and spatial correlation, and represent expected values at block support. Sample data have minimum values that are lower than kriged estimates, maximum values that are higher than kriged estimates, median values that are lower than kriged estimates, average values that are higher

than those observed in kriged estimates, and standard deviation values that are higher than kriged estimates (Table 6.4 and Table 6.14). The difference between the sample and kriged estimate statistics is due to the kriging smoothing effect, where extreme values are down-weighted by neighbouring information. This smoothing effect is also observed through the significant reduction of the standard deviation. The difference between the sample and kriged estimates' maximum and minimum values indicates an underestimation of the grades by ordinary kriging.

The use of geological domaining played a critical role in shaping the kriged estimates, as continuity patterns were preserved within each domain but did not extend across adjacent domains. For instance, high-grade zones that were spatially continuous in one domain terminated sharply at the domain boundary, with no influence on the estimates of the neighbouring domain (e.g., the boundary between domains 8 and 18). This independence arises from the assumption that domains are internally homogeneous and geostatistically distinct, validating that variograms and estimation parameters were defined separately for each domain-variable feature.

While the approach of delineating domains improves local accuracy and ensures that interpolation reflects geological controls, it also introduces abrupt changes in kriged estimates across boundaries. The discontinuities highlight the importance of domain definition, since poorly constructed boundaries can affect the perceived grade continuity. Overall, the domaining strategy ensured that spatial correlations were respected within domains, especially since the domain boundaries are structurally controlled (Fig. 6.16). Without the definition of domains, a single variogram would have been used across the entire study area, artificially increasing the perceived grade continuity and resulting in greater smoothing of the estimates, which would result in a loss of local variability and misleading classification.

Variogram analysis and kriging neighbourhood analysis play complementary roles in ensuring reliable estimates. The variogram is fundamental to capturing spatial continuity and grade variability, with experimental semi-variograms constructed in different directions and fitted to the spherical theoretical models to account for anisotropy. The semi-variogram models define structural parameters (range, sill, and nugget) that directly influence the weighting of sampled data in kriging. Kriging neighbourhood analysis evaluates how practical search parameters, such as the number of samples, search radius, and block discretisation, affect estimation quality by examining metrics such as slope of regression and kriging efficiency to ensure that block estimates are not excessively smoothed.

In this study, variogram maps were created in various azimuth directions within the study area for each domain-variable combination. Analysis of these variogram maps and semi-variograms reveals anisotropy with major and minor directions of continuity coinciding with the grade continuation trends observed in the raw data. The alignment confirms that the fitted variogram models are geologically reasonable. However, this does not eliminate the limitations that variography results are sensitive to outliers, sparse sampling, and subjective modelling decisions such as the choice of the range, sill, and nugget effect. A well-fitted variogram does not guarantee robust results if kriging neighbourhood parameters are poorly optimised. The combined application of variogram modelling and kriging neighbourhood analysis therefore provides a balanced approach, ensuring that spatial continuity is appropriately represented while practical estimation parameters are tuned to maximise reliability.

While geostatistical parameters influence estimation, geological structures also impose significant control on grade continuity. The influence of geological structures, such as faults and dykes, on both kriging estimates and kriging validation metrics is systematically assessed

across the study area for each variable-domain combination. Kriging estimate maps reveal a strong spatial relationship between high gold accumulation (cm.g/t) and channel width (cm) values and the locations of faults and dyke intrusions, thereby suggesting that geological structures play a significant role in disrupting continuity and influencing grade distribution.

Moderate kriging efficiency regions appear to be truncated by faults and dykes, reinforcing the idea that geological structures impact estimation reliability. Moderate to high kriging efficiency and slope of regression values across domains affirm the validity of the variogram models and parameter selections. However, since kriging variance is directly dependent on variogram parameters rather than spatial trends, no clear relationship was observed between kriging variance and structural controls. No direct assessment was conducted between the slope of regression values and structural variables, as the study area predominantly exhibits high slope of regression values, indicating minimal systematic bias in the kriging predictions.

Statistical analysis of both the kriged estimate results and kriging validation metrics was undertaken. The statistical results, drawn from Table 6.14, reflect spatial distribution and certainty associated with the ordinary kriging process and are comparable to the data that was used for resource estimation. The kriged estimate results are skewed, as evidenced by median values that are higher than the standard deviation and maximum values that are significantly higher than the 75^{th} percentile. However, the kriging validation metrics show that the maximum values are closer to the 75^{th} percentile values and contain relatively lower kriging standard deviation, and therefore lower spatial variance.

Key metrics such as kriging variance, kriging efficiency, and slope of regression were evaluated to quantify and assess the reliability of kriged estimates across the study area. A range of values for kriging variance as a measure of how well the block model fits the estimates

was observed for the different variables across all domains (Table 6.14). The relatively low kriging variance across all variables suggests that the estimation process is reasonably confident, though uncertainty still exists. However, high kriging variance values, concentrated in the northwestern region of the study area for both the gold accumulation (cm.g/t) and channel width (cm) and the northeastern region of the study area for Au (g/t), indicates that the kriged estimated values deviate from actual sample values, owing to the high range of sample influence. Kriging variance maps underscore the critical role of data density in ensuring prediction reliability.

The kriging efficiency is a measure of how well the kriged estimates reflect the true sample values. Areas with very low kriging efficiency suggest low confidence in predicted values throughout this study area. The highest kriging efficiency for all variables is closer to one, indicating that there are areas where kriging performs optimally. The high kriging efficiency regions are concentrated in the central and southwestern regions for the gold accumulation (cm.g/t) and channel with, and in the southwestern region for Au (g/t).

A narrow range of the kriged estimate's slope of regression values was observed. Generally, a high slope of regression value is observed throughout the study area, indicating conditional unbiasedness and no systematic over- or under-estimation of the variable's true values. The slope of regression values indicates that there exists low conditional bias in the kriged estimates, suggesting that the kriged estimates are reliable. However, the relatively lower kriging efficiency and higher kriged variance for channel width (cm) estimates suggest that the kriging process is less effective for channel width estimation, possibly due to the varying non-normal distribution of channel width values throughout the study area (Fig. 6.1).

The kriging estimation results demonstrate ordinary kriging's effectiveness in characterising the spatial distribution of mineral grades while minimising estimation variance. This is supported by the slope of regression closer to one, indicating that the estimated grades are closer to the true sample grades. However, ordinary kriging's reliance on spatial data coverage and variogram models underscores the importance of intense data collection and pre-processing. As such, future efforts should focus on infill drilling to reduce uncertainty in key areas to address specific geological complexities. This is because mineral resource classification must be based on a combination of criteria instead of only one (Glacken and Snowden, 2001).

Finally, swath plots offer a visual means of validation by comparing kriged estimates against input data along selected sections by highlighting local discrepancies and providing a spatial check on the robustness of the ordinary kriging model. Swath plot analyses show kriged values that are consistently below the true sample grades. This is an indication of conditional bias. However, the slope of regression values that are closer to one indicates minimal conditional bias (Vann *et al*., 2003; Mpanza, 2015). This conditional bias could therefore be a result of block discretisation since the KneeLocator function could not adequately determine the inflection point where the variance within blocks begins to flatten.

7.3. Confidence Intervals, Uncertainty Analysis, and Uncertainty Classification

Uncertainty in mineral resource estimation is traditionally assessed through geostatistical validation metrics such as kriging variance and kriging efficiency, and in the case of this study, through confidence interval assessment. These kriging metrics quantify the degree of reliability in block estimates by explicitly considering the spatial structure of data and the distribution of samples within each domain. Low kriging variance areas are classified as measured or indicated, while higher kriging variance areas are classified as inferred resources. The

difference between measured or indicated resources, apart from the value of the kriging variance, is also dependent on the geological interpretation and sample clustering (Emery *et al.,*2006). For example, domains 8 and 19 indicate lower kriging variance for the gold accumulation (cm.g/t) and channel width (cm) values as compared to domain 14's Au (g/t), which leads to the classification of domain 14's Au (g/t) as an inferred mineral resource. This outcome mirrors Emery *et al*. (2006) and Bargawa and Tobin (2020)'s proposal that categorising mineral resources can be distinguished based on kriging variance thresholds.

Lower kriging variance corresponds to lower uncertainty, thereby supporting the classification of measured mineral resources. Visualisation techniques further revealed that high uncertainty regions can exist within low uncertainty areas due to the block-by-block nature of uncertainty assessment, rather than domain-wide averaging. The block-by-block approach to mineral resource uncertainty and classification enhances reliability by preventing averaging in mineral resource classification. This is also evidenced by the fact that high certainty blocks may be found within largely moderate to low certainty blocks (*e.g*., Fig. 6.54 to Fig. 6.56).

In addition to kriging variance, uncertainty was quantified using confidence intervals, which introduce a probabilistic framework into the evaluation process. Confidence intervals define the range within which the true grade is expected to lie at a 90% confidence level, providing a measure of the variability and uncertainty associated with the kriging estimates. Confidence intervals provide insights regarding uncertainty levels, implications for decision-making, and risk management in resource evaluation and planning. Confidence intervals calculated using logarithmic transformation reveal an alignment between kriged estimates and true values. The lower-bound 90% kriged estimates determined through logarithmic transformation are below the maximum observed values for all variables.

Confidence interval percentages across all variables show relatively high percentages of confidence, generally above 70% indicating strong degrees of certainty and reliability in the kriged estimates. The expected confidence percentages deviate from the kriged estimates and exceed the industry-accepted 15% threshold (Davies and Crombie, 2009) with deviation percentages of 23% for the gold accumulation (cm.g/t), 44% for channel width (cm), and 29% for Au (g/t). These values are consistent with observations by Rezaee and Asghari (2012), classification of the Middelvlei Reef as an indicated mineral resource (see Table 6.19 for a guideline on these percentages). While confidence intervals provide an important probabilistic perspective, they also highlight sources of uncertainty that may not be captured by kriging variance alone.

A key insight from this analysis is the extent to which results derived from kriging validation metrics and confidence intervals converge or diverge. In several domains, notably domains 8 and 19, low kriging variance values were accompanied by higher confidence percentages, reinforcing the classification of these areas as measured or indicated resources. Such convergence provides reassurance that the classification outcomes are robust across both geostatistical and probabilistic frameworks. There is an alignment between kriging variation and confidence intervals in that while kriging variance provides a more deterministic measure rooted in data geometry, confidence intervals are sensitive to statistical assumptions and may highlight different aspects of uncertainty, particularly extreme deviations from the mean. The two approaches therefore illuminate different dimensions of uncertainty: kriging variance emphasises spatial data structure, while confidence intervals capture potential variability in block estimates.

The integration of both methods underscores the multifaceted nature of uncertainty analysis. Kriging variance offers a spatially grounded classification tool that aligns closely with

international reporting standards, while confidence intervals provide a probabilistic measure that communicates uncertainty in a more intuitive range-based form. Convergence between low kriging variance and high confidence percentages signals zones of higher reliability that could be prioritised in early planning. Thus, integrating multiple uncertainty metrics provides not only cross-validation of results but also a richer understanding of where estimation uncertainty could materially affect decision-making, providing stakeholders ample time to deterministically (through drilling programs) increase the certainty of their mineral resource.

This study highlights the importance of not relying on a single metric of uncertainty when classifying mineral resources. While kriging variance and efficiency remain the foundation of resource categorisation, the complementary use of confidence intervals expands the analytical framework, enabling both deterministic and probabilistic perspectives to inform decision-making. Importantly, divergences between the two approaches should not be seen as contradictions but as signals of complexity that warrant deeper geological and statistical investigation. A multi-metric approach, therefore, strengthens the classifications of mineral resources and provides a more nuanced foundation for risk management in mineral project evaluation.

7.4. Uncertainty Management

Uncertainty is an inherent aspect of mineral resource estimation, influenced by (1) variability in sampling density, (2) grade continuity, (3) geological complexity, (4) resource estimation methods, and (5) uncertainty quantification methods. Effectively calculating and managing uncertainty is essential for improving confidence in resource models and enabling informed decision-making in mine planning, resource extraction, and investment decisions. This study examines how the selection of resource estimation parameters and uncertainty quantification methods impacts uncertainty assessment and resource classification. The

results demonstrate that areas with dense sampling exhibit higher accuracy, whereas regions with sparse data show increased uncertainty.

Both the calculation and analysis of uncertainty using kriging validation metrics and confidence intervals have proven to be effective tools for understanding and managing the uncertainties associated with mineral resource estimation. The results underscore the critical role of data quality, sampling density, and variogram modelling in influencing uncertainty levels. To further reduce uncertainty and improve confidence in the estimates, future efforts should focus on: (1) conducting additional sampling in areas with broad confidence intervals and low confidence percentages; (2) refining variogram models to better capture spatial continuity, particularly in geologically complex regions; and (3) consistently computing resource models to evaluate the correlation between increased sampling and certainty.

As this study has demonstrated, uncertainty is dependent on factors such as variography, model parameters, geological domaining, and integration of multiple uncertainty quantification methods. Since the key factor that affects mineral resource uncertainty is variography, which is dependent on spatial variability (a factor of sample grade continuity), accurate sample collection is necessary for the improvement of grade continuity. Since most areas within the study area are classified as either medium or high uncertainty, they are flagged as requiring additional sampling. Varied infill drilling in high-variance or low-efficiency areas could significantly reduce uncertainty. Moreover, dynamic sampling plans based on uncertainty maps and confidence interval analyses should be implemented, where cross-validation will be routinely conducted to assess the effectiveness of uncertainty management strategies. Understanding the uncertainty of kriged estimates enables better resource allocation and mitigates the risk of unexpected outcomes during extraction, enhancing transparency by

explicitly communicating the level of confidence in the estimates and allowing resource managers to weigh potential risks and benefits when planning extraction strategies.

8. CONCLUSION

This study applied statistical techniques and ordinary kriging to quantify and manage uncertainty in mineral resource estimation. The research focused on three key objectives: (1) characterising spatial variability and mineral distribution, (2) estimating mineral resources using ordinary kriging, and (3) calculating confidence intervals for uncertainty analysis. By integrating geostatistical methods, the study provides practical insights for resource evaluation and extraction planning, contributing to more informed decision-making in the mining industry.

This research successfully achieved the aim of integrating statistical and geostatistical methods to characterise mineral resources, quantify uncertainty, and propose strategies for improving estimation accuracy. Through exploratory data analysis, variogram modelling, and ordinary kriging, the study provided reliable resource estimates while highlighting areas of high and low confidence. The incorporation of kriging validation metrics and confidence interval analysis further enhanced uncertainty assessment, offering valuable insights for resource classification and mine planning. The findings reinforce the importance of data quality, appropriate estimation parameters, and sound uncertainty quantification methods in mineral resource evaluation.

Exploratory data analysis and statistical assessments of the kriged estimates revealed anisotropy and spatial variability within the study area. Ordinary kriging effectively generated spatially continuous and reliable mineral resource estimates, yet dense sampling and high sample grades did not always correspond to higher extraction volumes or greater estimate certainty. Confidence interval analysis showed that, while the resource models were generally accurate, some mineral resource estimates exhibited errors exceeding the industry-accepted 15% threshold, highlighting persistent uncertainty.

The confidence interval results serve as a critical tool for risk-informed decision-making, enabling a more efficient and sustainable approach to mineral resource management by quantifying the uncertainty associated with a block model estimate instead of averaging the uncertainty of a domain or study area. Integrating confidence intervals into decision-making frameworks enhances mineral resource optimisation, mitigates financial and operational risks, and ensures that resource classification aligns with the degree of certainty in the estimates. High uncertainty areas require mitigation measures such as conservative mine designs that can be adjusted without significantly impacting expected grade-tonnage outputs.

Effective uncertainty management demands a combination of adaptive sampling strategies, sound model validation, and production volume scenario analysis. This study demonstrates that the choice of uncertainty quantification method significantly influences the reliability of resource estimation, emphasising the need for methodological alignment with the geological and sampling characteristics of the deposit.

REFERENCES

Abzalov, M. & Humphreys, M., 2002. Resource Estimation of Structurally Complex and Discontinous Mineralisation Using Non-linear Geostatics: A Case Study of a Mesothermal Gold Deposit in Northern Canada. *Exploration Mining Geology,* 11(1-4), pp. 19-29. DOI: 0964-1823/00 $17.00 + .00.

Amwaama, M., 2018. *Comparison of Kriging Neighbourhood Analysis (KNA) results from two different software packages- A case study.* Johannesburg: Unpublished M.Sc Thesis.

Ashrafpour, E., 2021. *Difference between Simple Kriging and Ordinary Kriging.* s.l.:s.n.

Atalay, F., 2025. Effect of Domaining in Mineral Resource Estimation with Machine Learning. *MINERALS,* p. Online 10.3390/min15040330.

Bai, T. & Tahmasebi, P., 2022. Sequential Gaussian Simulation for geosystems modeling: A machine learning approach. *Geoscience Fronteirs,* Issue 13, pp. 101258-101272. https://doi.org/10.1016/j.gsf.2021.101258.

Barboza, I. & Deutsch, C., 2024. *Quantitative Kriging Neighborhood Analysis (QKNA),* s.l.: J. L. Deutsch (Ed.), Geostatistics Lessons. Retrieved from http://www.geostatisticslessons.com/lessons/qkna.

Bardossy, A., 2017. *Introduction to Geostatistics.* Stuttgart: University of Stuttgart.

Bargawa, W. & Tobing, R., 2020. *Iron Ore Resource Modelling and Estimation using Geostatistics.* AIP Conference Proceedings 2245, Online. https://doi.org/10.1063/5.0006928.

Bariatska, N., 2023. *LinkedIn Pulse.* [Online]
Available at: https://www.linkedin.com/pulse/step-resource-model-validation-nataliia-bariatska/?trackingId=mZOUaCupTmWVum8ceOHoiA%3D%3D
[Accessed 15 January 2025].

Bastante, F., Ordóñez, C., Taboada, J. & Matías, J., 2008. Comparison of indicator kriging, conditional indicator simulation and multiple-point statistics used to model slate deposits. *Engineering Geology,* Volume 98, pp. 50-59. doi:10.1016/j.enggeo.2008.01.006.

Bosman, L., 2013. The relationship between mineral resource reporting, shareholder value and investor confidence. *Master's dissertation [Unpublished].*

Boyle, C., 2010. Kriging neighbourhood analysis by slope of regression and weight of mean – evaluation with the Jura data set. *Mining Technology: Institute of Materials, Minerals and Mining and The AusIMM,* 119(2), pp. 49-60. DOI 10.1179/037178410X12741755140804.

Brus, D. et al., 1996. The performance of spatial interpolation methods and choropleth maps to estimate properties at points: A soil survey case study. *Journal of Environmetrics,* 7(1), pp. 1-16.

Burrough, P. A. & McDonnell, R. A., 1998. *Principles of Geographical Information Systems.* Oxford: Oxford University Press.

Camana, F. & Deutsch, C., 2019. *The Nugget Effect.* [Online]
Available at: http://geostatisticslessons.com/lessons/nuggeteffect
[Accessed 06 April 2023].

Carvalho, D. & Deutsch, C. V., 2017. *An Overview of Multiple Indicator Kriging.* s.l.:J. L. Deutsch.

Choudhury, S., 2015. Comparative Study on Linear and Non-linear Geo-statistical Estimation Methods: A Case Study on Iron Deposit. *Procedia Earth and Planetary Science,* Volume 11 https://doi.org/10.1016/j.proeps.2015.06.017, pp. 131-139.

Clapham, M., 2015. *Matthew E. Clapham.* [Online]
Available at: https://youtu.be/Bs7z_2081T4
[Accessed 10 April 2023].

Coombes, J., 2008. *The art and science of resource estimation.* 1 ed. Perth, Australia: Coombes Capability.

CRIRSCO, 2012. *Standard definitions,* s.l.: CRIRSCO.

Davies, H. & Crombie, I., 2009. *What is Series.* [Online]
Available at: https://grunigen.lib.uci.edu/sites/all/docs/gml/what_are_conf_inter.pdf
[Accessed 12 January 2025].

Daya, A. & Bejari, H., 2015. A comparative study between simple kriging and ordinaru kriging for estimating and modellig the Cu concentration in Chehlkureh deposit, SE Iran. *Arab Journal of Geoscience,* Volume 8, pp. 6003–602. DOI 10.1007/s12517-014-1618-1.

de Costa, G., Hofmann, A. & Agangi, A., 2020. A revised classification scheme of pyrite in the Witwatersrand Basin and application to placer gold deposits. *Earth Science Reviews,* 201(https://doi.org/10.1016/j.earscirev.2019.103064).

de Smith, M., Goodchile, M. & Longley, P., 2021. *Geospatial Analysis: A Comprehensive Guide to Principles, Techniques and Software Tools.* 6 ed. s.l.:Winchelsea Press.

Delbari, M., Afrasiab, P. & Loiskandl, W., 2009. Using sequential Gaussian simulation to assess the field-scale spatial uncertainty of soil water content. *CATENA,* 79(2. doi:10.1016/j.catena.2009.08.001), pp. 163-169.

Deustch, J., Szymanski, J. & Deustch, C., 2014. Checks and measures of performance for kriging estimates. *Journal of the Southern African Institute of Mining and Metallurgy,* 114(3; ISSN 2411-9717), p. 223.

Dohm, C., 2005. Quantifiable Mineral Resource Classification: A Logical Approach. In: O. D. C. (. G. B. 2. Leuangthong, ed. *Quantitative Geology and Geostatistics, vol 14.* s.l.:Springer, Dordrecht, pp. 333-342.

Dominy, S., Noppe, M. & Annels, A., 2002. Errors and Uncertainty in Mineral Resource and Ore Reserve Estimation: The Importance of Getting it Right. *Explor. Mining Geol.,* 22(1-4. 0964-1823/00 $17.00 + .00), pp. 77-79.

Els, B., 1987. *The auriferous Middelvlei reef depositional system, West Wits Line, Witwatersrand Supergroup.,* Rand Afrikaans Univeristy, Johannesburg: Ph. D Thesis (Unpublished).

Els, B., 1988. Pebble Morphology of an Ancient Conglomerate: the Middelvlei Gold Placer, Witwatersrand, South Africa. *Journal of Sedimentary Petrology,* 58(5), pp. 894-901.

Els, B., 1991. Placer Formation during Progradational Fluvial Degradation: The Late Archaean Middelvlei Gold Placer, Witwatersrand, South Africa. *Economic Geology,* Volume 86, pp. 261-277.

Els, B., 1993. Anomalous pebble size variation in an erosive, Late Archaean braided stream: the Middelvlei gold placer, Witwatersrand, South Africa. *Sedimentology,* Volume 40, pp. 41-52.

Emery, X., Ortiz, J. & Rodr´ıguez, J., 2006. Quantifying Uncertainty in Mineral Resources by Use of Classification Schemes and Conditional Simulations. *Mathematical Geology,* 38(4), pp. 445-464.

Esri, 2012. *ArcGIS Resources.* [Online]
Available at: https://resources.arcgis.com/en/help/main/10.1/index.html#//009z00000075000000
[Accessed 25 April 2023].

Etherington, T., 2020. Discrete natural neighbour interpolation with uncertainty using cross-validation error-distance fields. *PeerJ Computer Science,* 6(3. DOI: 10.7717/peerj-cs.282).

Faraj, F., 2020. *Towards Data Science.* [Online]
Available at: https://towardsdatascience.com/why-data-scientists-should-decluster-their-geospatial-datasets-8425b0b2453f

Fonseca, C., Costa, J., Hundershausse, C. & Bassani, M., 2021. Kriging parameter optimisation: global versus local search strategies. *Applied Earth Science,* p. Online: DOI: 10.1080/25726838.2021.1930964.

Frimmel, H., 2014. A Giant Mesoarchaen Crustal Gold-Enrichment Episode: Possible Causes and Consequences for Exploration. *Society of Economic Geologists,* Special Publication(18), pp. 209-234. DOI: 10.5382/SP.18.10.

Frimmel, H., 2019. The Witwatersrand Basin and its Gold Deposits. In: A. Kröner & A. Hofmann, eds. *The Archaean Geology of the Kaapvaal Craton, Southern Africa.* s.l.:Springer, Cham, pp. 255-275. DOI: 10.1007/978-3-319-78652-0_10.

Frimmel, H. & Müller, J., 2011. Estimates of Mineral Resource Availability – How Reliable Are They ?. *Akad. Geowiss. Geotechn.,* Volume 28, pp. 39-62.

Frost, J., 2020. *Introduction to Statistics: An Intuitive Guide for Analyzing Data and Unlocking Discoveries..* s.l.:Statistics By Jim Publishing.

Gibson, M., Jolley, S. & Barnicoat, A., 2000. Interpretation of the Western Ultra Deep Levels 3-D Sesimic Survey. *The Leading Edge,* 19(7), pp. 730-735. DOI: 10.1190/1.1438704.

Gilday, A. & Emsley, S., 2017. Ore body modelling: A detailed study of domain definition and its impact on resource estimates. *Journal of Mining and Geology,* 63(4), pp. 457-475.

Glacken, I. & Snowden, D., 2001. Mineral Resource Estimation. *Mineral Resource and Ore Estimation - The Australasian Institute of Mining and Metallurgy Guide to Good Practice,* Volume 23, pp. 189-198.

Goovaerts, P., 1997. *Geostatistics for natural resources evaluation.* Oxford, England: Oxford University Press.

Hartkamp, A., De Beurs, K., Stein, A. & White, J., 1999. Interpolation techniques for Climate Variables. *NRG-GIS SERIES 99-01,* Volume Natural Resources Group. Geographic Information Systems Series 99-01.

Haslwanter, T., 2022. Statistics and Computing. In: W. I. 9. D. 1. Härdle, ed. *An Introduction to Statistics with Python with Applications in the Life Sciences.* s.l.:Springer International Publishing Switzerland, pp. 75-87.

Hekmat, A., Osanloo, M. & Moarefvand, P., 2011. Block size selection with the objective of minimizing the discrepancy in real and estimated block grade. *Arab Journal of Geosciences,* 6. Online(DOI 10.1007/s12517-011-0321-8).

Hespanhol, L., Vallio, C., Costa, L. & Saragiotto, B., 2019. Understanding and interpreting confidence and credible intervals around effect estimates. *Brazilian Journal of Therapy,* 23(4:290-301. doi: 10.1016/j.bjpt.2018.12.006. Epub 2018 Dec 31. PMID: 30638956; PMC), pp. 290-301.

Holbert, C., 2023. *Calculation of 95% Upper Confidence Limit for Left-Censored Data.* [Online]
Available at: https://www.cfholbert.com/blog/ucl95-calculation-censored-data/
[Accessed 09 September 2025].

Holbert, C., 2023. *Natural Neighbor Interpolation With R.* [Online]
Available at: https://www.cfholbert.com/blog/natural-neighbor-interpolation/
[Accessed 08 September 2025].

Hundelshaussen, J., Costa, J., Marques, D. & Bassani, M., 2018. Localised kriging parameter optimisation based on absolute error minimisation. *Applied Earth Science,* 127(4), pp. 153-162. DOI: 10.1080/25726838.2018.1539536.

Ibrahim, A. & Nasser, R., 2017. Comparison between Inverse Distance Weighted (IDW) and Kriging. *International Journal of Science and Research,* 6(11), p. Online. DOI: 10.21275/ART20177562.

Jara, J. et al., 2006. Block size selection and its impact on open-pit design and mine planning. *ournal of The Southern African Institute of Mining and Metallurgy,* 106(3), pp. 205-211.

Jolly, M., 1984. The sedimentology and economic potential of the auriferous Middelvlei reef on Driefontein consolidated Limites. *Unpublished M.c Thesis,* p. 122.

Journel, A. G. & Huijbregts, C. J., 1978. *Mining geostatistics.* London; New York: Academic Press..

Kim, J. & Deutsch, C., 2022. *Calculation and Modeling of Variogram and Anisotropy.* [Online]
Available at: https://geostatisticslessons.com/pdfs/variogramanisotropy.pdf
[Accessed 16 September 2025].

Krige, D., 1951. A statistical approach to some basic mine valuation problems on the Witwatersrand. *Journal of the Chemical, Metallurgical and Mining Society of South Africa,* pp. 119-137.

Kundu, R., 2022. *V7Labs.* [Online]
Available at: https://www.v7labs.com/blog/f1-score-guide
[Accessed 25 July 2024].

Letanta, D., 2020. *Application of sedimentological and gold assay data for resource estimation: A case study of the Middlevlei Reef, Witwatersrand BAsin (South Africa),* Johannesburg: Unpublished M.Sc Thesis.

Leuangthong, O., Lyster, S., Neufeld, C. & Deutsch, C., 2004. *Optimal Selection of Selective Mining Unit Size for Geostatistical Modeling,* Alberta, Canada: School of Mining and Petroleum Engineering, Department of Civil and Environmental Engineering.

Li, J. & Heap, A., 2014. Spatial interpolation methods applied in the environmental sciences: A review. *Environmental Modelling & Software,* 53(https://doi.org/10.1016/j.envsoft.2013.12.008), pp. 173-189.

Lindi, O., Aladejare, A., Ozoji, T. & Ranta, P., 2024. Uncertainty Quantification in Mineral Resource Estimation. *Natural Resources Research,* 33(https://doi.org/10.1007/s11053-024-10394-6), pp. 2503-2526.

Liu, Z. et al., 2021. An Adaptive Inverse-Distance Weighting Interpolation Method Considering Spatial Differentiation in 3D Geological Modeling. *Geosciences,* 11(51 https://doi.org/10.3390/geosciences11020051).

Mandava, S., Wanless, M. & Minnit, R., 2016. *Improved Grade Estimation Using Optimal Dynamic Anistrophy Resolution,* Johannesburg: Unpublished. SRK Consulting.

McCarthy, T., 1994. *A Review of the Regional Structural Controls on the Occurrence and Character of the Ventersdorp Contact Reef,* Johannesburg: Economic Geology Research Unit.

McManus, S., Rahman, A., Coombes, J. & Horta, A., 2021. Uncertainty assessment of spatial domain models in early stage mining projects- A review. *Ore Geology Reviews,* 133(ISSN 0169-1368), p. 104098. https://doi.org/10.1016/j.oregeorev.2021.104098.

Montgomery, D. C. & Runger, G. C., 2014. *Applied Statistics and Probability for Engineers.* 6 ed. s.l.:Wiley.

Moussa, A. & Abboud, M., 2024. Methodology of Applying Inverse Distance Weighting Interpolation Method in Determining Normal Heights. *Proceedings of Science and Technology ,* 4(DOI: 10.21625/resourceedings.v4i1.1068), pp. 1-6.

Mpanza, M., 2015. *A comparison of ordinary and simple kriging on a PGE resource in the Eastern Limb of the Bushveld Complex,* Johannesburg: Unpublished, M.Sc Eng thesis.

Mudau, M., 2014. *Linear and non-linear resource estimation techniques applied in the Kanzi phosphate project in the Democratic Republic of Congo,* Johannesburg: M.Sc Dissertation Unpublished.

Muntean, J., Frimmel, H., Phillips, N. & Myers, R., 2005. Controversies on the Origin of World-Class Gold Deposits, Part II: Witwatersrand Gold Deposits. *SEG Newsletter,* Volume 60, pp. 7-19.

Myers, R., McCarthy, T. & Stanistreet, I., 1990. A tectono-sedimentary reconstruction of the development and evolution of the Witwatersrand Basin, with particular emphasis on the Centrl rand Groups. *South African Journal of Geology,* 93(1), pp. 180-201.

Njowa, G., 2008. Salient issues in the reporting of mineral resources and mineral reserves in the vein and reef mining. *The South African Institute of Mining and Metallurgy,* pp. 1-15.

Nwaila, G. et al., 2021. The Significance of Erosion Channels on Gold Metallogeny in the Witwatersrand Basin (South Africa): Evidence from the Carbon Leader Reef in the Carletonville Gold Field. *Economic Geology,* 116(2), pp. 265-284. https://doi.org/10.5382/econgeo.4764.

Nwaila, G. et al., 2021. Valorisation of mine waste- Part II: Resource evaluation for consolidated and mineralised mine waste using the Central African Copperbelt as an example. *Journal of Environmental Management,* Issue 299, pp. 1-13. https://doi.org/10.1016/j.jenvman.2021.113553.

O'Donohue, D., 2023. *Understanding Inverse Distance Weighting: A Comprehensive Guide to Understanding and Implementing IDW Interpolation.* [Online] Available at: https://mapscaping.com/understanding-inverse-distance-

weighting/#:~:text=Inverse%20Distance%20Weighting%20%28IDW%29%20is%20an%20interpolation%20technique,based%20on%20the%20values%20of%20nearby%20measured%20points.

[Accessed 08 September 2025].

Ohlert, P., Bach, M. & Breuer, L., 2023. Accuracy assessment of inverse distance weighting interpolation of groundwater nitrate concentrations in Bavaria (Germany). *Environmental Science and Pollution Research ,* 30(https://doi.org/10.1007/s11356-022-22670-), pp. 9445-9455.

Oliver, M. & Webster, R., 2015. *Basic Steps in Geostatistics: The Variogram and Kriging.* Springer Cham Heidelberg New York Dordrecht London: SpringerBriefs in Agriculture; ISBN 978-3-319-15865-5.

Ortiz, J., 2006. Quantifying Uncertainty in Mineral resources based on Classification Schemes and Conditional Simulation. *Journal of the International Association for Mathematical Geology,* 38(4), pp. 445-464.

Owusu, S. & Dagdelen, K., 2019. Critical Review of Mineral Resource Classification Techniques in the Gold Mining Industry. *Insights in Mining Science & Technology,* 1(3. DOI: 10.19080/IMST.2019.01.555564), pp. 74-80.

Owusu, S. & Dagdelen, K., 2024. Impact of Competent Persons' udgements in Mineral Resources classification.. *The Journal of the Southern African Institute of Mining and Metallurgy,* 124(7), p. 371–382.

Phillips, G. & Law, J., 2000. Witwatersrand gold fields: Geology, genesis and exploration. *SEG Reviews,* Volume 13, pp. 439-500.

Phoona, K. et al., 2022. Geotechnical uncertainty, modeling, and decision making. *Soils and Foundations,* 62(5. https://doi.org/10.1016/j.sandf.2022.101189), pp. 1-21.

Pyrcz, M., 2023. *Python Numberical Demos.* [Online]

Available at:

https://github.com/GeostatsGuy/PythonNumericalDemos/blob/master/Interactive_Variogram_Modeling.ipynb

[Accessed August 2024].

Pyrcz, M. & Deutsch, C., 2002. *Declustering and Debias,* Alberta, Canada: s.n.

Randle, C., Bond, C., Lark, R. & Monaghan, A., 2019. Uncertainty in geological interpretations: Effectiveness of expert elicitations. *Geosphere,* 15(1 https://doi.org/10.1130/GES01586.1), pp. 108-119.

Rezaee, H. & Asghari, O., 2012. Accounting for Secondary Variable for the Classification of Mineral Resources using Cokriging Technique; a Case Study of Sarcheshmeh Porphyry Copper Deposit. *International Journal of Mining and Geo-Engineering, University of Tehran,* 46(1), pp. 67-80.

Shishvan, M. & Benndorf, J., 2016. The effect of geological uncertainty on achieving short-term targets: A quantitative approach using stochastic process simulation. *Journal of South African Institute of Mining and Metallurgy,* 116(3. https://doi.org/10.17159/2411-9717/2016/v116n3a7), pp. 259-264.

Silva, D. & Boisvert, J., 2014. Mineral resource classification: a comparison of new and existing techniques. *Journal of the South African Institute of Mining and Metallurgy,* Volume 114, pp. 265-274.

Sunday, C. & Deutsch, C., 2020. *Geostatistics Lessons.* [Online]

Available at: https://geostatisticslessons.com/lessons/discretization

[Accessed 24 October 2024].

Tucker, R., Viljoen, R. & Viljoen, M., 2016. A Review of the Witwatersrand Basin- The World's Greatest Goldfield. *Journal of International Geoscience,* 38(2), pp. 104-133. DOI: 10.18814/epiiugs/2016/v39i2/95771.

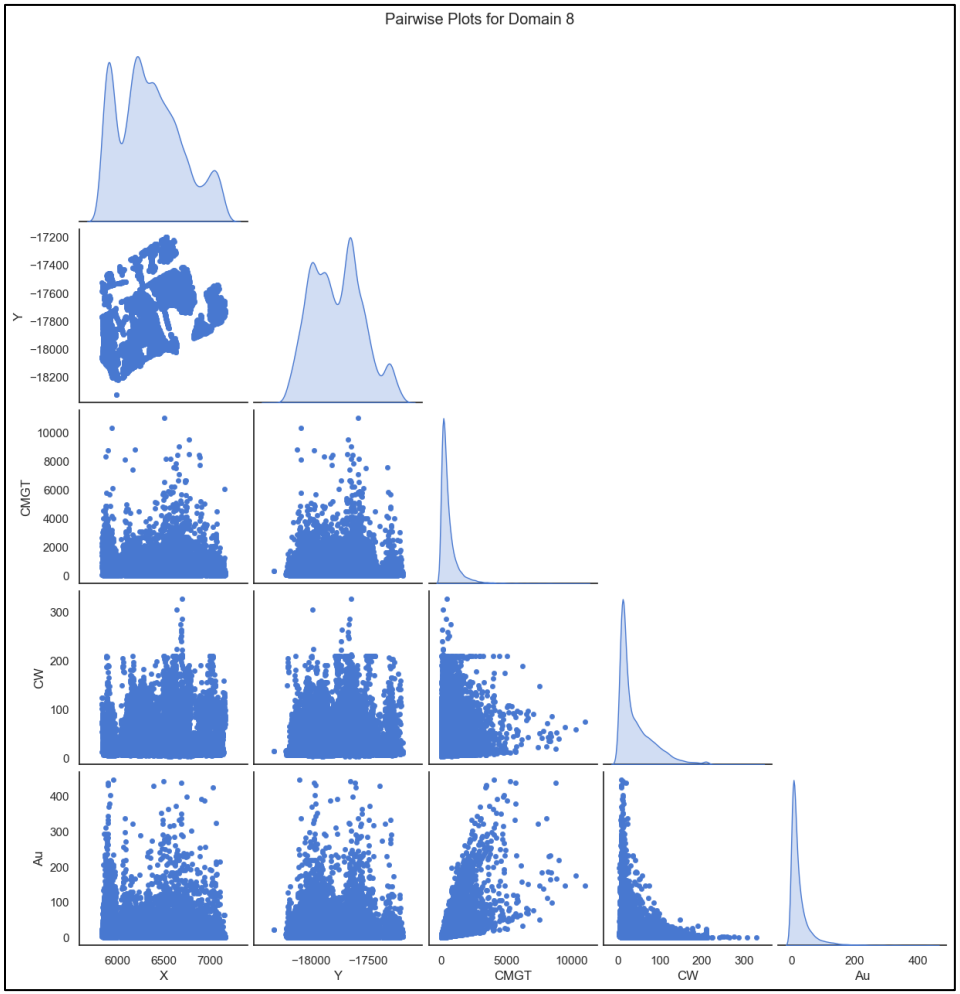
Vann, J., Jackson, S. & Bertoli, O., 2003. Quantitative kriging neighbourhood analysis pp. 215–223.. *Proceedings of the Fifth International Mining Geology Conference,* pp. 215-223.

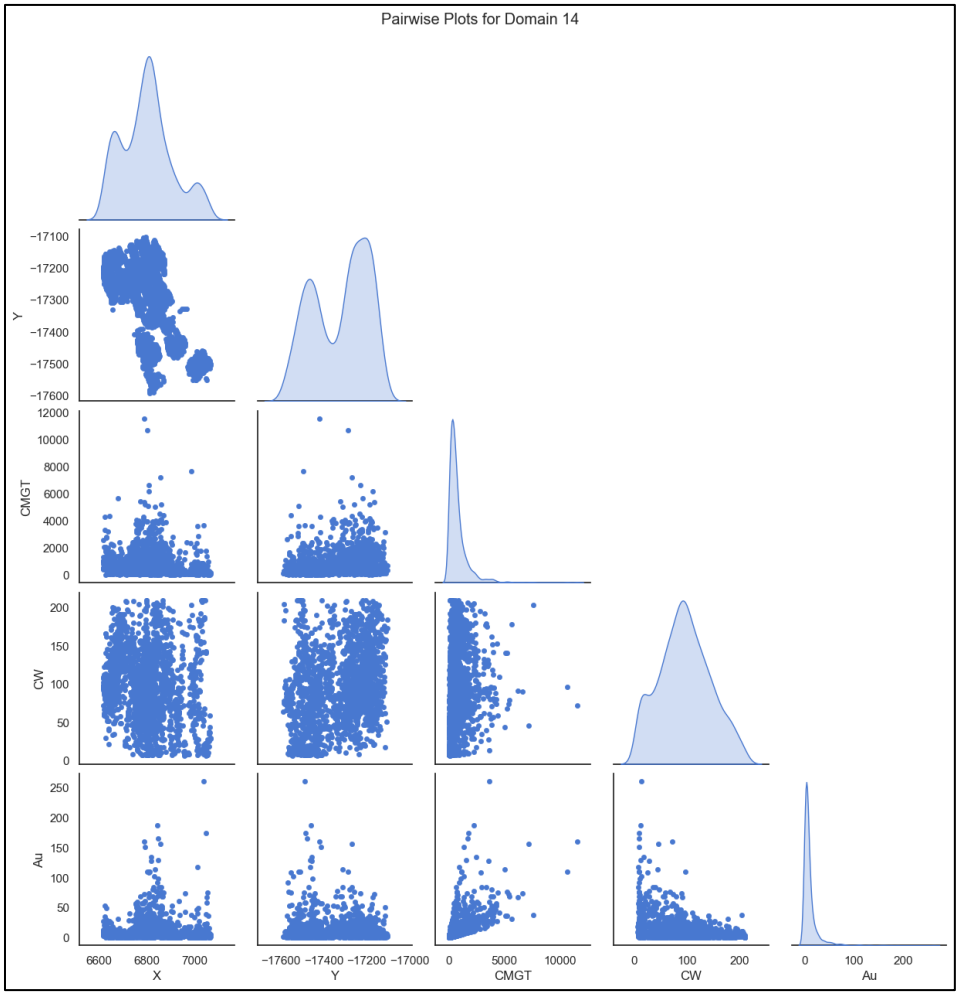
Wahid, M. & Winarno, E., 2024. Bauxite Resource Estimation Analysis Using Ordinary Kriging and Inverse Distance Weighting in West Kalimantan. *Journal of Earth and Marine Technology,* 4(2 ISSN 2723-8105), pp. 225-264.

Zhang, S. et al., 2023. Machine Learning-Based Delineation of Geodomain Boundaries: A Proof-of-Concept Study Using Data from the Witwatersrand Goldfields. *Natural Resources Research,* 32(3), pp. Online https://doi.org/10.1007/s11053-023-10159-7.

APPENDIX

Pairwise Plots





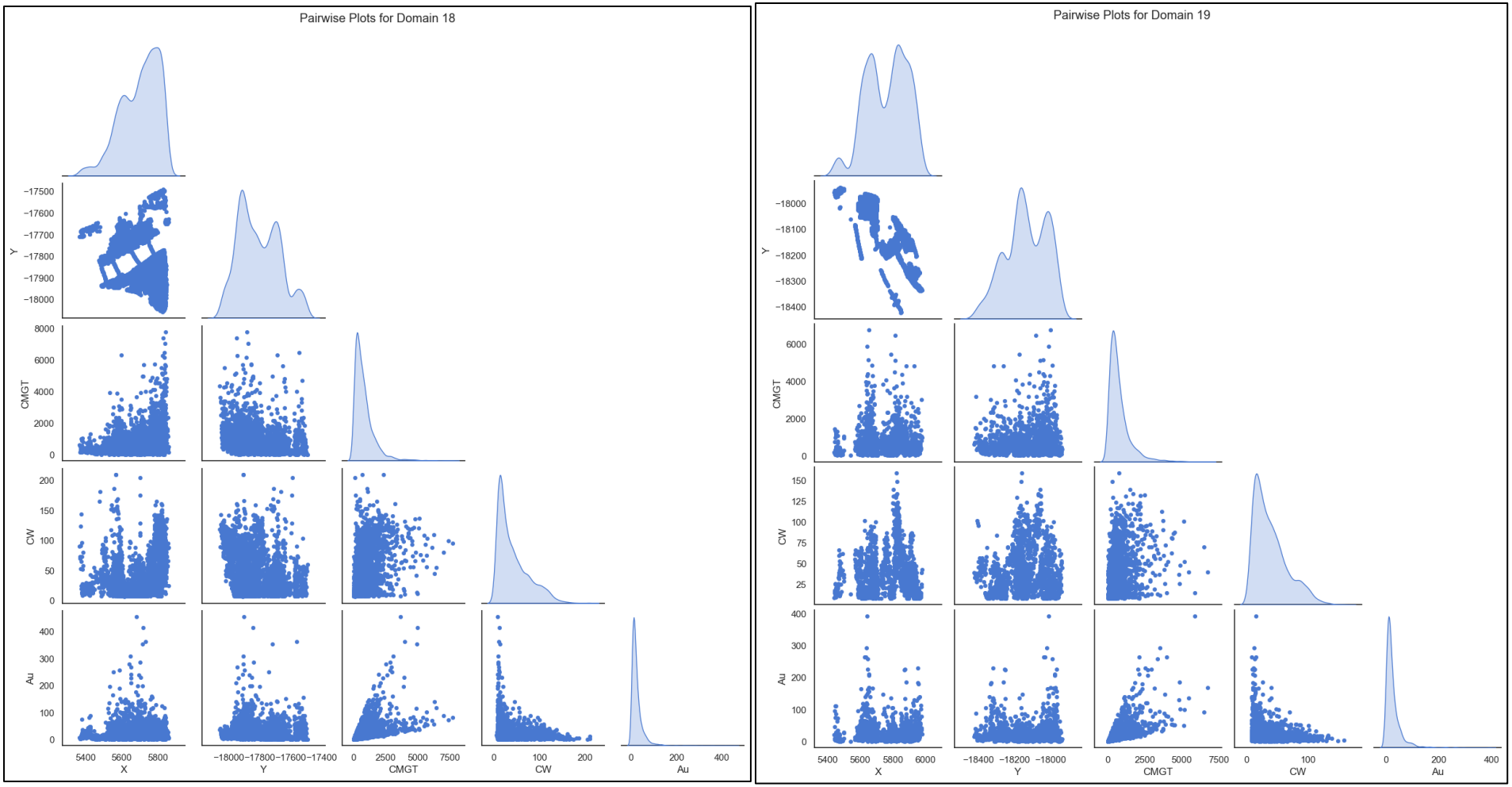


Figure A1: Pairwise plots showing the relationships between different variables within each domain.

Correlation Heatmaps

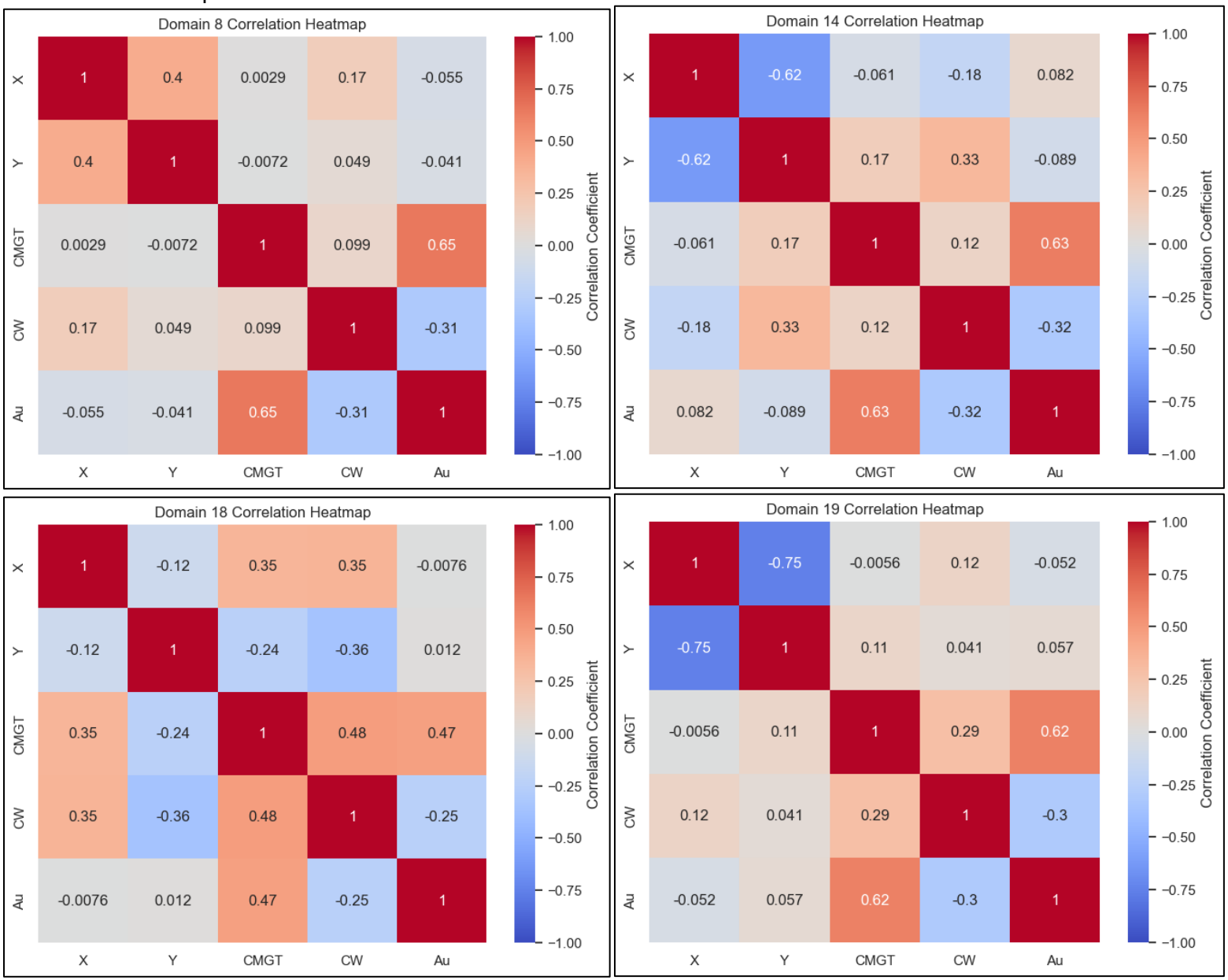
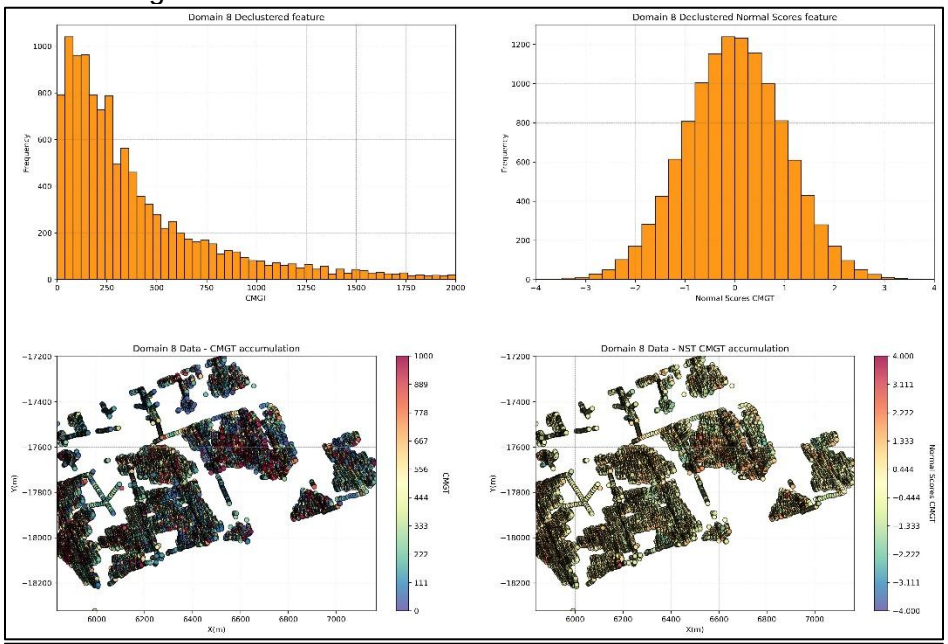
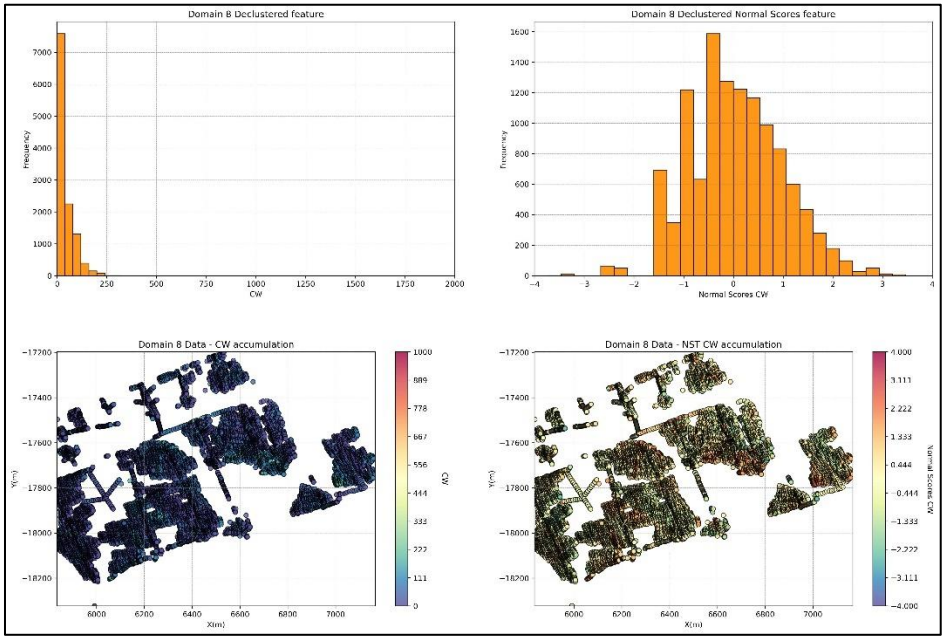
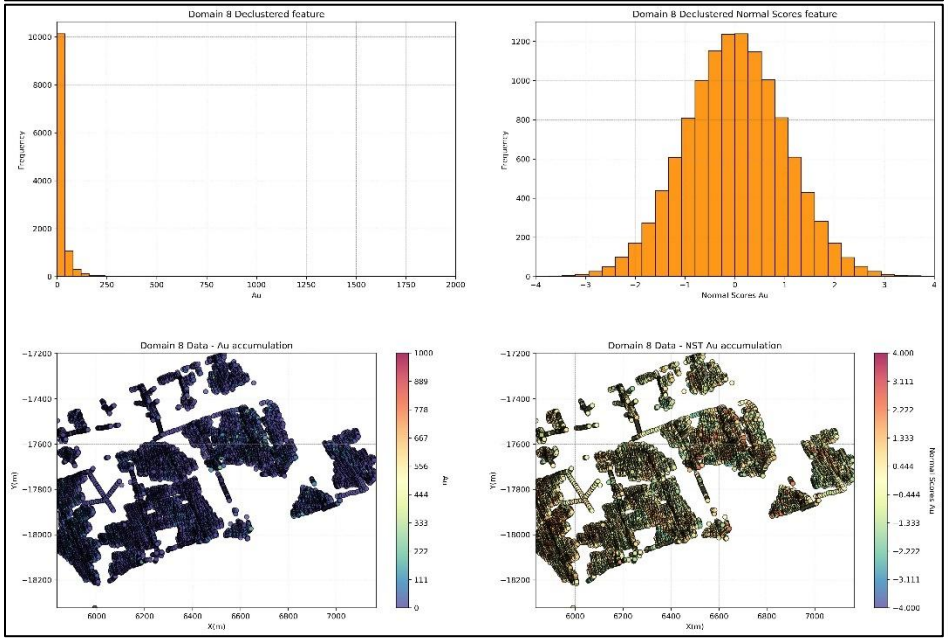


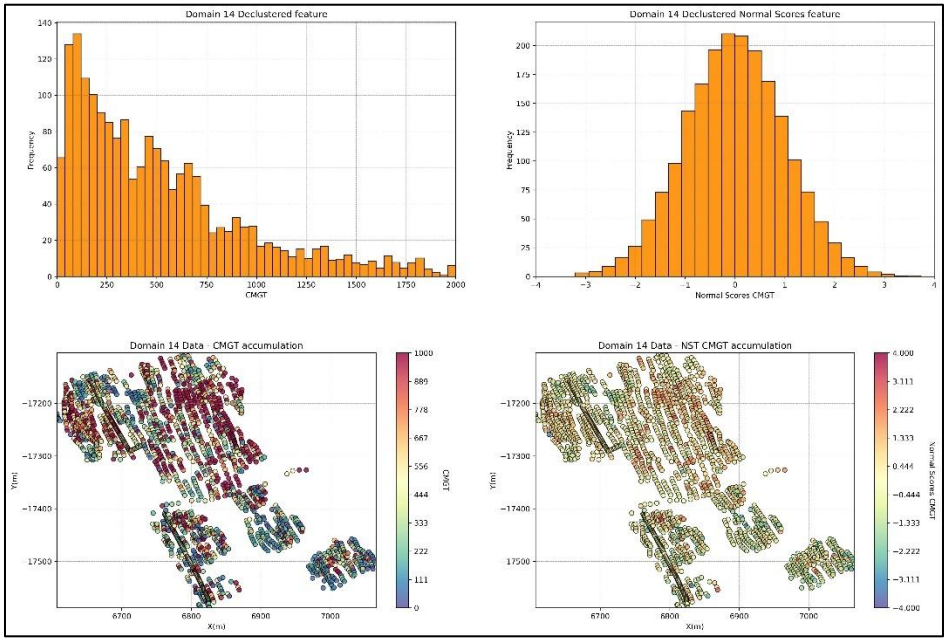
Figure A2: Pearson’s correlation heatmaps for the different domains

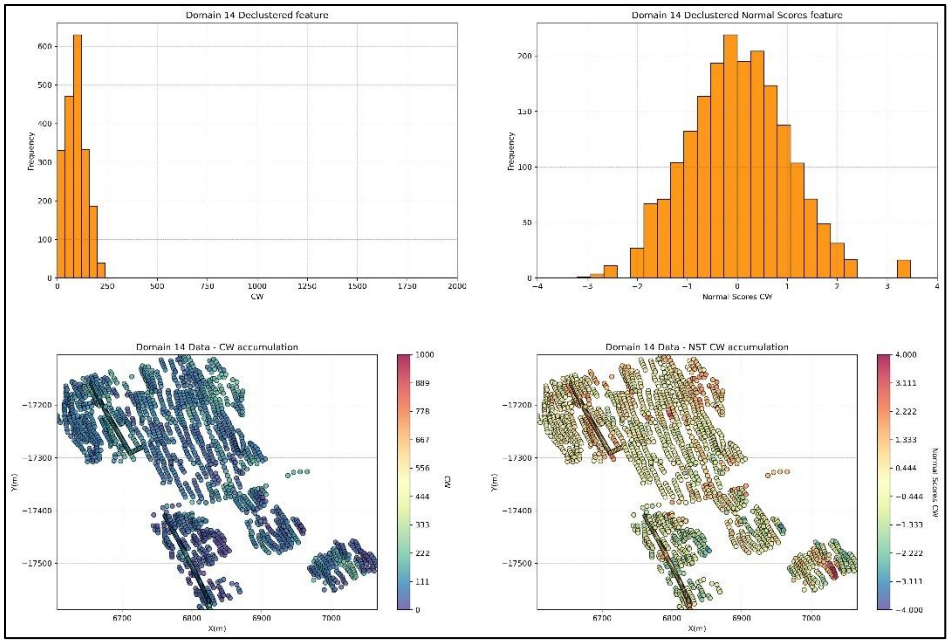
Declustering

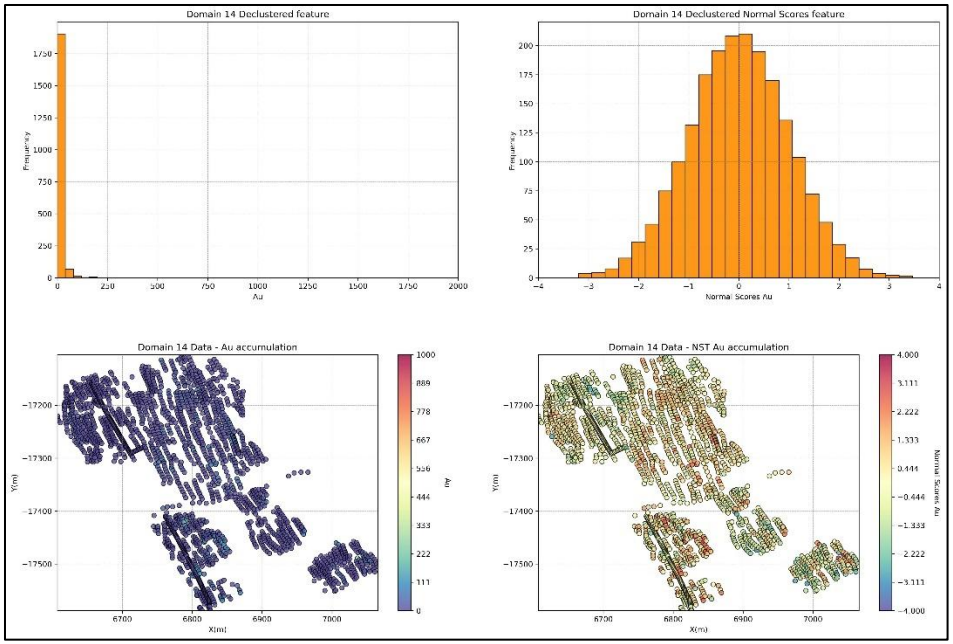


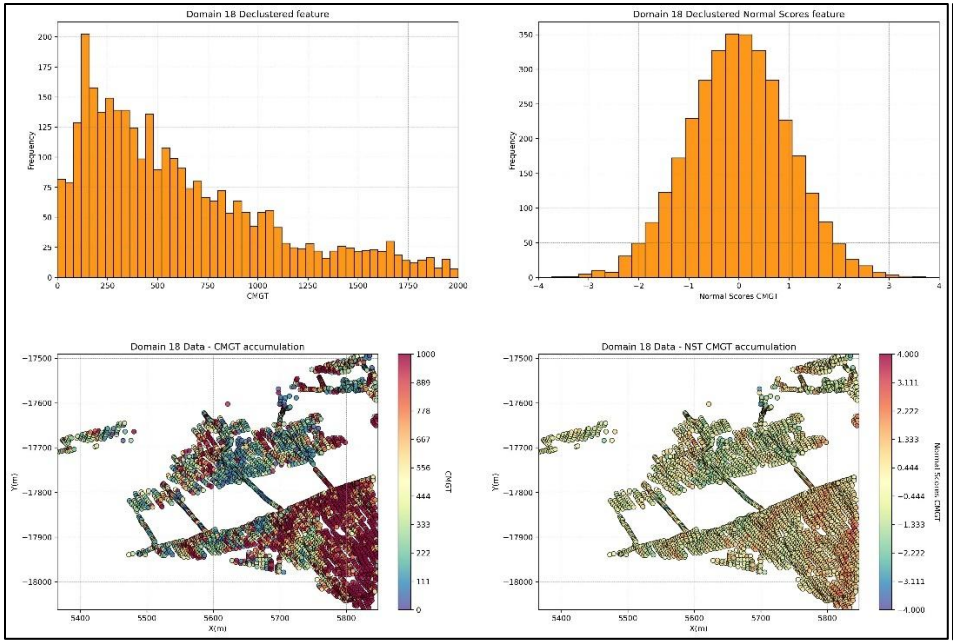


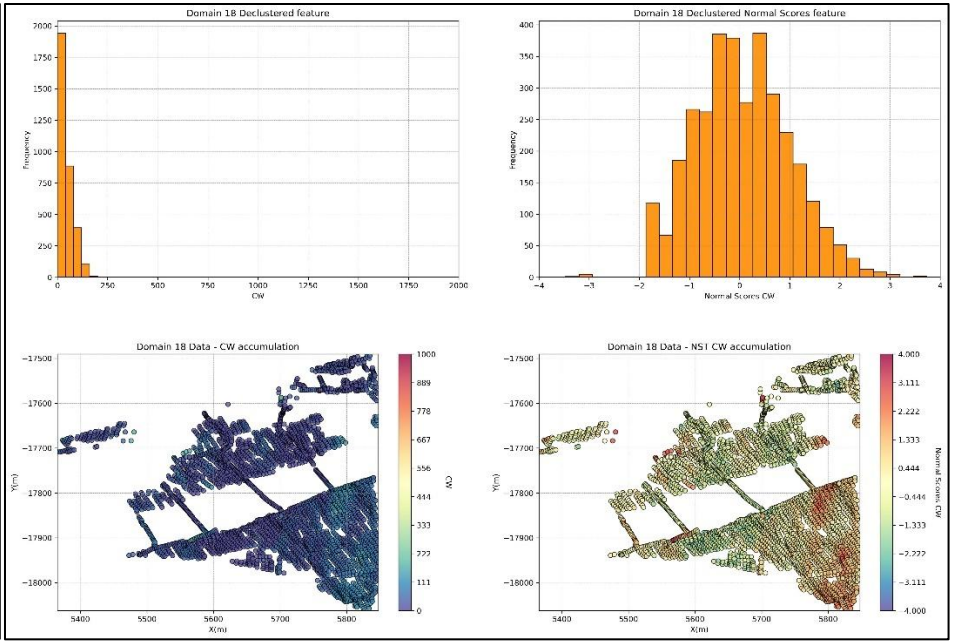


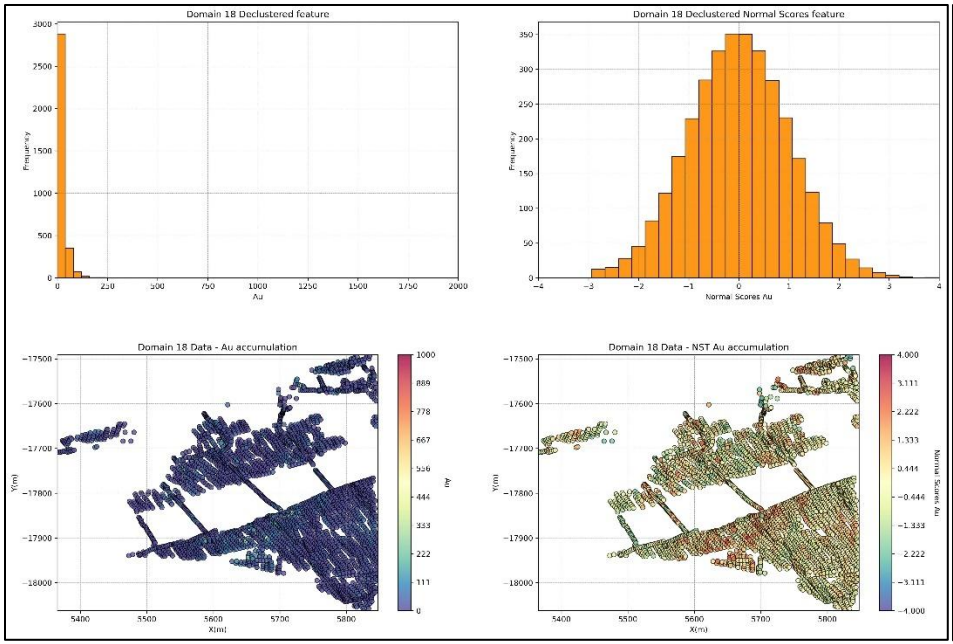


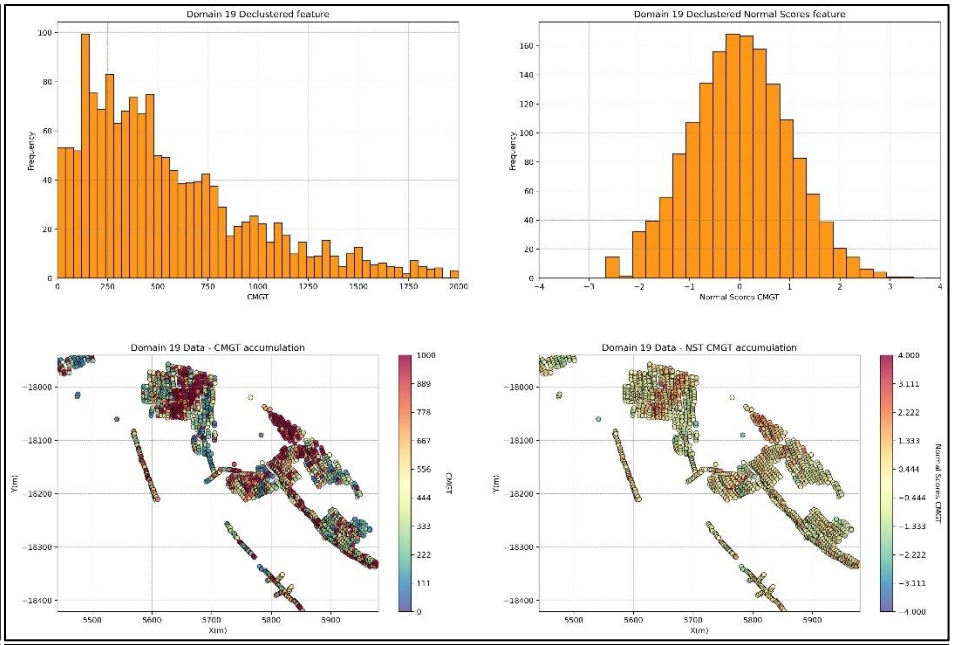

Domain 14 Declustered feature
Frequency
CW
Domain 14 Declustered Normal Scores feature
Frequency
Normal Scores CW
Domain 14 Data - CW accumulation
Y(m)
X(m)
CW
Domain 14 Data - NST CW accumulation
Y(m)
X(m)
Normal Scores CW

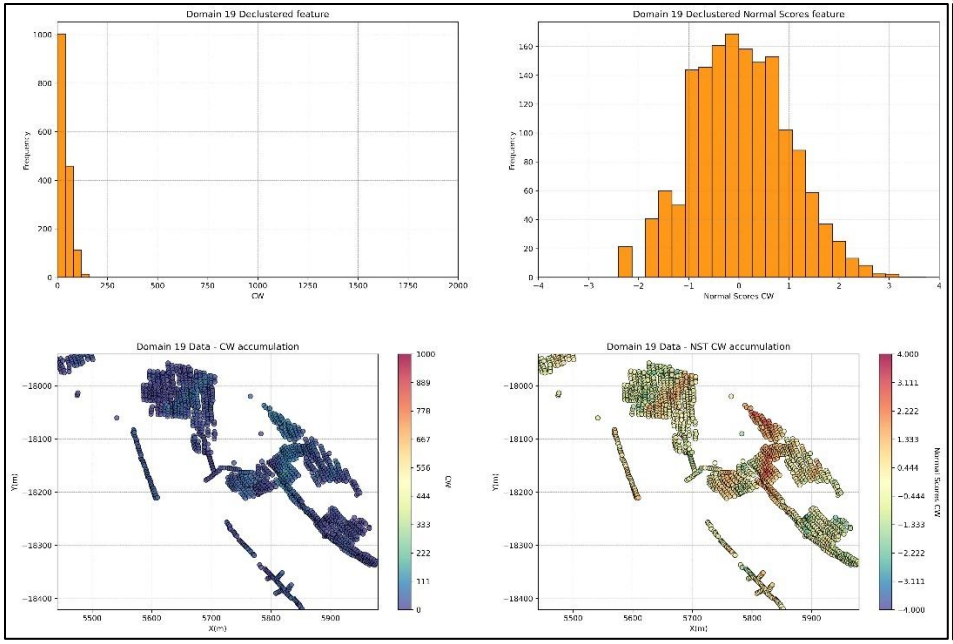

Domain 14 Declustered feature
Frequency
Au
Domain 14 Declustered Normal Scores feature
Frequency
Normal Scores Au
Domain 14 Data - Au accumulation
Y(m)
X(m)
Au
Domain 14 Data - NST Au accumulation
Y(m)
X(m)
Normal Scores Au


Domain 18 Declustered feature
Frequency
CMGT
Domain 18 Declustered Normal Scores feature
Frequency
Normal Scores CMGT
Domain 18 Data - CMGT accumulation
Y(m)
X(m)
CMGT
Domain 18 Data - NST CMGT accumulation
Y(m)
X(m)
Normal Scores CMGT


Domain 18 Declustered feature
Frequency
CW
Domain 18 Declustered Normal Scores feature
Frequency
Normal Scores CW
Domain 18 Data - CW accumulation
Y(m)
X(m)
CW
Domain 18 Data - NST CW accumulation
Y(m)
X(m)
Normal Scores CW


Domain 18 Declustered feature
Frequency
Au
Domain 18 Declustered Normal Scores feature
Frequency
Normal Scores Au
Domain 18 Data - Au accumulation
Y(m)
X(m)
Au
Domain 18 Data - NST Au accumulation
Y(m)
X(m)
Normal Scores Au


Domain 19 Declustered feature
Frequency
CMGT
Domain 19 Declustered Normal Scores feature
Frequency
Normal Scores CMGT
Domain 19 Data - CMGT accumulation
Y(m)
X(m)
CMGT
Domain 19 Data - NST CMGT accumulation
Y(m)
X(m)
Normal Scores CMGT


Domain 19 Declustered feature
Frequency
CW
Domain 19 Declustered Normal Scores feature
Frequency
Normal Scores CW
Domain 19 Data - CW accumulation
Y(m)
X(m)
CW
Domain 19 Data - NST CW accumulation
Y(m)
X(m)
Normal Scores CW

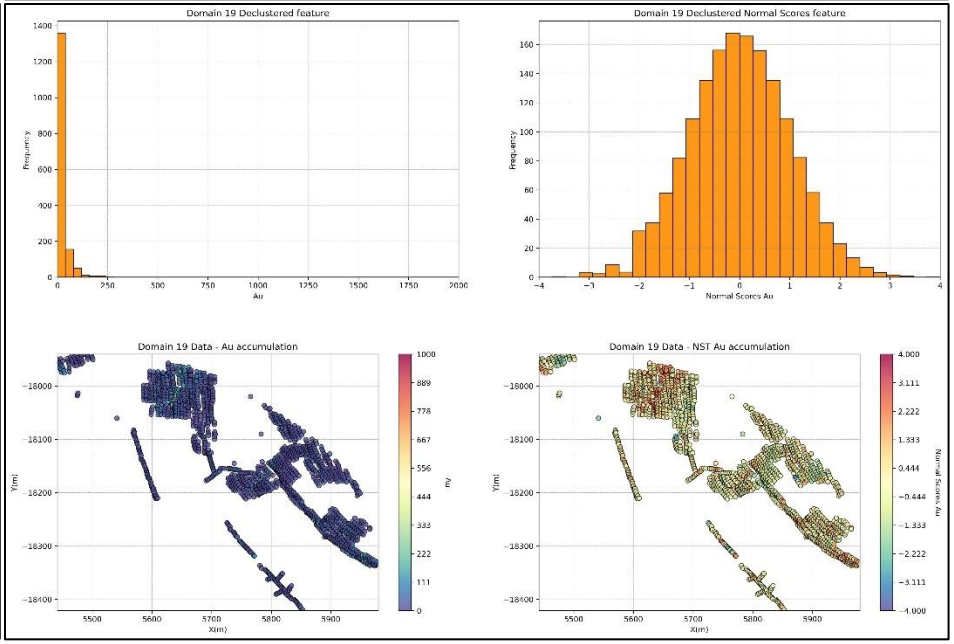

Domain 19 Declustered feature
Frequency
Au
Domain 19 Declustered Normal Scores feature
Frequency
Normal Scores Au
Domain 19 Data - Au accumulation
Y(m)
X(m)
Au
Domain 19 Data - NST Au accumulation
Y(m)
X(m)
Normal Scores Au

Figure A3: Scatter plots and histograms showing histograms and scatter plots for each variable-domain's combination for the declustered estimation data.

Table A1: Within-block variance for various discretisation block and discretisation number combinations for each variable.

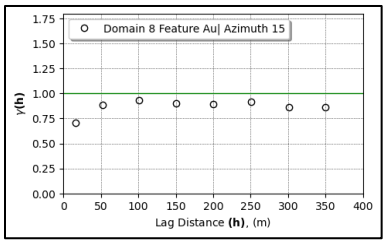
		Domain 8			Domain 14			Domain 18			Domain 19		
Discretisation Block	Discretisation number	CMGT within-blocks variance	CW within-blocks variance	Au within-blocks variance	CMGT within-blocks variance	CW within-blocks variance	Au within-blocks variance	CMGT within-blocks variance	CW within-blocks variance	Au within-blocks variance	CMGT Within Blocks Variance	CW within-blocks variance	Au within-blocks variance
4	2	0.7075	0.4115	0.6280	0.5933	0.6030	0.5847	0.4813	0.2609	0.6620	0.6447	0.3567	0.7403
9	3	0.7112	0.4198	0.6345	0.5978	0.6074	0.5894	0.4855	0.2651	0.6663	0.6520	0.3643	0.7444
16	4	0.7124	0.4223	0.6364	0.5992	0.6088	0.5908	0.4868	0.2663	0.6676	0.6542	0.3666	0.7456
25	5	0.7128	0.4234	0.6373	0.5998	0.6094	0.5914	0.4873	0.2669	0.6681	0.6552	0.3676	0.7461
36	6	0.7131	0.4240	0.6377	0.6001	0.6097	0.5917	0.4876	0.2672	0.6684	0.6557	0.3682	0.7464
49	7	0.7132	0.4243	0.6380	0.6003	0.6098	0.5919	0.4878	0.2673	0.6686	0.6559	0.3685	0.7466
64	8	0.7133	0.4245	0.6381	0.6004	0.6099	0.5920	0.4879	0.2674	0.6687	0.6561	0.3686	0.7467
81	9	0.7134	0.4246	0.6382	0.6004	0.6100	0.5921	0.4879	0.2675	0.6688	0.6562	0.3688	0.7467
100	10	0.7134	0.4247	0.6383	0.6005	0.6101	0.5922	0.4880	0.2675	0.6688	0.6563	0.3689	0.7468
121	11	0.7135	0.4248	0.6384	0.6005	0.6101	0.5922	0.4880	0.2676	0.6689	0.6564	0.3689	0.7468
144	12	0.7135	0.4248	0.6384	0.6006	0.6101	0.5922	0.4880	0.2676	0.6689	0.6564	0.3690	0.7468
169	13	0.7135	0.4249	0.6384	0.6006	0.6102	0.5923	0.4881	0.2676	0.6689	0.6565	0.3690	0.7469
196	14	0.7135	0.4249	0.6384	0.6006	0.6102	0.5923	0.4881	0.2676	0.6689	0.6565	0.3690	0.7469
225	15	0.7135	0.4249	0.6385	0.6006	0.6102	0.5923	0.4881	0.2677	0.6689	0.6565	0.3691	0.7469
256	16	0.7135	0.4250	0.6385	0.6006	0.6102	0.5923	0.4881	0.2677	0.6690	0.6565	0.3691	0.7469
289	17	0.7135	0.4250	0.6385	0.6006	0.6102	0.5923	0.4881	0.2677	0.6690	0.6566	0.3691	0.7469
324	18	0.7136	0.4250	0.6385	0.6006	0.6102	0.5923	0.4881	0.2677	0.6690	0.6566	0.3691	0.7469
361	19	0.7136	0.4250	0.6385	0.6006	0.6102	0.5923	0.4881	0.2677	0.6690	0.6566	0.3691	0.7469
400	20	0.7136	0.4250	0.6385	0.6006	0.6102	0.5923	0.4881	0.2677	0.6690	0.6566	0.3691	0.7469

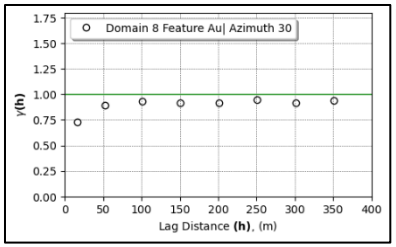
Table A2: Table showing results from quantitative neighbourhood analysis post validation

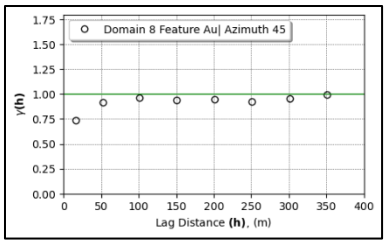
Domain	Number of samples	Gold accumulation index						Channel width						Au					
		Declustered mean	Kriging mean	Kriged etsimate	Kriging efficiency	Slope of regression	Absolute Error	Declustered mean	Kriging mean	Kriged etsimate	Kriging efficiency	Slope of regression	Absolute Error	Declustered mean	Kriging mean	Kriged etsimate	Kriging efficiency	Slope of regression	Absolute Error
8	5	585.496	494.952	494.952	0.943	0.908	90.544	42.500	45.604	45.604	0.935	0.915	3.104	25.877	19.080	19.080	0.949	0.920	6.798
	7	585.496	497.242	497.242	0.955	0.924	88.253	42.500	45.415	45.415	0.943	0.925	2.914	25.877	19.284	19.284	0.959	0.933	6.593
	9	585.496	498.986	498.986	0.961	0.934	86.510	42.500	44.939	44.939	0.948	0.932	2.439	25.877	19.688	19.688	0.964	0.941	6.189
	11	585.496	501.718	501.718	0.965	0.940	83.778	42.500	44.870	44.870	0.952	0.937	2.370	25.877	19.749	19.749	0.968	0.947	6.128
	13	585.496	500.239	500.239	0.968	0.946	85.256	42.500	44.826	44.826	0.955	0.941	2.326	25.877	19.770	19.770	0.971	0.952	6.107
	15	585.496	499.862	499.862	0.970	0.949	85.634	42.500	44.886	44.886	0.958	0.944	2.386	25.877	19.781	19.781	0.973	0.955	6.096
	17	585.496	499.657	499.657	0.972	0.953	85.839	42.500	44.823	44.823	0.960	0.947	2.323	25.877	19.818	19.818	0.975	0.958	6.059
	19	585.496	501.331	501.331	0.974	0.955	84.165	42.500	44.829	44.829	0.963	0.950	2.329	25.877	19.910	19.910	0.977	0.961	5.967
	21	585.496	501.736	501.736	0.975	0.958	83.760	42.500	44.793	44.793	0.965	0.952	2.293	25.877	19.878	19.878	0.978	0.963	5.999
	23	585.496	504.200	504.200	0.976	0.960	81.296	42.500	44.727	44.727	0.966	0.954	2.227	25.877	19.963	19.963	0.980	0.965	5.915
	25	585.496	503.323	503.323	0.977	0.962	82.172	42.500	44.698	44.698	0.968	0.955	2.198	25.877	19.967	19.967	0.981	0.967	5.910
	27	585.496	503.894	503.894	0.978	0.963	81.601	42.500	44.716	44.716	0.969	0.957	2.216	25.877	20.020	20.020	0.982	0.969	5.857
	29	585.496	503.110	503.110	0.979	0.964	82.385	42.500	44.768	44.768	0.970	0.958	2.268	25.877	19.978	19.978	0.983	0.970	5.899
	31	585.496	502.838	502.838	0.979	0.966	82.658	42.500	44.782	44.782	0.972	0.960	2.282	25.877	19.978	19.978	0.984	0.971	5.900
	33	585.496	502.804	502.804	0.980	0.967	82.692	42.500	44.874	44.874	0.972	0.961	2.374	25.877	19.951	19.951	0.984	0.972	5.927
	35	585.496	502.590	502.590	0.981	0.968	82.906	42.500	44.928	44.928	0.973	0.962	2.428	25.877	19.951	19.951	0.985	0.973	5.927
14	5	748.264	593.775	593.775	0.974	0.971	154.488	95.740	87.369	87.369	0.975	0.972	8.372	10.660	9.054	9.054	0.974	0.972	1.607
	7	748.264	589.153	589.153	0.978	0.975	159.110	95.740	86.542	86.542	0.978	0.975	9.199	10.660	9.289	9.289	0.978	0.975	1.371
	9	748.264	595.405	595.405	0.980	0.977	152.858	95.740	86.455	86.455	0.980	0.977	9.285	10.660	9.465	9.465	0.980	0.977	1.195
	11	748.264	599.733	599.733	0.981	0.979	148.530	95.740	86.611	86.611	0.982	0.979	9.129	10.660	9.596	9.596	0.981	0.979	1.064
	13	748.264	605.973	605.973	0.982	0.980	142.291	95.740	86.660	86.660	0.983	0.980	9.080	10.660	9.740	9.740	0.982	0.980	0.921
	15	748.264	607.979	607.979	0.983	0.980	140.285	95.740	86.347	86.347	0.983	0.981	9.393	10.660	9.801	9.801	0.983	0.981	0.860
	17	748.264	608.456	608.456	0.984	0.981	139.807	95.740	86.310	86.310	0.984	0.981	9.431	10.660	9.902	9.902	0.984	0.981	0.759
	19	748.264	610.405	610.405	0.984	0.982	137.859	95.740	86.453	86.453	0.985	0.982	9.287	10.660	9.977	9.977	0.985	0.982	0.683
	21	748.264	608.827	608.827	0.985	0.982	139.437	95.740	86.330	86.330	0.985	0.983	9.410	10.660	10.041	10.041	0.985	0.983	0.619
	23	748.264	613.112	613.112	0.985	0.983	135.152	95.740	86.245	86.245	0.986	0.984	9.495	10.660	10.164	10.164	0.986	0.983	0.497
	25	748.264	616.784	616.784	0.986	0.983	131.480	95.740	86.372	86.372	0.987	0.984	9.368	10.660	10.254	10.254	0.986	0.984	0.407
	27	748.264	619.633	619.633	0.986	0.984	128.631	95.740	86.163	86.163	0.987	0.984	9.577	10.660	10.283	10.283	0.987	0.984	0.377
	29	748.264	621.488	621.488	0.987	0.984	126.776	95.740	86.255	86.255	0.987	0.985	9.485	10.660	10.296	10.296	0.987	0.984	0.364
	31	748.264	622.108	622.108	0.987	0.985	126.155	95.740	85.994	85.994	0.988	0.985	9.746	10.660	10.338	10.338	0.987	0.985	0.323
	33	748.264	622.227	622.227	0.988	0.985	126.037	95.740	85.902	85.902	0.988	0.985	9.838	10.660	10.344	10.344	0.988	0.985	0.316
	35	748.264	622.121	622.121	0.988	0.985	126.143	95.740	85.895	85.895	0.988	0.986	9.845	10.660	10.359	10.359	0.988	0.985	0.302
18	5	807.175	903.909	903.909	0.946	0.947	96.734	41.920	56.685	56.685	0.896	0.915	14.765	25.273	21.563	21.563	0.973	0.967	3.710
	7	807.175	910.987	910.987	0.951	0.951	103.812	41.920	55.991	55.991	0.901	0.919	14.071	25.273	21.947	21.947	0.977	0.971	3.325
	9	807.175	906.249	906.249	0.954	0.954	99.074	41.920	55.101	55.101	0.906	0.922	13.181	25.273	22.505	22.505	0.979	0.974	2.768
	11	807.175	902.251	902.251	0.957	0.956	95.076	41.920	54.936	54.936	0.909	0.924	13.017	25.273	22.645	22.645	0.981	0.976	2.628
	13	807.175	900.671	900.671	0.959	0.958	93.495	41.920	54.884	54.884	0.911	0.925	12.965	25.273	22.709	22.709	0.983	0.978	2.564
	15	807.175	895.550	895.550	0.960	0.960	88.374	41.920	54.746	54.746	0.913	0.926	12.827	25.273	22.808	22.808	0.984	0.979	2.465
	17	807.175	895.372	895.372	0.962	0.961	88.196	41.920	54.682	54.682	0.915	0.928	12.762	25.273	22.801	22.801	0.985	0.980	2.472
	19	807.175	898.522	898.522	0.963	0.962	91.347	41.920	54.651	54.651	0.917	0.929	12.731	25.273	22.796	22.796	0.985	0.981	2.476
	21	807.175	899.521	899.521	0.963	0.962	92.345	41.920	54.656	54.656	0.917	0.930	12.737	25.273	22.742	22.742	0.986	0.982	2.530
	23	807.175	906.394	906.394	0.964	0.963	99.219	41.920	54.636	54.636	0.918	0.930	12.716	25.273	22.814	22.814	0.986	0.982	2.459
	25	807.175	907.788	907.788	0.965	0.964	100.612	41.920	54.601	54.601	0.920	0.931	12.681	25.273	22.858	22.858	0.987	0.983	2.415
	27	807.175	906.221	906.221	0.966	0.964	99.046	41.920	54.563	54.563	0.922	0.932	12.643	25.273	22.732	22.732	0.987	0.983	2.541
	29	807.175	905.543	905.543	0.966	0.965	98.368	41.920	54.544	54.544	0.923	0.933	12.624	25.273	22.770	22.770	0.988	0.984	2.503
	31	807.175	903.758	903.758	0.967	0.965	96.583	41.920	54.525	54.525	0.924	0.934	12.605	25.273	22.770	22.770	0.988	0.984	2.502
	33	807.175	904.847	904.847	0.967	0.966	97.671	41.920	54.473	54.473	0.924	0.934	12.554	25.273	22.779	22.779	0.988	0.985	2.494
	35	807.175	905.024	905.024	0.968	0.966	97.848	41.920	54.499	54.499	0.925	0.935	12.579	25.273	22.800	22.800	0.988	0.985	2.472
19	5	771.665	659.685	659.685	0.983	0.979	111.980	39.201	35.897	35.897	0.968	0.968	3.304	26.475	24.051	24.051	0.981	0.976	2.424
	7	771.665	662.303	662.303	0.986	0.982	109.362	39.201	35.922	35.922	0.971	0.970	3.279	26.475	24.766	24.766	0.985	0.980	1.709
	9	771.665	658.366	658.366	0.988	0.984	113.299	39.201	35.954	35.954	0.972	0.972	3.247	26.475	24.745	24.745	0.987	0.982	1.730
	11	771.665	664.394	664.394	0.989	0.985	107.271	39.201	35.810	35.810	0.974	0.973	3.390	26.475	25.071	25.071	0.988	0.984	1.404
	13	771.665	671.597	671.597	0.990	0.986	100.068	39.201	35.819	35.819	0.976	0.974	3.381	26.475	25.412	25.412	0.989	0.985	1.063
	15	771.665	672.318	672.318	0.991	0.987	99.347	39.201	35.829	35.829	0.977	0.976	3.372	26.475	25.311	25.311	0.990	0.986	1.164
	17	771.665	671.794	671.794	0.992	0.988	99.871	39.201	35.701	35.701	0.978	0.976	3.500	26.475	25.094	25.094	0.991	0.987	1.380
	19	771.665	668.001	668.001	0.992	0.989	103.664	39.201	35.646	35.646	0.979	0.977	3.555	26.475	24.991	24.991	0.991	0.987	1.483
	21	771.665	669.615	669.615	0.993	0.989	102.050	39.201	35.714	35.714	0.979	0.978	3.486	26.475	24.821	24.821	0.992	0.988	1.654
	23	771.665	668.863	668.863	0.993	0.990	102.802	39.201	35.628	35.628	0.980	0.978	3.573	26.475	24.817	24.817	0.993	0.989	1.657
	25	771.665	672.876	672.876	0.994	0.991	98.789	39.201	35.497	35.497	0.981	0.979	3.703	26.475	25.099	25.099	0.993	0.989	1.376
	27	771.665	676.577	676.577	0.995	0.991	95.088	39.201	35.526	35.526	0.982	0.980	3.674	26.475	25.167	25.167	0.993	0.990	1.308
	29	771.665	679.746	679.746	0.995	0.992	91.919	39.201	35.604	35.604	0.983	0.980	3.597	26.475	25.259	25.259	0.994	0.990	1.215
	31	771.665	678.189	678.189	0.995	0.992	93.476	39.201	35.638	35.638	0.983	0.981	3.563	26.475	25.272	25.272	0.994	0.991	1.202
	33	771.665	677.055	677.055	0.996	0.992	94.610	39.201	35.632	35.632	0.984	0.981	3.569	26.475	25.155	25.155	0.995	0.991	1.319
	35	771.665	678.179	678.179	0.996	0.993	93.486	39.201	35.513	35.513	0.984	0.982	3.688	26.475	25.195	25.195	0.995	0.991	1.279

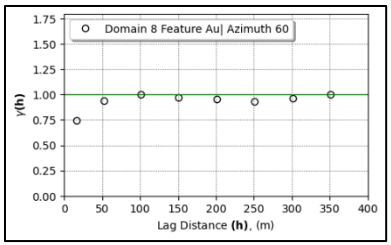
Experimental Variograms

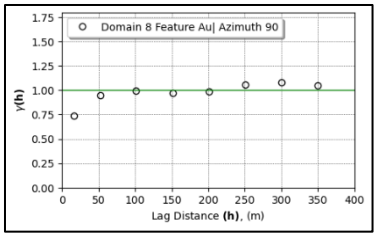


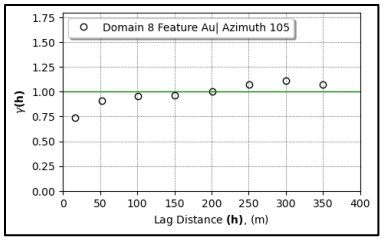

Domain 8 Feature Au| Azimuth 15
γ(h)
Lag Distance (h), (m)

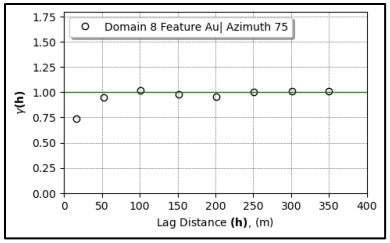

Domain 8 Feature Au| Azimuth 30
γ(h)
Lag Distance (h), (m)

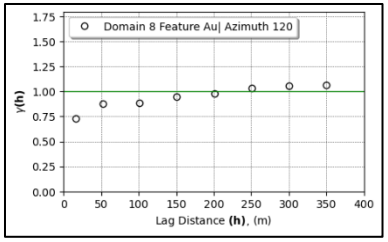

Domain 8 Feature Au| Azimuth 45
γ(h)
Lag Distance (h), (m)

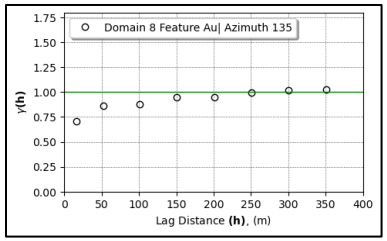

Domain 8 Feature Au| Azimuth 60
γ(h)
Lag Distance (h), (m)

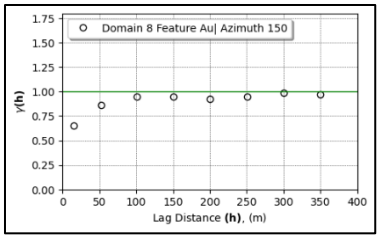

Domain 8 Feature Au| Azimuth 90
γ(h)
Lag Distance (h), (m)

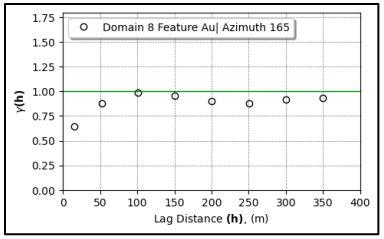

Domain 8 Feature Au| Azimuth 105
γ(h)
Lag Distance (h), (m)

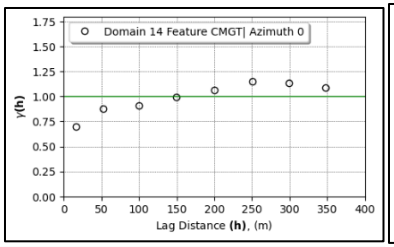

Domain 8 Feature Au| Azimuth 75
γ(h)
Lag Distance (h), (m)

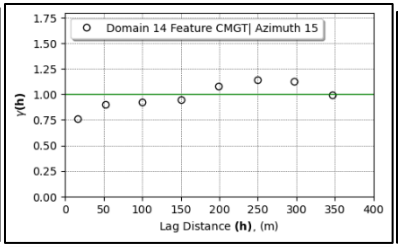

Domain 8 Feature Au| Azimuth 120
γ(h)
Lag Distance (h), (m)

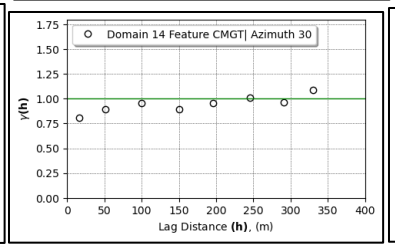

Domain 8 Feature Au| Azimuth 135
γ(h)
Lag Distance (h), (m)

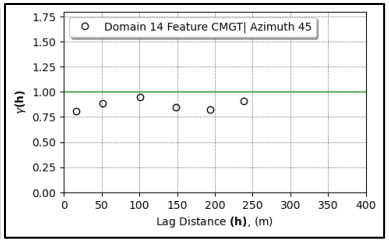

Domain 8 Feature Au| Azimuth 150
γ(h)
Lag Distance (h), (m)

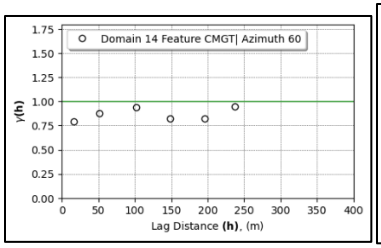

Domain 8 Feature Au| Azimuth 165
γ(h)
Lag Distance (h), (m)

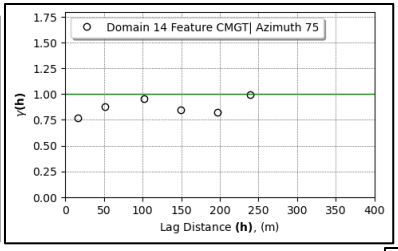

Domain 14 Feature CMGT| Azimuth 0
γ(h)
Lag Distance (h), (m)

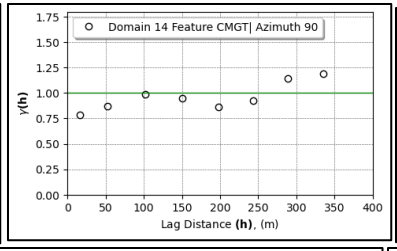

Domain 14 Feature CMGT| Azimuth 15
γ(h)
Lag Distance (h), (m)

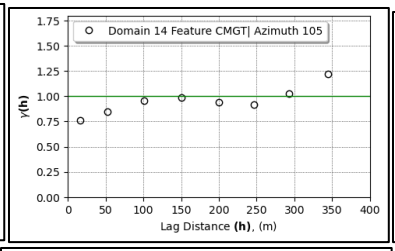

Domain 14 Feature CMGT| Azimuth 30
γ(h)
Lag Distance (h), (m)

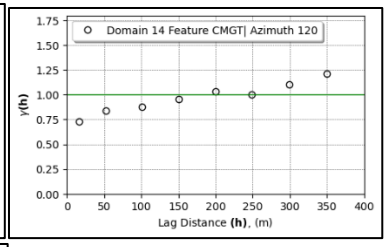

Domain 14 Feature CMGT| Azimuth 45
γ(h)
Lag Distance (h), (m)

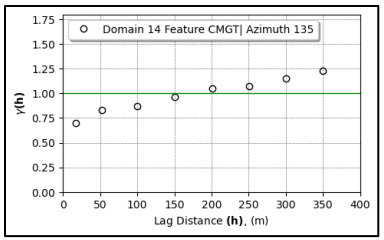

Domain 14 Feature CMGT| Azimuth 60
γ(h)
Lag Distance (h), (m)

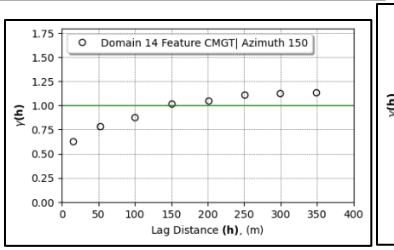

Domain 14 Feature CMGT| Azimuth 75
γ(h)
Lag Distance (h), (m)

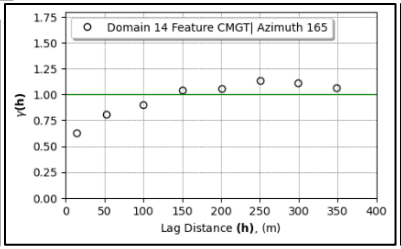

Domain 14 Feature CMGT| Azimuth 90
γ(h)
Lag Distance (h), (m)

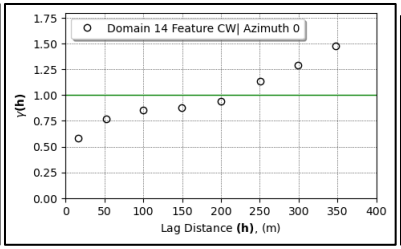

Domain 14 Feature CMGT| Azimuth 105
γ(h)
Lag Distance (h), (m)

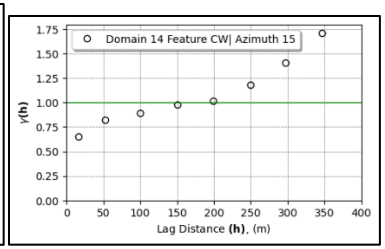

Domain 14 Feature CMGT| Azimuth 120
γ(h)
Lag Distance (h), (m)

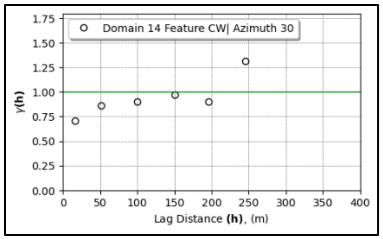

Domain 14 Feature CMGT| Azimuth 135
γ(h)
Lag Distance (h), (m)

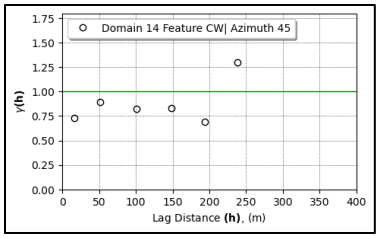

Domain 14 Feature CMGT| Azimuth 150
γ(h)
Lag Distance (h), (m)

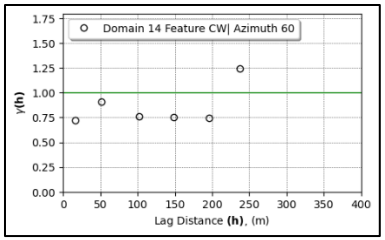

Domain 14 Feature CMGT| Azimuth 165
γ(h)
Lag Distance (h), (m)

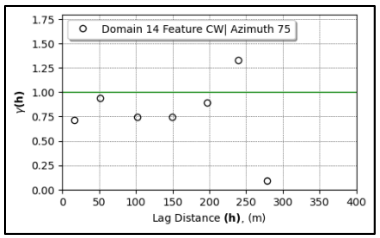

Domain 14 Feature CW| Azimuth 0
γ(h)
Lag Distance (h), (m)

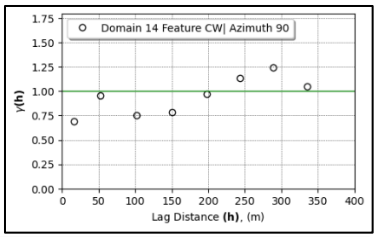

Domain 14 Feature CW| Azimuth 15
γ(h)
Lag Distance (h), (m)

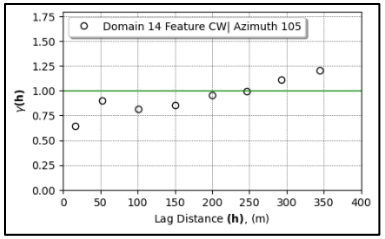

Domain 14 Feature CW| Azimuth 30
γ(h)
Lag Distance (h), (m)

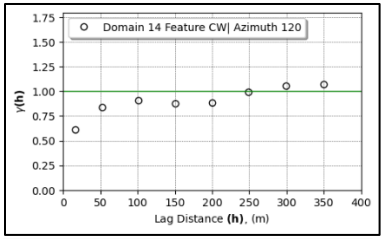

Domain 14 Feature CW| Azimuth 45
γ(h)
Lag Distance (h), (m)

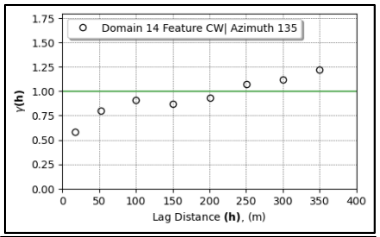

Domain 14 Feature CW| Azimuth 60
γ(h)
Lag Distance (h), (m)

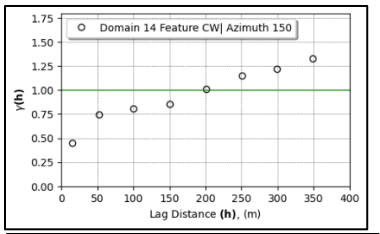

Domain 14 Feature CW| Azimuth 75
γ(h)
Lag Distance (h), (m)

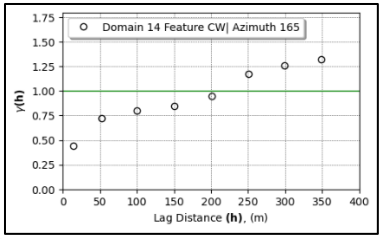

Domain 14 Feature CW| Azimuth 90
γ(h)
Lag Distance (h), (m)

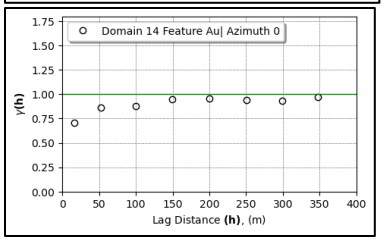

Domain 14 Feature CW| Azimuth 105
γ(h)
Lag Distance (h), (m)

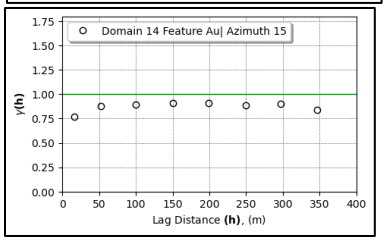

Domain 14 Feature CW| Azimuth 120
γ(h)
Lag Distance (h), (m)

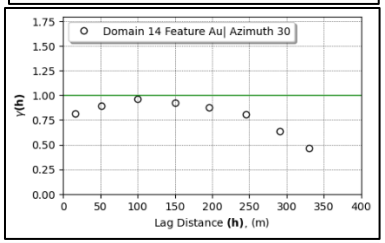

Domain 14 Feature CW| Azimuth 135
γ(h)
Lag Distance (h), (m)

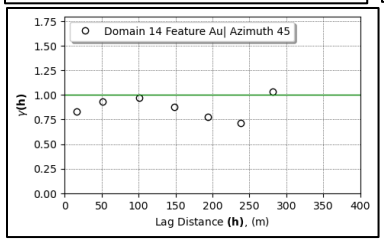

Domain 14 Feature CW| Azimuth 150
γ(h)
Lag Distance (h), (m)

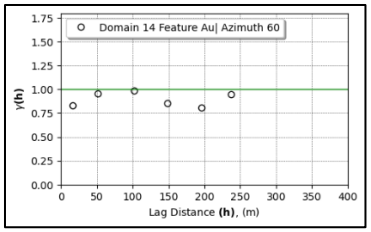

Domain 14 Feature CW| Azimuth 165
γ(h)
Lag Distance (h), (m)

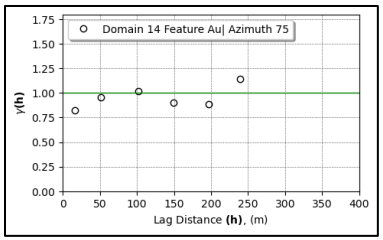

Domain 14 Feature Au| Azimuth 0
γ(h)
Lag Distance (h), (m)

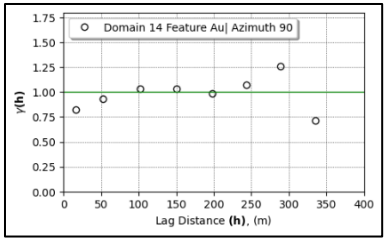

Domain 14 Feature Au| Azimuth 15
γ(h)
Lag Distance (h), (m)

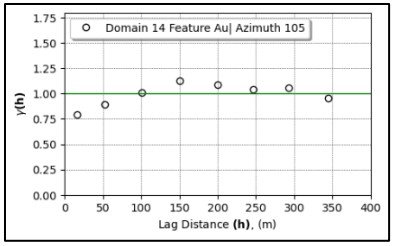

Domain 14 Feature Au| Azimuth 30
γ(h)
Lag Distance (h), (m)

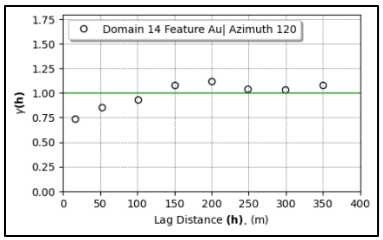

Domain 14 Feature Au| Azimuth 45
γ(h)
Lag Distance (h), (m)

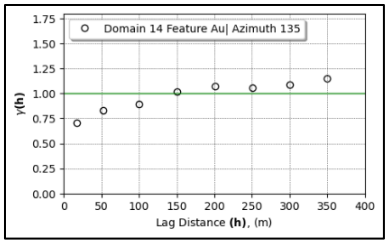

Domain 14 Feature Au| Azimuth 60
γ(h)
Lag Distance (h), (m)

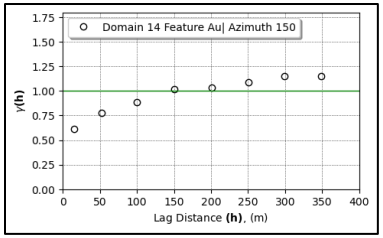

Domain 14 Feature Au| Azimuth 75
γ(h)
Lag Distance (h), (m)

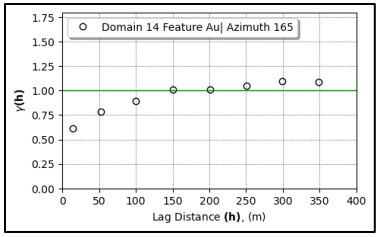

Domain 14 Feature Au| Azimuth 90
γ(h)
Lag Distance (h), (m)

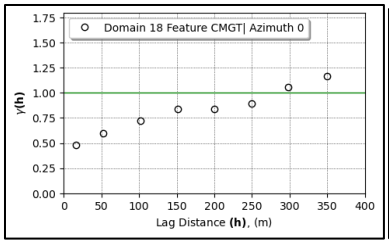

Domain 14 Feature Au| Azimuth 105
γ(h)
Lag Distance (h), (m)

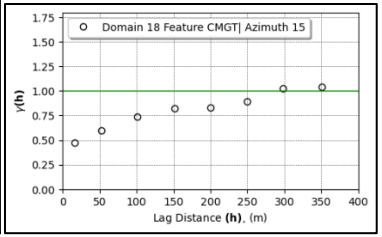

Domain 14 Feature Au| Azimuth 120
γ(h)
Lag Distance (h), (m)

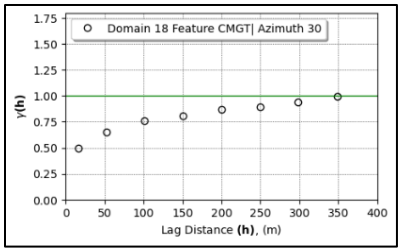

Domain 14 Feature Au| Azimuth 135
γ(h)
Lag Distance (h), (m)

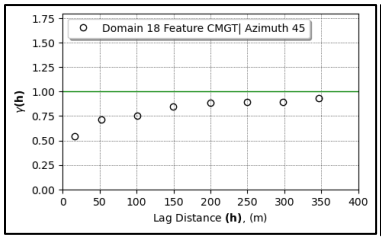

Domain 14 Feature Au| Azimuth 150
γ(h)
Lag Distance (h), (m)

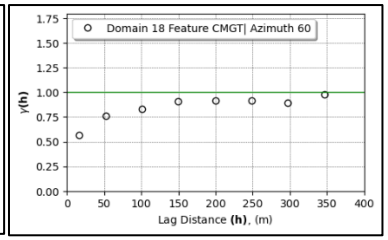

Domain 14 Feature Au| Azimuth 165
γ(h)
Lag Distance (h), (m)

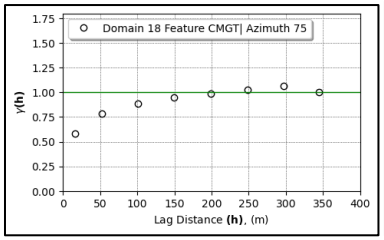

Domain 18 Feature CMGT| Azimuth 0
γ(h)
Lag Distance (h), (m)

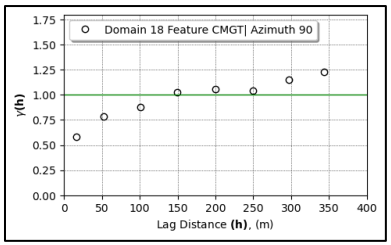

Domain 18 Feature CMGT| Azimuth 15
γ(h)
Lag Distance (h), (m)

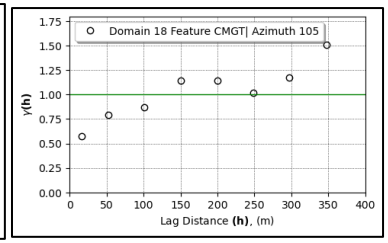

Domain 18 Feature CMGT| Azimuth 30
γ(h)
Lag Distance (h), (m)

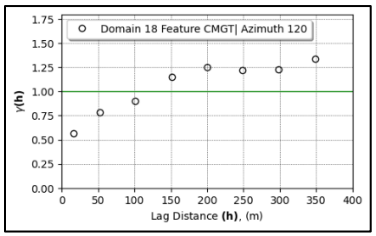

Domain 18 Feature CMGT| Azimuth 45
γ(h)
Lag Distance (h), (m)

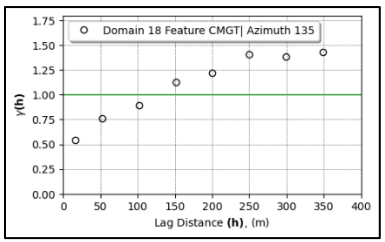

Domain 18 Feature CMGT| Azimuth 60
γ(h)
Lag Distance (h), (m)

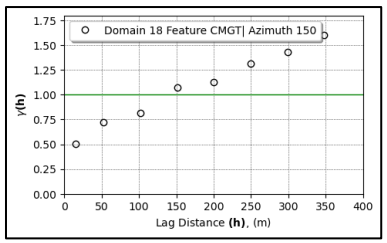

Domain 18 Feature CMGT| Azimuth 75
γ(h)
Lag Distance (h), (m)

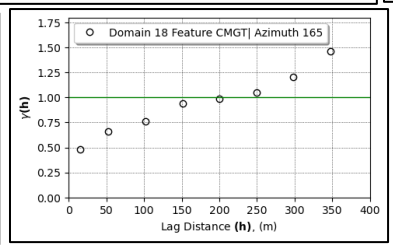

Domain 18 Feature CMGT| Azimuth 90
γ(h)
Lag Distance (h), (m)

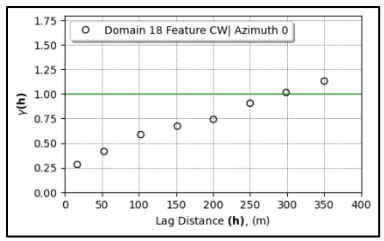

Domain 18 Feature CMGT| Azimuth 105
γ(h)
Lag Distance (h), (m)

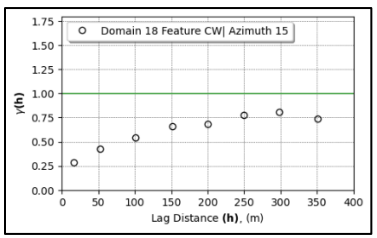

Domain 18 Feature CMGT| Azimuth 120
γ(h)
Lag Distance (h), (m)

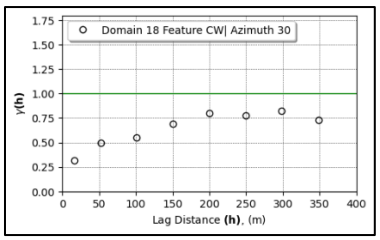

Domain 18 Feature CMGT| Azimuth 135
γ(h)
Lag Distance (h), (m)

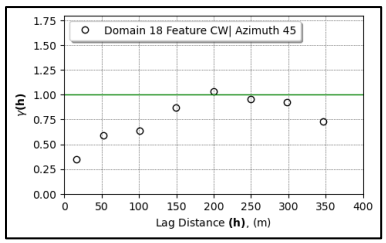

Domain 18 Feature CMGT| Azimuth 150
γ(h)
Lag Distance (h), (m)

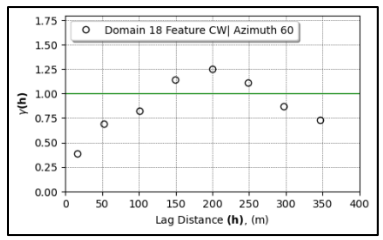

Domain 18 Feature CMGT| Azimuth 165
γ(h)
Lag Distance (h), (m)

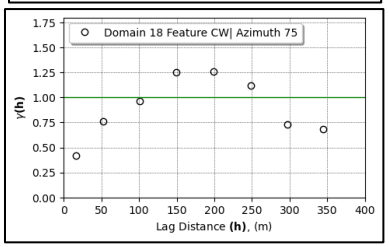

Domain 18 Feature CW| Azimuth 0
γ(h)
Lag Distance (h), (m)

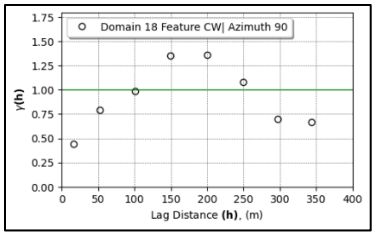

Domain 18 Feature CW| Azimuth 15
γ(h)
Lag Distance (h), (m)

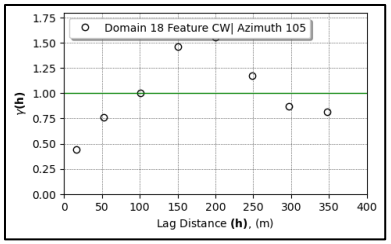

Domain 18 Feature CW| Azimuth 30
γ(h)
Lag Distance (h), (m)

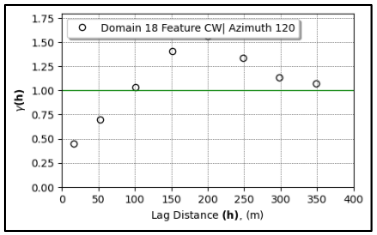

Domain 18 Feature CW| Azimuth 45
γ(h)
Lag Distance (h), (m)

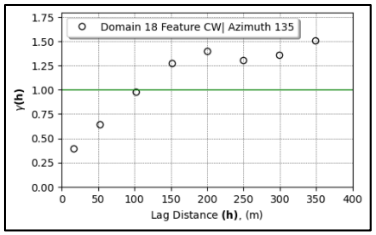

Domain 18 Feature CW| Azimuth 60
γ(h)
Lag Distance (h), (m)

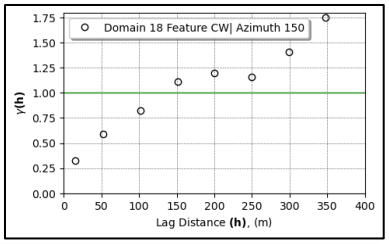

Domain 18 Feature CW| Azimuth 75
γ(h)
Lag Distance (h), (m)

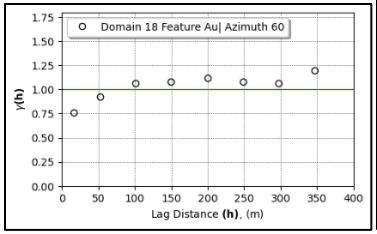

Domain 18 Feature CW| Azimuth 90
γ(h)
Lag Distance (h), (m)

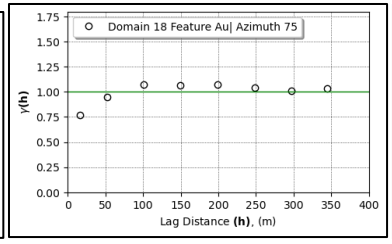

Domain 18 Feature CW| Azimuth 105
γ(h)
Lag Distance (h), (m)

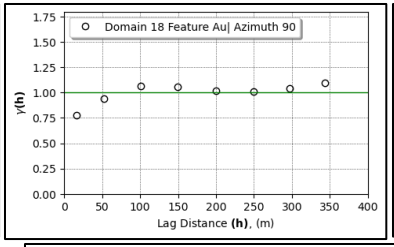

Domain 18 Feature CW| Azimuth 120
γ(h)
Lag Distance (h), (m)

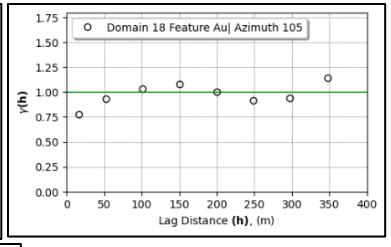

Domain 18 Feature CW| Azimuth 135
γ(h)
Lag Distance (h), (m)

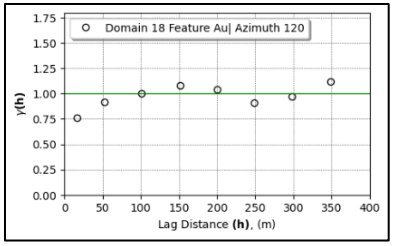

Domain 18 Feature CW| Azimuth 150
γ(h)
Lag Distance (h), (m)

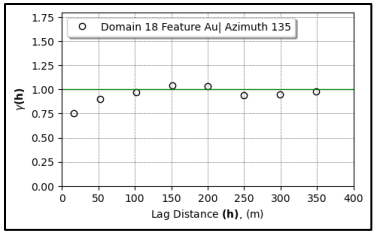

Domain 18 Feature Au| Azimuth 60
γ(h)
Lag Distance (h), (m)

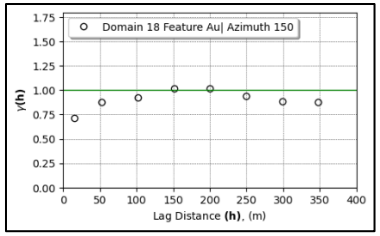

Domain 18 Feature Au| Azimuth 75
γ(h)
Lag Distance (h), (m)

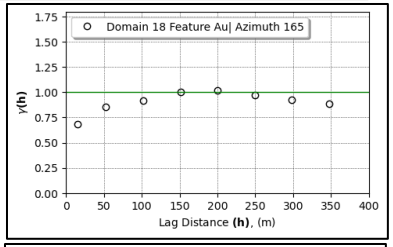

Domain 18 Feature Au| Azimuth 90
γ(h)
Lag Distance (h), (m)

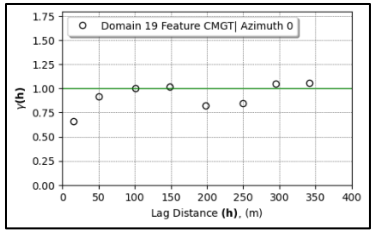

Domain 18 Feature Au| Azimuth 105
γ(h)
Lag Distance (h), (m)

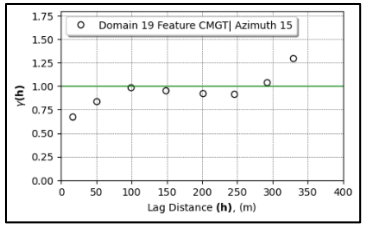

Domain 18 Feature Au| Azimuth 120
γ(h)
Lag Distance (h), (m)

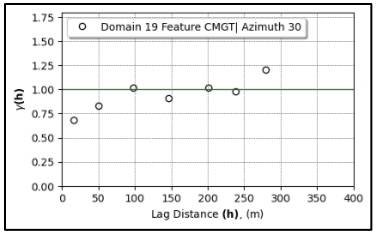

Domain 18 Feature Au| Azimuth 135
γ(h)
Lag Distance (h), (m)

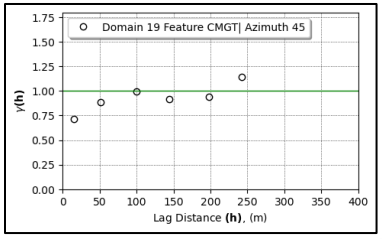

Domain 18 Feature Au| Azimuth 150
γ(h)
Lag Distance (h), (m)

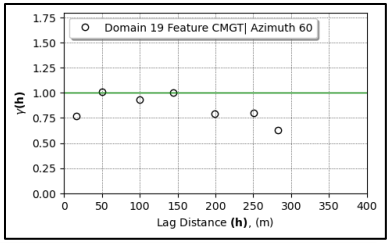

Domain 18 Feature Au| Azimuth 165
γ(h)
Lag Distance (h), (m)

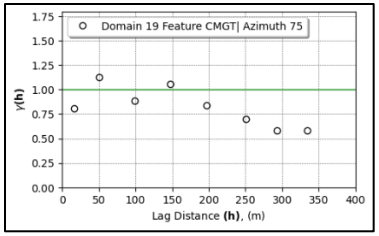

Domain 19 Feature CMGT| Azimuth 0
γ(h)
Lag Distance (h), (m)

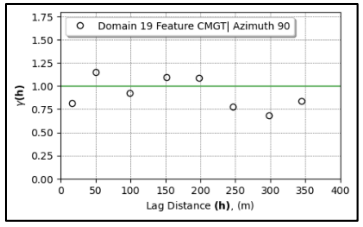

Domain 19 Feature CMGT| Azimuth 15
γ(h)
Lag Distance (h), (m)

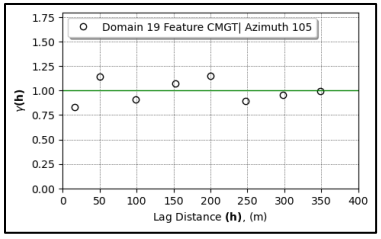

Domain 19 Feature CMGT| Azimuth 30
γ(h)
Lag Distance (h), (m)

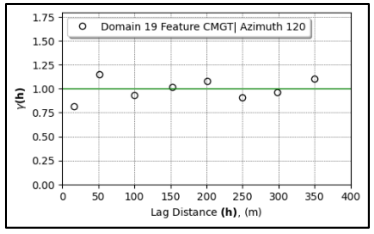

Domain 19 Feature CMGT| Azimuth 45
γ(h)
Lag Distance (h), (m)

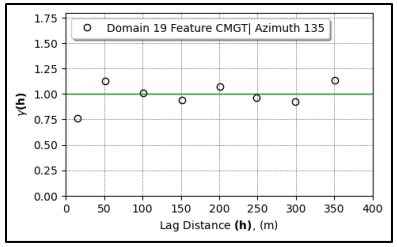

Domain 19 Feature CMGT| Azimuth 60
γ(h)
Lag Distance (h), (m)

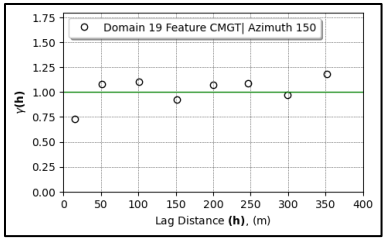

Domain 19 Feature CMGT| Azimuth 75
γ(h)
Lag Distance (h), (m)

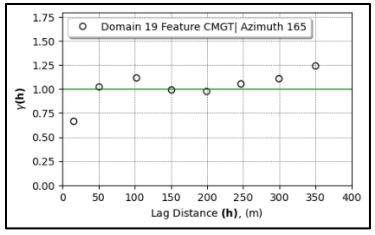

Domain 19 Feature CMGT| Azimuth 90
γ(h)
Lag Distance (h), (m)

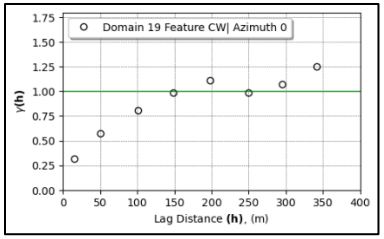

Domain 19 Feature CMGT| Azimuth 105
γ(h)
Lag Distance (h), (m)

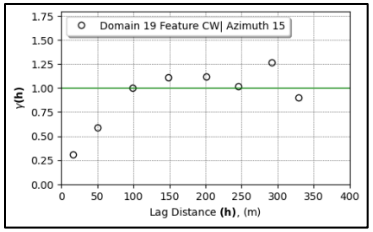

Domain 19 Feature CMGT| Azimuth 120
γ(h)
Lag Distance (h), (m)

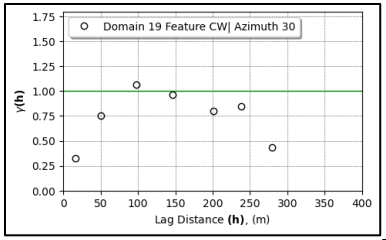

Domain 19 Feature CMGT| Azimuth 135
γ(h)
Lag Distance (h), (m)

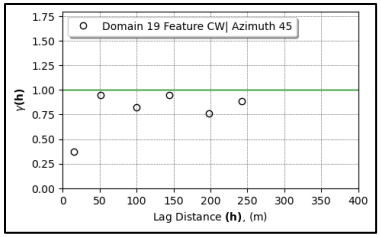

Domain 19 Feature CMGT| Azimuth 150
γ(h)
Lag Distance (h), (m)

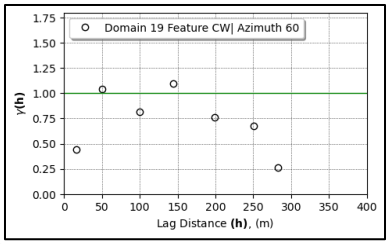

Domain 19 Feature CMGT| Azimuth 165
γ(h)
Lag Distance (h), (m)

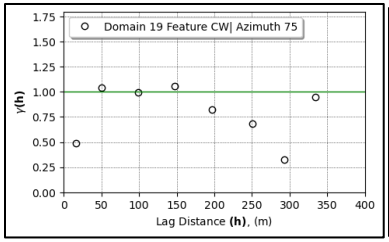

Domain 19 Feature CW| Azimuth 0
γ(h)
Lag Distance (h), (m)

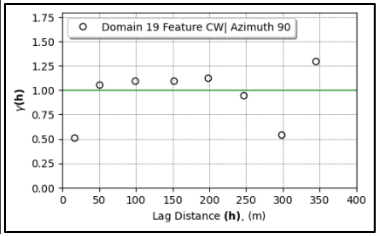

Domain 19 Feature CW| Azimuth 15
γ(h)
Lag Distance (h), (m)

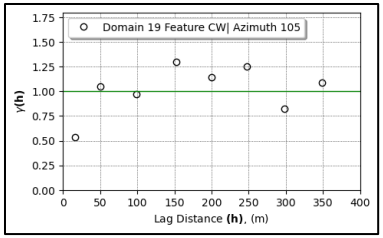

Domain 19 Feature CW| Azimuth 30
γ(h)
Lag Distance (h), (m)

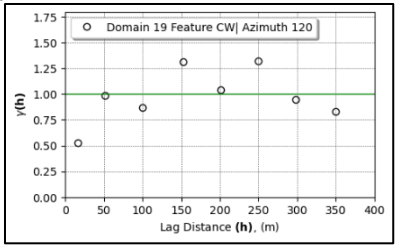

Domain 19 Feature CW| Azimuth 45
γ(h)
Lag Distance (h), (m)

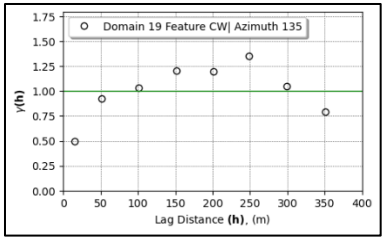

Domain 19 Feature CW| Azimuth 60
γ(h)
Lag Distance (h), (m)

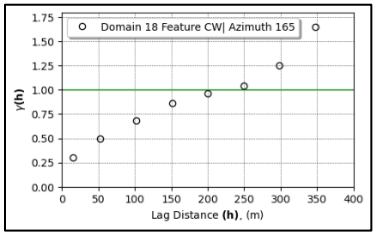

Domain 19 Feature CW| Azimuth 75
γ(h)
Lag Distance (h), (m)

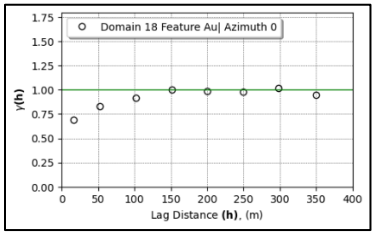

Domain 19 Feature CW| Azimuth 90
γ(h)
Lag Distance (h), (m)

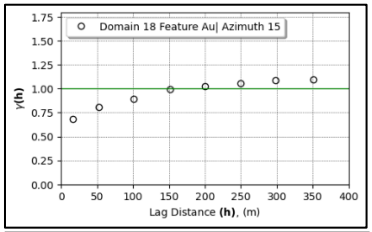

Domain 19 Feature CW| Azimuth 105
γ(h)
Lag Distance (h), (m)

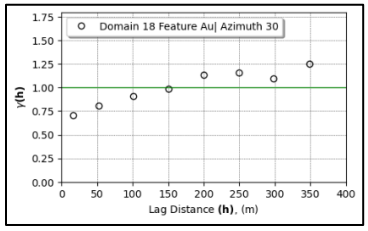

Domain 19 Feature CW| Azimuth 120
γ(h)
Lag Distance (h), (m)

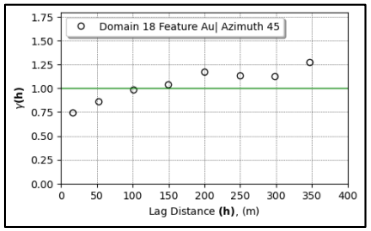

Domain 19 Feature CW| Azimuth 135
γ(h)
Lag Distance (h), (m)

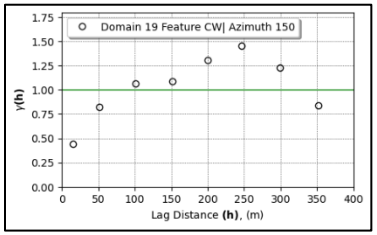

Domain 18 Feature CW| Azimuth 165
γ(h)
Lag Distance (h), (m)

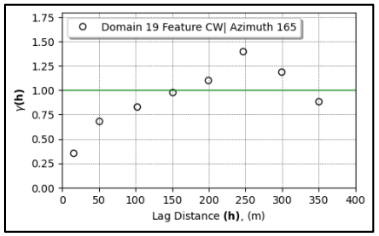

Domain 18 Feature Au| Azimuth 0
γ(h)
Lag Distance (h), (m)

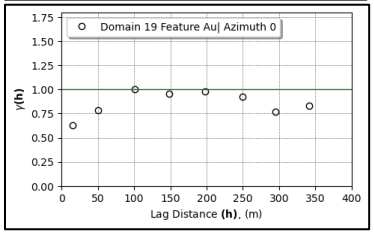

Domain 18 Feature Au| Azimuth 15
γ(h)
Lag Distance (h), (m)

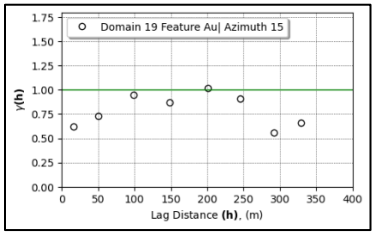

Domain 18 Feature Au| Azimuth 30
γ(h)
Lag Distance (h), (m)

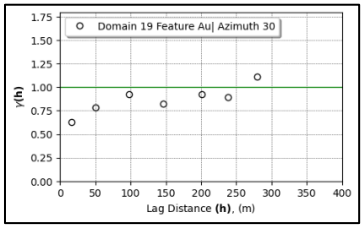

Domain 18 Feature Au| Azimuth 45
γ(h)
Lag Distance (h), (m)


Domain 19 Feature CW| Azimuth 150
γ(h)
Lag Distance (h), (m)


Domain 19 Feature CW| Azimuth 165
γ(h)
Lag Distance (h), (m)


Domain 19 Feature Au| Azimuth 0
γ(h)
Lag Distance (h), (m)


Domain 19 Feature Au| Azimuth 15
γ(h)
Lag Distance (h), (m)


Domain 19 Feature Au| Azimuth 30
γ(h)
Lag Distance (h), (m)

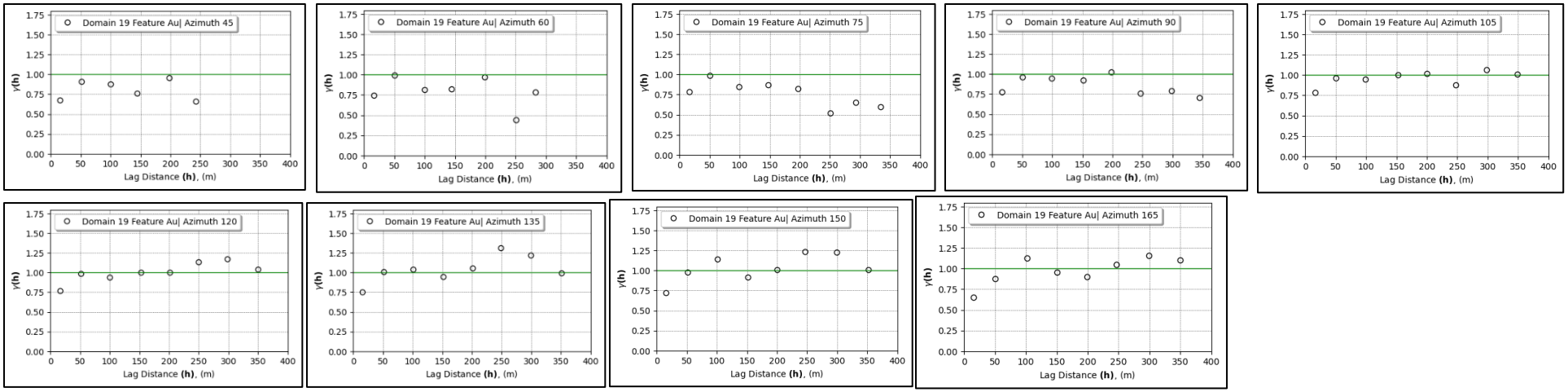
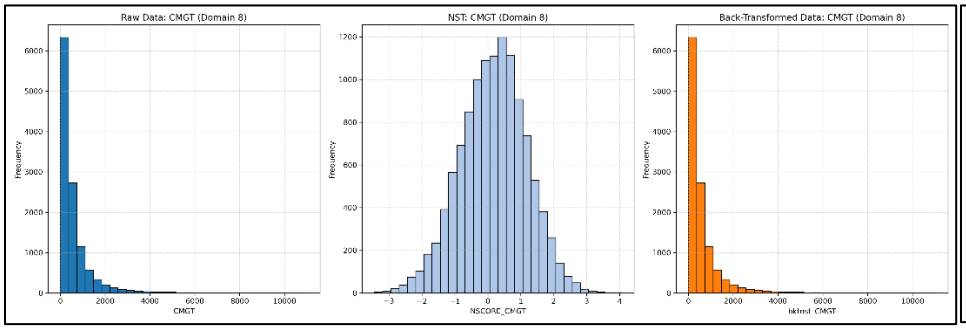
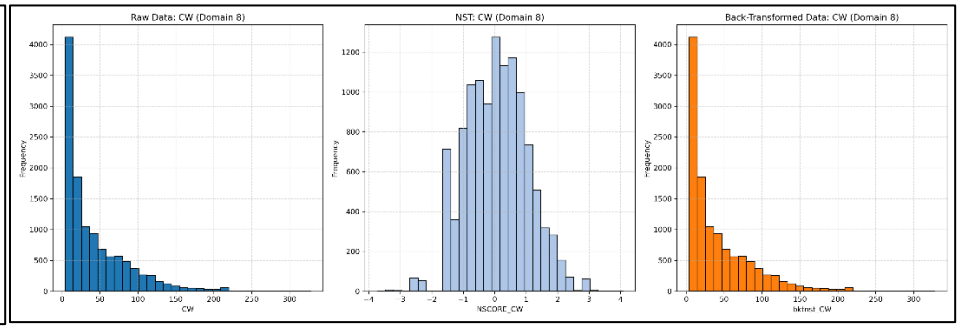
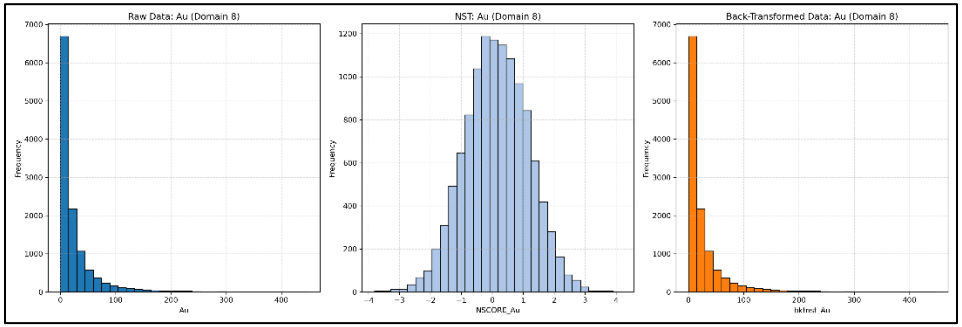


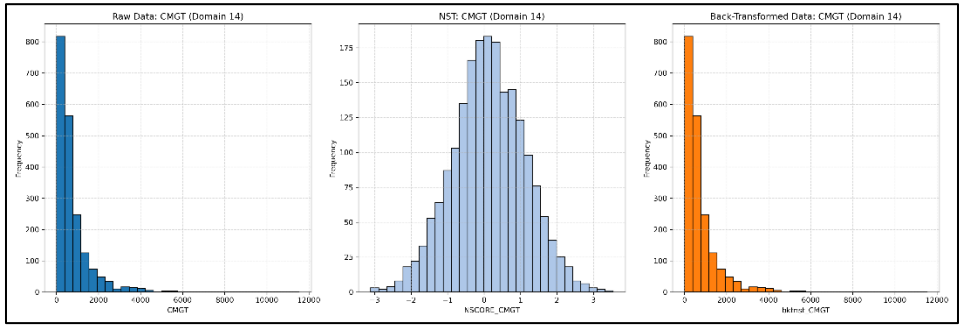
Figure A4: Experimental semi-variograms created for the variable-domain combinations at 15◦ intervals.

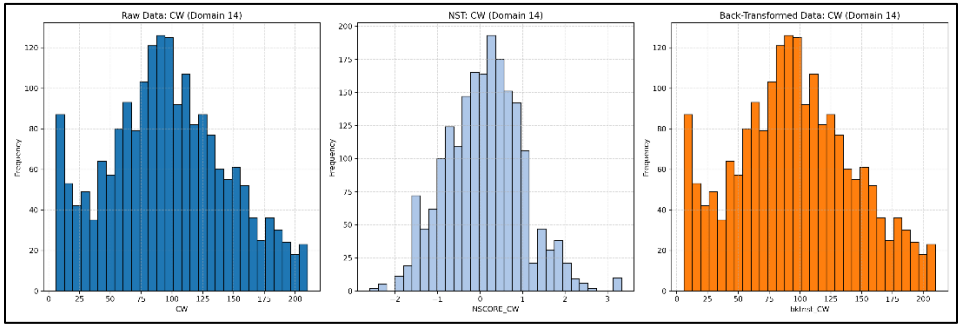
Normal Score Transformation and Back Transformation

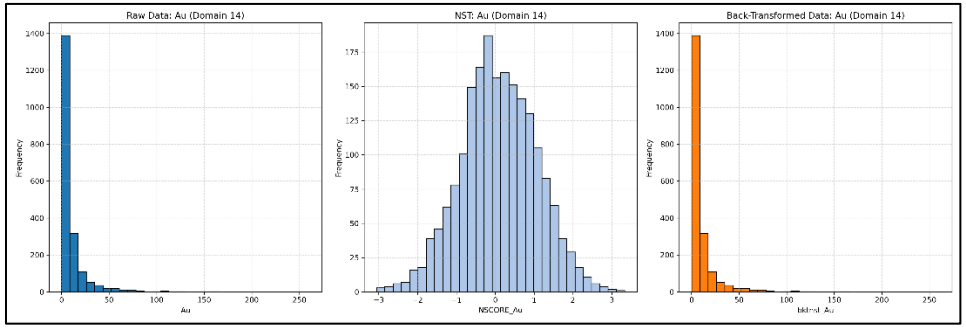












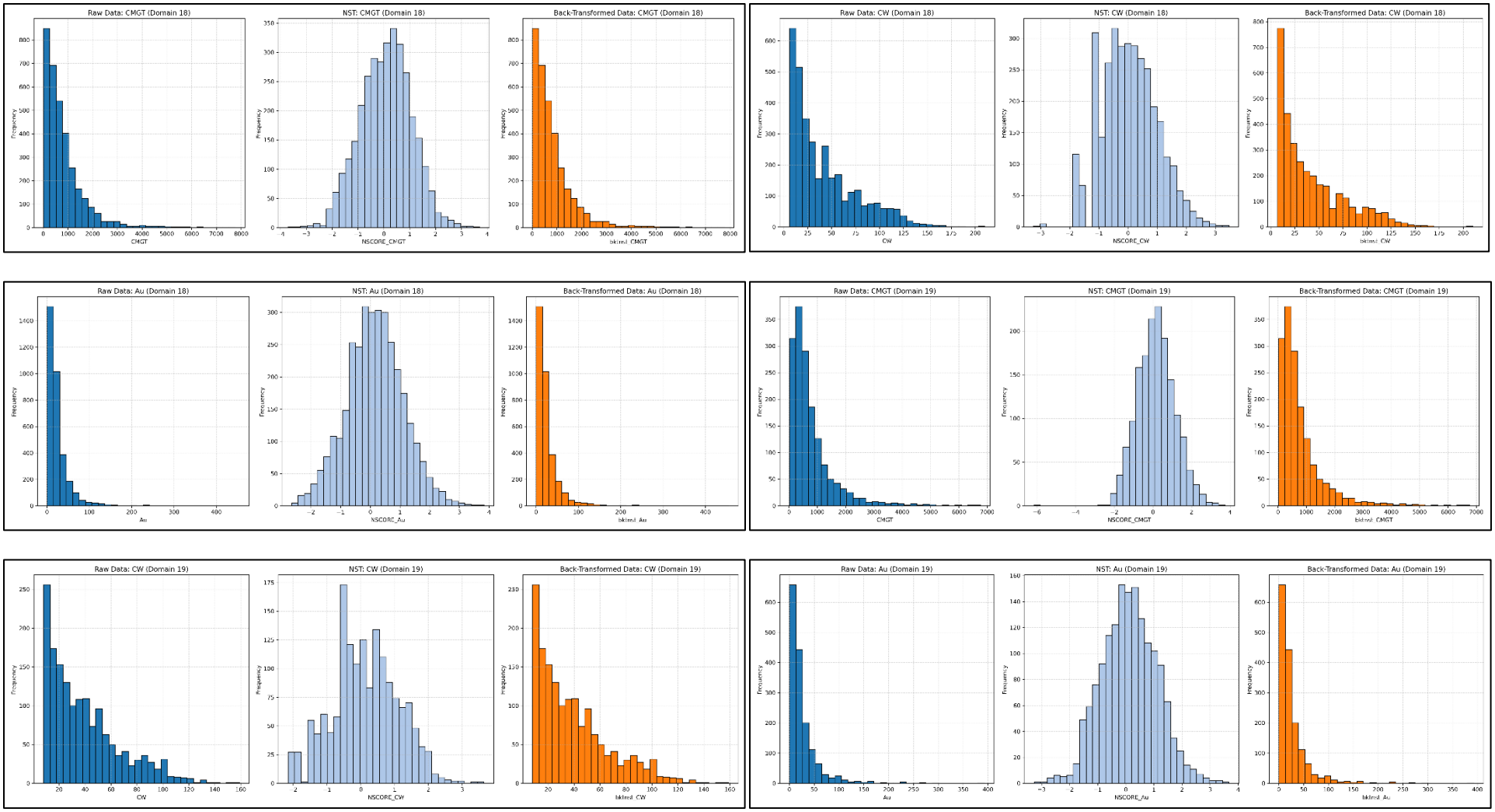


Figure A5: Histograms of each domain-variable combinations raw data, normal score transformed data and back-transformed data distribution